NASA/TM–1999-208769

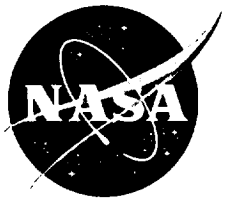

Steady Secondary Flows Generated by Periodic Compression and Expansion of an Ideal Gas in a Pulse Tube

Jeffrey M. Lee

September 1999

The NASA STI Program Office . . . in Profile

Since its founding, NASA has been dedicated to the advancement of aeronautics and space science. The NASA Scientific and Technical Information (STI) Program Office plays a key part in helping NASA maintain this important role.

The NASA STI Program Office is operated by Langley Research Center, the Lead Center for NASA's scientific and technical information. The NASA STI Program Office provides access to the NASA STI Database, the largest collection of aeronautical and space science STI in the world. The Program Office is also NASA's institutional mechanism for disseminating the results of its research and development activities. These results are published by NASA in the NASA STI Report Series, which includes the following report types:

- TECHNICAL PUBLICATION. Reports of completed research or a major significant phase of research that present the results of NASA programs and include extensive data or theoretical analysis. Includes compilations of significant scientific and technical data and information deemed to be of continuing reference value. NASA's counterpart of peer-reviewed formal professional papers but has less stringent limitations on manuscript length and extent of graphic presentations.

- TECHNICAL MEMORANDUM. Scientific and technical findings that are preliminary or of specialized interest, e.g., quick release reports, working papers, and bibliographies that contain minimal annotation. Does not contain extensive analysis.

- CONTRACTOR REPORT. Scientific and technical findings by NASA-sponsored contractors and grantees.

- CONFERENCE PUBLICATION. Collected papers from scientific and technical conferences, symposia, seminars, or other meetings sponsored or cosponsored by NASA.

- SPECIAL PUBLICATION. Scientific, technical, or historical information from NASA programs, projects, and missions, often concerned with subjects having substantial public interest.

- TECHNICAL TRANSLATION. English-language translations of foreign scientific and technical material pertinent to NASA's mission.

Specialized services that complement the STI Program Office's diverse offerings include creating custom thesauri, building customized databases, organizing and publishing research results . . . even providing videos.

For more information about the NASA STI Program Office, see the following:

- Access the NASA STI Program Home Page at *http://www.sti.nasa.gov*

- E-mail your question via the Internet to help@sti.nasa.gov

- Fax your question to the NASA Access Help Desk at (301) 621-0134

- Telephone the NASA Access Help Desk at (301) 621-0390

- Write to:
  NASA Access Help Desk
  NASA Center for AeroSpace Information
  7121 Standard Drive
  Hanover, MD 21076-1320

NASA/TM–1999-208769

Steady Secondary Flows Generated by Periodic Compression and Expansion of an Ideal Gas in a Pulse Tube

Jeffrey M. Lee
Ames Research Center, Moffett Field, California

National Aeronautics and
Space Administration

Ames Research Center
Moffett Field, California 94035-1000

September 1999

Acknowledgments

There are many persons I would like to acknowledge for their contributions.

Professor Klaus D. Timmerhaus and my advisory committee, Professors William B. Krantz, Robert Sani, and Howard Snyder of the University of Colorado at Boulder deserve many thanks for their critical assessments and insightful suggestion. Special thanks to Becky Phillips for pushing my paper work and registration through in the eleventh hour.

Dr. Ray Radebaugh of the National Institute of Standards and Technology served on the advisory committee and supplied the use of NIST facilities early-on for the initial flow visualization studies. Dr. Nicholas Rott contributed by offering his expertise on thermoacoustic systems.

Dr. Peter Kittel of the Cryogenics Group at NASA Ames Research Center served on the advisory committee and was a strong advocate of this work. Drs. Pat Roach, Ali Kashani, and Ben Helvensteijn also of the Cryogenics Group deserve special recognition for several stimulating discussions that led to the hashing-out of many technical details. Dr. Meng Wang guided my understanding of perturbation expansions. Mic Clark was instrumental in the construction of the experimental system. And thanks to my Branch Chief, Dr. Craig McCreight who patiently supported my "extended" program.

This work was funded by and conducted at NASA Ames Research Center.

CONTENTS

SYMBOLS v

SUMMARY 1

1. INTRODUCTION 3

Mechanics of Mean-Steady Secondary Transport in Oscillating Systems 3

Background 5

Conventions Used 12

Scope of This Study 12

2. GOVERNING EQUATIONS 15

Equations of Change for an Oscillating Fluid 15

Relevant Transport Quantities 16

Conditions for Acoustic and Anelastic Flows 17

3. TWO-DIMENSIONAL AXISYMMETRIC FORMULATION 21

System 21

Equations 22

Complex Embedding of the First-Order Equations 30

4. SOLUTION FOR THE THERMALLY STRONG CASE, $T_{0,z} = 0$ 35

Leading Order Results 35

Mean-Steady Secondary Flow 46

Discussion 64

5. EXPERIMENTAL MEASUREMENTS OF THE MEAN-STEADY PARTICLE VELOCITY 67

Experimental System 67

Comparison with Theory 68

Discussion 81

6. CONCLUDING REMARKS AND FUTURE WORK 83

APPENDIX A—SCALING 87

APPENDIX B—PARTICLE VELOCITY 91

APPENDIX C—ANELASTIC APPROXIMATION 93

APPENDIX D—TWO-DIMENSIONAL ANELASTIC EXPANSION AND ORDERING 95

APPENDIX E—REDUCING THE FIRST-ORDER EQUATIONS USING COMPLEX EMBEDDING 101

APPENDIX F—SOLUTION FOR THE THERMALLY STRONG CASE, $\nabla T_0 = 0$ 105

APPENDIX G—COMPUTATIONAL PROGRAM 113

APPENDIX H—EXPERIMENTAL DATA 139

REFERENCES 151

SYMBOLS

Note: All quantities are dimensionless unless designated with a superscript asterisk, in which case they are dimensional.

A area normal to flow

a speed of sound

C_p specific heat capacity at constant pressure

C_v specific heat capacity at constant volume

d displacement of gas at end of tube

$\mathcal{d}$ general diffusion term

f frequency

Fo Fourier number for the tube wall, $\mathrm{Fo} = \alpha_w^* / \left(\omega^* l^{*2}\right)$

H enthalpy

h specific enthalpy

i imaginary number, $i = \sqrt{-1}$

$\Im$ imaginary component of a complex number

J_n *nth* order Bessel function

$\mathbf{j}$ mass flux vector

k thermal conductivity of material

L length of tube

l thickness of tube wall

M Mach number, $\mathrm{M} = U_0^* / a^*$

m_n dimensionless radial function defined in table 5, equations (h), (i), and (j)

$\mathbf{n}$ unit normal vector

$\mathcal{P}$ anelastic pressure

Pr Prandtl number, $\mathrm{Pr} = \nu^* / \alpha^*$

p pressure

Q heat

$\mathbf{q}$ conduction heat flux, $\mathbf{q} = -k\nabla T$

R^* ideal gas constant

Re Reynolds number, $\mathrm{Re} = U_0^* r_w^* / \nu^* = \varepsilon \mathrm{Va}\, L^* / r_w^*$

$\Re$ real component of a complex quantity

r radial coordinate

r_w inner radius of tube

S entropy

$\mathcal{S}$ surface area enclosing domain

s specific entropy

T gas temperature

T_w temperature at interface between the gas and tube wall

t time

U_L velocity ratio, $U_L = U_L^* / U_0^*$

Velocity components

$\mathcal{U}$ higher-order Eulerian velocity vector

$\mathbf{u}$ Eulerian velocity vector

u axial Eulerian velocity

$\hat{u}$ axial Eulerian velocity phasor

v radial Eulerian velocity

$\hat{v}$ radial Eulerian velocity phasor

$\mathcal{u}$ axial higher order Eulerian velocity

$\mathbf{u}_p$ Lagrangian particle velocity vector

u_p axial Lagrangian particle velocity

v_p radial Lagrangian particle velocity

$\mathcal{v}$ radial higher order Eulerian velocity

Va Valensi number, $\mathrm{Va} = r_w^{*2} \omega^* / \nu^*$

$\mathcal{V}$ domain volume

W work

z axial coordinate

α thermal diffusivity

β thermal expansion coefficient, $\beta = -(1/\rho)(\partial\rho/\partial T)_p$

Γ gas domain length ratio $\Gamma = \left(r_w^*/\varepsilon L^*\right)$

Γ_w tube wall length ratio $\Gamma_w = \left(l^*/\varepsilon^2 L^*\right)$

γ heat capacity ratio, $\gamma = C_p/C_\upsilon$

ε inverse Strouhal number (expansion parameter), $\varepsilon = U_0^*/\left(\omega^* L^*\right) = d_0^*/L^*$

ζ_n Bessel function ratio $\zeta_n = J_n/J_0$, $n = 0, 1$

θ temperature of tube wall

κ bulk modulus, $\kappa = \rho(\partial p/\partial\rho)_T$

λ elasticity parameter, $\lambda = \gamma \mathrm{M}^2/\varepsilon = \gamma\left(U_0^*/a_0^*\right)\left(\omega^* L^*/a_0^*\right)$

μ dynamic viscosity

μ_2 second viscosity

ν kinematic viscosity

ϑ entropy of the tube wall

ρ density

τ stress tensor

Φ dissipation function

ϕ phase angle

ϕ_T phase angle between U_0 (velocity at $z = 0$) and temperature

ϕ_U phase angle between U_0 (velocity at $z = 0$) and U_L (velocity at $z = 1$)

χ arbitrary thermodynamic variable

ψ stream function

ω angular frequency

Superscripts

$\bar{}$ mean-steady, time average over a period

^	complex quantity containing amplitude and phase angle
*	dimensional quantity (no asterisk represents dimensionless quantity)
~	amplitude of a real quantity
'	exact derivative
°	definite integral
cc	complex conjugate

Subscripts

0	zeroth-order, quantity at $z = 0$, reference quantity
1	first-order
2	second-order
3	third-order
a	aftercooler
c	cold end of pulse tube
g	gas
h	hot end of pulse tube
L	quantity at $z = 1$
osc	oscillating quantity
w	tube wall

Dimensionless Numbers

ε	inverse Strouhal number (expansion parameter), $\varepsilon = U_0^*/(\omega^* L^*) = d_0^*/L^*$
λ	elasticity parameter, $\lambda = \gamma \mathrm{M}^2/\varepsilon = \gamma(U_0^*/a_0^*)(\omega^* L^*/a_0^*)$
Fo	Fourier number, $\mathrm{Fo} = \alpha_w^*/(\omega^* l^{*2})$
M	Mach number, $\mathrm{M} = U_0^*/a^*$
Pr	Prandtl number, $\mathrm{Pr} = \nu^*/\alpha^*$
Re	Reynolds number, $\mathrm{Re} = U_0^* r_w^*/\nu^* = \varepsilon \mathrm{Va}\, L^*/r_w^*$
U_L	velocity ratio, $U_L = U_L^*/U_0^*$
Va	Valensi number, $\mathrm{Va} = r_w^{*2}\omega^*/\nu^*$

STEADY SECONDARY FLOWS GENERATED BY PERIODIC COMPRESSION AND EXPANSION OF AN IDEAL GAS IN A PULSE TUBE

Jeffrey M. Lee

Ames Research Center

SUMMARY

This study establishes a consistent set of differential equations for use in describing the steady secondary flows generated by periodic compression and expansion of an ideal gas in pulse tubes. A small-amplitude series expansion solution in the inverse Strouhal number at the anelastic limit is proposed for the two-dimensional axisymmetric mass, momentum, and energy equations. The anelastic approach applies when shock and acoustic energies are small compared with the energy needed to compress and expand the gas, such as for pulse tubes.

Seven independent dimensionless numbers are used to scale the system. The reciprocal Strouhal number and Valensi number are used to linearize the mass and momentum equations. The Fourier number is used to characterize heat transfer within the tube wall. The Mach number, the Prandtl number, the velocity amplitude, and the velocity phase angle at the tube ends complete the dimensionless scales.

The ordered equations show that the zeroth-, first-, and second-order equations, are coupled through the zeroth-order temperature. An analytic solution is obtained in the strong temperature limit where the zeroth-order temperature is constant. The solution shows that periodic heat transfer between the gas and tube, characterized by the complex Nusselt number, is independent of axial velocity boundary conditions and Fourier number. Steady velocities increase linearly for small Valensi number and can be of order 1 for large Valensi number. Decreasing heat transfer between the gas and the tube decreases steady velocities for orifice pulse tubes. The opposite is true for basic pulse tubes. A conversion of steady work flow to heat flow occurs whenever temperature, velocity, or phase-angle gradients are present. Steady enthalpy flow is reduced by heat transfer and is scaled by the Prandtl times Valensi numbers.

Particle velocities from a smoke-wire experiment were compared with predictions for basic and orifice pulse tube configurations. The theory predicted the observed mass streaming and flow reversals between the centerline and diffusion layers. The results indicate that the theory is valid for pulse tubes and that it can be used to solve for the zeroth-order temperature, to compute enthalpy flows, and to determine losses associated with steady secondary streaming.

1. INTRODUCTION

A gas subject to periodic compression and expansion generates higher-order steady secondary flows. The steady flows can manifest themselves as mass, momentum, and energy streaming. The pulse tube refrigerator, in which the generated steady flow of enthalpy can lead to temperature differences of over 200 K, is a practical use of this type of transport.

The behavior results from nonlinear steady secondary transport. What appears to be strictly a linear periodic system— oscillating temperatures and oscillating mass flows— in fact, gives rise to mean-steady enthalpy flows. These enthalpy flows produce the observed refrigeration effect. The term "mean-steady flow" refers to the time-averaged secondary flow.[1] Other types of mean-steady flows, or streaming, include momentum streaming (such as acoustic streaming) and mass-species streaming. Although the magnitude of mean-steady flows may be small, the fact that they are steady and unidirectional can lead to sizable gradients over extended times.

This work examines mean-steady secondary transport for the pulse tube refrigerator. The phenomenon is examined in the limit of a linear anelastic approximation. Oscillating anelastic[2] flows are characterized by low Mach numbers and oscillating frequencies that are much lower than the resonance frequency defined by the system geometry. The anelastic approximation filters shocks from the fluid equations while retaining the effects of density variations resulting from "slow" compression and expansion of the gas. This applies when the energies of acoustic waves and shock waves are negligible relative to the energy needed to compress and expand the bulk gas.[3] This work investigates steady secondary momentum and energy flows of an ideal compressible gas in the limit of linear anelasticity.

Mechanics of Mean-Steady Secondary Transport in Oscillating Systems

Mean-steady secondary flows have been investigated for a number of systems. For such flows, the nonlinear advection terms of the appropriate transport equation produce the "driving force" for the mean-steady flow. Mean-steady flows can produce energy streaming, mass streaming (refs. 3–5), and even a mechanism for separating different mass species in multicomponent mixtures (refs. 6, 7). An example of mass streaming for a single component fluid is shown in figure 1. Figure 1(a) shows the observed mean-steady pathlines external to an extended cylinder oscillating along its diameter in water, and figure 1(b) shows the corresponding calculated pathlines.

In this section, a simple linear mathematical model for describing mean-steady secondary flows is developed. Consider the unsteady advection-diffusion equation where u is the velocity, χ is

---

[1]This is different from 'quasi-steady' flow which refers to periodic oscillations, or 'steady-state' flow which is absolutely constant in time.

[2]Anelastic flows are described in more detail by Sherman (ref. 1) and Paolucci (ref. 2).

[3]The arguments are similar to Boussinesq flow, except that the flow is driven by applied pressure forces instead of buoyancy forces.

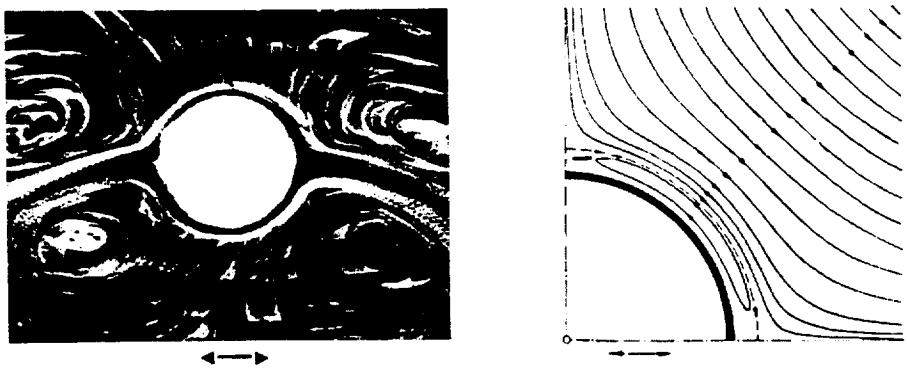

(a) (b)

Figure 1. Example of mean-steady flows in oscillating systems: from Schlichting's oscillating cylinder (ref. 8).

a thermodynamic quantity (such as temperature or pressure), and $\mathcal{d}$ is the term containing diffusion of χ,

$$\frac{\partial \chi}{\partial t} + \varepsilon \frac{\partial}{\partial z}(\chi u) = \mathcal{d} \tag{1}$$

Now consider a time-periodic series expansion solution of u and χ that is expanded in the small parameter ε, valid for $\varepsilon \ll 1$:

$$u = \tilde{u}_0(z)\cos\omega t + \varepsilon u_1(z,t) + \boldsymbol{O}\left(\varepsilon^2\right) \tag{2}$$

$$\chi = \tilde{\chi}_0(z)\cos(\omega t + \phi) + \varepsilon \chi_1(z,t) + \boldsymbol{O}\left(\varepsilon^2\right) \tag{3}$$

$$\mathcal{d} = \mathcal{d}_0(z,t) + \varepsilon \mathcal{d}_1(z,t) + \boldsymbol{O}\left(\varepsilon^2\right) \tag{4}$$

where ϕ is the phase angle between u and χ. Substituting the series solution into the differential equation and equating terms of like order in ε results in

$$\boldsymbol{O}(1): \quad \mathcal{d}_0 = \frac{\partial}{\partial t}\tilde{\chi}_0 \cos(\omega t + \phi) \tag{5}$$

$$\boldsymbol{O}(\varepsilon): \quad \mathcal{d}_1 = \frac{\partial}{\partial t}\chi_1(z,t) + \frac{\partial}{\partial z}\left[\tilde{u}_0 \cos\omega t \cdot \tilde{\chi}_0 \cos(\omega t + \phi)\right] \tag{6}$$

where $\boldsymbol{O}$ means "of order." Equation (5) is the linear oscillating equation of $\boldsymbol{O}(1)$. Its solution allows evaluation of equation (6) which describes a secondary flow of $\boldsymbol{O}(\varepsilon)$. By time-averaging equation (6) over a period the relation for the mean-steady flow is obtained:

$$\bar{\dot{q}}_1 = \frac{\partial}{\partial z}\omega \oint_{1/\omega} \dot{q}_1 dt = \frac{\partial}{\partial z}\left\{(\tilde{u}_0\tilde{\chi}_0)\left(\cos\phi + \frac{1}{2}\oint_{1/\omega}\cos 2\omega t dt\right)\right\} \tag{7}$$

$$= \frac{\partial(\tilde{u}_0\tilde{\chi}_0)}{\partial z}\cos\phi - \tilde{u}_0\tilde{\chi}_0 \sin\phi \frac{\partial\phi}{\partial z}$$

Equation (7) shows that the secondary flow depends on the gradients of amplitude and phase angle.

Two limiting flows are characterized by being either of the standing wave type, in which phase is independent of position $\partial\phi/\partial z = 0$, or the progressive wave type, in which amplitude is independent of position $\partial(\tilde{u}_0\tilde{\chi}_0)/\partial z = 0$. An acoustic oscillator is an example of the standing wave type. An example of the progressive wave type is water of uniform depth oscillating near the shore of a pond. The oscillating water generates mean-steady momentum forces that form periodic ridges in the fine sediment.

The above illustrates the mathematical basis for a linearized pulse tube model. The time-averaged product of velocity (kinematic quantity) and temperature (thermodynamic quantity) results in a mean-steady unidirectional flow of enthalpy. The mean-steady enthalpy flow will be non-zero when there are gradients in the phase angle and product amplitudes. This can be accomplished by heat transfer between the gas and the tube wall such that the thermal and viscous penetration depths are not equal, or by independently controlling the amplitude and phase angle of velocity at the tube ends. The first case is the enthalpy flow mechanism in the basic pulse tube, and the second is the mechanism in the orifice pulse tube.

Background

The following is a chronological summary of pulse tube development. A historical brief on pulse tube development is given by Longsworth (ref. 9), Kittel (ref. 10), and Radebaugh (ref. 11). Ames Research Center's pulse tube home page[4] provides a comprehensive list of published pulse tube research papers through 1994. A variation of the pulse tube is the acoustic refrigerator, a detailed account of which was prepared by Swift (ref. 12).

Gifford and Longsworth

In 1963 Gifford and Longsworth reported on a new type of regenerative refrigerator (ref. 13). Their "pulse tube refrigerator," aptly named because of the use of pressure pulses to alternately compress and expand the gas, was innovative and very promising because there were no cold moving parts which could limit reliability. Comparable systems at that time were based on Stirling systems which required both a compressor and a cold expander for operation. Figure 2 shows a schematic of this early basic pulse tube (BPT). The BPT consists of a hot heat exchanger, an open tube, a cold heat exchanger, a regenerator, an aftercooler, and a reciprocating compressor. Work is supplied by the compressor, heat is rejected at T_h and T_a, and cooling is produced at T_c.

[4]http://irtek.arc.nasa.gov/CryoGroup/PTDatabase/database.htm

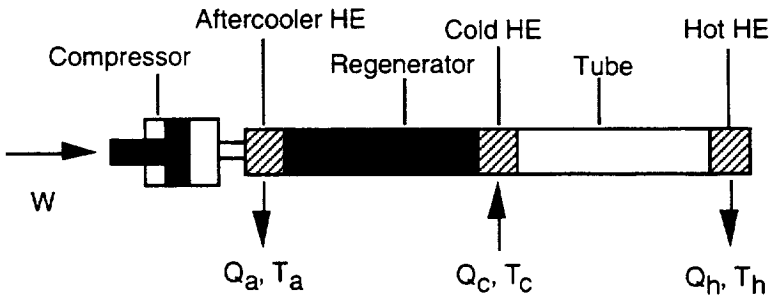

Figure 2. Basic pulse tube.

Longsworth's experiments demonstrated the performance of a BPT, obtaining temperatures of 169 K with a single stage and of 123 K with two stages using helium (ref. 14).

Gifford and Longsworth formulated a "step-wise" heat-transfer theory to describe their results (ref. 15), and recently, de Boer extended the analysis (ref. 16). The basis of his model consists of four steps: adiabatic compression of the gas and displacement toward the hot end of the pulse tube; isobaric heat transfer from the hot gas to the cooler tube wall; adiabatic expansion of the gas and displacement back toward the cold end of the pulse tube; and isobaric heat transfer from the wall of the pulse tube to the cooler gas. This description enables one to visualize how an "energy packet" can migrate between the gas and the tube wall in such a fashion as to result in a net transport of energy from one end of the tube to the other. Heat transfer between the tube wall—which acts as a second thermodynamic medium—and the gas is required to produce the phase shift necessary for the flow of enthalpy, as explained above. After a decade of research, however, interest waned because the BPT was unable to obtain temperatures and efficiencies comparable to those of Stirling cryocoolers.

Wheatley, Swift, Hoffler

Following the BPT, Wheatley et al. at the Los Alamos National Laboratory began investigating "naturally irreversible engines," that is, those processes in which a downhill flow of entropy, say for example, heat conduction, can be used for conversion into mechanical energy, such as a thermally driven engine or prime mover (ref. 17). This work is still in progress by Swift at Los Alamos. A complete account of the theory of acoustic engines given by Swift (ref. 12) and a similitude analysis has been done by Olsen and Swift (ref. 18).

The work on heat engines was applied to refrigeration by reversing the thermodynamic process. Hoffler examined an acoustic refrigerator in which a pressure driver was placed at one end of the system shown in figure 3 (ref. 19). Temperatures of 193 K were demonstrated using helium, with the stack acting as the second thermodynamic medium serving the same purpose as with the tube of the BPT.

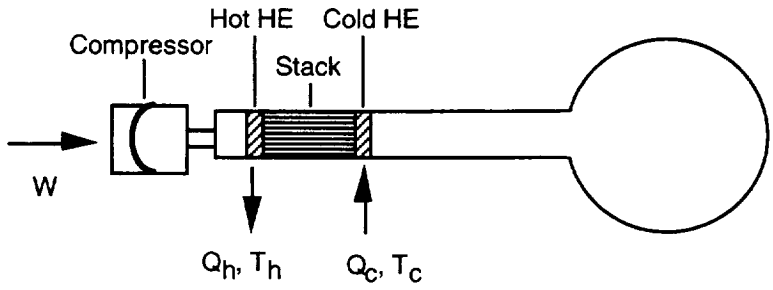

Figure 3. Acoustic refrigerator.

Rott

Previous to Wheatley's work, Rott formulated a set of linear acoustic equations which included transverse diffusion (refs. 20, 21). Müller, studying under Rott, detailed much of the analyses in reference 22. The equations were examined for a number of conditions, including stability limits for thermally driven oscillations (ref. 23), tubes with variable cross section (ref. 24), gas-liquid oscillations (ref. 25), and efficiency analysis of thermoacoustic oscillations operating as heat engines (ref. 26). Of primary interest are Rott's papers on second-order mean-steady heat flux (refs. 27–29), which focus on enthalpy and mass streaming in the limit of constant axial temperature. Rott has termed this limit the "strong" temperature case (Rott, N. 1993: personal communication).

Merkli

Merkli and Thomann (ref. 30) experimentally investigated an acoustic refrigerator and examined their results using Rott's acoustic equations. They found good correlation between experiment and prediction, with local heating at velocity nodes and cooling at antinodes. This and the experimental work of Wheatley laid the theoretical foundation for acoustic refrigerators and acoustic engines as accepted today.

Mikulin

The fundamental principle behind the acoustic devices and the BPT requires heat transfer between a solid boundary and the working gas. This necessitates a spacing between solid boundaries of the order of the thermal and viscous diffusion lengths. However, this limits enthalpy flow, because temperature and velocity amplitudes and phase-angle are restrained and because the dynamics are governed by transverse diffusion. However, Mikulin et al. showed that enthalpy transport need not require diffusion to produce the required phase shift between gas temperature and velocity, but that the phase and amplitude relation between velocity and temperature can be separately managed by controlling the boundary conditions at the tube ends (ref. 31). In their experiments, Mikulin et al. demonstrated the first orifice pulse tube (OPT) refrigerator, obtaining temperatures of 105 K with air.

A variation of the OPT device is shown in figure 4. The approach Mikulin et al. used was to place an orifice and reservoir volume at the closed end of a basic pulse tube, thus allowing for a

finite gas flow. The result is to greatly increase enthalpy flow at the hot end[5] and to change the phase angle between velocity and temperature at the cold end so that pressure and velocity are closer to being in-phase. This eliminates the need for a second thermodynamic medium and the inherent restrictions associated with diffusion. It was also accomplished without the need for any type of mechanical device. The OPT results in lower temperatures, increased cooling, and higher efficiencies. Since the tube of the ideal OPT does not require heat transfer to transport energy, the transport process within the tube is ideally reversible.

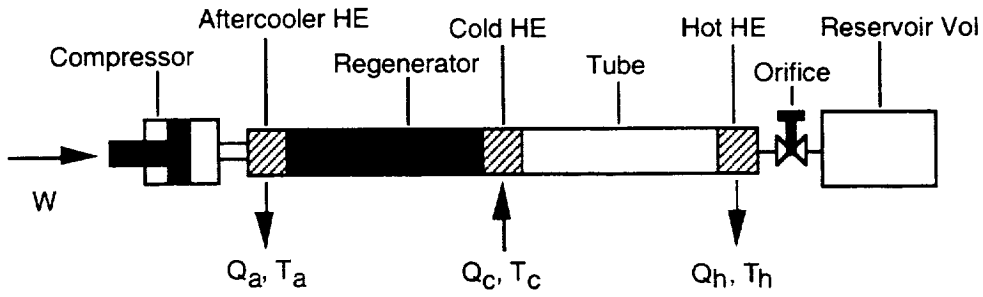

Figure 4. Orifice pulse tube.

Radebaugh

After reviewing Mikulin's work, Radebaugh and his coworkers recognized the intrinsic value of a cooler without any cold moving mechanical parts, and so began work on the OPT as it is known today. Their initial work demonstrated a single-stage 60 K refrigerator using helium, a substantially lower temperature than had been achieved by any previous PT device (ref. 32). Other investigators have since demonstrated temperatures of 4 K (ref. 33) and even lower by using multiple-stages (ref. 34).

A description of the transport process for OPT devices was first given by Storch et al. based on a one-dimensional thermodynamic model that assumed adiabatic processes within the tube (ref. 35). A primary advantage of the one-dimensional (1-D) model is the convenience in using phasor diagrams to describe the phase relation between oscillating temperature, pressure, and mass flow. David et al. extended one-dimensional analysis for arbitrary time-dependence of pressure (ref. 36), and Kittel reviewed and extended the theory for entropy and work flows, temperature gradients, thermal conduction, and viscosity (ref. 37). For large systems in which transverse diffusion is confined to thin-boundary layers, this approach works well. However, for smaller systems in which diffusion is significant, large discrepancies arise (from 2 to 5 times, depending on tube diameter-to-length ratio (ref. 35)).

Beyond one dimension

The one-dimensional description of the transport process within pulse tubes is unable to describe transverse transport. To account for transverse effects, lumped-parameter corrections to the 1-D model have been used. The complex Nusselt number developed by K. Lee (ref. 38) and

[5]Whereas in the BPT, enthalpy flow goes to zero at the closed end of the tube because the velocity goes to zero.

extended by Kornhauser and Smith (refs. 39, 40) was used by Roach and Kashani (ref. 41). The complex Nusselt number allows for lumped-parameter corrections to the oscillating heat transfer between the gas and the tube wall by accounting for amplitude and phase-shift owing to diffusion.

A number of investigators have taken the 2-D dissipative acoustic equations of Rott (ref. 20) and applied them to pulse tubes. Though the dynamics of the pulse tube are not within the constraints of the acoustic approximation, nevertheless, the corrections offered by considering diffusion do increase the predictability.

Jeong calculated 2-D steady secondary flows between flat plates with velocity oscillations for a BPT-configured system (ref. 42). His leading-order solution is in the limit of a boundary-layer approximation (thin diffusion layer). He applies the leading-order solution to the higher-order mean-steady problem and extends the solution over the complete transverse domain, with the solution for the core region corresponding well to the mean-steady parabolic solution of Rott. Previous solutions of the dissipative acoustic equations for a cylindrical geometry by J. Lee and coworkers have shown similar results for mean-steady mass flow, and have been extended to enthalpy flow (ref. 43).

Xiao formulated the problem in the acoustic limit. His three papers present a general set of 2-D acoustic equations with transverse effects averaged out (by integrating over the area normal to axial flow), thereby obtaining equations amenable to solution for "flow quantities" (integrated quantities as opposed to local vector quantities) (refs. 44–46). Xiao's subsequent solutions are offered for isothermal zeroth-order temperature and adiabatic conditions at the tube wall. His analysis has yielded insightful understanding of axial mean-steady work, heat, and energy flows, and is a step above a 1-D analysis because it includes lower-order transverse diffusion; however, it cannot be used to determine the vector fields, nor the higher-order mean-steady transverse diffusion heat transfer.

Bauwens takes an anelastic approach of the leading-order problem for very narrow tubes and small Mach numbers, and arrives at a solution for the axial temperature profile and mean-steady enthalpy flow (refs. 47, 48). Velocity conditions at the tube ends are treated as independent, and the temperature of the tube wall is fixed (high heat capacity). His analysis is applicable for very small Peclet numbers of the gas (small tube diameters) such as for regenerators.

Only a few experimental investigations have been conducted to validate the predictions offered by the above solutions. Linear oscillating flow for low speeds was measured by Shiraishi et al. (ref. 49) and Nakamura et al. (ref. 50). Velocity phase shifts in the diffusion layer have been observed, corresponding to a Stokes solution of the linearized momentum equation. Hoffman et al. (ref. 51) compared pulse tube performance with the acoustic solutions of Xiao (refs. 44–46) and obtained good agreement. Previous work by J. Lee and coworkers had shown the existence of mean-steady streaming with characteristic lengths of the tube length, in agreement with higher-order solutions obtained from linear analysis (ref. 52).

Other phase-shifting mechanisms

The OPT goes beyond the capabilities of a BPT by utilizing a valve and reservoir volume at the hot end to increased phase shift and mass flow. The valve/reservoir combination, however, is still limiting. Two other new pulse tube configurations have the potential to further increase performance: the double-inlet pulse tube and the inertance pulse tube.

Double-Inlet Pulse Tube

The double-inlet pulse tube, illustrated in figure 5, adds a flow path from the compressor to the tube hot end. This allows the gas to be compressed from the hot end of the tube, thereby increasing the phase angle and reducing the mass flow through the regenerator. Reducing the mass flow through the regenerator reduces enthalpy flow losses. Zhu et al. (ref. 53) first demonstrated the advantages of the double-inlet pulse tube, and Lewis and Radebaugh (ref. 54) recently obtained a temperature of 35 K for a 4 - cm^3 compressor using a double-inlet. Seo et al. measured axial and radial temperatures for the basic, orifice, and double-inlet pulse tubes and examined the phase and amplitude differences between the three (ref. 55). Shiraishi et al. measured axial mass flow between the three pulse tubes and showed that the double-inlet decreases flow in the middle of the tube while maintaining generally the same flow at the ends of the tube (ref. 56). This suggests that a primary advantage of the double-inlet is to increase phase angles.

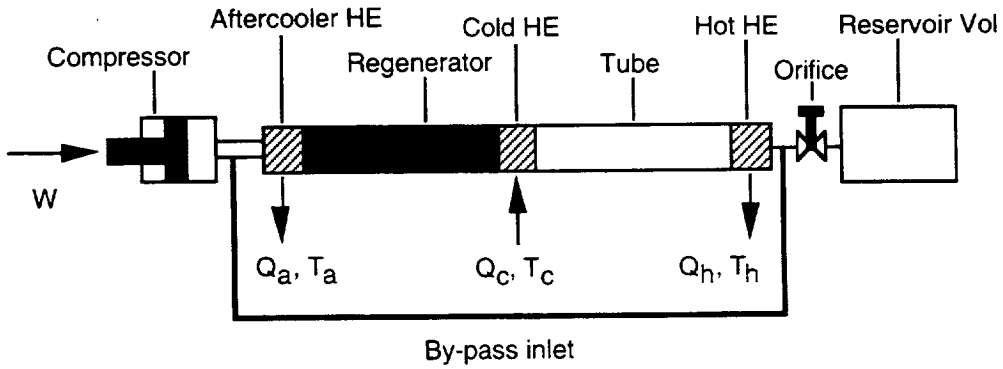

Figure 5. Double-inlet pulse tube.

The concept of the double-inlet can be extended to multi-inlets by providing flow communication between the regenerator and pulse tube at locations with similar temperatures. In theory, the effect is a multi-stage device with cooling stages at the multi-inlets, but in practice, it is difficult to obtain the proper flow amplitudes and phase angles.

Inertance Pulse Tube

Use of an inertance tube to replace the orifice has been reported by Godshalk et al. (ref. 57), Zhu et al. (ref. 58), Gardner and Swift (ref. 59), and Roach and Kashani (ref. 60). The inertance pulse tube is shown in figure 6. The idea is to use the inertia of the gas in a long tube to provide added phase shift, analogous to the inductance in an electrical circuit. Hence the term *inertance*, a combination of inertia and inductance. Matching the gas inertia in the inertance tube to the gas spring compliance of the compressor, regenerator, and tube combination can result in near resonant operation with higher performance.

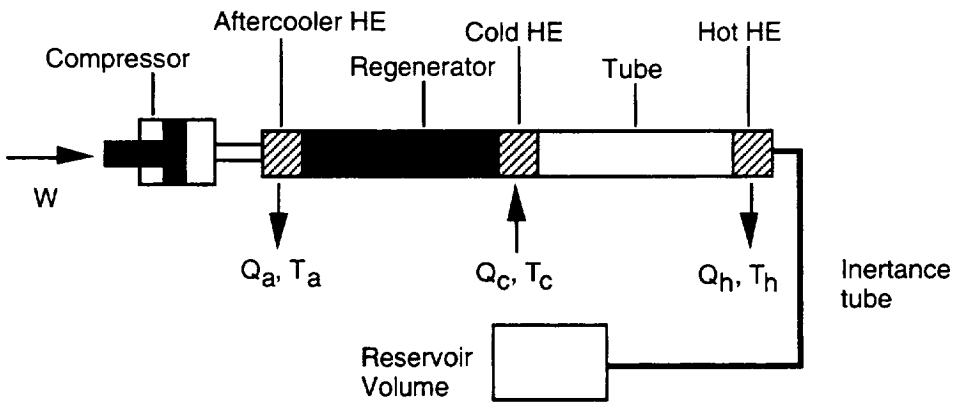

Figure 6. Inertance pulse tube.

A qualitative comparison of different modeling approaches is shown in table 1. Two-dimensional anelastic modeling is seen to yield a high return on modeling effort. With 2-D modeling, transverse diffusion effects (which represent viscous effects and heat transfer between the gas and the tube wall) can be evaluated to obtain transverse temperatures profiles and higher-order mean-steady flows. The information obtained from a 2-D model is significantly more than from a 1-D model, and anelastic approximations are computationally less intensive than fully compressible CFD (computational fluid dynamic) codes.

Table 1. Qualitative comparison of different modeling approaches.

Model comparison chart	**Integral**	**Differential analytic**		**CFD**			
				Compressible		**Anelastic**	
	Phasor	1-D	2-D	1-D	2-D	3-D	2-D
Primary measures							
Refrigeration (enthalpy flow)	√	√	√	√	√	√	√
Temperature, axial profile		√	√	√	√	√	√
Temperature, transverse profile			√		√	√	√
Mean-steady secondary flows			√		√	√	√
Heat transfer between tube and gas			√		√	√	√
Secondary measures							
Temperature-dependent properties		√	√	√	√	√	√
Oscillating temperature at tube ends		√	√	√	√	√	√
Nonlinearities				√	√	√	√
Buoyancy effects (free convection)			√		√	√	√
Flow end effects					√	√	√
Qualitative measures							
System optimization		√	√	√	√	√	√
Transient simulation				√	√	√	√
Physics are easily understandable	√	√	√				

Conventions Used

The following conventions are used for variables in this study:

u = scalar	$\Rightarrow$	lightface italic are scalars
$\mathbf{U}$ = vector	$\Rightarrow$	boldface are vectors
τ = tensor	$\Rightarrow$	lightface non-italic Greek are tensors
u^* = dimensional	$\Rightarrow$	with asterisk denotes a dimensional quantity
u = dimensionless	$\Rightarrow$	without asterisk denotes a nondimensional quantity
$O(\varepsilon)$	$\Rightarrow$	of order of ε
$\chi_{,t} = \partial\chi/\partial t$	$\Rightarrow$	partial differential notation

Complex embedding will be used to eliminate the time variable. For periodic χ,

$$\chi = \Re\left[\hat{\chi} e^{it}\right] = \Re\left[\tilde{\chi} e^{i(t+\phi)}\right] \tag{8}$$

where $t = \omega^* t^*$, $\hat{\chi}$ is complex, $\tilde{\chi}$ is a real number, ϕ is the phase angle, and $\Re$ extracts the real component of the complex quantity.

Scope of This Study

Previous attempts to model the dynamic workings of pulse tube coolers have typically used thermodynamic or acoustic analysis. The first, being an integral approach, fails in its attempt to capture local transport. It is also inherently one-dimensional, and so neglects transverse thermal and viscous diffusion. The consequence is to oversimplify phase angles and overestimate velocity, temperature, and pressure amplitudes, resulting in overprediction of enthalpy flows, particularly for small pulse tubes in which fields dominated by diffusion constitute a significant amount of the mean-steady flow. To account for transverse diffusion, lumped-parameter heat-transfer relations have been introduced with some success.

The second approach, acoustic analysis, examines the differential acoustic equations first formulated by Rott. The transverse diffusion terms are retained, thus allowing for transverse 2-D effects. Typically, however, the solution for the linear system has been simplified by approximating the diffusion layer as being very thin, thereby obtaining the pressure function at the 1-D inviscid limit. This is applicable to pulse tubes that have large Valensi numbers. The higher-order mean-steady flows have been examined for flow in a BPT. However, for the OPT, the transverse effects have been integrated-out, thereby making vector fields unobtainable. For these cases, the acoustic ordering is not completely consistent with demonstrated pulse tubes since pulse tubes operate at frequencies considerably below resonance. This is not a weakness, however, since the acoustic

solutions are smooth and well-behaved, and so can be used in engineering models. None of the previous work has compared measured mean-steady velocity fields to predictions in order to validate the solutions.

This study goes beyond previous analyses by calculating the anelastic 2-D vector fields for enthalpy and velocity, and transverse temperature. Included are the effects of heat transfer between the gas and the tube wall of finite thickness. Finally, experimentally measured mean-steady particle velocities are compared with the theory's predictions.

Section 2 focuses on the fluid equations and the conditions in which they can be approximated for acoustic, anelastic, and linear anelastic flows. The enthalpy flow, mean-steady particle velocity, and entropy equations, useful in this study, are presented.

Section 3 reduces the fluid equations for linear anelastic flow of a gas in a tube. The system taken is two-dimensional axisymmetric. Heat transfer between the gas and a thin-walled tube is included. An expansion series solution is taken, and the leading-order problem and the mean-steady higher-order equations are presented. The linearized equations are then simplified by using complex embedding for time.

Section 4 presents the linearized solutions for the strong temperature case in which the zeroth-order temperature is constant. Examined are oscillating flows for velocity and temperature, oscillating heat transfer between the gas and the tube wall, and oscillating shear. Correlations and use of the complex Nusselt number are given. Mean-steady flows are calculated for the Eulerian and Lagrangian (particle) velocities, enthalpy flux fields, and temperature. The interaction between enthalpy flow, work flow, and heat conduction is discussed.

In section 5 the predicted mean-steady particle velocities are compared with measured velocities. The measured velocities are obtained using smoke-wire flow visualization for air contained in a transparent tube with oscillating compressors at each end.

Study results and suggestions for future work are summarized in section 6.

2. GOVERNING EQUATIONS

This chapter examines and simplifies the governing fluid equations for slow oscillating compressible flows. The equations are scaled, and dimensionless numbers are defined. Next, secondary transport quantities are derived, and then series solutions are identified for the limiting cases of acoustic and anelastic flow.

Equations of Change for an Oscillating Fluid

The three governing equations for a compressible viscous fluid are defined by the laws of mass, momentum, and energy conservation. Supplementing the fluid equations are four auxiliary relations for density, enthalpy (energy), thermal conductivity, and viscosity in terms of pressure and temperature. Linear diffusion transport is assumed: Newtonian flow relating shear and velocity gradient through viscosity, and Fourier heat transfer relating heat conduction and temperature gradient through thermal conductivity. Stokes's hypothesis for the bulk viscosity is assumed, and body forces are neglected. A detailed formulation of the governing fluid equations can be found in Batchelor (ref. 61).[1]

The system and the boundary conditions dictate how the equations are scaled. Details of scaling are given in appendix A and a dimensional analysis is provided by J. Lee et al. (ref. 62). Consider an ideal gas contained in a system with characteristic length L^*. At each end of the tube the gas is displaced a distance d_0^*, with frequency f^* and characteristic velocity amplitude U_0^*. The imposed oscillating displacements also produce oscillations in the velocity vector $\mathbf{u}^*$, pressure p^*, density ρ^*, and temperature T^*. Pressure, density, and temperature oscillate about mean reference bulk values p_0^*, ρ_0^*, and T_0^*, respectively, which are taken as the scaling constants. The scaling for $\mathbf{u}^*$ is U_0^* and the scaling for time is the inverse angular frequency, $\omega^* = 2\pi f^*$. Using the above scaling constants, the conservation equations for mass, momentum and energy are, respectively,

$$0 = \rho_{,t} + \varepsilon \nabla \cdot (\rho \mathbf{u}) \tag{9}$$

$$\rho \mathbf{u}_{,t} + \varepsilon \rho \mathbf{u} \cdot \nabla \mathbf{u} = -\frac{1}{\lambda} \nabla p - \frac{1}{\mathrm{Va}} \nabla \cdot \tau \tag{10}$$

$$\rho T_{,t} + \varepsilon \rho \mathbf{u} \cdot \nabla T = \frac{\gamma - 1}{\gamma} \left(p_{,t} + \varepsilon \mathbf{u} \cdot \nabla p \right) - \frac{1}{\mathrm{Pr\ Va}} \nabla \cdot \mathbf{q} + (\gamma + 1) \frac{\mathrm{M}^2}{\mathrm{Va}} \tau : \nabla \mathbf{u} \tag{11}$$

where

$$\tau = \mu_2 (\nabla \cdot \mathbf{u}) \mathbf{I} + 2\mu \, def\, \mathbf{u}; \quad 3\mu_2 + 2\mu = 0; \quad def\, \mathbf{u} = \frac{1}{2} \left[\nabla \mathbf{u} + (\nabla \mathbf{u})^{\mathrm{tr}} \right] \tag{12}$$

[1]For additional references, see Sherman (ref. 1), White (ref. 63), or Bird et al. (ref. 64).

and μ_2 is the second viscosity, $\mathbf{q} = -k\nabla T$ is the conduction heat flux vector, and τ is the viscous stress tensor. The dimensionless parameters are the inverse Strouhal number, ε; the Mach number, M; the Prandtl number, Pr; the Valensi number, Va; and the elasticity parameter, λ, which is a measure of the resilience of the gas (ref. 2). The parameters are defined as

$$\varepsilon = \frac{U_0^*}{\omega^* L^*} \qquad \mathrm{M}^2 = \frac{U_0^{*2}}{\gamma R^* T_0^*} \qquad \mathrm{Pr} = \frac{\nu^*}{\alpha^*} \qquad \mathrm{Va} = \frac{L^{*2}\omega^*}{\nu^*} \qquad \lambda = \frac{\gamma \mathrm{M}^2}{\varepsilon} \tag{13}$$

where ν^* is the kinematic viscosity, α^* is the thermal diffusivity, γ is the heat capacity ratio C_p^*/C_v^*, $a^* = \sqrt{\gamma R^* T_0^*}$ is the speed of sound for an ideal gas, and R^* is the ideal gas constant with the ideal gas law reducing to

$$p = \rho T \tag{14}$$

Note that only two of the three parameters ε, M, and λ are mutually independent. For sinusoidal motion of velocity at the tube ends, $\varepsilon = d_0^*/L^*$. Rewriting $\lambda = \gamma \mathrm{M}\,\omega^* L^*/a^*$ shows that it is composed of the Mach number and the ratio of the oscillation frequency to the system acoustic resonance frequency. For the problems we will address, $\mathrm{M} \ll 1$, $\omega^* L^*/a^* \ll 1$, and $\gamma = O(1)$.

Relevant Transport Quantities

Mean-Steady Enthalpy Flow

The local mean-steady enthalpy flow is evaluated by integrating the enthalpy flux over the cross-sectional area normal to the flow and time-averaging over a period,

$$\overline{H} = \int_A \oint \rho \mathbf{n} \cdot \mathbf{u} T dt\, dA \tag{15}$$

where the overbar represents mean-steady values, and $\mathbf{n}$ is the unit vector pointing in the positive direction and normal to the cross-sectional area A. Enthalpy flux is scaled as $h_0^* = \rho_0^* U_0^* T_0^* C_p^*$ and enthalpy flow as $H_0^* = h_0^* A^*$.

Mean-Steady Particle Velocity

For absolute steady-state conditions, the stream function represents lines of constant mass flow (ref. 63) and is identical to the path along which particles travel (particle path). However, for oscillating flow in which quadratic products of the linear solutions produce higher-order mean-steady flows, the mean-steady stream function does not represent the mean-steady particle path. To find the mean-steady particle path, the mean-steady particle velocity must be determined.

The instantaneous particle velocity, $\mathbf{u}_p(\mathbf{x},t)$, is the Lagrangian velocity, as opposed to $\mathbf{u}(\mathbf{x},t)$, which is the Eulerian velocity. For small displacement, $\mathbf{u}_p(\mathbf{x},t)$ can be obtained by a Taylor expansion of $\mathbf{u}(\mathbf{x},t)$ about the initial position $\mathbf{x}_i$ at $t = 0$. Details are given by Batchelor in

reference 61 and they are reviewed in appendix B. The mean-steady particle velocity for an oscillating flow is given as

$$\bar{\mathbf{u}}_p(\mathbf{x}) \approx \bar{\mathbf{u}}(\mathbf{x}_i) + \left(\overline{\int_0^t \mathbf{u}(\mathbf{x},\tau)\, d\tau \cdot \nabla \mathbf{u}} \right)_{\mathbf{x}_i} \tag{16}$$

where the first term on the right-hand side is the mean-steady field velocity at the initial position $\mathbf{x}_i$ at $t = 0$, and the second term is the velocity component due to time-averaged particle oscillations that transverse $\bar{\mathbf{u}}(\mathbf{x})$.

The mean-steady Lagrangian transport of other quantities has a similar form. Let χ be such a quantity (for example, enthalpy **h**; entropy **s**; or the acceleration $\mathbf{u}_{,t} + \mathbf{u} \cdot \nabla \mathbf{u}$). Then the mean-steady value of χ associated with the particle velocity is

$$\bar{\chi}_p(\mathbf{x}) \approx \bar{\chi}(\mathbf{x}_i) + \left(\overline{\int_0^t \mathbf{u}(\mathbf{x},\tau)\, d\tau \cdot \nabla \chi} \right)_{\mathbf{x}_i} \tag{17}$$

Entropy

The entropy equation is given by

$$\rho s_{,t} + \varepsilon \rho \mathbf{u} \cdot \nabla s = (\gamma - 1)\frac{\mathrm{M}^2}{\mathrm{Va}}\Phi - \frac{1}{\mathrm{Pr\,Va}}\nabla \cdot \mathbf{q} \tag{18}$$

where $\Phi = \tau : \nabla \mathbf{u}$ is the dissipation function. The entropy equation is an alternative form of the energy equation and is useful for optimization studies.

Conditions for Acoustic and Anelastic Flows

For the limiting condition of very small ε, equations (9)–(11) can be reduced to a set of linear equations that are amenable to an expansion series solution. The parameter λ serves by helping to identify the distinguished limit between ε and M.

Acoustic Flow

The equations can be reduced to an acoustic form for $\lambda = O(1)$ and $\varepsilon << 1$. Here the first-order pressure $p_1(\mathbf{x},t)$, is coupled between the mass conservation and momentum equations. The acoustic equations are linear (ref. 65) and allow a series solution in ε where $\mathrm{M} = \varepsilon^{0.5}$ is the distinguished limit. The expansion for $p(\mathbf{x},t)$ is

$$p(\mathbf{x},t) = p_0(\mathbf{x}) + \varepsilon\, p_1(\mathbf{x},t) + \varepsilon^2 p_2(\mathbf{x},t) + O(\varepsilon^3) \tag{19}$$

Equation (19) shows that the first correction to the pressure, p_1, is spatially dependent, and that pressure gradients are of the order of the bulk temporal pressure oscillations. The rest of the variables are also expanded in ε,

$$\rho(\mathbf{x},t) = \rho_0(\mathbf{x}) + \varepsilon\rho_1(\mathbf{x},t) + \varepsilon^2\rho_2(\mathbf{x},t) + O(\varepsilon^3) \tag{20}$$

$$T(\mathbf{x},t) = T_0(\mathbf{x}) + \varepsilon T_1(\mathbf{x},t) + \varepsilon^2 T_2(\mathbf{x},t) + O(\varepsilon^3) \tag{21}$$

$$u(\mathbf{x},t) = u_0(\mathbf{x},t) + \varepsilon u_1(\mathbf{x},t) + O(\varepsilon^2) \tag{22}$$

$$v(\mathbf{x},t) = v_0(\mathbf{x},t) + \varepsilon v_1(\mathbf{x},t) + O(\varepsilon^2) \tag{23}$$

Anelastic Flow

An anelastic approximation of the fluid equations neglects density changes due to pressure gradients. Its effect is to "remove acoustic phenomena from theoretical considerations" (ref. 1) and it can be used to "filter sound" from the fluid equations with the advantage that the equations do not propagate numerical shocks (ref. 2). The anelastic approximation applies when shock and acoustic energies are small relative to the energy needed to compress and expand the gas.

The condition $\lambda \le \varepsilon << 1$, defines the anelastic approximation. The corresponding distinguished limit is $\mathrm{M} \le \varepsilon$. The pressure is expanded as

$$p(\mathbf{x},t) = \mathcal{P}(t) + \lambda\, p_2(\mathbf{x},t) + \textit{higher order terms} \tag{24}$$

The anelastic equations are similar to the acoustic equations except that now there is no coupling (through the pressure gradient) between the mass conservation equation and the momentum equation at leading-order, that is, at leading-order $\mathcal{P}(t)$ is not present in the momentum equation, but remains in the mass and energy conservation equations, and in the equation of state. The next pressure term is $O(\lambda)$; it is the kinematic pressure that drives the flow in the momentum equation. A consequence of this ordering is that there is an inaccuracy in the mass conservation equation of $O(\lambda)$. Appendix C details the anelastic scaling.

The added unknown $\mathcal{P}(t)$ requires an additional relation. The relation comes from the integral form of the energy equation. For a calorically perfect gas (ideal gas with constant heat capacity), the integral equation is

$$\mathcal{P}'(t) = \frac{\gamma}{\mathcal{V}} \frac{1}{\mathrm{Pr\,Va}} \int_{\mathcal{S}} \mathbf{n}\cdot\nabla T \, d\mathcal{S} - \frac{\gamma}{\mathcal{V}} \int_{\mathcal{S}} \mathcal{P}(t)\mathbf{n}\cdot\mathbf{u} \, d\mathcal{S} \tag{25}$$

where $\mathbf{n}$ is the outward pointing unit normal vector, $\mathcal{S}$ is the surface area enclosing the domain, and $\mathcal{V}$ is the domain volume. Equation (25) defines $\mathcal{P}(t)$ in terms of boundary conditions only, hence, $\mathcal{P}(t)$ is the thermodynamic equilibrium pressure and is the integral equivalent of the first law used in macroscopic thermodynamics.

Now consider a subset of the above case in which $\lambda << \varepsilon << 1$. An appropriate expansion of pressure is

$$p(\mathbf{x},t) = p_0 + \varepsilon\, p_1(t) + \lambda\, p_2(\mathbf{x},t) + \varepsilon\lambda\, p_3(\mathbf{x},t) + O(\varepsilon^2\lambda) \tag{26}$$

The expansion given by equation (26) is applicable for pulse tubes where $\mathcal{P}(t)$ of equation (24) has been split into two terms, $p_0 + \varepsilon p_1(t)$. The first term represents $O(1)$ time-dependence of pressure, such as when the pulse tube is cooling or warming; for quasi-steady conditions it is constant. The second term represents $O(\varepsilon)$ time-dependence given by the oscillating pressure in the pulse tube. As before, the thermodynamic pressure p_1 is determined from the energy integral, equation (25). The expansion in ε of the other variables is given by equations (20)–(23).

Linear Anelastic Flow

The added condition $\varepsilon \mathrm{Va} \ll 1$ allows linearization of momentum, that is, a linear anelastic approximation. The product $\varepsilon \mathrm{Va}$ is the Reynolds number. In this study, the linear anelastic problem is investigated. Though the acoustic problem is not addressed here, it has been addressed elsewhere (ref. 20); it is, however, summarized, along with the anelastic equations, in table 3 of section 3.

3. TWO-DIMENSIONAL AXISYMMETRIC FORMULATION

In this section, the two-dimensional axisymmetric linear anelastic problem is derived for oscillating flow in a tube. Heat transfer between the gas and a tube wall of thin but finite thickness is considered. Mean-steady relations are derived and summarized for both the anelastic and acoustic limits. Finally, the equations are simplified for sinusoidal time using complex embedding.

System

Consider an ideal gas contained in a long cylindrical tube of finite wall thickness. The thickness of the tube wall is very thin relative to the tube radius. The system is thermally insulated, and the gas velocities at the tube ends are of small amplitude and sinusoidal. Figure 7 is a sketch of the system. A summary of the assumptions and approximations made in the analysis is as follows:

1. Two-dimensional, axisymmetric cylindrical geometry
2. Inert single component ideal gas
3. Constant properties—thermal conductivity, heat capacity, dynamic viscosity
4. Enthalpy a function of temperature only
5. Stokes hypothesis for second viscosity, $3\mu_2 + 2\mu = 0$
6. $r_w^*/L^* << 1$ implying that the radial momentum equation is negligible, $p_{,r} \approx 0$, and that $p = p(z,t)$
7. No body forces
8. $l^* << r_w^*$ so that the tube wall domain can be approximated with rectangular Cartesian coordinates
9. Sinusoidal time-periodic velocity boundary conditions

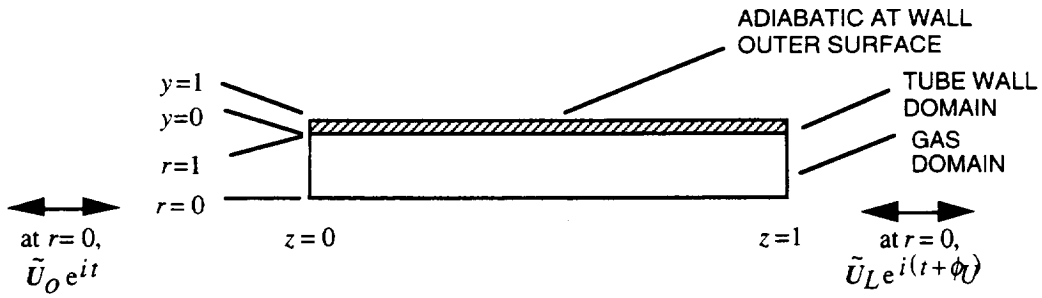

Figure 7. Two-dimensional axisymmetric system for oscillating flow.

The problem is divided into two domains. In the gas domain, only the gas inside the tube is considered; it extends from $r = 0$ to $r = 1$, and from $z = 0$ to $z = 1$. In the tube-wall domain, only the tube wall thickness is considered; it extends from $y = 0$ to $y = 1$, and from $z = 0$ to $z = 1$. The two problems are coupled through the boundary conditions between the gas and the tube wall which require that the temperature and heat flux be continuous across the interface. In the gas domain, the thermodynamic variables of temperature T and density ρ are functions of spatial coordinates r and z, and of time t. For the tube-wall domain, the tube-wall temperature θ is a function of y, z, and t. The normalized velocity field for the gas domain is composed of the axial velocity u and the radial velocity v. The periodic boundary condition at $r = 0$ and $z = 0$ is $u = \tilde{U}_0 e^{it}$ and at $r = 0$ and $z = 1$ it is $u = \tilde{U}_L e^{i(t+\phi_U)}$ where $i = \sqrt{-1}$. The velocity is scaled by $\tilde{U}_0^*$ so that $\tilde{U}_0 = 1$ and $\tilde{U}_L = \tilde{U}_L^*/\tilde{U}_0^*$. Finally, at the outer surface of the tube ($y = 1$) the radial heat flux is zero (adiabatic).

Equations

The dimensionless fluid equations for mass and energy conservation, the equation of motion, and energy conservation for the tube wall are

$$\rho_{,t} + \varepsilon\left[\frac{(\rho v r)_{,r}}{r} + (\rho u)_{,z}\right] = 0 \tag{27}$$

$$(\rho u)_{,t} + \varepsilon\left(\frac{(\rho v u)_{,r}}{r} + (\rho u u)_{,z}\right) = -\frac{1}{\lambda} p_{,z} + \frac{1}{\mathrm{Va}} \frac{\left(r u_{,r}\right)_{,r}}{r} \tag{28}$$

$$\frac{p_{,t}}{\gamma} + \varepsilon\left[\frac{(p v r)_{,r}}{r} + (p u)_{,z}\right] = \frac{\gamma - 1}{\gamma} \varepsilon u p_{,z} + \frac{1}{\mathrm{Pr\ Va}}\left(\frac{\left(r T_{,r}\right)_{,r}}{r} + \varepsilon^2 \Gamma^2 T_{,zz}\right) + (\gamma - 1)\frac{\mathrm{M}^2}{\mathrm{Va}} u_{,r}^2 \tag{29}$$

$$p = \rho T \tag{30}$$

$$\theta_{,t} = \mathrm{Fo}\left(\theta_{,yy} + \varepsilon^4 \Gamma_w^2 \theta_{,zz}\right) \tag{31}$$

where $\Gamma^2 = \left(r_w^*/\varepsilon L^*\right)^2$ and $\Gamma_w^2 = \left(l^*/\varepsilon^2 L^*\right)^2$. The last two relations, Γ and Γ_w, are of $\boldsymbol{O}(1)$. This ordering for equations (29) and (31) applies when the axial conduction of energy due to the tube wall is two orders higher than the corresponding conduction of the gas. The equations do not allow for azimuthal flow; however, it is noted that one should not necessarily rule out the possibility of azimuthal flow in pulse tubes.

In addition to the dimensionless numbers previously introduced (ε, M, Pr, Va, and λ) there are several other dimensionless quantities that result from the boundary conditions and the system geometry. These are the velocity amplitude ratio, $\tilde{U}_L$; the normalized velocity phase angle, ϕ_U, which is the phase angle between the velocities U_0^* and U_L^* where U_0^* leads U_L^* and $0 \le \phi_U < 1$; the

Fourier number for the tube wall, $\mathrm{Fo} = \alpha_w^* / \left(l^{*2}\omega^*\right)$; and dimensionless length ratios, r_w^*/L^* and l^*/L^*. Table 2 lists the complete set of dimensionless parameters.

Table 2. Dimensionless numbers.

	Range	Name	Definition	Comments
ε	10^{-3} to 10^{-1}	Expansion parameter	$\tilde{U}_0^*/\left(\omega^* L^*\right) = d_0^*/L^*$	Ratio of displacement length d_0^* to tube length L^*, $\omega^* = 2\pi f^*$
λ	10^{-8} to 10^{-5}	Elasticity parameter	$\gamma \frac{\mathrm{M}^2}{\varepsilon} = \gamma \frac{\tilde{U}_0^*}{a^*} \frac{\omega^* L^*}{a^*}$	$\gamma = \frac{C_p^*}{C_v^*}$ and $a^* = \sqrt{\gamma R^* T_0^*}$
M	10^{-5} to 10^{-3}	Mach number	$\tilde{U}_0^*/a^*$	Ratio of velocity at $z = 0$ to speed of sound
Va	1 to 10^2	Valensi number	$r_w^{*2}\omega^*/\nu^*$	Squared ratio of tube inner radius to viscous diffusion length
Pr	0.7	Prandtl number	ν^*/α^*	Squared ratio of viscous to thermal diffusion length of gas
Fo	0 to 10^2	Fourier number	$\alpha_w^*/\left(l^{*2}\omega^*\right)$	Squared ratio of tube-wall thermal diffusion length to tube-wall thickness
r_w^*/L^*	10^{-1}	Gas domain length ratio		Ratio of tube radius to tube length
l^*/L^*	10^{-2}	Tube wall length ratio		Ratio of tube-wall thickness to tube length
$\tilde{U}_L$	0 to 1	Velocity ratio	$\tilde{U}_L^*/\tilde{U}_0^*$	Ratio of velocity amplitude at $z = 1$ to amplitude at $z = 0$
ϕ_U	–0.5 to 0	Velocity phase angle		Velocity phase angle where U_0 at $z = 0$ leads U_L at $z = 1$
$\overline{H}$		Normalized enthalpy flow	$\overline{H}^*/\overline{H}_{ref}^*$	Ratio of mean-steady enthalpy flow to oscillating enthalpy flow $\overline{H}_{ref}^* = \rho_0^* T_0^* \tilde{U}_0^* C_p^* \pi r_w^{*2}$

To illustrate the values of the dimensionless numbers, consider a small-sized pulse tube operating at 10 Hz, with a stainless steel tube of wall thickness $l^* = 0.01$ cm, inner radius $r_w^* = 0.35$ cm, length $L^* = 5$ cm; thermal diffusivity of the tube wall $\alpha_w^* = 0.045$ cm^2/sec; helium gas mean pressure at 10^6 Pa; kinematic viscosity $\nu^* = 0.124$ cm^2/sec; Prandtl number Pr = 0.7; speed of sound $a^* = 10^3$ m/sec; and gas displacement $d_0^* = 0.04$ cm. The calculated dimensionless numbers become $\varepsilon = 8\mathrm{x}10^{-3}$, Va = 62, εVa = 0.497, $\mathrm{M} = 2.5\mathrm{x}10^{-5}$, $\lambda = 4.8\mathrm{x}10^{-8}$, Fo = 7.2, and

$M^2/Va = O(10^{-11}) << \varepsilon^2$. The value of εVa shows that these conditions are at the limit of the linear approximation, and the relation for M^2/Va shows that viscous dissipation is not important.

Now consider a pulse tube operating with a more typical $\varepsilon = 0.1$. This results in $\varepsilon Va = 6.2$, which is not strictly within the constraints of the linear approximation. However, if the measured values of mean-steady flow for $\varepsilon Va \geq 1$ are in agreement with calculations using a linear approach, then an argument can be made for describing mean-steady flows for pulse tubes using a linear theory. It will be shown that this is the case.

Series Expansion

The anelastic criterion that applies to pulse tubes is

$$\lambda << \varepsilon << 1 \tag{32}$$

We are interested in the quasi-steady periodic solution for the leading-order problem. Equations (27)–(31) are linearized using a two-parameter series expansion for pressure in ε and λ,

$$p(z,t) = 1 + \varepsilon\, p_1(t) + \lambda\, p_2(z,t) + \varepsilon\lambda\, p_3(z,t) + O(\varepsilon^2\lambda) \tag{33}$$

and an expansion in ε for the other variables,

$$\rho(r,z,t) = \rho_0(z) + \varepsilon\rho_1(r,z,t) + \varepsilon^2\rho_2(r,z,t) + O(\varepsilon^3) \tag{34}$$

$$T(r,z,t) = T_0(z) + \varepsilon T_1(r,z,t) + \varepsilon^2 T_2(r,z,t) + O(\varepsilon^3) \tag{35}$$

$$u(r,z,t) = u_0(r,z,t) + \varepsilon u_1(r,z,t) + O(\varepsilon^2) \tag{36}$$

$$v(r,z,t) = v_0(r,z,t) + \varepsilon v_1(r,z,t) + O(\varepsilon^2) \tag{37}$$

For details as to why the expansion takes the form of integer powers in ε and λ refer to appendix D. Equation (33) reflects that the leading-order equation of state is

$$1 = p_0 = \rho_0(z)T_0(z) \tag{38}$$

and the first-order correction for pressure is

$$p_1 = p_1(t) \tag{39}$$

Details for obtaining equation (39) are also given in appendix D.

First-Order Oscillating Equations

The resulting first-order equations for mass and energy conservation, the equation of state, and the energy equation for the tube wall are, respectively,

$$\rho_{1,t} + \frac{(\rho_0 u_0 r)_{,r}}{r} + (\rho_0 u_0)_{,z} = 0 \tag{40}$$

$$\frac{p_{1,t}}{\gamma}+\frac{(p_0 v_0 r)_{,r}}{r}+(p_0 u_0)_{,z}=\frac{1}{\mathrm{Pr\,Va}}\frac{(rT_{1,r})_{,r}}{r} \tag{41}$$

$$p_1=\rho_0 T_1+\rho_1 T_0 \tag{42}$$

$$\theta_{1,t}=\mathrm{Fo}\,\theta_{1,yy} \tag{43}$$

The condition $\varepsilon \mathrm{Va} \ll 1$ allows linearization of momentum. Ordering the momentum equation shows that the flow is driven by the $p_2(z,t)$ pressure gradient

$$(\rho_0 u_0)_{,t}=-p_{2,z}+\frac{1}{\mathrm{Va}}\frac{(ru_{0,r})_{,r}}{r} \tag{44}$$

The energy integral over the gas domain defines the relation for $p_1(t)$

$$p_1'(t)=\frac{\gamma}{V}\left(\frac{1}{\mathrm{Pr\,Va}}\int_S \mathbf{n}\cdot T_{1,r}\,dS-\int_S \mathbf{n}\cdot p_0 u_0\,dS\right) \tag{45}$$

where the prime denotes an exact derivative. Equation (45) shows that the thermodynamic oscillating pressure $p_1(t)$, results from the forced oscillations at the tube ends and from periodic radial heat conduction at the tube walls.[1] Details of the expansion are given in appendix D.

The above coupled set of linear equations still does not completely define the basic state problem. This is because the zeroth-order temperature, $T_0(z)$, is coupled to the mean-steady, second-order energy equation. To completely define the basic state problem, the mean-steady equations of next order must be determined.

Mean-Steady Equations

Mean-steady velocity component due to Reynolds stresses, $\bar{\mathbf{u}}_1$

The mean-steady, second-order momentum equation is given by

$$\frac{(\rho_0 \overline{v_0 u_0})_{,r}}{r}+(\rho_0 \overline{u_0 u_0})_{,z}=-\bar{p}_{3,z}+\frac{1}{\mathrm{Va}}\frac{(r\bar{u}_{1,r})_{,r}}{r} \tag{46}$$

The left-hand side of equation (46) contains the Reynolds stresses. The right-hand side is the resulting mean-steady velocity $\bar{u}_1$, and the mean-steady pressure $\bar{p}_3$. These two are unknown. A second relation comes from the zero-net-mass-flow constraint, which requires that the integration of the steady axial mass flux over the area normal to the axial flow be zero,

$$0=\int_0^1 (\rho_0 \bar{u}_1+\overline{\rho_1 u_0})\,r\,dr \tag{47}$$

[1]Periodic axial heat transfer at the tube ends is not considered here.

The above two equations are used to solve for $\overline{u}_1$ and $\overline{p}_3$. The mass conservation equation is then used to solve for $\overline{v}_1$,

$$0 = \frac{\left(\rho_0 \overline{v_1} r + \overline{\rho_1 v_0} r\right)_{,r}}{r} + \left(\rho_0 \overline{u_1} + \overline{\rho_1 u_0}\right)_{,z} \tag{48}$$

Mean-steady temperature distribution and the equation of state

The mean-steady, second-order energy equation is used to find $\overline{T}_2$,

$$\frac{1}{\mathrm{Pr\,Va}}\left\{\frac{\left(r\overline{T}_{2,r}\right)_{,r}}{r} + \Gamma^2 T_{0,zz}\right\} = \nabla_a \cdot \left(p_0 \overline{\mathbf{u}_1} + \overline{p_1 \mathbf{u}_0}\right) \tag{49}$$

where $\Gamma^2 = \boldsymbol{O}(1)$ and $(\nabla_a \cdot)$ is the axisymmetric divergence operator, that is, $\nabla_a \cdot \left(p_0 \overline{\mathbf{u}_1} + \overline{p_1 \mathbf{u}_0}\right) = \left(p_0 \overline{u_1} + \overline{p_1 u_0}\right)_{,z} + \frac{1}{r}\left(r p_0 \overline{u_1} + r \overline{p_1 u_0}\right)_{,r}$. Here we see that $T_0(z)$ is coupled to the second-order energy equation. The equation of state is used to find the density

$$\overline{p}_2 = \rho_0 \overline{T}_2 + \overline{\rho_1 T_1} + \overline{\rho}_2 T_0 \tag{50}$$

The gas-domain equation is coupled to the tube-wall domain

$$0 = \overline{\theta}_{2,yy} \tag{51}$$

which implies $\overline{\theta}_2 = 0$ after requiring that the temperature boundary condition at $y = 1$ be adiabatic. The zeroth-order temperature of the tube wall, $\theta_{0,zz}$, is of $\boldsymbol{O}(\varepsilon^4)$ so it does not enter into the problem at $\boldsymbol{O}(\varepsilon^2)$.

The complete leading-order problem requires $T_0(z)$ to be solved simultaneously at zeroth-order (eq. (38)), oscillating first-order (eq. (42)), and mean-steady, second-order (eq. (49)). Table 3 summarizes the leading-order and mean-steady equations and boundary conditions.

Table 3. Summary of equations: leading order and mean-steady boundary conditions.[a]

		Eq.
Zeroth-order relations		
$p_0 = 1$	Zeroth-order equation of state	(a)
$p_0 = \rho_0(z)T_0(z)$		(b)
$\theta_0(z) = T_0(z)$		(c)
First-order oscillating equations		
$(\rho_0 u_0)_{,t} = -p_{2,z} + \frac{1}{\mathrm{Va}}\frac{(r u_{0,r})_{,r}}{r}$	$\boldsymbol{O}(\lambda)$ pressure *gradient* drives the $\boldsymbol{O}(1)$ velocity	(d)
$\rho_{1,t} + \nabla_a \cdot (\rho_0 \mathbf{u}_0) = 0$	Mass conservation	(e)
$p_{1,t} = \gamma\left(\frac{1}{\mathrm{Pr\,Va}}\frac{(rT_{1,r})_{,r}}{r} - \nabla_a \cdot (p_0 \mathbf{u}_0)\right)$	Energy	(f)
$p_{1,t} = \frac{\gamma}{\mathcal{V}}\left(\frac{1}{\mathrm{Pr\,Va}}\int_{\mathcal{S}} \mathbf{n}\cdot T_{1,r}\, d\mathcal{S} - \int_{\mathcal{S}} \mathbf{n}\cdot p_0 u_0\, d\mathcal{S}\right)$	Volume integrated energy	(g)
$p_1 = \rho_0 T_1 + \rho_1 T_0$	Equation of state	(h)
$\theta_{1,t} = \mathrm{Fo}\,\theta_{1,yy}$	Energy equation for tube wall	(i)
Mean-steady equations		
$\nabla_a \cdot \left(\rho_0 \overline{\mathbf{u}_0^2}\right) = -\bar{p}_{3,z} + \frac{1}{\mathrm{Va}}\frac{(r\bar{u}_{1,r})_{,r}}{r}$	Solve with the axial mass flow constraint to obtain $\bar{p}_3$ and $\bar{u}_1$ average	(j)
$0 = \int_0^1 \left(\rho_0 \overline{u_1} + \overline{\rho_1 u_0}\right) r\, dr$	Axial mass flow constraint	(k)
$\nabla_a \cdot \left(\rho_0 \bar{\mathbf{u}}_1 + \overline{\rho_1 \mathbf{u}_0}\right) = 0$	Single quadrature to find $\bar{v}_1$	(l)
$\frac{1}{\mathrm{Pr\,Va}}\frac{(r\bar{T}_{2,r})_{,r}}{r} = \nabla_a \cdot \left(p_0 \bar{\mathbf{u}}_1 + \overline{\rho_1 \mathbf{u}_0}\right) - \frac{\Gamma^2}{\mathrm{Pr\,Va}} T_{0,zz}$	Second-order mean-steady energy equation	(m)
$\bar{p}_2 = \rho_0 \bar{T}_2 + \overline{\rho_1 T_1} + \bar{\rho}_2 T_0$		(n)
$0 = \bar{\theta}_{2,yy}$		(o)

[a]The acoustic problem is obtained by replacing p_2 in eq. (d) with $\frac{p_1(z,t)}{\lambda}$, replacing p_3 in eq. (j) with $\frac{p_2(z,t)}{\lambda}$; and eliminating eq. (g).

Table 3. Concluded.

Boundary conditions for oscillating problem			
$0 = u_{0,r} = v_0$	at $r = 0$	Symmetry	(p)
$0 = u_0$	at $r = 1$	No slip	
$0 = v_0$	at $r = 1$	No-penetration condition	
$u_0 = U_0 = \Re\left[\hat{U}_0 e^{it}\right]$	at $z = 0$ and $r = 0$	Two boundary conditions in z needed for	
$u_0 = U_L = \Re\left[\hat{U}_L e^{it}\right]$	at $z = 1$ and $r = 0$	$u_{0,zz}$	
$0 = T_{1,r}$	at $r = 0$	Symmetry	
$T_1 = \theta_1$ and $k_g T_{1,r} = k_w \theta_{1,y}$	at $y = 0$ and $r = 1$	Temperature and heat flux continuity	
$0 = \theta_{1,y}$	at $y = 1$	Adiabatic at outer wall	
Boundary conditions for mean-steady problem			(q)
$0 = \bar{u}_{1,r} = \bar{v}_1$	at $r = 0$	Symmetry	
$0 = \bar{u}_1$	at $r = 1$	No slip and isothermal	
$0 = \bar{v}_1$	at $r = 1$	No-penetration condition	
$T_0 = T\|_{z=0}$	at $z = 0$	Two boundary conditions in z	
$T_0 = T\|_{z=1}$	at $z = 1$	needed for $T_{0,zz}$	
$0 = \bar{T}_{2,r}$	at $r = 0$	Symmetry	
$0 = \bar{\theta}_2 = \bar{T}_2$	at $y = 0$ and $r = 1$	Results from solution of eq. (o) and applying boundary condition where it is	
$0 = \bar{\theta}_{2,y}$	at $y = 1$	adiabatic at outer wall	

Comments

The complete problem involves 15 variables (u_0, v_0, $\bar{u}_1$, $\bar{v}_1$, ρ_0, ρ_1, $\bar{\rho}_2$ T_0, T_1, $\bar{T}_2$, θ_1, $\bar{\theta}_2$, p_1, p_2, $\bar{p}_3$) in the 15 equations listed by equations (b) and (d) – (q) in table 3. There are 12 continuum equations, one integral equation (g), and two boundary constraints (p) and (q). The boundary constraints are independent equations, since in the differential equation for mass conservation, v_0 has only a single derivative and need satisfy only a single boundary condition. Note that the zeroth-, first-, and second-order equations must be solved simultaneously for the leading-order problem because T_0 is coupled between the zeroth- and first-order equations of state, and the mean-steady energy equation.

Thermally strong approximation, $T_{0,z} = 0$

The problem can be greatly simplified for the case of negligible zeroth-order axial temperature gradient, $T_{0,z} = 0$. This would apply for a strongly imposed heat sink/source on the system. This leads to decoupling of the zeroth-order equation of state from the mean-steady energy equations. The zeroth-order equation of state is exactly known ($p_0 = \rho_0 = T_0 = 1$) so that the first-order oscillating equations become self-contained and can be solved independently. The result is seven equations (eqs. (d) to (i) and boundary constraint eq. (p)) with seven unknowns (u_0, v_0, p_1, p_2, ρ_1, T_1, θ_1). This simplified case applies to the experimental investigations of section 5.

Acoustic limit

As shown in section 2, the acoustic limit requires $\lambda \approx \varepsilon << 1$ which results in $p(z,t) = 1 + \varepsilon\, p_1(z,t) + \varepsilon^2 p_2(z,t) + O(\varepsilon^3)$. The equations in table 3 can be rewritten in acoustic form by replacing $p_2(z,t)$ in equation (d) with $p_1(z,t)$; replacing $p_3(z,t)$ in equation (j) with $p_2(z,t)$; and eliminating equation (g).

Entropy production

The mean-steady generation of entropy can be used to optimize enthalpy flow by minimizing entropy production. The entropy equation is expanded to second-order and integrated over the domain. The zeroth- and first-order entropy equations do not contribute to mean-steady entropy production since they describe only linear oscillating entropy transfer in the form of heat transfer and entropy advection, and not generation.[2] Entropy generation is quadratic at second-order.

Integrating the second-order entropy equation over the domain results in the steady generation of entropy $\bar{S}_2$,

---

[2]Entropy generation is different than accumulation which can come in at first-order if the flow of heat at each end of the tube is different. This would result in a bulk temperature transient. In this case, the first-order accumulation of entropy is given by $\bar{S}_1 = \dfrac{\Gamma}{\mathrm{Pr\,Va}} \displaystyle\int_S \mathbf{n} \cdot \frac{T_{0,z}}{T_0}\, dS$ which requires the system to be heating or cooling.

$$\bar{S}_2 = \int_{\mathcal{V}} \left(\rho_0 \overline{s_2} + \overline{\rho_1 s_1} + \overline{\rho_2} s_0\right) d\mathcal{V}$$

$$= \frac{1}{\mathrm{Pr\,Va}} \left\{ \int_{\mathcal{V}} \left[\overline{\left(\frac{T_{1,r}}{T_0}\right)^2} + \Gamma \left(\frac{T_{1,r}}{T_0} \frac{T_{0,z}}{T_0} \right) + \Gamma^2 \left(\frac{T_{0,z}}{T_0} \right)^2 \right] d\mathcal{V} + \int_{\mathcal{S}} \mathbf{n} \cdot \frac{\bar{T}_{2,r}}{T_0} \, d\mathcal{S} \right\}$$

$$- \int_{\mathcal{S}} \mathbf{n} \cdot \left(\rho_0 \overline{\mathbf{u}_0 s_1} + \rho_0 \overline{\mathbf{u}_1} s_0 + \overline{\rho_1 \mathbf{u}_0} s_0\right) d\mathcal{S} \tag{52}$$

Viscous dissipation does not come in at second-order—irreversibilities are due only to heat transfer.

The entropy produced in the tube wall must be added. The entropy equation for the wall at second-order is

$$\bar{\vartheta}_2 = \mathrm{Fo} \left\{ \int_{\mathcal{V}_w} \left\{ \overline{\left(\frac{\theta_{1,r}}{T_0}\right)^2} + \Gamma_w^2 \overline{\left(\frac{\theta_{0,z}}{T_0}\right)^2} \right\} d\mathcal{V}_w + \int_{\mathcal{S}_w} \mathbf{n} \cdot \frac{\theta_{2,r}}{T_0} \, d\mathcal{S}_w \right\} \tag{53}$$

The total entropy generated by the combined gas and tube wall system is the sum, $\left(\bar{S}_2 + \bar{\vartheta}_2\right)$. In the limit of an isothermal or an adiabatic wall boundary condition, the wall-domain problem need not be considered, and the gas-domain equation, $\bar{S}_2$, by itself, is sufficient because in both idealized cases there are no temperature gradients present in the wall.

Complex Embedding of the First-Order Equations

To obtain a periodic solution for the linear equations of table 3, complex embedding can be used to eliminate the time-dependence. The problem is then solved in the complex plane with the real part of the complex solution being of physical significance. The complex solution takes the form

$$\chi = \Re\left[\hat{\chi}(\mathbf{x}) e^{it}\right] \tag{54}$$

where χ represents the real part of the complex function $\hat{\chi}(\mathbf{x})e^{it}$. In general, $\hat{\chi}(\mathbf{x})$is spatially dependent and is itself complex. Appendix E details the procedure for simplifying the first-order equations; only the important points are summarized here.

The first-order momentum equation given in table 3, equation (d), is reduced to a solution in z. The solution for u_0 is explicit in r with the z-dependence contained in $p_2(z)$ and $\rho_0(z)$, both unknown at this time:

$$\hat{u}_0 = i \frac{\hat{p}_2'(z)}{\rho_0(z)} \left[1 - \zeta_0\left(r, z; \sqrt{\mathrm{Va}}\right)\right] \tag{55}$$

where

$$\zeta_n(r,z;\sigma)=\frac{J_n\left(r\sigma\sqrt{-i\rho_0(z)}\right)}{J_0\left(\sigma\sqrt{-i\rho_0(z)}\right)} \qquad n=0,1 \tag{56}$$

with J_n being the Bessel function of the nth-order. In a similar manner, the energy equation can be solved explicitly in r with unknown dependence in z. The energy equation is rearranged using the equation of state and the mass conservation equation to arrive at

$$\begin{aligned}\hat{T}_1=&\frac{\gamma-1}{\gamma}\hat{p}_1T_0\left[1-\zeta_0\left(r,z;\sqrt{\mathrm{PrVa}}\right)\right]+\tilde{T}_we^{i\phi_T}\zeta_0\left(r,z;\sqrt{\mathrm{PrVa}}\right)\\&-T_0T_0'\hat{p}_2'\left\{\left[1-\zeta_0\left(r,z;\sqrt{\mathrm{PrVa}}\right)\right]-\left(\frac{\mathrm{Pr}}{\mathrm{Pr}-1}\right)\left[\zeta_0\left(r,z;\sqrt{\mathrm{Va}}\right)-\zeta_0\left(r,z;\sqrt{\mathrm{Pr\,Va}}\right)\right]\right\}\end{aligned} \tag{57}$$

where $\tilde{T}_w$ is the amplitude and ϕ_T is the phase angle of the temperature at the interface between the gas and the tube wall. The first term on the right-hand side of equation (57) contains the factor $\frac{\gamma-1}{\gamma}\hat{p}_1T_0$. This factor represents the leading term of a series expansion of the thermodynamic relation for isentropic compression of an ideal gas, $\frac{dT}{T}=\frac{\gamma-1}{\gamma}\frac{dp}{p}$. The first term also includes the Bessel function expression $\left[1-\zeta_0\left(r,z;\sqrt{\mathrm{Pr\,Va}}\right)\right]$, which describes the transverse diffusion temperature fall-off between the center of the gas and the tube wall.

The second term of equation (57) is the effect due to the heat transfer between the gas and the tube wall. For an isothermal tube wall, $\tilde{T}_w=0$. For a non-isothermal wall of finite thickness, $\hat{T}_1$ is coupled to the temperature $\hat{\theta}_1$ of the tube wall. The governing equation for the tube wall is given in table 3 by equation (i). The solution is

$$\hat{\theta}_1=\tilde{T}_we^{i\phi_T}\left[e^{i\chi y}-e^{i\chi}\left(\frac{i\sin\chi y}{\cos\chi}\right)\right] \tag{58}$$

where $\chi=\sqrt{\frac{-i}{\mathrm{Fo}}}$.

The third term is due to advection of gas along the axial temperature gradient. The dependence on T_0 suggests that the oscillating temperature T_1 should increase with local mean temperature. Experimental measurements of the oscillating temperature in a pulse tube suggest this is the case (ref. 35, p. 54). For $\mathrm{Pr}\to 1$, L' Hospital's rule shows that the term remains finite. Moreover, for a BPT with $\mathrm{Pr}\to 1$ and $T_w=0$, the phase shift between temperature and velocity—provided by the difference between thermal and viscous diffusion lengths—is everywhere orthogonal, which results in zero enthalpy flux. However, for an OPT, a phase shift is imposed by the velocity conditions at the tube ends, hence, enthalpy flux remains finite for $\mathrm{Pr}=1$.

Equation (57) shows that the unknown temperature, $\hat{T}_1$, is now described as a function of the axial temperature $T_0(z)$, the kinematic pressure $\hat{p}_2(z)$, the bulk oscillating pressure $\hat{p}_1$, and the temperature amplitude $\tilde{T}_w$ and phase angle ϕ_T between the gas and tube wall. Equation (57) is combined with the zeroth- and first-order equations of state and with the first-order mass conservation equation to obtain a second-order ordinary differential equation for v_0 which is explicit in r and unknown in z:

$$\begin{aligned} v_0 = i\Bigg\{ & m_1\left(r,z;\sqrt{\mathrm{Va}}\right)T_0\hat{p}_2'' \\ & + \left(m_1\left(r,z;\sqrt{\mathrm{Va}}\right) - \frac{\mathrm{Pr}}{\mathrm{Pr}-1}\left[m_3\left(r,z;\sqrt{\mathrm{Va}}\right) - m_3\left(r,z;\sqrt{\mathrm{PrVa}}\right)\right]\right) T_0'\hat{p}_2' \\ & + m_2\left(r,z;\sqrt{\mathrm{PrVa}}\right)\hat{p}_1 + m_3\left(r,z;\sqrt{\mathrm{PrVa}}\right)\frac{\tilde{T}_w}{T_0}e^{i\phi_T} \Bigg\} \end{aligned} \tag{59}$$

where

$$m_1\left(r,z;\sqrt{\mathrm{Va}}\right) = -\left[\frac{r}{2} - m_3\left(r,z;\sqrt{\mathrm{Va}}\right)\right] \tag{60}$$

$$m_2\left(r,z;\sqrt{\mathrm{PrVa}}\right) = -\left[\frac{r}{2\gamma} + \frac{\gamma-1}{\gamma}m_3\left(r,z;\sqrt{\mathrm{PrVa}}\right)\right] \tag{61}$$

$$m_3(r,z;\sigma) = \frac{1}{\sigma\sqrt{-i\rho_0(z)}}\zeta_1(r,z;\sigma) \tag{62}$$

Details about the derivation of equation (59) are given in appendix E. Equation (62) shows that when $T_{0,z} = 0$, ρ_0 is constant and that v_0 becomes independent of z.The boundary condition $v_0 = 0$ at $r = 1$ is used with equation (69) to obtain a quasi-linear, second-order ordinary differential equation for $\hat{p}_2(z)$ with unknown constant $\hat{p}_1$.

$$\begin{aligned} 0 = \hat{p}_2'' + & \left\{ \frac{m_1\left(1,z;\sqrt{\mathrm{PrVa}}\right)}{m_1\left(1,z;\sqrt{\mathrm{Va}}\right)} - \frac{\mathrm{Pr}}{\mathrm{Pr}-1}\left[\frac{m_3\left(1,z;\sqrt{\mathrm{Va}}\right)}{m_1\left(1,z;\sqrt{\mathrm{Va}}\right)} - \frac{m_3\left(1,z;\sqrt{\mathrm{PrVa}}\right)}{m_1\left(1,z;\sqrt{\mathrm{Va}}\right)}\right]\right\}\left[\ln T_0(z)\right]'\hat{p}_2' \\ & + \frac{m_2\left(1,z;\sqrt{\mathrm{PrVa}}\right)}{m_1\left(1,z;\sqrt{\mathrm{Va}}\right)}\frac{\hat{p}_1}{T_0} + \frac{m_3\left(1,z;\sqrt{\mathrm{PrVa}}\right)}{m_1\left(1,z;\sqrt{\mathrm{Va}}\right)}\frac{\tilde{T}_w}{T_0^2}e^{i\phi_T} \end{aligned} \tag{63}$$

This is the pressure equation for $\hat{p}_2(z)$. The volume-integrated energy equation is required for the unknown $\hat{p}_1$,

$$i\hat{p}_1 = \frac{\gamma}{\mathcal{V}}\left(\frac{1}{\mathrm{Pr\,Va}}\int_{\mathcal{S}} \mathbf{n}\cdot\hat{T}_{1,r}\,d\mathcal{S} - \int_{\mathcal{S}} \mathbf{n}\cdot\hat{u}_0\,d\mathcal{S}\right) \tag{64}$$

Table 4 summarizes the reduced set of oscillating first-order equations. These equations, along with the mean-steady equations and boundary conditions of table 3, complete the formulation of the linear anelastic problem.

Table 4. Reduced set of oscillating first-order equations.

$$\hat{u}_0 = i\frac{\hat{p}_2'(z)}{\rho_0(z)}\left[1-\zeta_0\left(r,z;\sqrt{\mathrm{Va}}\right)\right] \qquad \text{(a)}$$

$$\hat{T}_1 = \frac{\gamma-1}{\gamma}\hat{p}_1 T_0\left[1-\zeta_0\left(r,z;\sqrt{\mathrm{PrVa}}\right)\right]+\tilde{T}_w e^{i\phi_T}\zeta_0\left(r,z;\sqrt{\mathrm{PrVa}}\right)$$
$$-T_0 T_0'\,\hat{p}_2'\left\{\left[1-\zeta_0\left(r,z;\sqrt{\mathrm{PrVa}}\right)\right]-\left(\frac{\mathrm{Pr}}{\mathrm{Pr}-1}\right)\left[\zeta_0\left(r,z;\sqrt{\mathrm{Va}}\right)-\zeta_0\left(r,z;\sqrt{\mathrm{PrVa}}\right)\right]\right\} \qquad \text{(b)}$$

$$\hat{\theta}_1 = \left\{e^{i\chi y}-e^{i\chi}\left(\frac{i\sin\chi y}{\cos\chi}\right)\right\}\tilde{T}_w e^{i\phi_T} \qquad \text{(c)}$$

$$\hat{v}_0 = i\left\{m_1\left(r,z;\sqrt{\mathrm{Va}}\right)T_0\hat{p}_2''\right.$$
$$+\left(m_1\left(r,z;\sqrt{\mathrm{Va}}\right)-\frac{\mathrm{Pr}}{\mathrm{Pr}-1}\left[m_3\left(r,z;\sqrt{\mathrm{Va}}\right)-m_3\left(r,z;\sqrt{\mathrm{PrVa}}\right)\right]\right)T_0'\hat{p}_2' \qquad \text{(d)}$$
$$\left.+m_2\left(r,z;\sqrt{\mathrm{PrVa}}\right)\hat{p}_1+m_3\left(r,z;\sqrt{\mathrm{PrVa}}\right)\frac{\tilde{T}_w}{T_0}e^{i\phi_T}\right\}$$

$$0 = \hat{p}_2''+\left\{\frac{m_1\left(1,z;\sqrt{\mathrm{PrVa}}\right)}{m_1\left(1,z;\sqrt{\mathrm{Va}}\right)}-\frac{\mathrm{Pr}}{\mathrm{Pr}-1}\left[\frac{m_3\left(1,z;\sqrt{\mathrm{Va}}\right)}{m_1\left(1,z;\sqrt{\mathrm{Va}}\right)}-\frac{m_3\left(1,z;\sqrt{\mathrm{PrVa}}\right)}{m_1\left(1,z;\sqrt{\mathrm{Va}}\right)}\right]\right\}\left[\ln T_0(z)\right]'\hat{p}_2' \qquad \text{(e)}$$
$$+\frac{m_2\left(1,z;\sqrt{\mathrm{PrVa}}\right)}{m_1\left(1,z;\sqrt{\mathrm{Va}}\right)}\frac{\hat{p}_1}{T_0}+\frac{m_3\left(1,z;\sqrt{\mathrm{PrVa}}\right)}{m_1\left(1,z;\sqrt{\mathrm{Va}}\right)}\frac{\tilde{T}_w}{T_0^2}e^{i\phi_T}$$

$$i\hat{p}_1 = \left\{\frac{1}{\mathrm{Pr\ Va}}\int_S \mathbf{n}\cdot\hat{T}_{1,r}\,dS-\int_S \mathbf{n}\cdot\hat{u}_0\,dS\right\}\frac{\gamma}{\mathcal{V}} \qquad \text{(f)}$$

Considerations for the Leading-Order Temperature, $T_0(z)$

Solving the most general case requires simultaneous solution of the zeroth-, first-, and mean-steady, second-order equations because of the temperature coupling of $T_0(z)$. However, there are three limiting cases that specify $T_0(z)$, a priori, thus allowing decoupling of the first-order and mean-steady equations. Following is a summary of the general case along with the three limiting cases:

1. $T_0(z)$ is unknown

   This is the most general case in which $T_0(z)$ is part of the solution to the set of coupled zeroth-, first-, and second-order equations.

2. $\left(\ln T_0\right)' = \text{constant} \Rightarrow T_0(z) = T_0(0)\left[\dfrac{T_0(1)}{T_0(0)}\right]^z$

   Here $T_0(z)$ is exponential. This requires solving a coupled set of quasi-linear differential equations.

3. $T_0' = \text{constant} \Rightarrow \left(\ln T_0\right)' = \dfrac{m}{mz+a}$

   Here $T_0(z)$ is linear in z with slope m. This case also requires solving a coupled set of quasi-linear differential equations.

4. $T_0' = \left(\ln T_0\right)' = 0$

   Here T_0 is a constant. This is the thermally strong case, implying that $p_0 = \rho_0 = T_0 = 1$, where thermal sources and sinks are imposed on the system to maintain a constant temperature T_0.

Case 4 describes the thermally strong condition and is the simplest since the pressure equation is reduced to a second-order ordinary differential equation with constant coefficients, which allows an analytic solution. In addition, $\hat{p}_1$ is now one of two unknown constants in the pressure equation and is found by using the second boundary condition on u_0; hence, the volume integral of the energy equation is not required (eq. (f) in table 4). The remaining part of this study will focus on the thermally strong condition of Case 4.

4. SOLUTION FOR THE THERMALLY STRONG CASE, $T_{0,z} = 0$

The equation sets in tables 3 and 4 can be analytically solved for the case of $\nabla T_0 = 0$. The condition $\nabla T_0 = 0$ implies $p_0 = \rho_0 = T_0 = 1$ and thus allows the quasi-linear differential equation for pressure (eq. (e) in table 4) to be reduced to one with constant coefficients. This is Case 4 described in the previous section— a hypothetical condition in which heat sources and sinks maintain T_0 constant. Rott (1993: personal communication) termed this case thermally dominant or "strong." The solution is tabulated in table 5, and solution details are given in appendix F.

Leading-Order Results

In this section, flow fields are calculated for BPT ($U_L = 0$) and OPT ($\tilde{U}_L = 1$) configurations as a function of Va, ϕ_U, and Fo for fixed values of $\varepsilon = 0.002$, $\gamma = 5/3$, $\left(l^*/L^*\right)^2 \sim O\left(\varepsilon^4\right)$, $\left(r_w^*/L^*\right)^2 \sim O\left(\varepsilon^2\right)$, $\lambda \sim O\left(10^{-9}\right)$, and $\mathrm{M}^2 \sim O\left(10^{-11}\right)$. For these conditions, $\mathrm{M}^2/\mathrm{Va} < O\left(10^{-12}\right)$ so viscous dissipation is not important.

Table 5 shows that the pressure, equation (a), and the temperature, equation (c), are constant in z and depend only on the velocity boundary conditions and the tube-wall temperature. There is no dependence on pressure gradient; this is a result of the anelastic approach, and reflects thermodynamic equilibrium. The axial velocity, equation (b), also reflects thermodynamic equilibrium in its linear z-dependence, while the radial velocity, equation (d), is constant in z. The temperature of the tube-wall domain is given by equation (f), and the effect of heat transfer between the gas and the tube wall is contained in the terms represented by $\tilde{T}_w e^{i\phi_T}$. Appendix G lists the code used for computing the solutions.

Comparison of $\hat{p}_1$ and $\hat{\mathcal{P}}_1$

The equation for integrated bulk oscillating pressure is given by equation (f) in table 4. After integration, it is

$$\hat{\mathcal{P}}_1 = -2i\gamma\left(\frac{1}{\mathrm{Pr\,Va}}\left[r\hat{T}_{1,r}\right]_{r=1} - m_1\left(1;\sqrt{\mathrm{Va}}\right)\frac{1-\tilde{U}_L e^{i\phi_U}}{1-\zeta_0\left(0;\sqrt{\mathrm{Va}}\right)}\right) \tag{65}$$

This is more general than the solution pressure given by equation (a) in table 5. For the present solution, equation (65) is not required for determining the bulk oscillating pressure $\hat{p}_1$, because the bulk oscillating pressure is an unknown constant in the leading-order momentum equation and is determined by the velocity boundary conditions at the tube ends (details in appendix F). The pressure $\hat{p}_1$ that results is the thermodynamic pressure calculated along the centerline of the tube. In contrast, the integrated pressure $\hat{\mathcal{P}}_1$ of equation (65) is determined by integrating over the volume domain of the gas. This results in a discrepancy between $\hat{\mathcal{P}}_1$ and $\hat{p}_1$. The difference should be of order of the thermal diffusion layer thickness, $O\left(\frac{1}{\mathrm{PrVa}}\right)$.

Table 5. Summary of leading-order solutions for strong-temperature case, $T_{0,z}=0$.

	Eq.
$\hat{p}_1 = -i\dfrac{1-\tilde{U}_L e^{i\phi_U}}{1-\zeta_0\left(0;\sqrt{\mathrm{Va}}\right)}\dfrac{m_1\left(1;\sqrt{\mathrm{Va}}\right)}{m_2\left(1;\sqrt{\mathrm{PrVa}}\right)} - \dfrac{m_3\left(1;\sqrt{\mathrm{PrVa}}\right)}{m_2\left(1;\sqrt{\mathrm{PrVa}}\right)}\tilde{T}_w e^{i\phi_T}$	(a)
$\hat{u}_0 = \left[1-\left(1-\tilde{U}_L e^{i\phi_U}\right)z\right]\left\{\dfrac{1-\zeta_0\left(r;\sqrt{\mathrm{Va}}\right)}{1-\zeta_0\left(0;\sqrt{\mathrm{Va}}\right)}\right\}$	(b)
$\hat{T}_1 = -i\dfrac{\gamma-1}{\gamma}\dfrac{m_1\left(1;\sqrt{\mathrm{Va}}\right)}{m_2\left(1;\sqrt{\mathrm{PrVa}}\right)}\left\{\dfrac{1-\zeta_0\left(r;\sqrt{\mathrm{PrVa}}\right)}{1-\zeta_0\left(0;\sqrt{\mathrm{Va}}\right)}\right\}\left(1-\tilde{U}_L e^{i\phi_U}\right)$ $+\left(\zeta_0\left(r;\sqrt{\mathrm{PrVa}}\right)-\dfrac{\gamma-1}{\gamma}\dfrac{m_3\left(1;\sqrt{\mathrm{PrVa}}\right)}{m_2\left(1;\sqrt{\mathrm{PrVa}}\right)}\left[1-\zeta_0\left(r;\sqrt{\mathrm{PrVa}}\right)\right]\right)\tilde{T}_w e^{i\phi_T}$	(c)
$\hat{v}_0 = \dfrac{m_1\left(1;\sqrt{\mathrm{Va}}\right)}{1-\zeta_0\left(0;\sqrt{\mathrm{Va}}\right)}\left\{\dfrac{m_2\left(r;\sqrt{\mathrm{PrVa}}\right)}{m_2\left(1;\sqrt{\mathrm{PrVa}}\right)}-\dfrac{m_1\left(r;\sqrt{\mathrm{Va}}\right)}{m_1\left(1;\sqrt{\mathrm{Va}}\right)}\right\}\left(1-\tilde{U}_L e^{i\phi_U}\right)$ $-im_3\left(1;\sqrt{\mathrm{PrVa}}\right)\left\{\dfrac{m_2\left(r;\sqrt{\mathrm{PrVa}}\right)}{m_2\left(1;\sqrt{\mathrm{PrVa}}\right)}-\dfrac{m_3\left(r;\sqrt{\mathrm{PrVa}}\right)}{m_3\left(1;\sqrt{\mathrm{PrVa}}\right)}\right\}\tilde{T}_w e^{i\phi_T}$	(d)
$\hat{\rho}_1 = \hat{p}_1 - \hat{T}_1$	(e)
$\hat{\theta}_1 = \tilde{T}_w e^{i\phi_T}\left[e^{i\chi y} - e^{i\chi}\left(\dfrac{i\sin\chi y}{\cos\chi}\right)\right]$	(f)
$\zeta_n(r,z;\sigma) = \dfrac{J_n\left(r\sigma\sqrt{-i\rho_0(z)}\right)}{J_0\left(\sigma\sqrt{-i\rho_0(z)}\right)}\quad n=0,1$ $J_0(0)=1$ $J_1(0)=0$	(g)
$m_1\left(r,z;\sqrt{\mathrm{Va}}\right) = -\left[\dfrac{r}{2}-m_3\left(r,z;\sqrt{\mathrm{Va}}\right)\right]$ $m_1\left(0,z;\sqrt{\mathrm{Va}}\right)=0$	(h)
$m_2\left(r,z;\sqrt{\mathrm{PrVa}}\right) = -\left[\dfrac{r}{2\gamma}+\dfrac{\gamma-1}{\gamma}m_3\left(r,z;\sqrt{\mathrm{PrVa}}\right)\right]$ $m_2\left(0,z;\sqrt{\mathrm{PrVa}}\right)=0$	(i)
$m_3(r,z;\sigma) = \dfrac{1}{\sigma\sqrt{-i\rho_0(z)}}\zeta_1(r,z;\sigma)$ $m_3(0,z;\sigma)=0$	(j)

The bulk pressures $\hat{p}_1$ and $\hat{\mathcal{P}}_1$ for a BPT ($U_L = 0$) with $\varepsilon = 2 \times 10^{-3}$ and $\lambda = 6.46 \times 10^{-9}$ are given in figure 8. The difference between $\hat{p}_1$ and $\hat{\mathcal{P}}_1$ for small PrVa is significant, being about 40% for PrVa = 0.7. As PrVa increases (7< PrVa < 21), the difference is less than 5%, and for PrVa = 70 the difference is less than 1%. The difference between $\hat{p}_1$ and $\hat{\mathcal{P}}_1$ is consistent with a PrVa scaling.

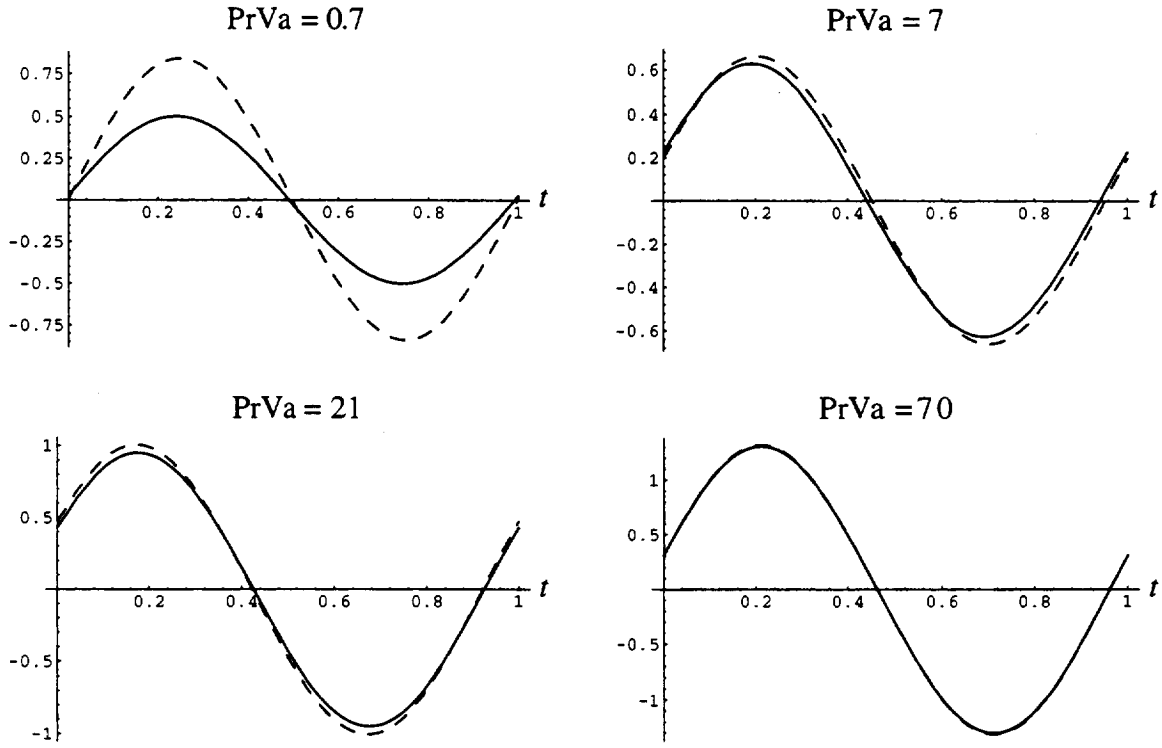

Figure 8. Pressure vs. time for $\hat{p}_1$ (—) and $\hat{\mathcal{P}}_1$ (– –) with $\lambda = 6.46 \times 10^{-9}$, $\hat{T}_w = 0$, $\tilde{U}_L = 0$.

Leading-Order Temperature and Pressure Phasors

Figure 9 shows how heat transfer between the gas and the tube wall affects the temperature, pressure, and velocity phasors[1] for a BPT and an OPT. Phasors for $\hat{p}_1$, $\hat{U}_0$, $\hat{U}_L$, and $\hat{T}_b$ for the conditions Fo → 0 and Fo = 100, and Va = 1, 30, and 100 are shown where $\hat{T}_b$ is the bulk oscillating temperature (temperature averaged over the tube cross-sectional area),

$$\hat{T}_b = 2\int_0^1 r\hat{T}_1\, dr \tag{66}$$

[1]Phasors are complex vector quantities whose magnitude and angular position, when plotted in the complex plane, represent, respectively, the amplitude and phase angle of a sinusoid.

The BPT is a standing wave device and so the velocity phasor $\hat{u}_0$ has a constant phase angle along the tube length; hence $\hat{u}_0$ lies along the real axis. Because $\hat{u}_0$ lies only along the real axis, the temperature phasor $\hat{T}_b$ is out of phase with the velocity. This is seen in figures 9(a)–9(c) for a BPT. The result is very small enthalpy fluxes since enthalpy flux depends on the cosine of the phase angle between temperature and velocity according to the general relation given by equation (7) where χ_0 is the temperature phasor and u_0 is the velocity phasor.

Three more observations are illustrated by figure 9. The first is that for the BPT phasor diagrams, figures 9(a)–9(c), which show that $\hat{T}_b$ and $\hat{u}_0$ are closer to being in-phase for Fo $\rightarrow$ 0 than for Fo = 100. This is due to the large heat transfer between the gas and the tube wall for Fo $\rightarrow$ 0. The condition Fo $\rightarrow$ 0 represents isothermal wall conditions. The condition Fo = 100 represents near adiabatic conditions on the gas. That is, the condition Fo = 100 represents a very thin-walled tube relative to the thermal penetration in the tube wall. This illustrates how heat transfer is required for the BPT in order to obtain a favorable phase shift between temperature and velocity.

The second interesting observation is shown for the OPT in figures 9(c)–9(e). The results are for $\tilde{U}_L = 1$ and $\phi_U = -0.1$. The velocity phasor at $z = 0$ is $\hat{U}_0$, which lies along the real axis with amplitude 1, and the velocity phasor at $z = 1$ is $\hat{U}_L$. The shaded area between $\hat{U}_0$ and $\hat{U}_L$ represents all velocity phasors between $z = 0$ and $z = 1$, hence the OPT is more of a progressive wave device because of the presence of phase-angle gradients.

The OPT shows that $\hat{T}_b$ can be adjusted through the velocity boundary conditions so that it is more nearly in-phase with $\hat{u}_0$. This is most easily seen in figures 9(d) and 9(e) for Va = 30 and Va = 100. Here $\hat{T}_b$ is more in-phase with $\hat{u}_0$ when compared with the BPT. Also, it is apparent that for the OPT the adiabatic conditions imposed on the gas by the tube wall result in the temperature and velocity phasors becoming more in phase. This is most easily seen for Va = 100 and Fo = 100 where $\hat{T}_b$ is now in the shaded area representing the velocity phasors within the tube. For the isothermal wall condition of Fo $\rightarrow$ 0, $\hat{T}_b$ is pushed out of phase (out of the shaded region) with velocity. This results in less enthalpy flow. Heat transfer, then, is not advantageous for an OPT.

Third, when there is significant heat transfer between the gas and tube wall, the pressure and temperature phasors move out of phase relative to each other for both BPT and OPT. This is seen by comparing $\hat{p}_1$ and $\hat{T}_b$ for Fo $\rightarrow$ 0, with $\hat{p}_1$ and $\hat{T}_b$ for Fo = 100. For Fo = 100, $\hat{p}_1$ and $\hat{T}_b$ are nearly in phase (Va = 30 and Va = 100), whereas for Fo $\rightarrow$ 0, they are not in phase. Calculations show that the phase shift can be about 20%. This is important because in simple 1-D models it is often assumed that there are adiabatic conditions on the gas and so there is a presumption that temperature is always in phase with pressure. A discrepancy between experimental measurements and model predictions may then arise. Most pulse tubes operate at Fo = $\boldsymbol{O}(1)$, which is closer to isothermal wall conditions.

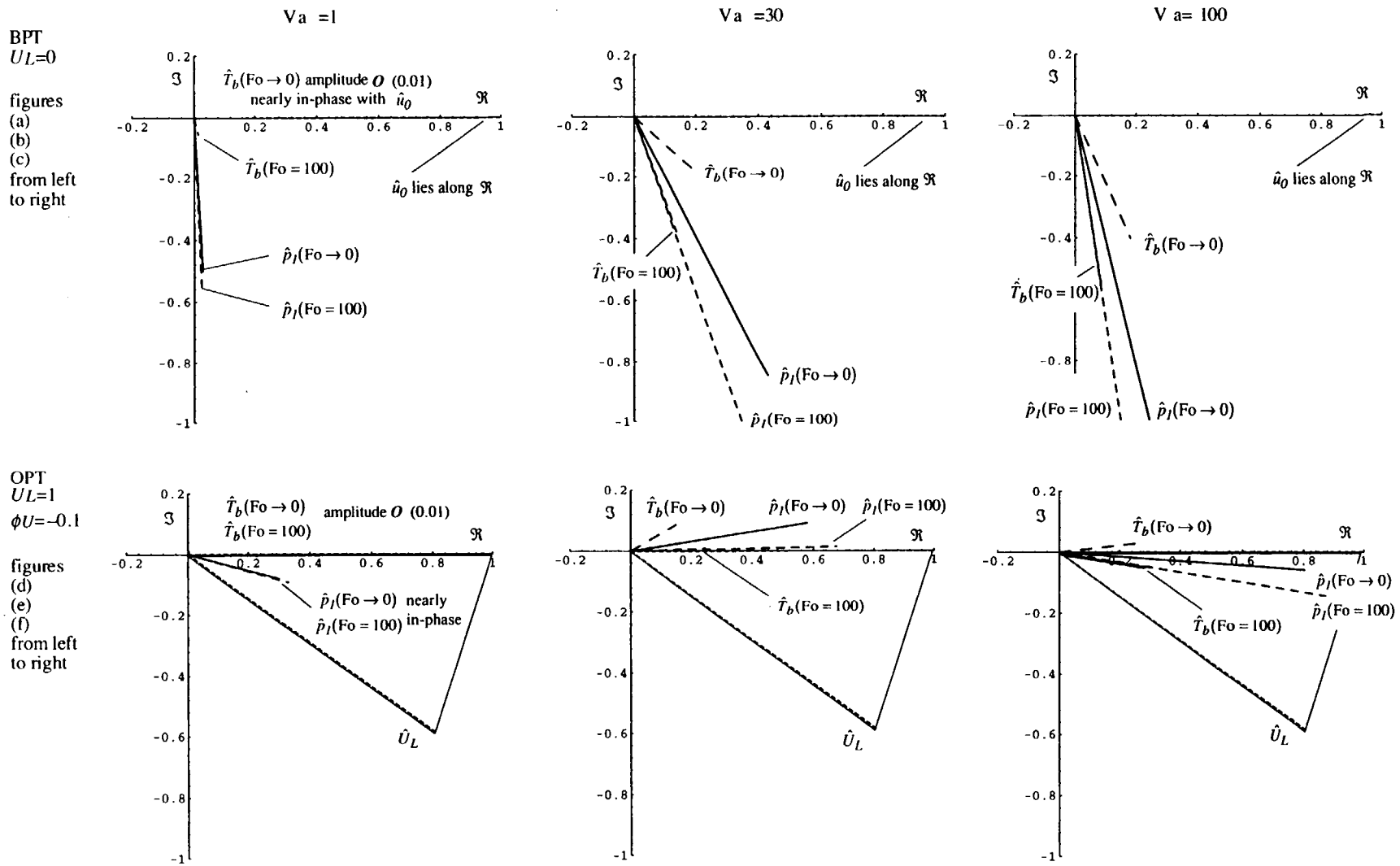

Figure 9. Effect of Va and Fo on pressure and temperature phasors for BPT ($U_L = 0$) and OPT ($\tilde{U}_L = 1$, $\phi_U = -0.1$). Reference velocity phasor $\hat{U}_0$ along real axis with unit amplitude.

Transverse Diffusion of Oscillating Velocity and Temperature

Velocity

Figure 10 shows $u_0(r)$ at $z = 0$ for Va = 1 and $U_L = 0$ at t = 0, 0.1, 0.2, 0.3, and 0.4. For small Va, the profile is parabolic as in steady-state flow. Increasing Va to Va = 10 shows that the velocity near the wall begins to lead the velocity at the centerline. Further increasing Va to 30 and to 100 shows that the velocity very near the wall substantially leads that of the centerline, and that the velocity in the vicinity of the centerline begins to flatten and take on an inviscid profile, with the velocity amplitude near the wall leading and overshooting the velocity at the centerline. Figure 11 shows $v_0(r)$. For small Va, v_0 is in phase (with itself) at all r-locations. Increasing Va, however, results in v_0 near the wall leading v_0 at the centerline region.

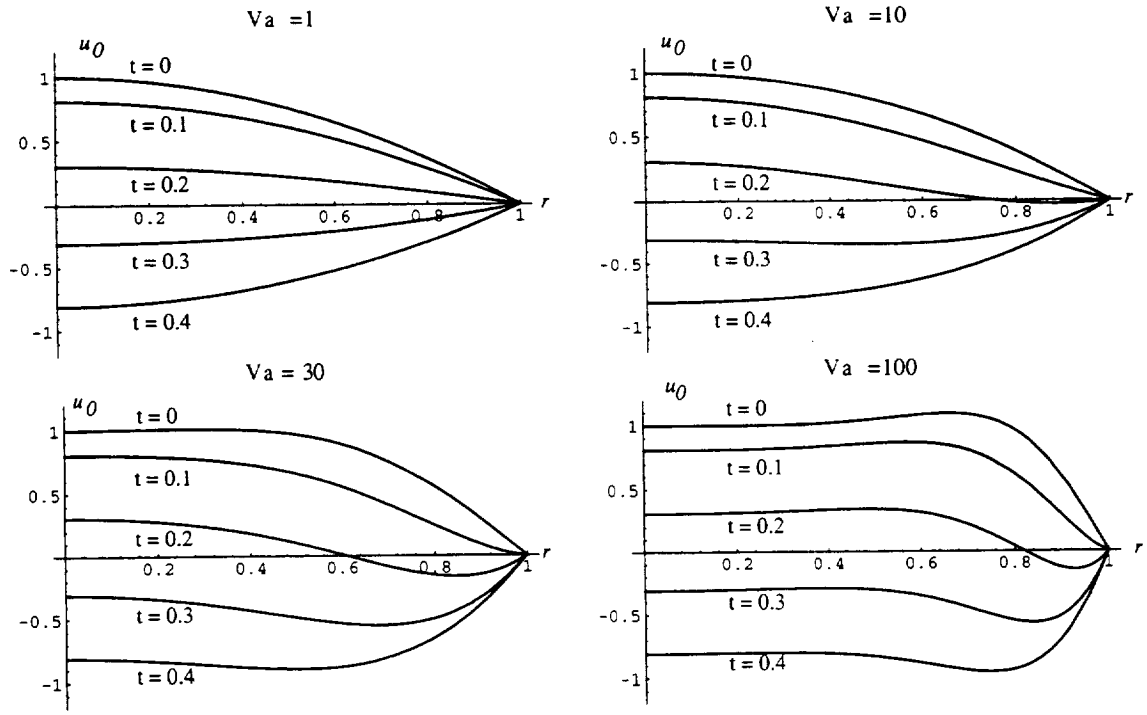

Figure 10. Oscillating axial velocity, $u_0(r)$.

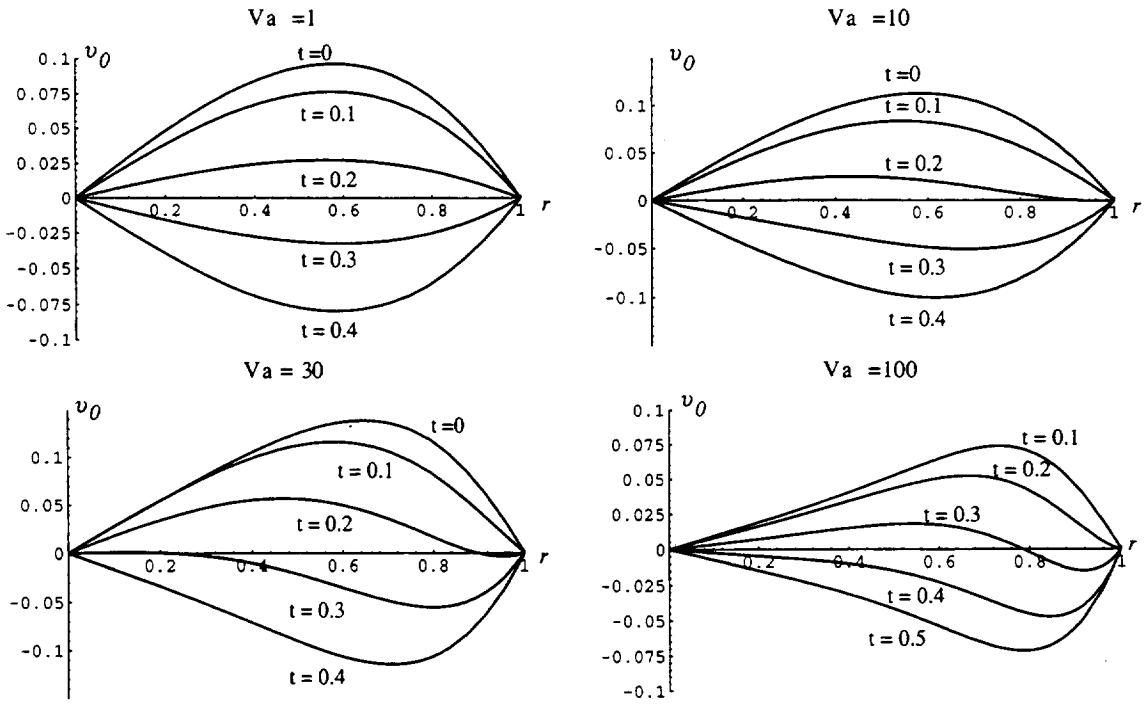

Figure 11. Oscillating radial velocity, $v_0(r)$.

Temperature

Figure 12 shows the $T_1(r)$ profile for PrVa = 0.7, 7, 21, and 70 with Fo → 0 and Fo = 100. For the isothermal wall condition of Fo → 0, the temperature profiles are similar to the velocity profiles of figure 10, just scaled by the Prandtl number. For the near-adiabatic case of Fo = 100, in all cases of PrVa, the temperature at the wall is seen to float. This is because the wall temperature responds to the imposed oscillating gas temperature—the wall temperature is not fixed as it is for an isothermal wall. The ability of the wall temperature to float for the adiabatic wall allows for the temperature at the centerline region to be larger when compared with that of the isothermal wall. This is apparent for PrVa = 0.7 and PrVa = 7. As Va increases, the centerline temperature for Fo → 0 begins to approach that of Fo = 100 in both amplitude and phase. This is because diffusion is now confined near the wall in the boundary layer. Figure 12 shows that the effect of the floating wall temperature on gas temperature is primarily confined to the diffusion layer, and that an adiabatic wall condition will have a greater relative effect on gas temperature amplitude for small PrVa than for large PrVa.

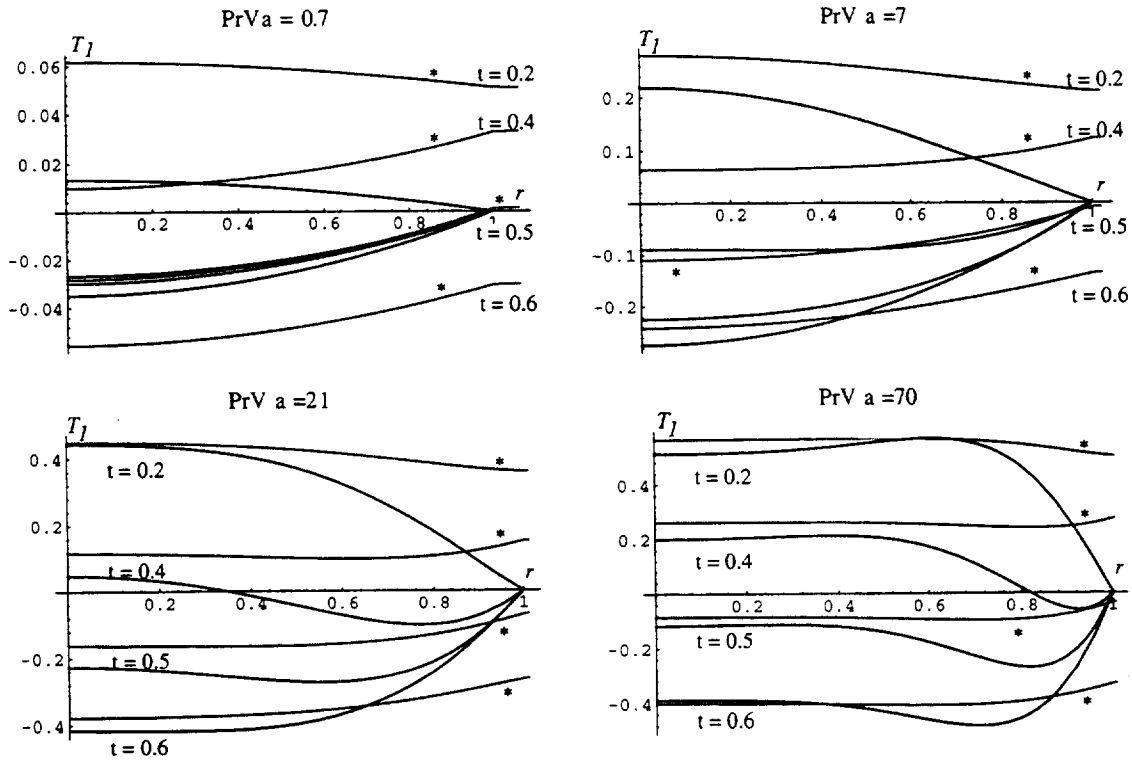

Figure 12. Oscillating temperature, $T_1(r)$. Temperature profiles for Fo → 0 are pinned at r = 1, and profiles for Fo = 100 (identified with '') float at r = 1.*

Oscillating Heat Transfer and Oscillating Shear

Complex Nusselt number for oscillating heat transfer

The thermal diffusion and temperature phase shifts are now examined within the context of the complex Nusselt number proposed by K. Lee (ref. 38). His work focused on BPT-type systems. We now extend our analysis for OPT systems. The complex Nusselt number $\hat{\mathrm{Nu}}$ is defined as the heat flux at the wall divided by the difference in temperature between the tube wall and the bulk gas,

$$\hat{\mathrm{Nu}} = \frac{\hat{q}_w e^{it}}{\left(\hat{T}_w - \hat{T}_b\right)e^{it}} \tag{67}$$

$$= \frac{-\hat{T}_{1,r}\Big|_{r=1}}{\hat{T}_1\Big|_{r=1} - 2\int_0^1 r\hat{T}_1\,dr} \tag{68}$$

where $\hat{q}_w = -\hat{T}_{1,r}\Big|_{r=1}$, $\hat{T}_w = \hat{T}_1\Big|_{r=1}$, and $\hat{T}_b$ is defined by equation (66).

Figure 13 shows phasors for $\hat{\mathrm{Nu}}$, $\hat{T}_b$, $\Delta\hat{T} = \hat{T}_w - 2\int_0^1 r\hat{T}_1\,dr$ and $\hat{q}_w$ as functions of PrVa = 0.7, 21, and 70, and Fo $\rightarrow$ 0 and Fo = 100 for the BPT and OPT, respectively. For PrVa = 0.7 and Fo $\rightarrow$ 0, the above phasors are of very small amplitude, and are generally in phase (or 180° out of phase) with $\hat{U}_0$ (the phasor of $\hat{U}_0$ is along the positive real axis and is of unit amplitude). Steady-state heat transfer coefficients can be used under these conditions. Continuing with Fo $\rightarrow$ 0, as Va increases to PrVa = 21 and beyond, phase angles also increase with $\hat{q}_w$ lagging $\hat{U}_0$. At Va = 70, $\phi_{\hat{N}u} = -0.397$, and for Va > 70, $\phi_{\hat{N}u} \approx -0.38$ (not shown), which corresponds well with K. Lee's value of $\phi_{\hat{N}u} \approx -0.375$ for rectangular geometry in the limit of large PrVa.

The effect of Fo shown in figure 13 is to shift the phase of $\hat{q}_w$ ahead so that now $\hat{q}_w$ leads $\hat{U}_0$. A curious observation is that $\hat{\mathrm{Nu}}$ is independent of Fo. This is proven mathematically in appendix F. A scaling of equation (68) shows that $\hat{\mathrm{Nu}} \sim \sqrt{\mathrm{Pr\,Va}}$. The thermal penetration in the gas is only affected by $\sqrt{\mathrm{Pr\,Va}}$, whereas Fo only affects the tube-wall temperature boundary condition.

Figure 14 shows plots for the same phasors as shown in figure 13 with the same values of PrVa and Fo for an OPT with $\tilde{U}_L = 1.0$ and $\phi_U = -0.1$, where $\hat{U}_L = \tilde{U}_L e^{i\phi_U}$. Comparing figure 14 with figure 13 for corresponding PrVa and Fo shows that all phasors are shifted forward, except for $\hat{\mathrm{Nu}}$, which remains with the same relative phase angle. That is, $\hat{\mathrm{Nu}}$ is independent of $\hat{U}_L$. This is shown mathematically in appendix F. Thus $\hat{\mathrm{Nu}}$ is only a function of PrVa and is independent of Fo and $\hat{U}_L$. F $\hat{\mathrm{Nu}}$ versus PrVa is plotted in figure 15; the figure can be used for either BPT or OPT systems, independent of Fo, $\tilde{U}_L$, and ϕ_U.

The complex Nusselt number may be used for one-dimensional linear oscillating flow in a tube to correct for radial heat transfer,

$$i\hat{T}_{osc} = i\hat{p}_1 + \hat{\mathrm{Nu}}(\mathrm{PrVa})\hat{T}_{osc} \tag{69}$$

where $\hat{T}_{osc}$ is the local oscillating temperature and $\hat{\mathrm{Nu}} = \tilde{A}\,e^{i\phi}$.

Complex wall shear factor for oscillating shear

A similar relation can also be defined for oscillating shear and oscillating bulk velocity. Gedeon termed this the "complex wall shear factor," F (ref. 66). It is defined as

$$\hat{\mathrm{F}} = \frac{\hat{\tau}_w}{\hat{u}_b} \tag{70}$$

where

$$\hat{\tau}_w = \hat{u}_{0,r}\big|_{r=1} \quad \text{and} \quad \hat{u}_b = 2\int_0^1 r\hat{u}_{0,r}\,dr \tag{71}$$

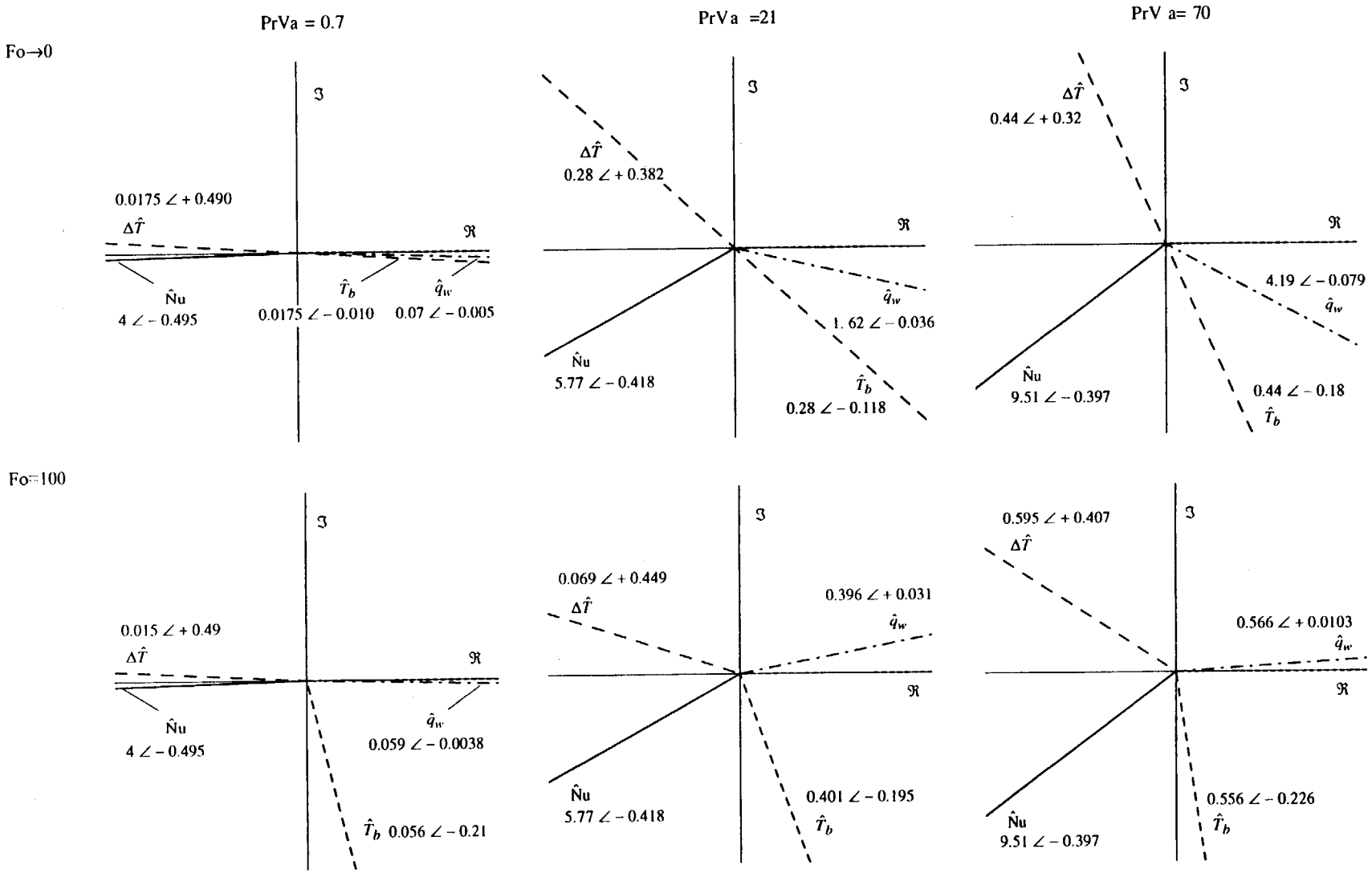

Figure 13. Effect of PrVa and Fo on heat-transfer amplitude and heat-transfer phase angles for BPT. Reference velocity phasor $\hat{U}_0$ along real axis with unit amplitude.

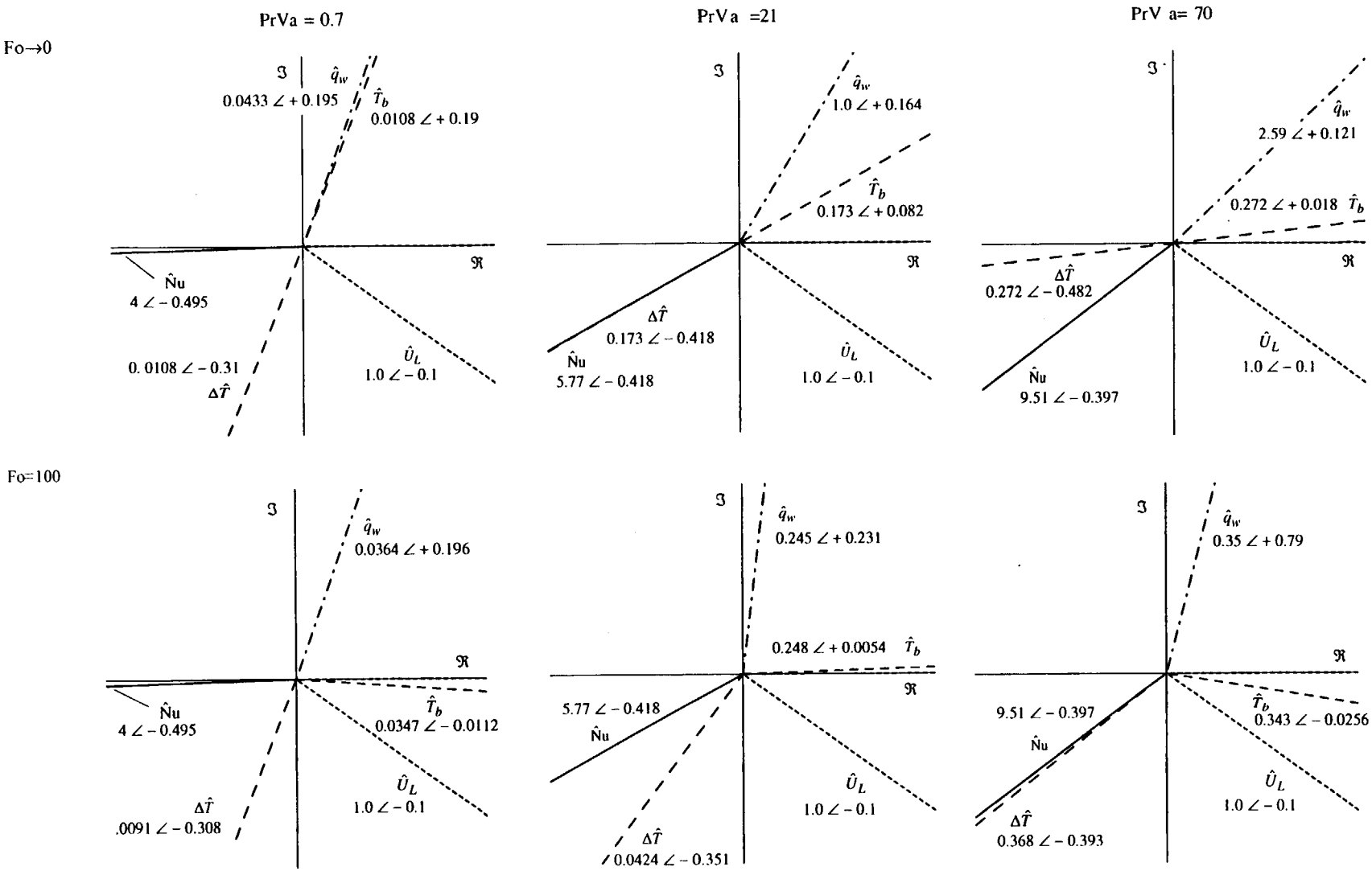

Figure 14. Effect of PrVa and Fo on heat-transfer amplitude and phase angles for OPT: ($\tilde{U}_L = 1$, $\phi_U = -0.1$). Reference velocity phasor $\hat{U}_0$ along real axis with unit amplitude.

These relations are of the same form as the complex Nusselt number, and so figure 15 may be used in a similar manner with the scaling length characterized by Va. The complex wall-shear factor may be used as a lumped-parameter approximation of shear for one-dimensional linear oscillating flow,

$$i\hat{u}_{osc} = -\hat{p}_{2,z} + \hat{\mathrm{F}}(\mathrm{Va})\hat{u}_{osc} \tag{72}$$

where $\hat{u}_{osc}$ is the area-averaged oscillating velocity and $\hat{\mathrm{F}} = \tilde{A}\, e^{i\phi}$.

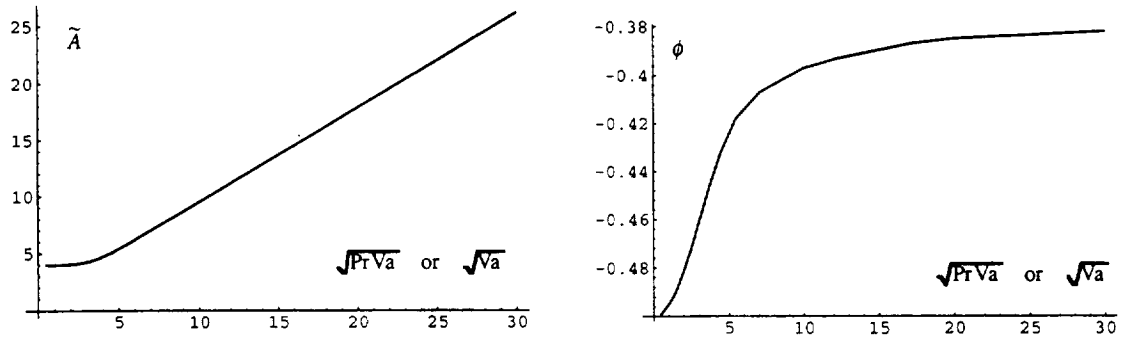

Figure 15. Amplitude and phase of the complex Nusselt number, $\hat{\mathrm{Nu}}(\mathrm{PrVa}) = \tilde{A}\, e^{i\phi}$, *or complex wall shear factor,* $\hat{\mathrm{F}}(\mathrm{Va}) = \tilde{A}\, e^{i\phi}$.

Mean-Steady Secondary Flow

The mean-steady flows are composed of the time-averaged product of two oscillating quantities. The first is velocity; the second may be density for mass flux streaming, temperature for enthalpy streaming, pressure for work streaming, entropy for heat streaming, or velocity itself for momentum streaming. In all cases, each oscillating quantity depends on the axial velocity amplitude, as seen in table 5. Thus, all mean-steady fluxes have a quadratic dependence on axial velocity. Details for the mean-steady secondary flow solutions for $T_{0,z} = 0$ are found in appendix F. The results are summarized here.

Eulerian Velocity, $\overline{\mathcal{U}_1}(r,z)$

The Eulerian mean-steady velocity results from two nonlinear flow components. These components are the Reynolds stresses $\overline{\mathbf{u}}_1$ and the nonlinear product of the oscillating first-order density and leading-order velocity, $\overline{\rho_1 \mathbf{u}_0}$. Although the two components are not themselves independently measured, they do constitute separate components of the mean-steady Eulerian velocity $\overline{\mathcal{U}_1}(r,z)$,which is measured. $\mathcal{U}(\mathbf{x},t)$ is defined as the observed velocity component of the mass flux vector j where $\mathbf{j}(\mathbf{x},t) = \rho\mathbf{u}$; hence,

$\mathcal{U}(\mathbf{x},t)$ and $\mathbf{j}$ are expandable in ε,

$$\mathcal{U}(\mathbf{x},t) = \mathcal{U}_0 + \varepsilon\mathcal{U}_1 + O\left(\varepsilon^2\right) \tag{74}$$

$$\mathbf{j}(\mathbf{x},t) = \rho_0\mathbf{u}_0 + \varepsilon\left(\rho_0\mathbf{u}_1 + \rho_1\mathbf{u}_0\right) + O\left(\varepsilon^2\right) \tag{75}$$

Substituting equations (74) and (75) into equation (73) and equating like orders in ε results in

$$\mathcal{U}_0 = \mathbf{u}_0 \quad \text{and} \quad \mathcal{U}_1 = \mathbf{u}_1 + \frac{\rho_1\mathbf{u}_0}{\rho_0} \tag{76}$$

where $\rho_0 = 1$ for the strong-temperature case. $\overline{\mathcal{U}}_1(r,z)$ is composed of the axial component $\overline{u}_1$ and the radial component $\overline{v}_1$

$$\overline{u}_1 = \overline{u}_1 + \overline{\rho_1 u_0} \tag{77}$$

and

$$\overline{v}_1 = \overline{v}_1 + \overline{\rho_1 v_0} \tag{78}$$

Figure 16 shows calculated mean-steady Eulerian velocities for a BPT with an isothermal wall, Fo $\rightarrow$ 0. The left column shows the velocity field $\overline{\mathcal{U}}_1(r,z)$, and the right column plots $\overline{u}_1(r)$ and $\overline{v}_1(r)$ at $z = 0$. The z-dependencies are such that $\overline{u}_1$ is linear in z, and $\overline{v}_1$ is constant in z. This can be seen by examining equations (b) and (d) in table 5. For the viscous case in which Va = 1, the mean-steady velocity components are of order $\overline{u}_1 = O\left(10^{-2}\right)$ and $\overline{v}_1 = O\left(10^{-3}\right)$ due to the dominance of diffusion throughout the gas domain. Flow in the vicinity of the centerline ($r = 0$) moves toward the closed end, and flow near the wall is toward the oscillating end. There is a radial component of flow at $z = 1$, because no-slip at the tube ends is not enforced in the equations. The r-momentum equation, which contains axial diffusion of the radial velocity, is of $O\left(\varepsilon^2\right)$ and so is not included in the $O(\varepsilon)$ mean-steady problem.

As Va increases to Va = 10, the mean-steady flux increases by the same order, and the steady flows remain in the same directions. Upon further increasing to Va = 50, flow at the centerline decreases and flow near the wall increases. For $\text{Va} < 50$, the radial flow component (dashed-line plot) is seen to be always outward toward the walls, that is, streaming flows down the center of the tube toward the closed end and radially outward toward the tube wall, and then back to the oscillating end along the tube wall. At Va = 60, the flow at the centerline decreases to the point where the flow reverses itself and begins moving toward the oscillating end. At this point, a double boundary layer develops. This is consistent with the analysis of Stuart (ref. 67). Stuart refers to the diffusion layer near the wall as the "inner layer," and the transition layer between the inner layer and the centerline as the "outer layer." His terminology is adopted here. For $\text{Va} > 60$, the development of the double boundary layer requires streaming to now flow from the outer layer to either the inner layer or to the centerline region, as shown by the negative and positive radial velocities in the plot for Va = 100. The Va = 100 plot distinctly shows the inner and outer layers, and the centerline region. For Va > 100 (not shown) the centerline and outer layer flows increase in magnitude, and the inner layer flow remains relatively constant.

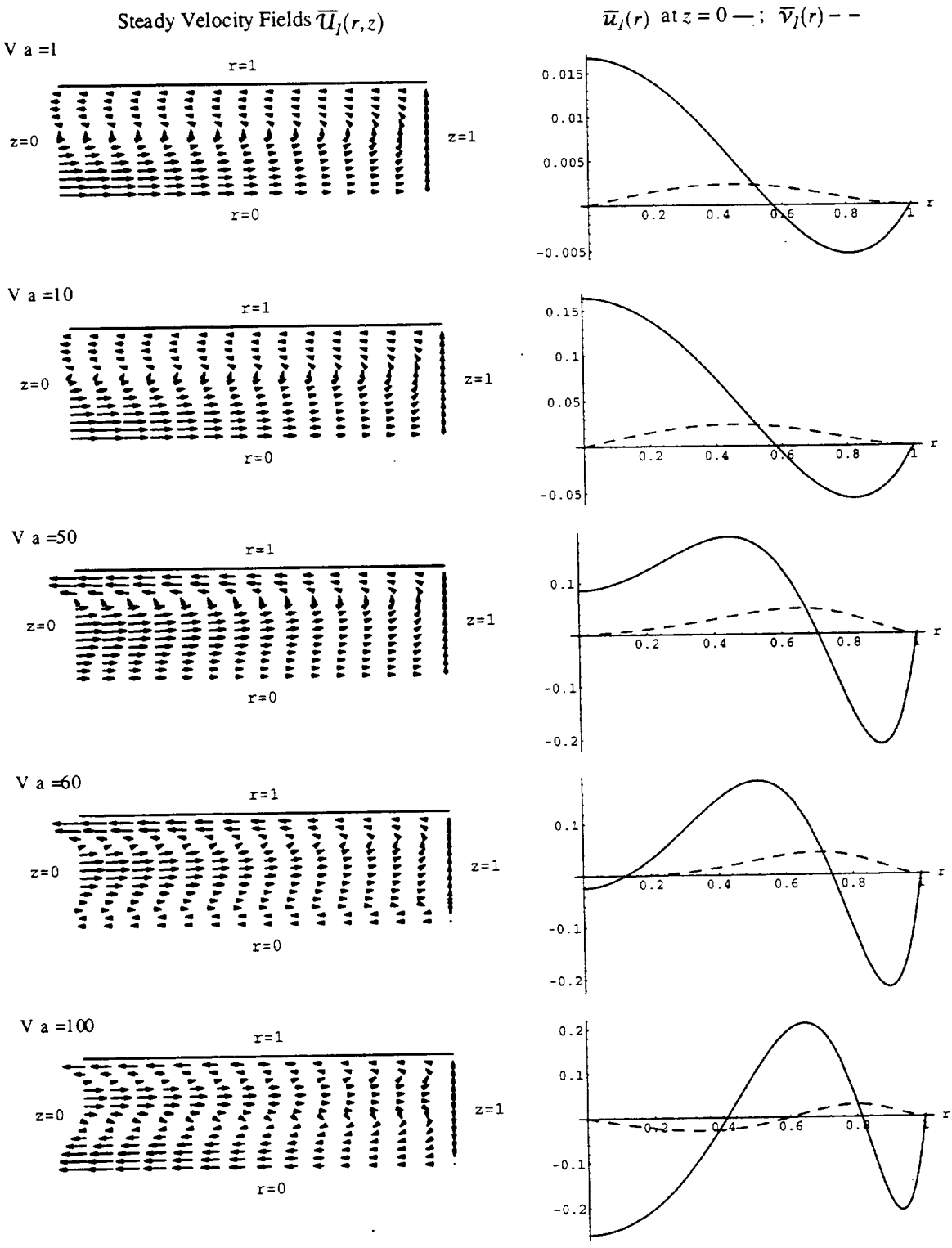

Figure 16. Effect of Va on the Eulerian mean-steady velocity for a BPT: $\varepsilon = 0.002$.

The results shown in figure 16 correspond well with the results of Grotberg (ref. 3) for mean-steady mass flux of oscillating incompressible flow in a diverging tube. In Grotberg's analysis, the larger end of the tube corresponds to lower amplitude oscillations, whereas for this analysis the closed end of the tube corresponds to lower amplitude oscillations. The present results for comparable ε and Va are consistent with those of Grotberg in both direction and magnitude of the component velocities, including the predicted double boundary layer.

Figure 17 presents the mean-steady velocity fields $\overline{u}_1(r,z)$, and velocity plots $\overline{u}_1(r)$ at $z = 0$, 0.5, and 1, respectively, for an OPT-type system (oscillating flow at both ends). Fixed parameters are $\tilde{U}_L = 1$, $\phi_U = -0.25$, and Fo $\rightarrow 0$. The range of Va examined is from Va = 10 to Va = 100. For Va = 10, the velocity enters the tube at the centerline from both ends, reverses flow within the tube, and then exits in the diffusion layer near the wall. The plot for Va = 10 shows that $\overline{u}_1 = O\left(10^{-1}\right)$ which is of the same order as the previous BPT case for Va = 10. For Va < 10, $\overline{u}_1$ scales with Va as with the BPT. Increasing to Va = 30, the centerline velocity at $z = 0$ is seen to decrease to zero, while the velocities at $z = 0.5$ and $z = 1$ decrease further in the negative direction. For $30 < \text{Va} < 50$, the centerline velocities at all three z-locations become negative, and a double boundary layer develops at $z = 0$. Continued increase in Va results in decreasing the inner layer at $z = 0$. At Va = 50, the remnants of the inner layer at $z = 0$ can be seen. Further increasing Va, the centerline velocity for $z = 0$ and $z = 0.5$ continues to decrease and the diffusion layers near the wall increase. At Va = 60, the centerline velocities have all converged at about $\overline{u}_1 = -0.7$, and the inner layer at $z = 0$ has almost disappeared. Further increasing to Va = 100 shows that the velocities for $z = 0$, 0.5, and 1 have inverted, with the centerline velocity at $z = 0$ still decreasing while at $z = 1$ the centerline velocity is now increasing, and the inner layer now completely disappears. For Va = 100 there is very strong streaming of the order of the oscillating velocity.

The results shown in figure 17 give a sense of how the second oscillating velocity (at $z = 1$) of an OPT can lead to streaming patterns that are much more complex than those of a BPT. For small Va < 10 streaming is small and it scales with Va. For large Va = 100, streaming is very strong and is of the order of the oscillating velocity.

The effect of phase angle on mean-steady flow is given in figure 18. The calculations are based on Va = 100, $\tilde{U}_L = 1$, and Fo $\rightarrow 0$. The plots are for $\overline{u}_1(r)$ at $z = 0$, 0.5, and 1. For $0 > \phi_U > -0.25$ there is only a single boundary layer at all three z-locations.[2] For $\phi_U < -0.30$ at $z = 0$ (not shown) a double boundary layer begins to develop. For $\phi_U < -0.40$ at $z = 1$ a double boundary layer develops with a direction opposite to that at $z = 0$. At $\phi_U = -0.50$, the flow is mirrored across $z = 0.5$, and at $\phi_U = -0.55$ the flow is mirrored to that of $\phi_U = -0.45$ (not shown).

---

[2]The case $\phi_U = 0$ and $\tilde{U}_L = 1$ is incompressible flow, hence mean-steady flow is zero since $u_{0,z} = 0$, that is, the Reynolds stresses are zero.

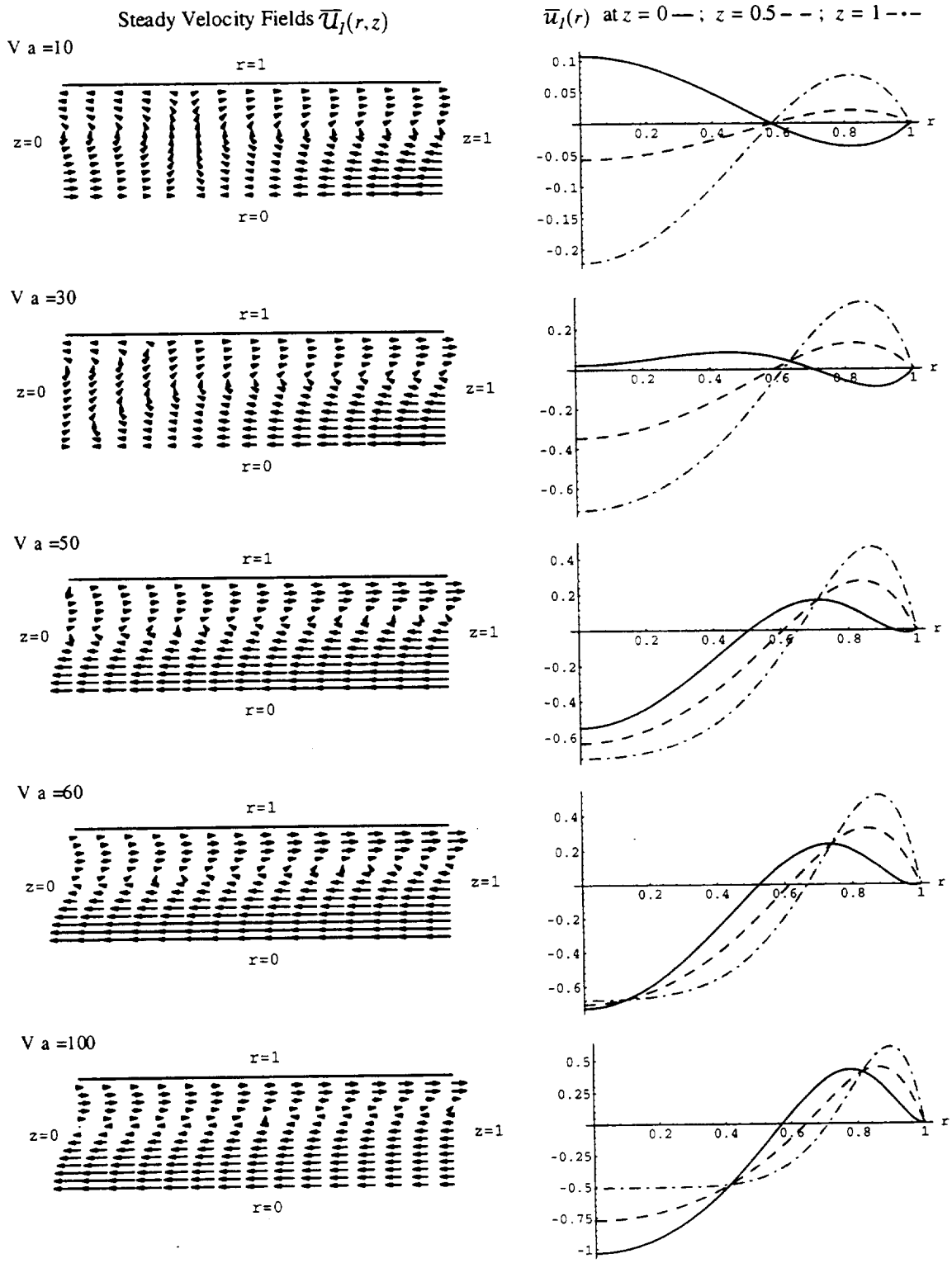

Figure 17. Effect of Va on steady velocity for OPT: $\varepsilon = 0.002$, $\tilde{U}_L = 1$, $\phi_U = -0.25$.

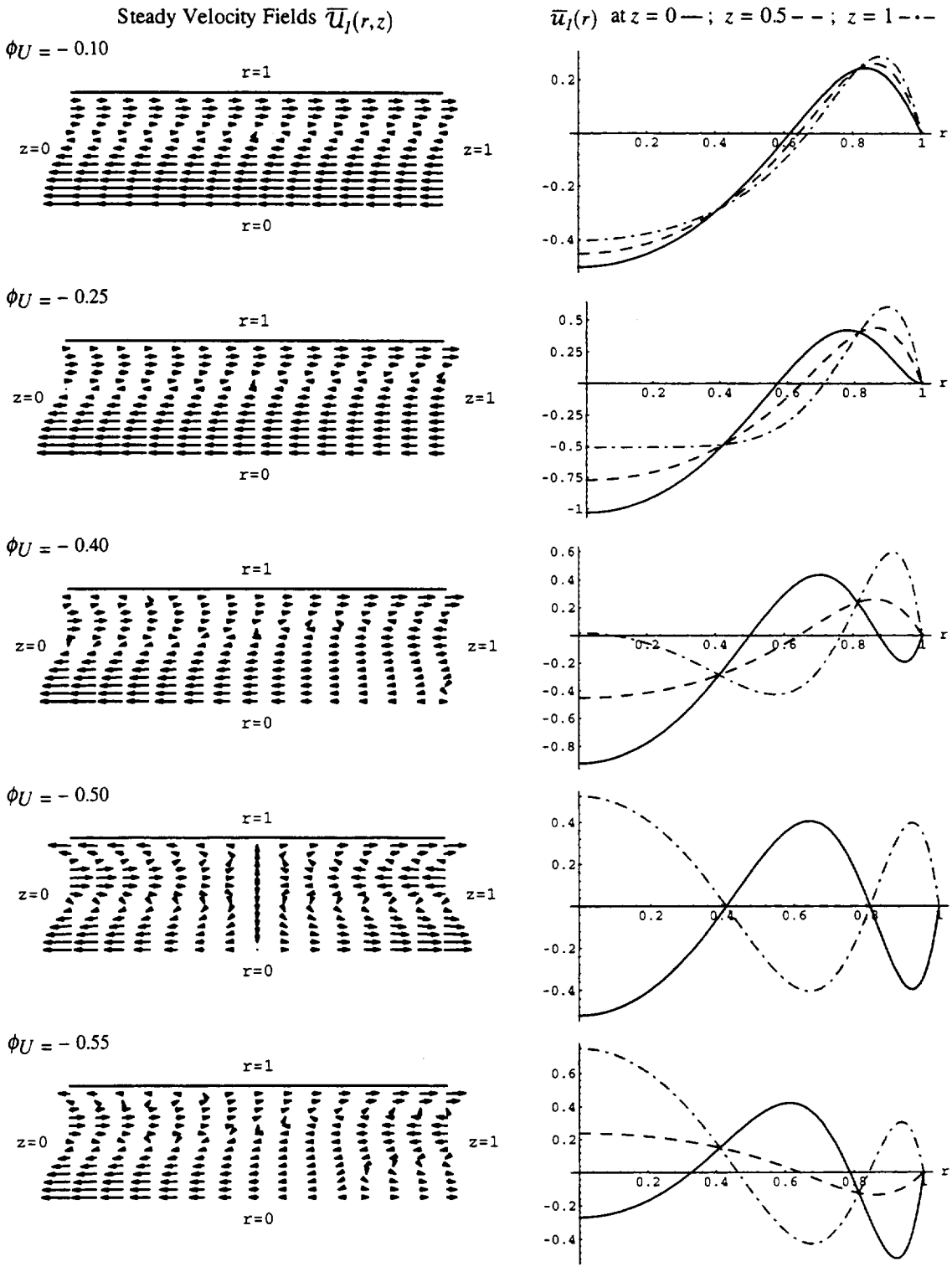

Figure 18. Effect of ϕ_U on the steady velocity for OPT: $\varepsilon = 0.002$, $Va = 100$, $\tilde{U}_L = 1$.

The mean-steady velocity field is a complicated function of velocity phase angle. In general, for $\phi_U < -0.40$ the centerline and diffusion-layer regions flow in opposite directions. For $\phi_U < -0.40$, flow reversals between the centerline and diffusion-layer regions become more pronounced because radial flow components become stronger. For $\phi_U = -0.25$, streaming is strongest, implying that at this phase angle, mean-steady flow quantities such as enthalpy flow, will be largest. Later, the mean-steady enthalpy flow will be shown to be a maximum at $\phi_U = -0.25$.

Particle Velocity, $\bar{\mathbf{u}}_p$

The mean-steady particle velocity, $\bar{\mathbf{u}}_p$, is used to compute the particle path, or pathline. It is the velocity in Lagrangian coordinates and it is different from the observed mean-steady Eulerian velocity given by $\overline{U_1}$. Appendix B provides details on the formulation of $\bar{\mathbf{u}}_p$, and appendix F outlines its computation. For $\varepsilon \ll 1$ the components of $\bar{\mathbf{u}}_p$ are

$$\bar{u}_p(r,z) = \overline{u_1} + \overline{u_{0,r}\int_0^t v_0 d\tau} + \overline{u_{0,z}\int_0^t u_0 d\tau} \tag{79}$$

and

$$\bar{v}_p(r,z) = \overline{v_1} + \overline{v_{0,r}\int_0^t v_0 d\tau} + \overline{v_{0,z}\int_0^t u_0 d\tau} \tag{80}$$

Equations (79) and (80) are simply the steady velocity conversions between Eulerian and Lagrangian coordinates. Interpreted physically, the oscillating components of velocity $\mathbf{u}_0$ push particles across mean-steady streamlines $\overline{U_1}$, which results in an additional drift quantified by the quadratic term $\left(\int_0^t \mathbf{u}_0\, d\tau \cdot \nabla \mathbf{u}_0\right)$.

Figure 19 plots $\bar{\mathbf{u}}_p(r)$ and $\overline{U_1}(r)$ at $z = 0$ for a BPT, with Va = 1, 10, and 100. The Eulerian and Lagrangian velocities are seen to be very similar for both axial and radial velocities. The BPT is a standing wave device, hence all local velocities generally are in-phase. The additional quadratic terms of equations (79) and (80) each contain a time integral of velocity, which when integrated, results in a 90° phase shift. The quadratic product thus becomes nearly zero since the product of two phasors that are 90° out of phase is zero. (The mean-steady product of two standing wave phasors is proportional to the cosine of their relative phase angle, according to eq. (7).)

Figure 20 shows the fields for $\overline{U_1}(r,z)$ and $\bar{\mathbf{u}}_p(r,z)$ for an OPT with $\tilde{U}_L = 1$, $\phi_U = -0.1$, and Va = 1, 10, and 100. Also shown are plots for $\overline{u_1}(r)$ and $\bar{u}_p(r)$ at $z = 0$, and $\overline{v_1}(r)$ and $\bar{v}_p(r)$ at $z = 0$. For Va = 1 and 10 there is a significant difference in the field plots between $\overline{U_1}$ and $\bar{\mathbf{u}}_p$. For Va = 1, $\overline{U_1}$ is seen to flow toward the middle of the tube at the centerline and then reverse flow near the walls, with $\overline{u_1} \approx 0$ near $z = 0.45$. The corresponding flow for $\bar{\mathbf{u}}_p$ shows a centerline flow that is continuous from left to right, with a reverse flow near the walls. The plot shows that $\overline{u_1}(r)$ is significantly smaller than $\bar{u}_p(r)$ for Va = 1 and 10, and the radial flows $\overline{v_1}(r)$ and $\bar{v}_p(r)$ are nearly equal. For Va = 100, $\overline{U_1}$ and $\bar{\mathbf{u}}_p$ are nearly the same.

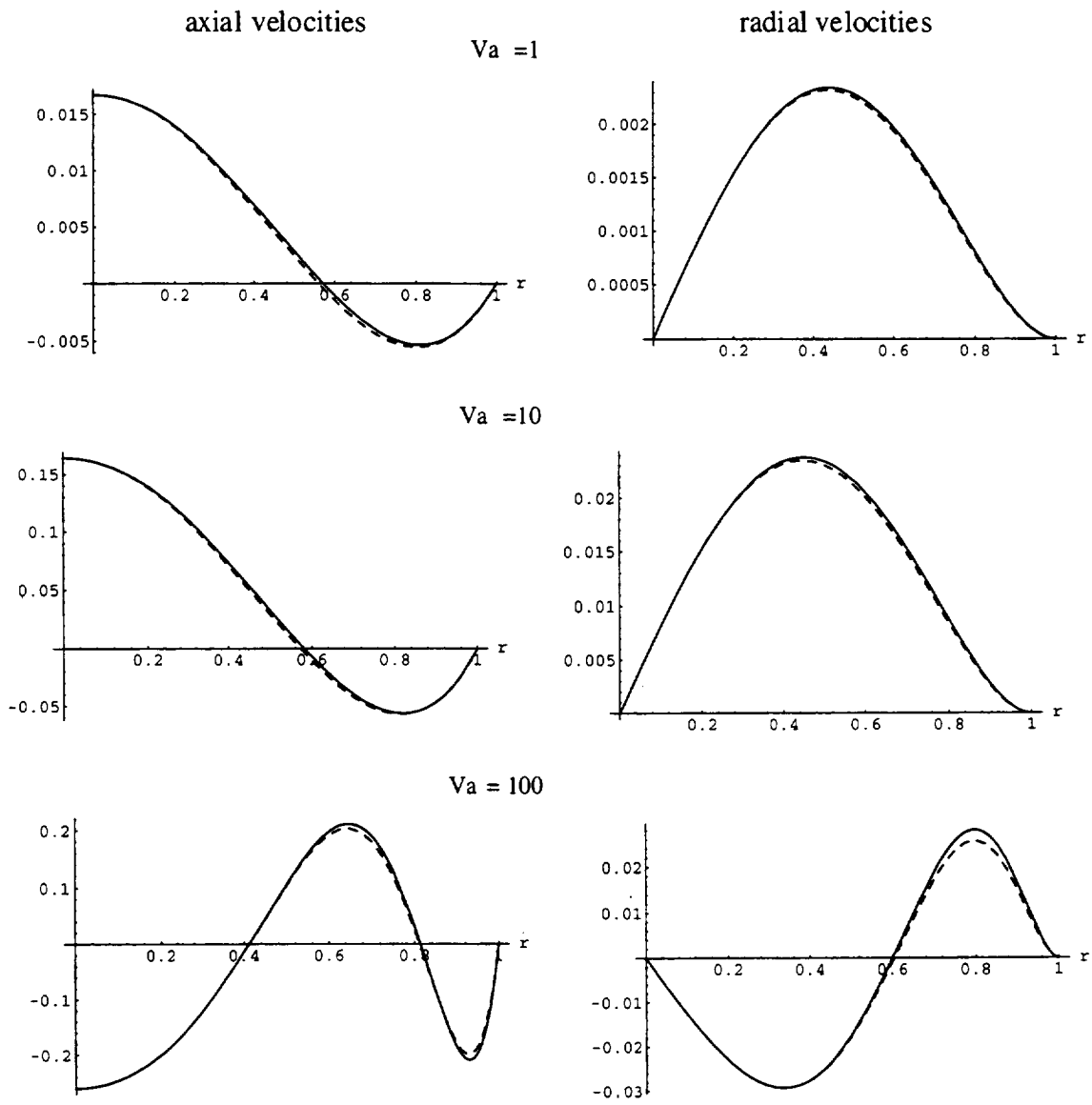

Figure 19. Comparison of Eulerian and Lagrangian particle velocities for the BPT at z = 0 and with Fo → 0: $\overline{U_1}(r)$ —; $\bar{u}_p(r)$ – –.

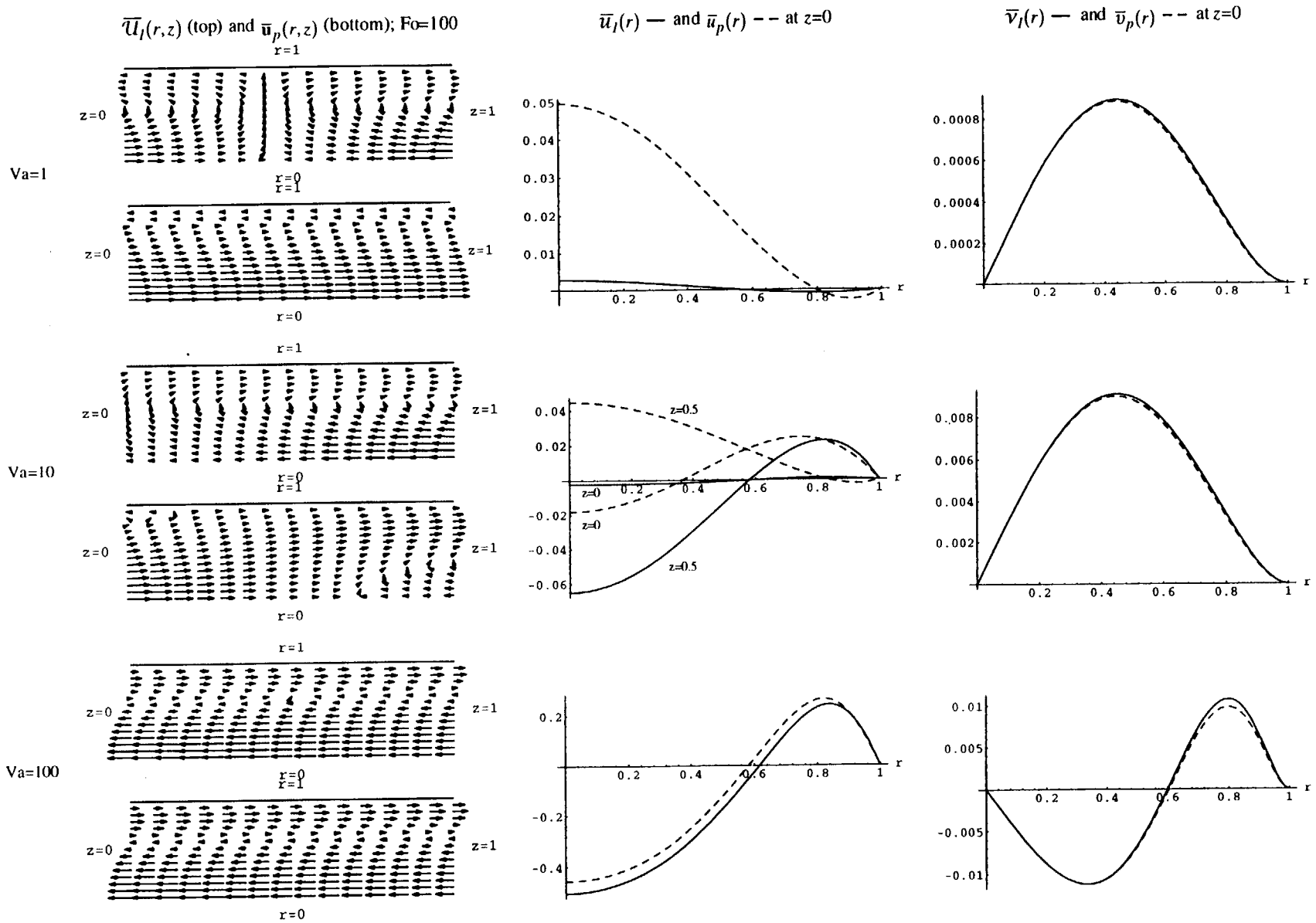

Figure 20. Comparison of Eulerian and Lagrangian particle velocities for OPT at z = 0, $\tilde{U}_L = 1$, and $\phi_U = -0.1$.

In general, for Va of about 1, the axial Eulerian and particle velocities have similar profiles; however, the Eulerian velocities are much more restrained. As Va increases to 10, the axial velocity profiles are no longer similar, being quite different in both direction and magnitude. For Va of 100, the fields become nearly identical in both speed and direction. The results reflect the large influence of the progressive wave component contained in the additional quadratic term of the particle velocity.

Effect of Heat Transfer on Particle Velocity

Figure 21 illustrates how heat transfer between the gas and the tube wall affects the mean-steady particle velocity for the BPT. The figure compares $\bar{u}_p$ at Fo $\rightarrow$ 0 and Fo = 100 for PrVa = 0.7, 7, and 70. For PrVa = 0.7, the axial velocity $\bar{u}_p$ for isothermal wall conditions (Fo $\rightarrow$ 0) is nearly the same as for the near adiabatic case (Fo = 100). Upon increasing to PrVa = 7, the adiabatic condition increases the axial velocity until it is about 30% greater than for the isothermal condition. For PrVa = 70, the adiabatic condition now reduces the axial velocity to about 50% less than that for the isothermal condition at the centerline; they are about equal in the outer layer; and the adiabatic case is greater by about 30% in the inner layer. For the radial velocity $\bar{v}_p$, the difference between the adiabatic and isothermal conditions increases with increasing PrVa.

Figure 22 illustrates the affect of heat transfer for the OPT on particle velocity and plots the same conditions for Fo and PrVa as for the BPT of figure 21. In general, Fo and PrVa have the same affect on the OPT velocities as for the BPT. One exception is that for PrVa = 70 the double boundary layer is not present in the OPT so that the streaming in the diffusion layer near the tube wall is in the opposite direction compared with the inner layer of the BPT. Also for the OPT at PrVa = 70, the streaming in the diffusion layer near the tube wall for adiabatic conditions is less than it is for isothermal conditions, whereas for the BPT, the streaming in the inner layer is greater for the adiabatic conditions than it is for the isothermal conditions.

The mean-steady velocity reduces pulse tube performance because it directly transports gas from the hot end to the cold end, and vice versa, thereby destroying the temperature gradient. The mean-steady velocity is rather a complicated function of Fo and its effect on velocities is not easily determined by simple examination of the solutions. The benefit of figures 21 and 22 is to give a general understanding of how PrVa and Fo influence mass streaming for the BPT and OPT.

For the BPT, the difference in viscous and thermal diffusion lengths provides the phase-shifting mechanism between velocity and temperature to produce enthalpy flow. In this case it is best that the PrVa be sized so that diffusion fills the entire gas domain and that the tube wall be sized for Fo $\rightarrow$ 0 (isothermal wall condition). A good value of PrVa is about 7, as indicated in figure 21. These conditions allow diffusion over the gas domain while at the same time reducing mean-steady streaming (relative to the adiabatic wall condition).

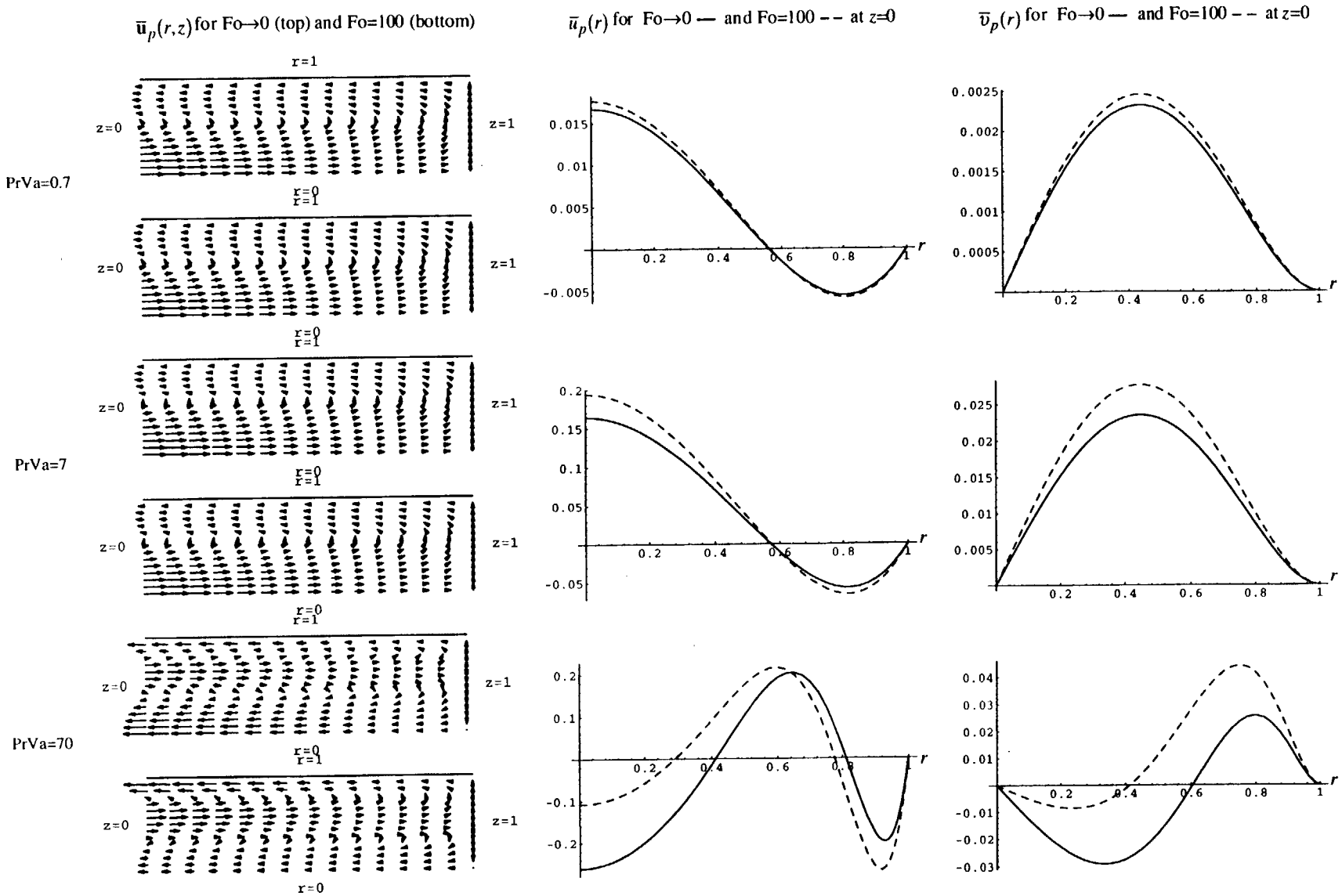

Figure 21. Heat-transfer effect on particle velocity for BPT.

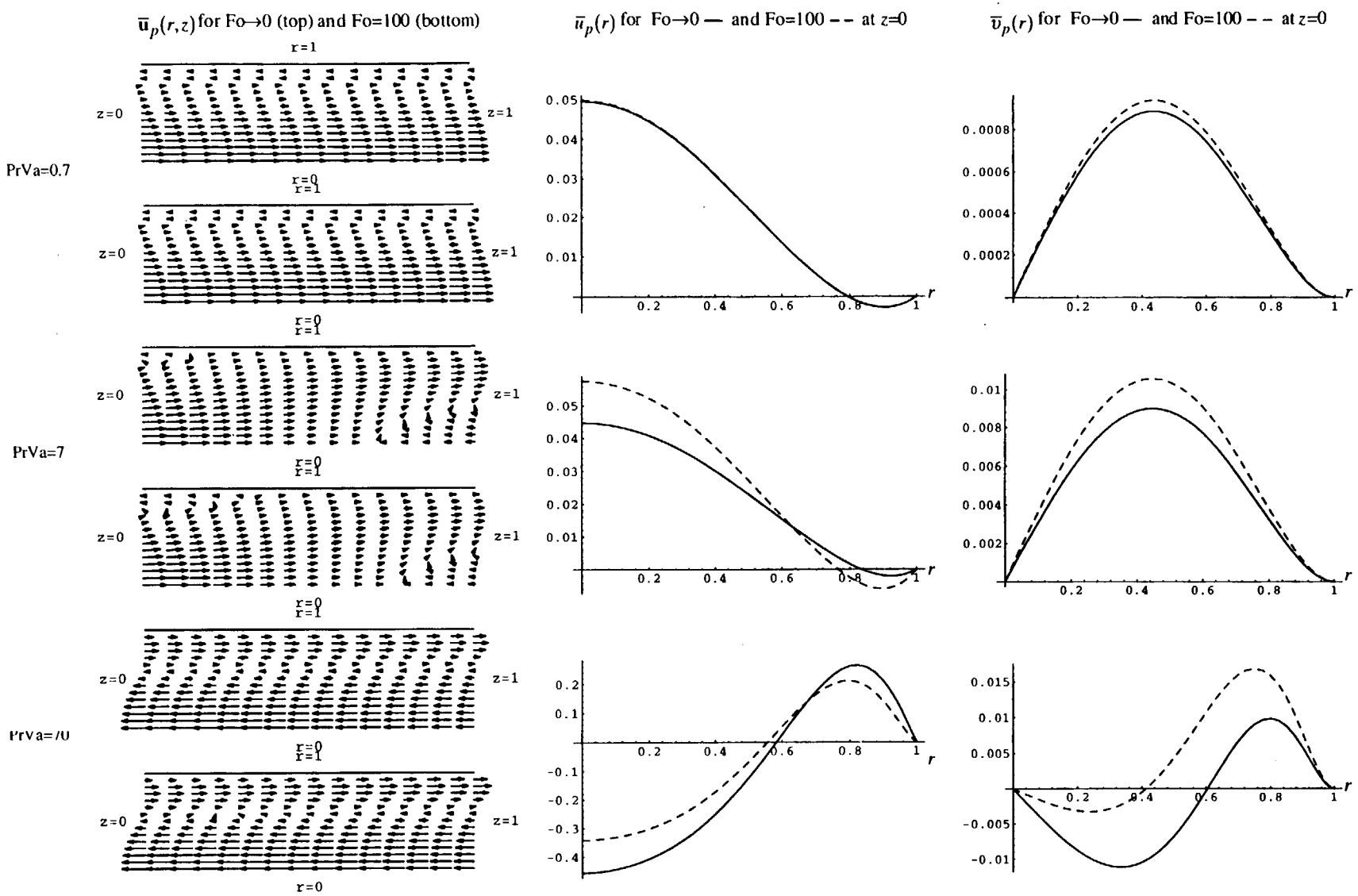

Figure 22. Heat-transfer effect on particle velocity for OPT: $\varepsilon = 0.002$, $\tilde{U}_L = 1$, and $\phi_U = -0.1$.

For the OPT, the velocity boundary conditions at the tube ends provide the phase-shifting mechanism. Diffusion is not required and, in fact, diffusion will reduce enthalpy flow by reducing the velocity and temperature amplitudes near the tube wall. Operation at large PrVa and large Fo (adiabatic wall conditions) is desirable because the diffusion layer now is confined to a thin layer near the tube wall. From figure 22 for PrVa = 70, the mean-steady axial velocity plot shows that for Fo = 100, the steady axial particle velocity is reduced relative to Fo $\rightarrow$ 0. The combination of large PrVa and large Fo confines the diffusion layer to be thin while at the same time it reduces mean-steady streaming (relative to the isothermal wall condition).

Mean-Steady Temperature, $\overline{T}_2$

The mean-steady temperature $\overline{T}_2$ is found by a double quadrature of equation (m) in table 3 with $T_{0,z} = 0$. In conservative form it is

$$\frac{1}{\mathrm{Pr\,Va}} \frac{\left(r\overline{T}_{2,r}\right)_{,r}}{r} = \left(\overline{u}_1 + \overline{p_1 u_0}\right)_{,z} + \frac{1}{r}\left(\overline{v}_1 r + \overline{p_1 v_0} r\right)_{,r} \tag{81}$$

which shows that $\overline{T}_2$ is a result of the axial and radial work flows. That is, gradients in conductive heat transfer are a result of gradients in work flow.

Figure 23 shows $\overline{T}_2(r)$ for the BPT and OPT with Fo $\rightarrow$ 0 and Fo = 100, and PrVa = 0.7, 7, and 70. The mean-steady temperature is constant in z. The plots show that for PrVa = 0.7 and 7, heat is continuously being transferred to the wall. For PrVa = 70, heat is also being transferred to the centerline region. Physically, this would result in the centerline region heating. However, for the present thermally strong approximation ($T_{0,z} = 0$), there is an "imposed" thermal sink that maintains T_0 constant.

Axial Enthalpy Flow, $\overline{H}_1$

The first-order steady enthalpy flux is given by $\overline{h}_1 = T_0 \rho_0 \overline{u}_1 + T_0 \overline{\rho_1 u_0} + \rho_0 \overline{T_1 u_0}$, which after rearrangement becomes

$$\overline{h}_1 = T_0\left(\rho_0 \overline{u}_1 + \overline{\rho_1 u_0}\right) + \rho_0 \overline{T_1 u_0} \tag{82}$$

When integrated over the cross-sectional area, equation (82) is the enthalpy flow. It is important because it quantifies cooling,

$$\overline{H}_1 = \int_0^1 \left[T_0\left(\rho_0 \overline{u}_1 + \overline{\rho_1 u_0}\right) + \rho_0 \overline{T_1 u_0}\right] r dr \tag{83}$$

From the zero-net-mass-flow constraint (eq. (48)) and since $T_0(z)$ is independent of r, the first term in equation (83) is zero. Recalling that $\rho_0 = 1$, the enthalpy flow becomes

$$\overline{H}_1 = \int_0^1 \overline{T_1 u_0} r\, dr \tag{84}$$

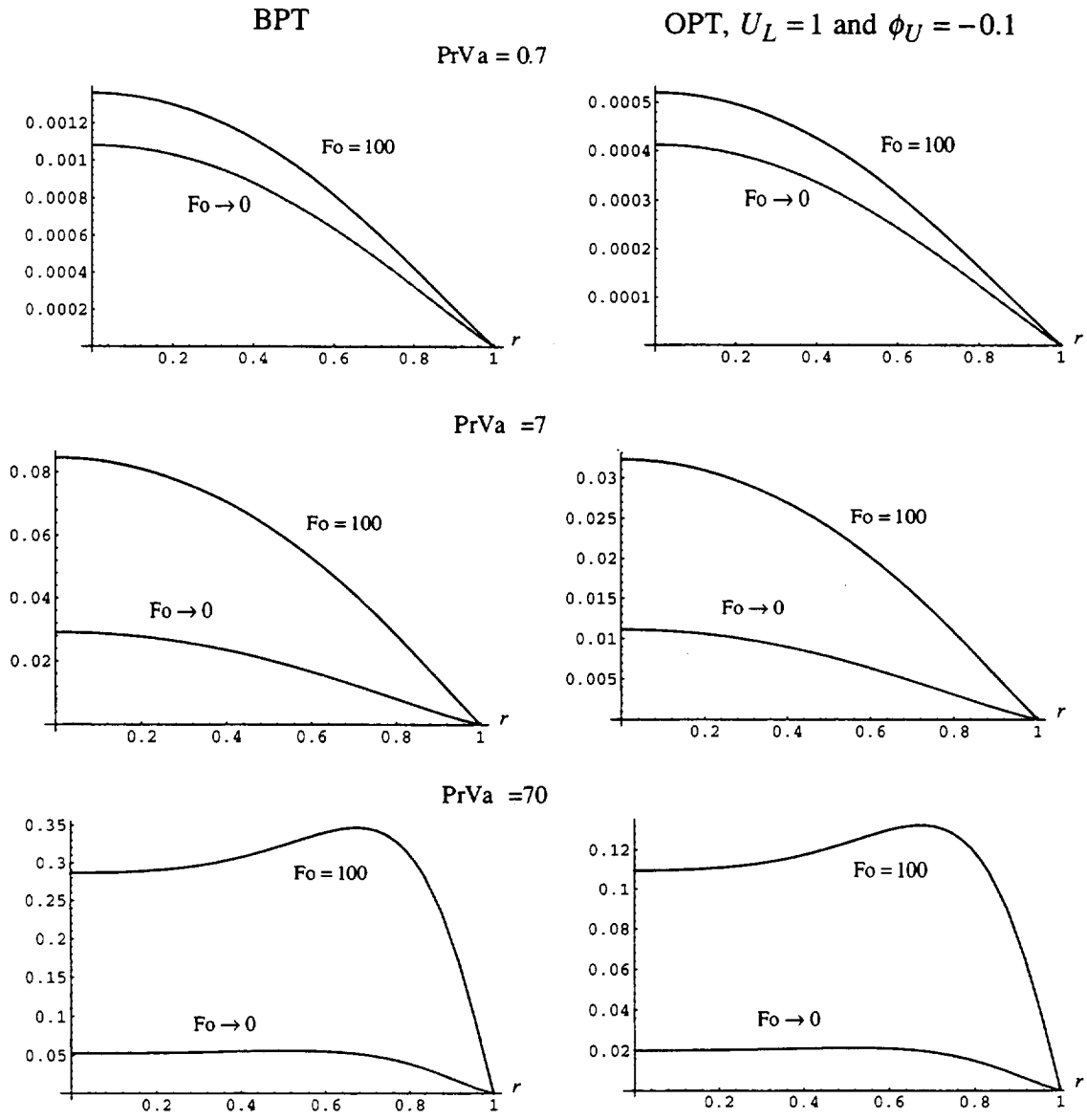

Figure 23. Comparison of $\overline{T}_2(r)$ for BPT and OPT at z = 0 and z = 1 forFo → 0 and Fo = 100.

which shows that the mean-steady enthalpy flow at $O(\varepsilon)$ is due to the time-averaged product of the oscillating temperature and the oscillating velocity.

Using the equation of state, equation (84) can be rewritten in terms of the work flow pu,

$$\overline{H}_1 = \int_0^1 \left(\overline{u_1} + \overline{p_1 u_0}\right) r\, dr \tag{85}$$

which shows that the enthalpy has two work flow components: the product of the oscillating pressure and oscillating velocity, and work flow due to mean-steady streaming, $p_0\bar{u}_1$, where $p_0 = 1$.

Figure 24 shows enthalpy transport for the BPT. Shown are enthalpy flux fields $\bar{h}_1(r,z)$ for PrVa = 0.7, 7, and 70 and Fo $\rightarrow$ 0 and Fo = 100. Corresponding plots for $\bar{h}_1(r)$ are for $z = 0$ and $z = 0.5$, with $\bar{h}_1 = 0$ at $z = 1$. For the isothermal wall condition of Fo $\rightarrow$ 0, axial enthalpy flux decreases from $z = 0$ to $z = 1$.

For Fo = 100, there is a reversal of enthalpy flux in the vicinity of the wall. The enthalpy reversal results from the inability of radial temperature gradients to be generated because of the near-adiabatic wall conditions for Fo = 100, that is, sufficient heat cannot be transferred to the wall. Operating a BPT with high Fo is undesirable because of the large enthalpy flow reversal near the tube wall.

Figure 25 shows the corresponding enthalpy transport for the OPT with $\tilde{U}_L = 1$ and $\phi_U = -0.1$. The plots of $\bar{h}_1(r)$ are shown for $z = 0$, 0.5, and 1. The OPT allows velocity oscillations at $z = 1$, which enable enthalpy to flow out of the tube, whereas in the BPT enthalpy flow goes to zero at $z = 1$ since the velocity goes to zero. For the case of PrVa = 0.7 and Fo $\rightarrow$ 0, enthalpy flows in the reverse direction from $z = 1$ to about $z = 0.6$, showing that an OPT operating with isothermal walls and small PrVa is not desirable.

In general, a BPT should be operated with the thermal diffusion length and tube radius sized so that PrVa $\approx$ 10 and the tube wall is near isothermal, Fo $\rightarrow$ 0. The Fo $\rightarrow$ 0 condition allows good heat transfer between the gas and wall so that the phase angles between the velocity and temperature are advantageous for enthalpy flow. The PrVa $\approx$ 10 condition sizes the gas domain so that all of the gas is efficiently transporting enthalpy. Figure 24 illustrates the enthalpy flux for these conditions.

The OPT should be operated with the thermal diffusion region confined to a thin layer near the tube wall and the tube wall near adiabatic. These conditions correspond to large PrVa and large Fo. For the OPT, diffusion is no longer necessary in order to supply the correct phase angle between velocity and temperature. The phase angle is supplied by the velocity boundary conditions at the tube ends. An example of the enthalpy flux for these conditions is shown in figure 25 for PrVa = 70 and Fo = 100.

In figure 26, enthalpy flow $\bar{H}_1(z)$ is plotted for the BPT and OPT with $\tilde{U}_L = 1$ and $\phi_U = -0.1$ for PrVa = 0.7, 7, and 70; and for Fo $\rightarrow$ 0 and Fo = 100. For the BPT (first column), adiabatic wall conditions (Fo = 100, dashed line) reduce enthalpy flow, particularly for large PrVa. For the OPT (second column), enthalpy flow is greater and more constant for adiabatic wall conditions. This is very apparent for large values of PrVa.

The plots of figure 26 reiterate the previous assertion regarding heat transfer to the tube wall. For the BPT, heat transfer between the gas and the tube wall is necessary and desirable to allow for the proper phase angle between velocity and temperature, whereas for the OPT, heat transfer is undesirable. For the OPT, the phase shift is supplied by the velocity boundary conditions at the tube ends.

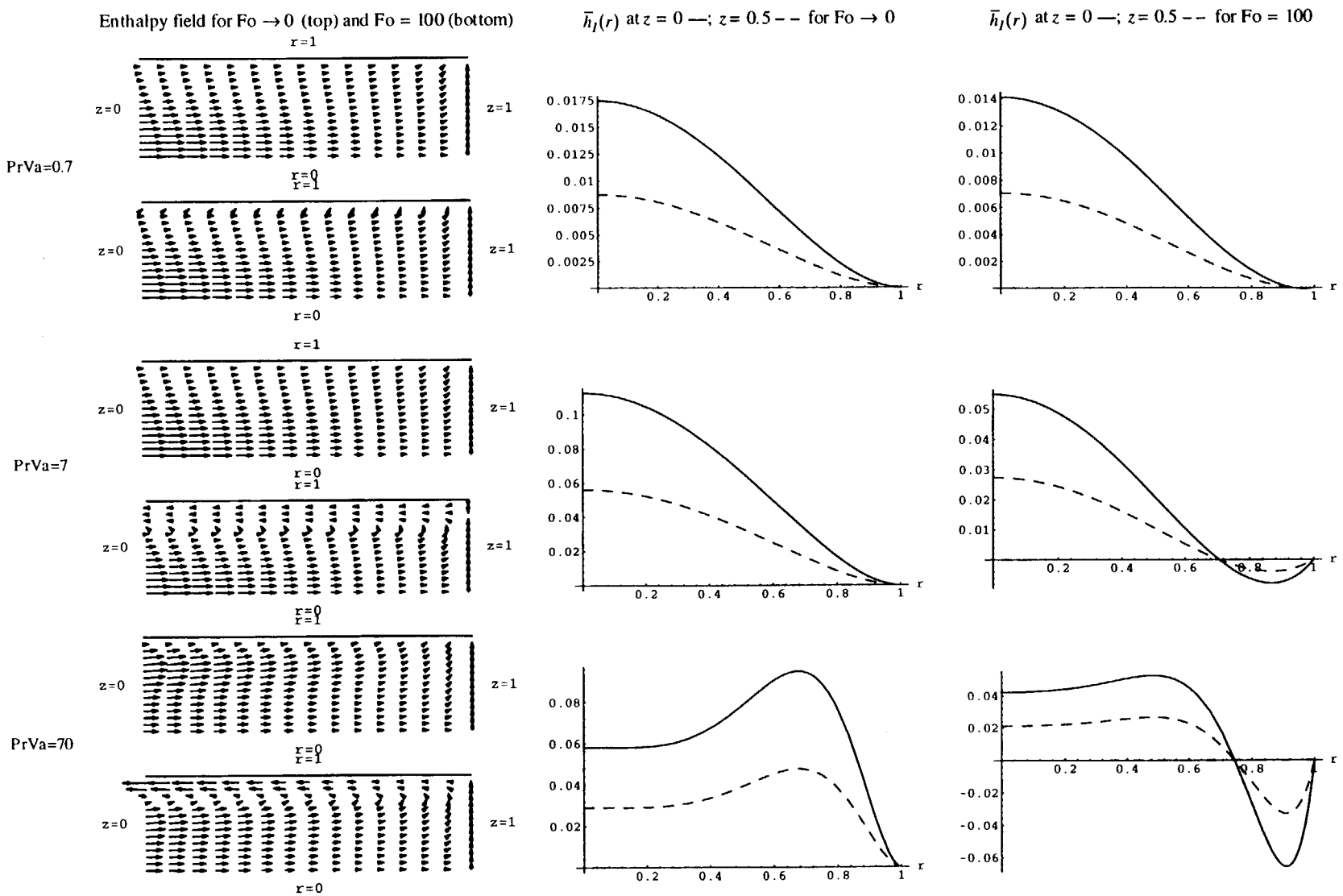

Figure 24. Enthalpy transport for BPT.

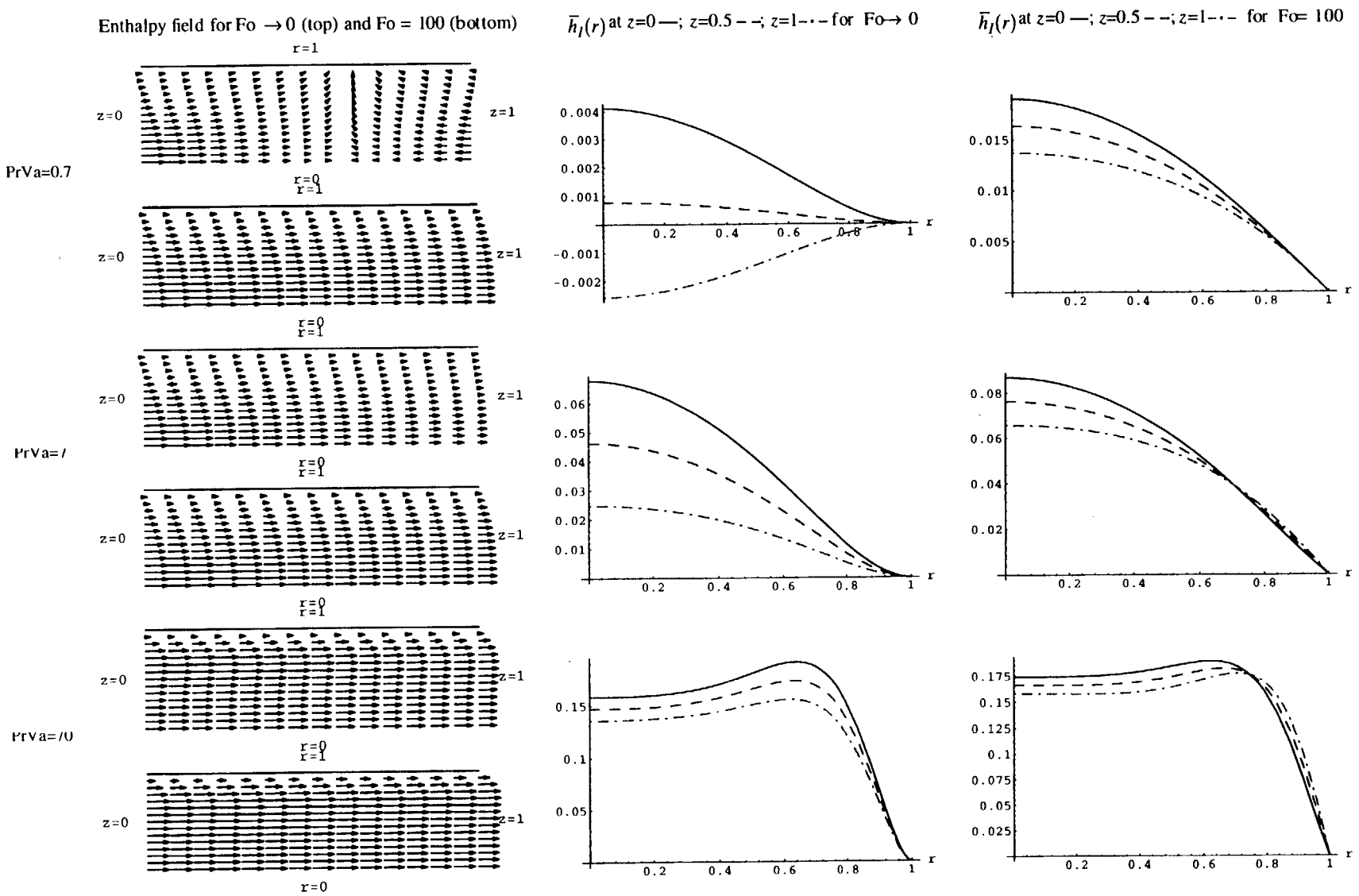

Figure 25. Enthalpy transport for OPT with $\tilde{U}_L = 1$ and $\phi_U = -0.1$.

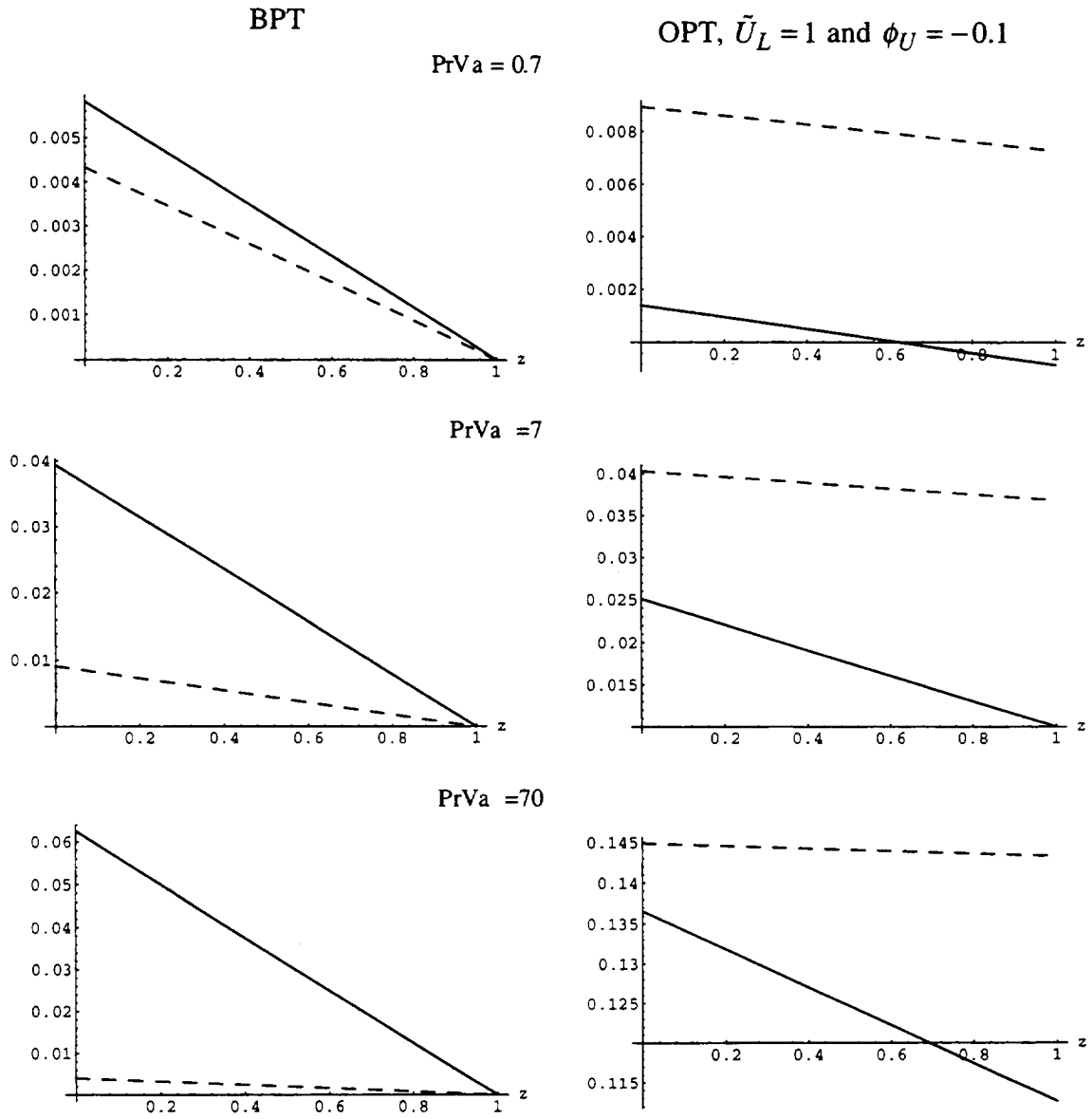

Figure 26. The effect of heat transfer on enthalpy flow, $\overline{H}_1(z)$, for the BPT and OPT for Fo → 0 —; Fo = 100 – –.

The amplitude-squared dependence of the mean-steady quantities on leading-order velocity was previously mentioned at the beginning of this section. Although it has not been investigated here, Storch et al. found refrigeration to depend on the square of the pressure ratio, where the pressure ratio is defined as the maximum pressure divided by the minimum pressure (ref. 35). This is consistent with the results of the present study since, for a given frequency, the oscillating pressure depends on fluid displacement at the tube ends, which is the integrated velocity at leading order.

In figure 27, the area-normalized enthalpy flux versus ϕ_U is plotted for the conditions of $\varepsilon = 0.1$, $\mathrm{Va} = 250$, $\mathrm{Pr} = 0.7$, $\tilde{U}_L = 1.0$, $\mathrm{Fo} = 20$, and $\gamma = 5/3$. The figure shows a peak in the area-averaged enthalpy flux at $\phi_U \approx -0.25$. This is reasonable considering that maximum mean-steady velocity streaming was seen in figure 18 to be at $\phi_U \approx -0.25$. Kasuya et al. (ref. 68) measured optimum phase angles, and Radebaugh reported that for a typical OPT, $\phi_U \approx -0.1$ (ref. 11). However, increasing the phase angle leads to increased velocities in the regenerator, which results in larger regenerator losses. Thus $\phi_U \approx -0.1$ would be relevant for use as a system optimum.

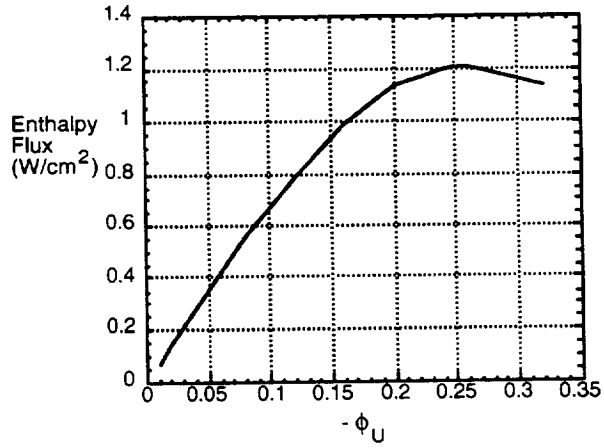

Figure 27. Area-normalized enthalpy flux versus velocity phase angle. Maximum occurs at $\phi_U \approx -0.25$.

Discussion

The calculated leading-order quantities for pressure, temperature, velocity, and heat transfer, the mean-steady velocity and enthalpy flux fields, and the mean-steady temperature give an understanding of the transport mechanisms for pulse tubes.

The BPT is essentially a standing wave device, because there are no phase-angle gradients along the tube length. Phase shifts between velocity and temperature—required for enthalpy flow—are obtained through differences in the viscous and thermal diffusion lengths. The ratio is quantified in the Prandtl number. A BPT is able to operate when $\mathrm{Pr} < 1$; the lower the Prandtl number the better. A Prandtl number of $\mathrm{Pr} = 1$ results in zero enthalpy flow.

The BPT should be operated with an isothermal tube wall to enable a large heat transfer between the gas and tube wall. This requires the Fourier number to be near zero, $\mathrm{Fo} \to 0$. Operating a BPT with a large value for Fo (adiabatic wall condition) would result in enthalpy flow reversals (enthalpy flow from hot to cold ends) near the tube wall, a result of the inability of the work flow to convert to heat flow. Calculations also show that an isothermal tube wall reduces mass streaming relative to an adiabatic wall. Mass streaming has a negative affect on performance, because streaming directly transports hot gas to the cold end, and vice versa. This tends to destroy the axial temperature gradient. The tube radius of the BPT should also be sized to the thermal diffusion length

so that all of the gas is efficiently transporting enthalpy. The calculations show that to accomplish this, the Prandtl number times the Valensi number should be PrVa ≈ 10 for the BPT.

The OPT is more of a progressive wave device and so it does not rely on diffusion to obtain the appropriate phase angles between velocity and temperature. Phase angles are obtained through the velocity boundary conditions. The OPT should be operated with the thermal diffusion region confined to a thin layer near the tube wall. This condition requires PrVa and Fo to both be large. The calculated plots of mean-steady velocity show that large Fo reduces mass streaming relative to Fo $\rightarrow$ 0. However, large Va tends to increase mass streaming.

Operating at small PrVa and small Fo is detrimental to an OPT because heat transfer between the gas and the tube wall (1) reduces the oscillating temperature amplitude near the tube wall, and (2) creates unwanted phase angles between velocity and temperature. Both of these effects tend to reduce enthalpy flow. There is a practical limitation to having both PrVa and Fo very large, for these requirements lead to a system that must contain high pressures with a large diameter, thin-walled tube. Also, the compressor must be large to drive a larger system with a large tube diameter.

An additional advantage of the OPT over the BPT is the ability to also have independent control of the velocity amplitudes. The large velocity amplitude of the OPT at the hot end of pulse tube ($z = 1$) allows much more enthalpy flow relative to the BPT whose velocity goes to zero. For the BPT, because of the steep velocity gradients along the tube, enthalpy flow is continuously being converted to heat flow along the tube at a high rate. The heat then flows back to the cold end as heat conduction. As a consequence, only a small amount of enthalpy flow arrives near the hot heat exchanger for rejection to the environment. For the OPT, because the velocity is finite at the hot end of the tube, more enthalpy flow can arrive near the hot heat exchanger. Larger amounts of enthalpy flow can then be rejected at the hot heat exchanger.

Heat transfer between the gas and the tube wall has an important effect on the pressure and temperature phasors. When there is significant heat transfer between the gas and tube wall, Fo = $\boldsymbol{O}(1)$, the pressure and temperature phasors move out of phase relative to each other for both the BPT and OPT; calculations indicate this difference to be as much as 20°. This is important, because 1-D models often assume adiabatic conditions on the gas and so there is a presumption that the temperature is always in phase with pressure. Most pulse tubes operate at Fo = $\boldsymbol{O}(1)$, which is closer to isothermal wall conditions.

At the tube ends, the complex Nusselt number is found to be independent of Fo, of the velocity amplitude ratio $\tilde{U}_L$, and of the velocity phase angle ϕ_U. When written in the form $\hat{\mathrm{Nu}}(\mathrm{PrVa}) = \tilde{A}\, e^{i\phi}$, $\tilde{A}$ is about 4 for PrVa < 3 and is linear with PrVa for PrVa > 25. The phase angle for PrVa < 0.5 is $\phi \rightarrow -0.5$ and for PrVa > 500, $\phi \rightarrow -0.38$. A similar relation for the complex shear wall factor exists, using only Va as the independent parameter. The complex Nusselt number and shear wall factor can be used for one-dimensional linear oscillating flow in a tube to account for radial heat transfer or shear at the tube wall.

The axial velocity was found to be a complicated function of Va and ϕ_U. The mean-steady velocity increases linearly with Va for Va < 10, and can be of $\boldsymbol{O}(1)$ for Va > 100. It is strongest when $\phi_U \approx -0.25$.

In general, an OPT should be operated with large PrVa and $\phi_U \approx -0.25$. This maximizes mean-steady enthalpy flow. However, since mass streaming is of the same mechanism as the mean-steady enthalpy flow, losses owing to mass streaming and the destruction of the axial temperature gradient will also be maximum. Understanding the trade-off between mean-steady enthalpy flow, mass streaming, and axial temperature gradient requires a solution to the coupled zeroth-, first-, and second-order equations. That is left for future work.

5. EXPERIMENTAL MEASUREMENTS OF THE MEAN-STEADY PARTICLE VELOCITY

A flow-visualization system was constructed to permit observation of particle flow patterns and measurement of particle velocities. In this section, the observed patterns are presented and interpreted within the framework of the anelastic solution.

Experimental System

A schematic of the experimental flow-visualization system is illustrated in figure 28. A clear polycarbonate tube (38.9 cm long, 2.22 cm i.d., and 2.54 cm o.d.) is filled with air at 1 atm mean pressure. Diaphragm compressors are attached to each end of the tube and are sealed from the ambient. The compressors are each driven by separate stepper motors capable of 25,000 steps per revolution. The compressor/motor assemblies can be independently controlled in order to adjust the relative phase angle between them. Three 0.00- cm stainless steel wires are strung across the tube diameter at the indicated positions, and a light oil is applied to the wires before operation. The surface tension of the oil is sufficient to hold a thin film on the wires. During operation, when the compressors are producing an oscillating flow, a short pulse of electrical current (~0.1 sec duration) is applied to a wire. This quickly heats and vaporizes the oil from the wire. There is no combustion of the oil— only vaporization. The vaporized oil quickly cools and condenses into an oil fog or "smoke" that stretches across the tube diameter. One can now observe the leading-order oscillating flow and the secondary mean-steady flow of the smoke, which represent particle paths of the gas.[1] A CCD video camera (30 frames/sec) is used to record the smoke flow patterns.

Figure 28 also shows the physical dimensions of the system. The volume displacement of the two compressors is 13.5 cm^3 each, and the total system volume is 155.2 cm^3, resulting in $\varepsilon = 0$ .0435. The volumes of the connections between the compressors and tubes are converted into equivalent lengths by dividing the volumes by the connector cross-sectional area (3.88 cm^2). The range of speed of the compressors is 5 to 20 Hz. Smoke-wires are positioned at z = 11.0 cm, 20.4 cm, and 32.1 cm. The tube was oriented with the gravity force acting in the positive z-direction. During operation, the smoke is generally neutrally buoyant.

When operating, the speed and the relative phase angle between the two compressors are fixed. The compressors are then started and allowed to come up to the final operating speed, at which time the video camera begins recording. After about 10 sec have elapsed (to ensure quasi-steady flow), the smoke-wire is pulsed with electrical current, and the smoke is seen to immediately leave the wire. Initially, when the smoke comes off the wire, it rises against the gravitational-force vector because of buoyancy, that is, the smoke is warmer (less dense) than the surrounding air. This condition exists for about 2 sec until the smoke temperature and the surrounding air temperature equilibrate. The video camera records the particle paths of the smoke at 30 frames/sec, and records a time tag on each frame. After the smoke dissipates, which takes from 20 to 80 sec, the system is shut down and reset for the next run.

---

[1] The "particles" tracked were more like "blobs," diffuse yet distinguishable.

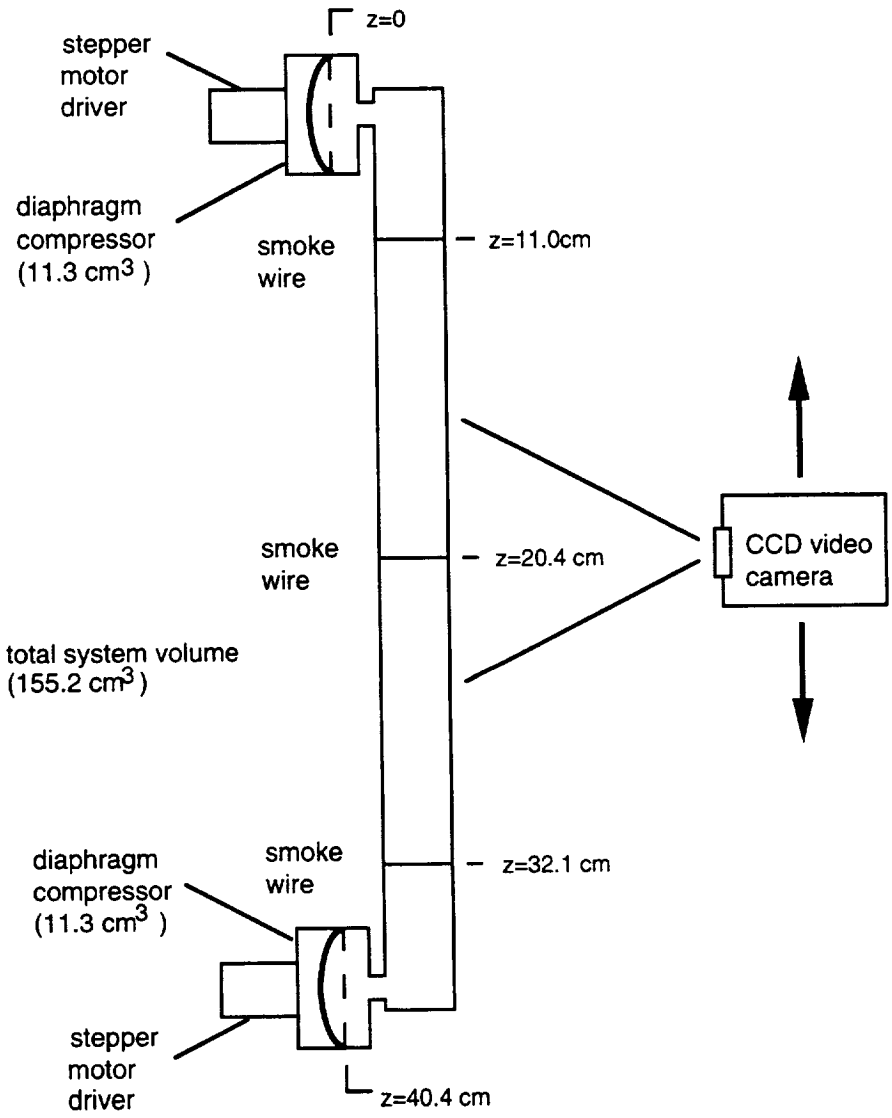

Figure 28. Schematic of the smoke-wire flow-visualization experiment.

Coordinate positions of the smoke for each time were determined by digitizing each individual video frame. Particle velocities were determined from the coordinates and incremental times. The measured particle velocities were then compared with predicted values.

Comparison with Theory

Several runs were conducted to compare the experimentally measured mean-steady axial particle velocities with those predicted by equation (79). Table 6 summarizes the dimensionless quantities investigated. The BPT configuration was tested for varying Va, and the OPT configuration was tested for varying Va and ϕ_U. There was no independent variation of $\tilde{U}_L$, because the velocity boundary conditions defined by $\tilde{U}_L$ should have no unusual effects on $\bar{u}_p(r,z)$ since $\bar{u}_p(r,z)$ is simply linear along z. There was also no variation in Fo since Fo << 1 for any of the runs

(isothermal wall conditions). The following section presents and compares the experimental results against calculations. The code for computing the solutions is given in appendix G, and the data are tabulated in appendix H.

Table 6. Range of dimensionless numbers investigated

Run	1	2	3	4	5	6
Configuration	BPT	BPT	OPT	OPT	OPT	OPT
Evaluation	Velocity	Velocity	Observation	Observation	Velocity	Velocity
ε	0.0434	0.0434	0.0434	0.0434	0.0434	0.0434
Va	**34**	**103**	**137**	**137**	**68**	**68**
M	1.66×10^{-3}	5.06×10^{-3}	6.7×10^{-3}	6.7×10^{-3}	3.14×10^{-3}	3.14×10^{-3}
λ	4.5×10^{-5}	4.13×10^{-4}	7.3×10^{-4}	7.3×10^{-4}	1.62×10^{-4}	1.62×10^{-4}
$\tilde{U}_L$	0	0	1	1	1	1
ϕ_U	n/a	n/a	**– 0.5**	**– 0.94**	**– 0.254**	**– 0.125**

Basic Pulse Tube Configuration

Axial particle velocities $\bar{u}_p(r,z)$ were measured near the centerline of a BPT configured system for Va = 34 and Va = 103. The measured velocities were in the vicinity of the centerline region.

Run 1: BPT, Va = 34

Figure 29 shows the mean-steady particle path and particle velocity of a smoke particle. This is shown by plotting the axial particle velocity $\bar{u}_p(r,z)$ at the specified r and z positions and comparing this with the calculated $\bar{u}_p(r,z)$ given by equation (79). Figure 29(a) shows the calculated flow field $\bar{\mathbf{u}}_p(r,z)$, figure 29(b) plots $\bar{u}_p(r)$ and $\bar{v}_p(r)$ at $z = 0$, and figure 29(c) compares the measured

values of $\bar{u}_p(r,z)$ with those predicted by theory. The ordinate of figure 29(c) gives the measured and calculated values for $\bar{u}_p(r,z)$, and the corresponding r and z coordinates. The abscissa identifies the corresponding time for each $\bar{u}_p(r,z)$. Figure 29(c) shows that the calculated velocities are in general agreement with the measured values in terms of speed and direction. Velocities are positive for the particle coordinate range $r \approx 0.2$ to 0.24 and $z \approx 0.67$ to 0.72. As time progresses, the particle moves toward $z = 1$, as shown by the flow field in figure 29(a). Since the particle is at $r = 0$, there is

Fig. (a) Steady velocity fields $\bar{\mathbf{u}}_p(r,z)$

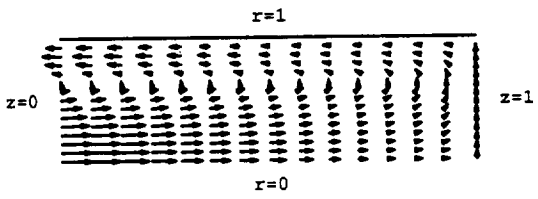

Fig. (b) $\bar{u}_p(r)$ — at $z = 0$; $\bar{v}_p(r)$ - - -

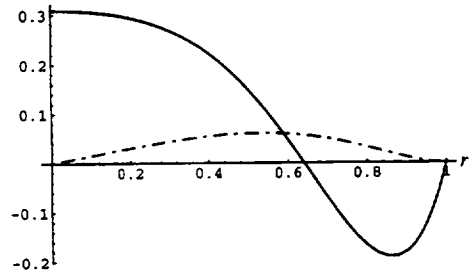

Fig. (c) Comparison of measured and calculated $\bar{u}_p(r,z)$

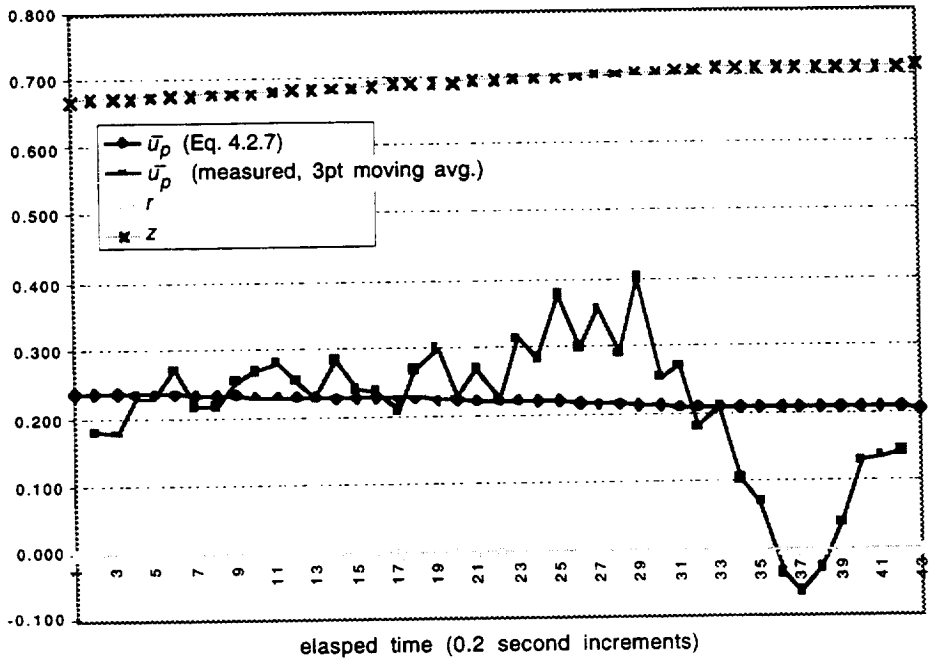

Figure 29. Particle velocity for BPT, $\varepsilon = 0.0435$, $Va = 34$, $U_L = 0$: (a) particle velocity field, $\bar{\mathbf{u}}_p(r,z)$; (b) calculated component velocities $\bar{u}_p(r)$ and $\bar{v}_p(r)$ at $z = 0$; (c) plot of measured particle coordinates, and measured and calculated axial particle velocity $\bar{u}_p(r,z)$ for corresponding elapsed times.

no radial flow component and so the particle remains at $r = 0$. It is unclear why the measured velocities decrease to zero for elapsed times greater than 35 sec although it may be a result of inaccurate particle tracking, since the smoke dissipates as time progresses.

Run 2: BPT, Va = 103

The particle flow field shown in figure 30(a) shows that for higher Va a double boundary layer is formed. Figure 30(b) shows that the velocity in the inner layer ($r = 0.8$ to 1) is negative, then reverses in the outer layer ($r = 0.38$ to 0.8) to positive, then again reverses itself in the centerline region ($r = 0$ to 0.38) back to negative. A positive and negative radial flow maintains mass conservation.

The measured $\bar{u}_p(r,z)$, the calculated $\bar{u}_p(r,z)$, and r and z coordinates at the given time intervals are plotted in figure 30(c). The measured negative velocities are in the centerline region and are comparable to those predicted. The larger negative velocities measured at the initial points are a result of the buoyancy forces present after the initial pulse. As time progresses, the temperature equilibrates between the smoke and the air, and so the velocity levels off.

The presence of the inner and outer layers of the double boundary layer predicted by theory could not be confirmed experimentally. This is because the smoke did not distribute itself in either of these two layers after pulsing. The simplicity of these experiments did not allow for observation of velocities throughout the entire field. Future work—perhaps with laser Doppler or anemometer velocity measuring instruments—will allow for further validation.

Orifice Pulse Tube Configuration

Orifice pulse tube observations

Mean-steady secondary flow observations for an OPT configuration are described for Va = 137, $\tilde{U}_L = 1.0$ with $\phi_U = -0.5$ and $\phi_U = -0.94$. The observed smoke flow is in qualitative agreement with the predicted particle velocity fields.

Run 3: smoke flow observations for $\phi_U = -0.5$

Figure 31 shows the observed steady flow for Va = 137, $\tilde{U}_L = 1$, and $\phi_U = -0.5$. Figures 31(a) and 31(b) predict large negative radial velocities at $r \approx 0.4$ and large axial velocities in both the negative and positive directions symmetric about $z = 0.5$. This is verified from the smoke observation data shown in figure 31(c) where the two smoke lines are seen to "stretch" in the axial direction and "compress" together in the negative radial direction. This is predicted by the particle velocity field of figure 31(a), and is an indication of the presence of the outer layer and centerline flow regions. Unfortunately, smoke did not distribute near the tube wall, so the presence of the inner layer could not be directly confirmed.

Fig. (a) Steady velocity fields $\overline{\mathbf{u}}_p(r,z)$

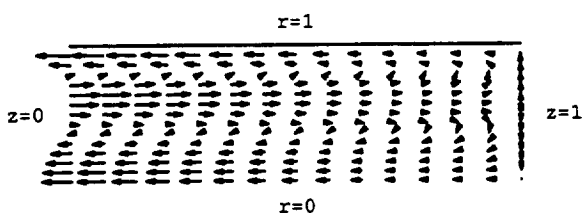

Fig. (b) $\overline{u}_p(r)$ — at $z = 0$; $\overline{v}_p(r)$ -·-

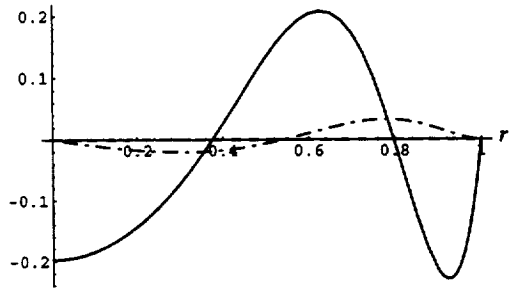

Fig. (c) Comparison of measured and calculated $\overline{u}_p(r,z)$

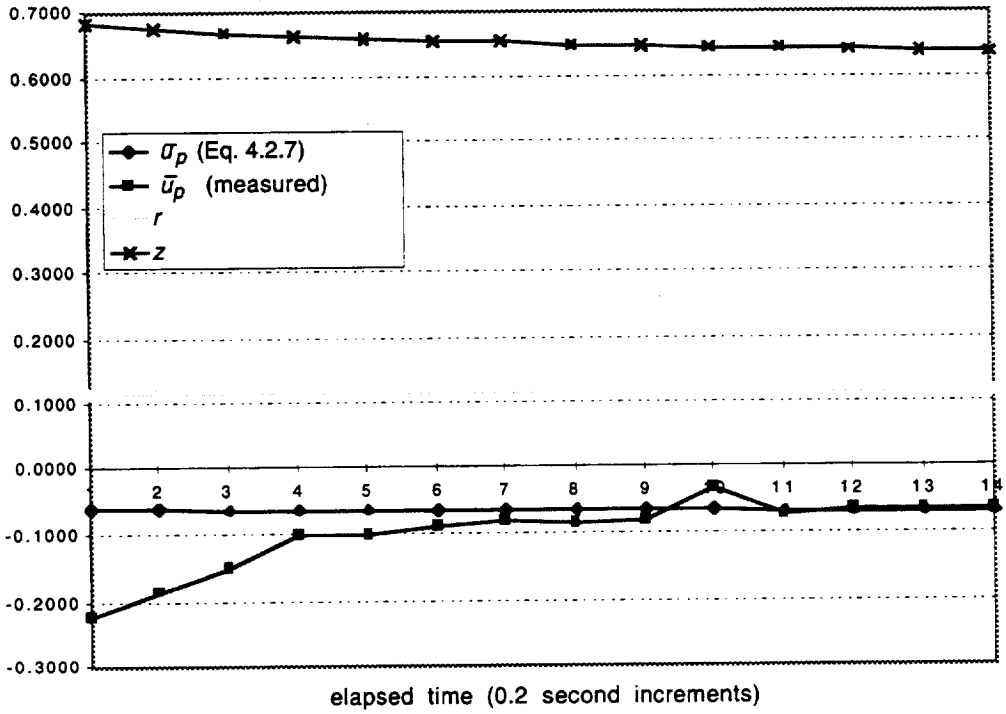

Figure 30. Particle velocity for BPT, $\varepsilon = 0.0435$, $Va = 103$, $U_L = 0$: (a) particle velocity field, $\overline{\mathbf{u}}_p(r,z)$; (b) calculated component velocities $\overline{u}_p(r)$ and $\overline{v}_p(r)$ at $z = 0$; (c) plot of measured particle coordinates, and measured and calculated axial particle velocity $\overline{u}_p(r,z)$ for corresponding elapsed times.

Fig. (a) Steady velocity fields $\bar{\mathbf{u}}_p(r,z)$

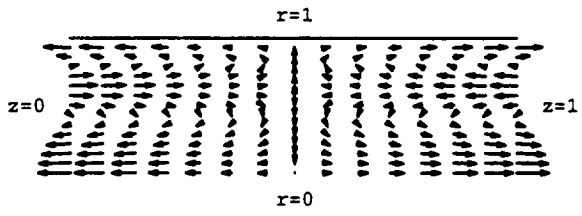

Fig. (b) $\bar{u}_p(r)$ at $z = 0$ —;
$\bar{u}_p(r)$ at $z = 1$ – – ; $\bar{v}_p(r)$ –·–

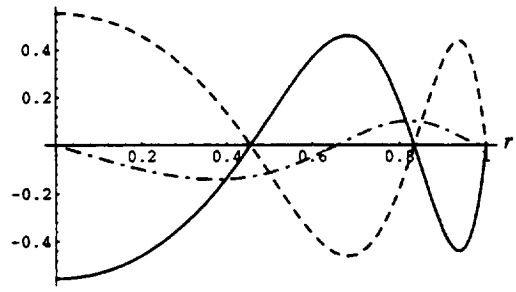

Fig. (c) Time elapsed observed mean -steady particle flow

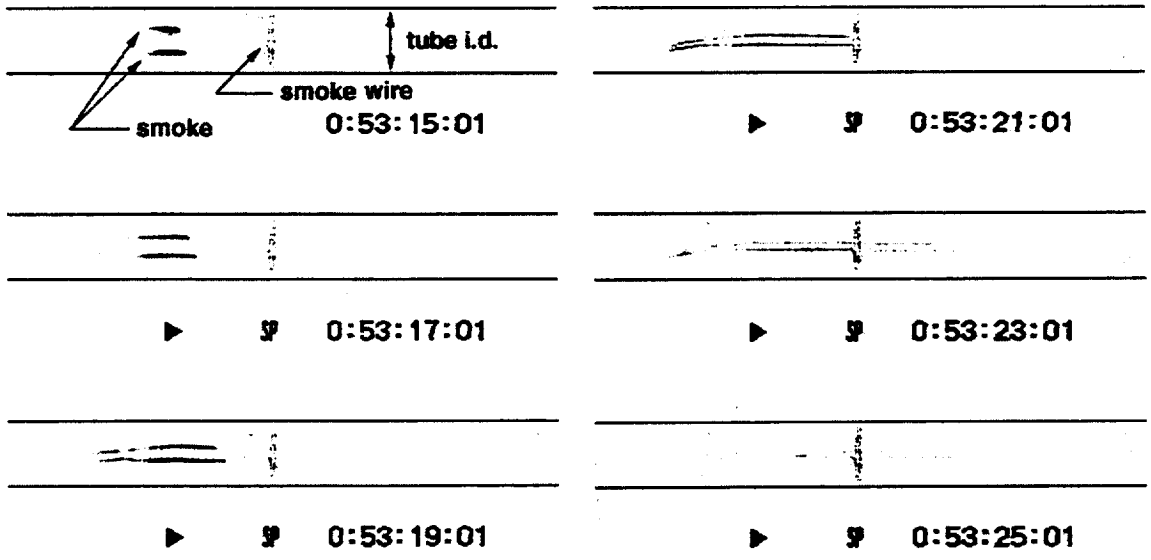

Figure 31. Particle velocity for OPT, ε = 0.0434, Va = 137, $\tilde{U}_L = 1$, $\phi_U = -0.5$: (a) particle velocity field, $\bar{\mathbf{u}}_p(r,z)$; (b) calculated component velocities $\bar{u}_p(r)$ at z = 0 and z = 1 and $\bar{v}_p(r)$; (c) observed smoke flow at indicated times. The observed flow is seen to stretch axially and compress radially as predicted by the flow field of (a).

Though the smoke-wire is positioned at $z \approx 0.5$, the observed smoke flow shows that at $t = 53{:}15{:}01$, the smoke is skewed at a location $z < 0.5$. This is because of the buoyancy effect immediately after the smoke is pulsed. Also, we would expect the flow to be symmetric about $z = 0.5$, hence, we would not expect the smoke to cross the $z = 0.5$ plane. However, at $t > 53{:}21{:}01$, smoke can be seen at locations $z > 0.5$, possibly because the smoke was of a slightly higher density than the air, or because of the instability of a purely zero velocity plane at $z = 0.5$. This second

possibility would allow smoke to cross at $z = 0.5$, allowing the smoke to get caught in the positive direction centerline flow fields for $z > 0.5$.

The smoke observations are seen to "curve" at the ends of the tube. This is because the connections from the compressors to the visualization tube are at right angles. The curved flow is generally restricted to $z < 0.3$ and $z > 0.7$. Flow measurements are taken within the range of $0.3 < z < 0.7$.

Run 4: smoke flow observations for $\phi_U = -0.94$

Figure 32 shows the observed steady flow for Va = 137, $\tilde{U}_L = 1$, and $\phi_U = -0.94$. Figures 32(a) and 32(b) show strong positive velocities in the centerline region and negative velocities in the viscous layer near the tube wall. Radial velocities are very small. Figure 32(c) shows that the observed smoke flow qualitatively confirms the model. The observed flows are in the centerline region and are seen to quickly flow in the positive direction with little radial displacement, except near the positive end ($z = 1$) where the curved flow due to end effects begins to compress the pathlines.

Orifice pulse tube measurements

Mean-steady particle velocity measurements were taken near the centerline and within the viscous layer near the tube wall for an OPT configuration for Va = 68, $\tilde{U}_L = 1$ with $\phi_U = -0.254$, and $\phi_U = -0.125$. Particles were observed flowing with the directional sense and speed as predicted by equation (79). Circulating flow from the centerline region to the viscous layer near the tube wall was observed; it also was in general agreement with predictions.

Run 5: particle velocity measurements for $\phi_U = -0.254$

Centerline and viscous layer flow near tube wall

Figure 33(a) shows the measured and predicted velocities for flow in the centerline region. Calculations correspond well with measured values. The measured velocities at times greater than 18 time-increments (1.8 sec) are due to the curved flow end-effects as described in the observation section. The inlets to the tubes from the compressors are at right angles to the tube, and so the flow is curved at the tube ends. This results in a significant particle position change in r as z approaches 0.3.

Figure 33(b) shows the five-point moving average of axial particle velocity in the viscous layer near the tube wall. Although there is scatter in the data, the results are still in general agreement with prediction.

Fig. (a) Steady velocity fields $\bar{\mathbf{u}}_p(r,z)$

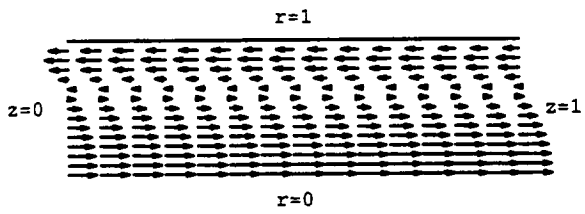

Fig. (b) $\bar{u}_p(r)$ at $z = 0$ —;
$\bar{u}_p(r)$ at $z = 1$ – – ; $\bar{v}_p(r)$ –·–

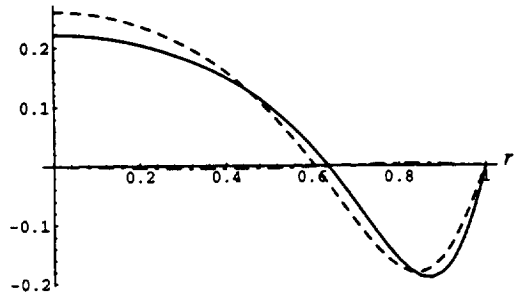

Fig. (c) Time elapsed observed mean -steady particle flow

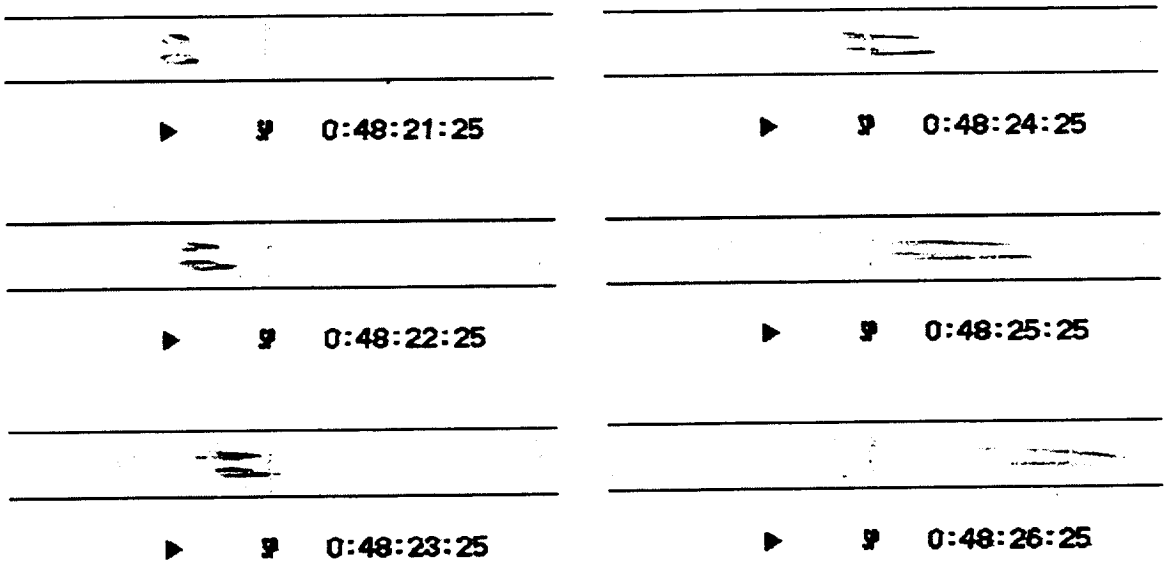

Figure 32. Particle velocity for OPT, ε = 0.0435, Va = 137, $\tilde{U}_L = 1$, $\phi_U = -0.94$: (a) particle velocity field, $\bar{\mathbf{u}}_p(r,z)$; (b) calculated component velocities $\bar{u}_p(r)$ at z = 0 and z = 1 and $\bar{v}_p(r)$; (c) observed smoke flow at indicated times. The observed flow is seen to stretch axially in the positive direction with little radial displacement, as predicted by the flow field of (a).

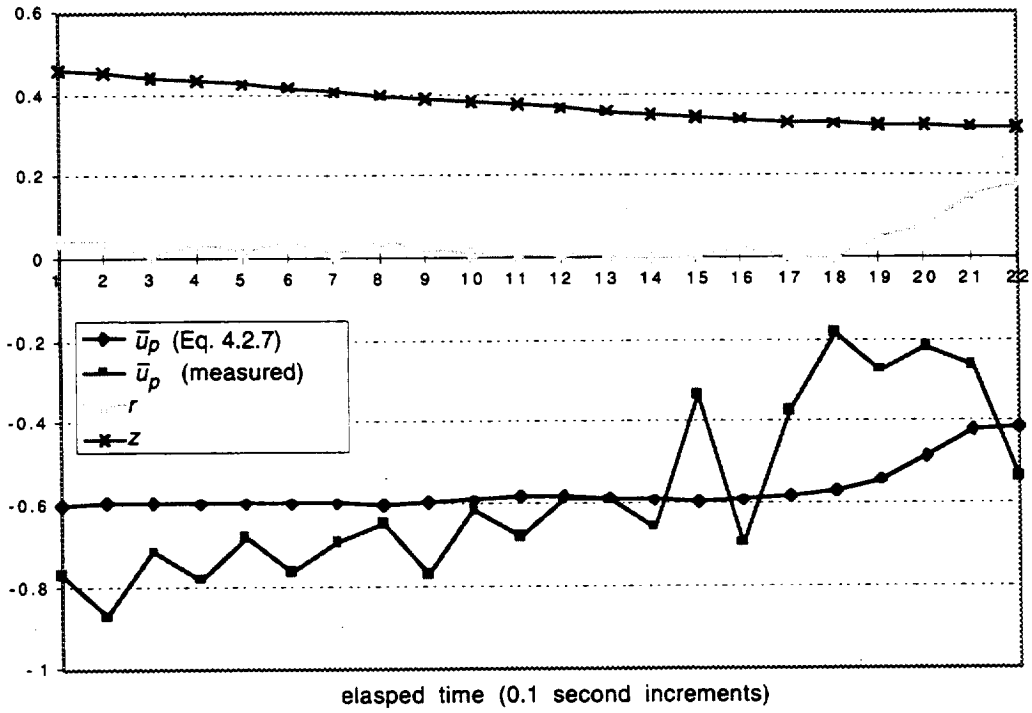

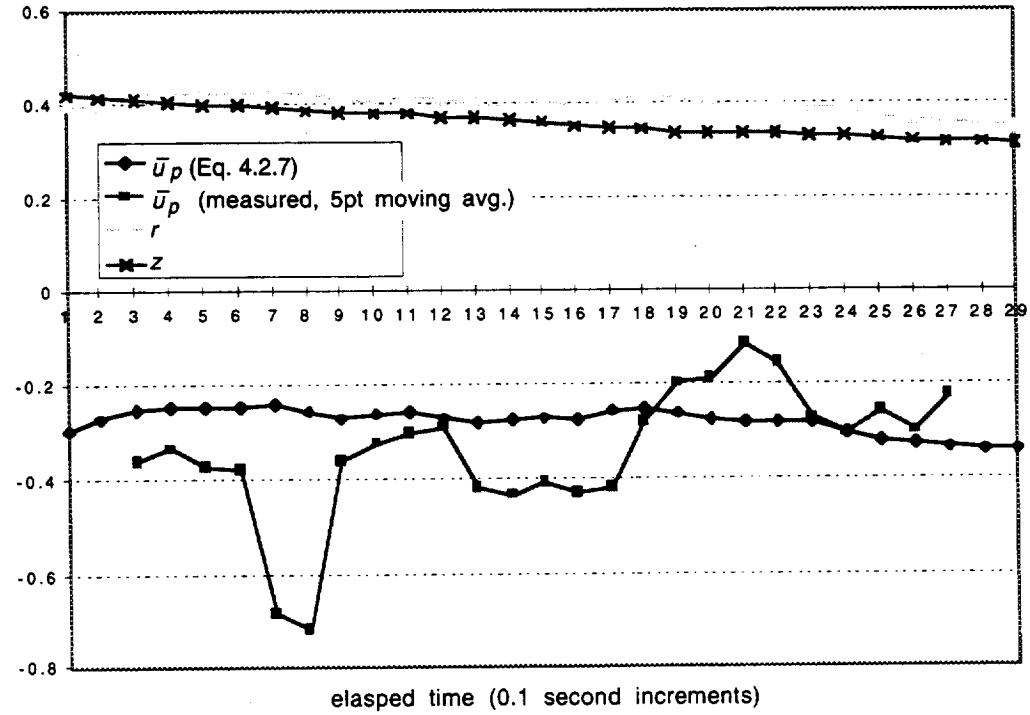

Figure 33. Particle velocities for OPT at indicated r *and* z *positions for corresponding elapsed times:* $\varepsilon = 0.0435$, $Va = 68$, $\tilde{U}_L = 1$, $\phi_U = -0.254$; *(a) is measured and calculated axial velocities* $\bar{u}_p(r,z)$ *at centerline; (b) plot is measured and calculated axial velocities* $\bar{u}_p(r,z)$ *in the viscous layer*

Circulating flow between centerline region and viscous layer near tube wall

Figure 34 shows the flow for an OPT configuration with Va = 68, $\tilde{U}_L = 1$, and $\phi_U = -0.254$. The flow field of figure 34(a) shows negative flow in the centerline region and positive flow near the wall. Figure 34(b) predicts a radial component of flow that is significant between r 0.5 and r 0.8. The radial velocity allows for flow reversal where fluid particles can move from the negative axial flow region to the positive axial flow region.

Fig. (a) Steady velocity fields $\bar{u}_p(r,z)$

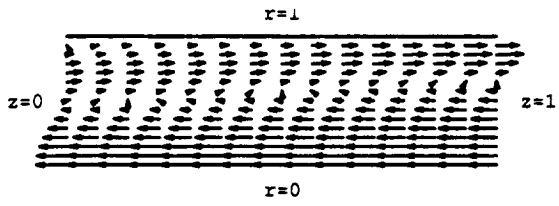

Fig. (b) $\bar{u}_p(r)$ at $z = 0$ —;
$\bar{u}_p(r)$ at $z = 1$ – –; $\bar{v}_p(r)$ –·–

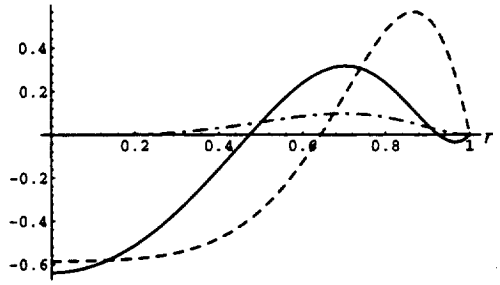

Fig. (c) Comparison of measured and calculated $\bar{u}_p(r,z)$

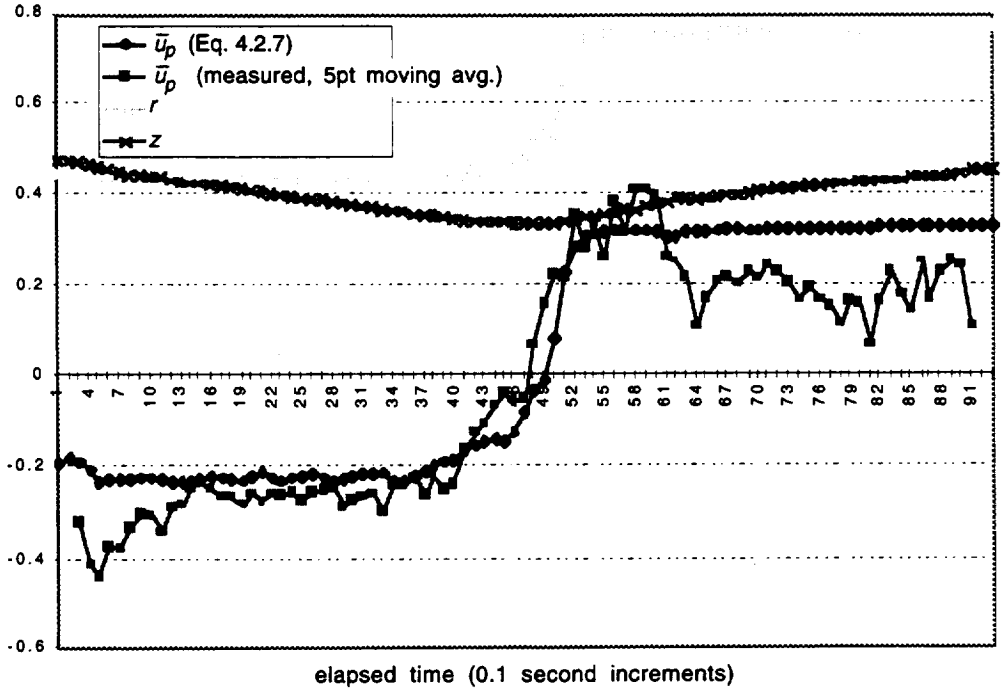

Figure 34. Particle velocity for OPT, ε = 0.0435, Va = 68, $\tilde{U}_L = 1$, $\phi_U = -0.254$: (a) particle velocity field, $\bar{u}_p(r,z)$; (b) calculated component velocities $\bar{u}_p(r)$ at z = 0 and z = 1 and $\bar{v}_p(r)$; (c) plot of measured particle coordinates, and measured and calculated axial particle velocity $\bar{u}_p(r,z)$ for corresponding elapsed times.

Figure 34(c) plots the measured and calculated velocities of equation (79). The data confirm flow reversal between the negative-flow centerline region and the positive-flow viscous layer near the tube wall. Particles, initially at $r \approx 0.42$ and $z \approx 0.45$ have negative velocities. As time progresses, the positive radial component of flow moves the particles outward toward the viscous layer which has positive velocities. The particles enter the viscous layer region and so reverse from negative to positive flow. Equation (79) predicts reasonably well both the magnitude and direction of the particle velocities, and the location at which the particles flow from the negative to the positive velocity regions.

Run 6: particle velocity measurements for $\phi_U = -0.125$

Figure 35(a) shows the mean-steady particle velocity field and figure 35(b) shows a plot of the axial and radial particle velocities for an OPT with Va = 68, $\tilde{U}_L = 1$, and $\phi_U = -0.125$. The flow field is negative in the centerline region and positive in the viscous layer near the tube wall, with radial flow significant between $r = 0.5$ and $r = 0.8$. This is similar to the previous case in which $\phi_U = -0.254$. However, the magnitude of the flows is about 30% less than for $\phi_U = -0.254$. The plots of figure 35 are the predicted fields for the data presented in figures 36 and 37.

Fig. (a) Steady velocity fields $\bar{\mathbf{u}}_p(r,z)$

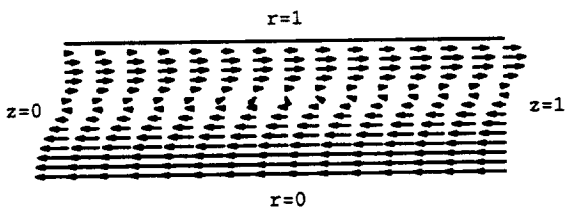

Fig. (b) $\bar{u}_p(r)$ at $z = 0$ — ;
$\bar{u}_p(r)$ at $z = 1$ — — ; $\bar{v}_p(r)$

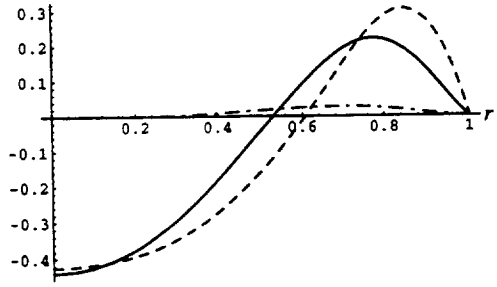

Figure 35. Particle velocity for OPT, ε = 0.0435, Va = 68, $\tilde{U}_L = 1$, $\phi_U = -0.125$: (a) particle velocity field, $\bar{\mathbf{u}}_p(r,z)$; (b) calculated component velocities $\bar{u}_p(r)$ at z = 0 and z = 1 and $\bar{v}_p(r)$

Flow near centerline

Figure 36 shows the measured and predicted velocities for the centerline region. The data for elapsed times greater than 15 time-increments are again due to the flow end-effects as described previously. The measured results are in general agreement with prediction.

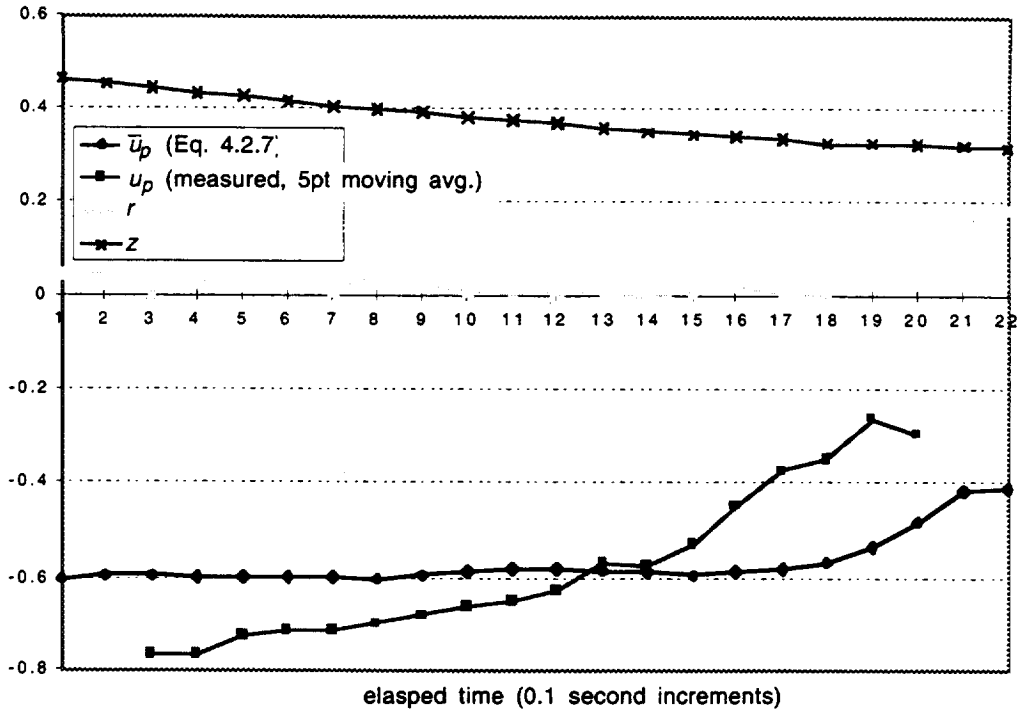

Figure 36. Plots of measured and calculated axial particle velocity $\bar{u}_p(r,z)$ *at the indicated* r *and* z *coordinates and given elapsed times for OPT in the centerline region,* $\varepsilon = 0.0435$, $Va = 68$, $\tilde{U}_L = 1$, $\phi_U = -0.125$.

Circulating flow between centerline region and viscous layer near tube wall

Figure 37 shows the measured axial velocity and position corresponding to the calculated results of figure 35. Figure 37(a) shows a plot of the results for one-half of the radial domain and figure 37(b) is a plot of the results for the other half.[2] Figure 37 shows flow reversal between the centerline region and the viscous layer near the tube wall. The calculated velocity using equation (79) shows good prediction of axial particle speed and direction. There is also good prediction in the transition region where flow goes from being negative to being positive. The transition from negative to positive flow is not as steep as that for the case of $\phi_U = -0.254$, figure 34(c). This is due to the much smaller radial velocity in the flow-reversal region between $r \approx 0.5$ to $r \approx 0.6$ of figure 37.

[2]The smoke comes off the wire nearly axisymmetric within a single plane perpendicular to the camera view. Subsequently, two "smoke blobs" can be tracked, one on either side of the centerline.

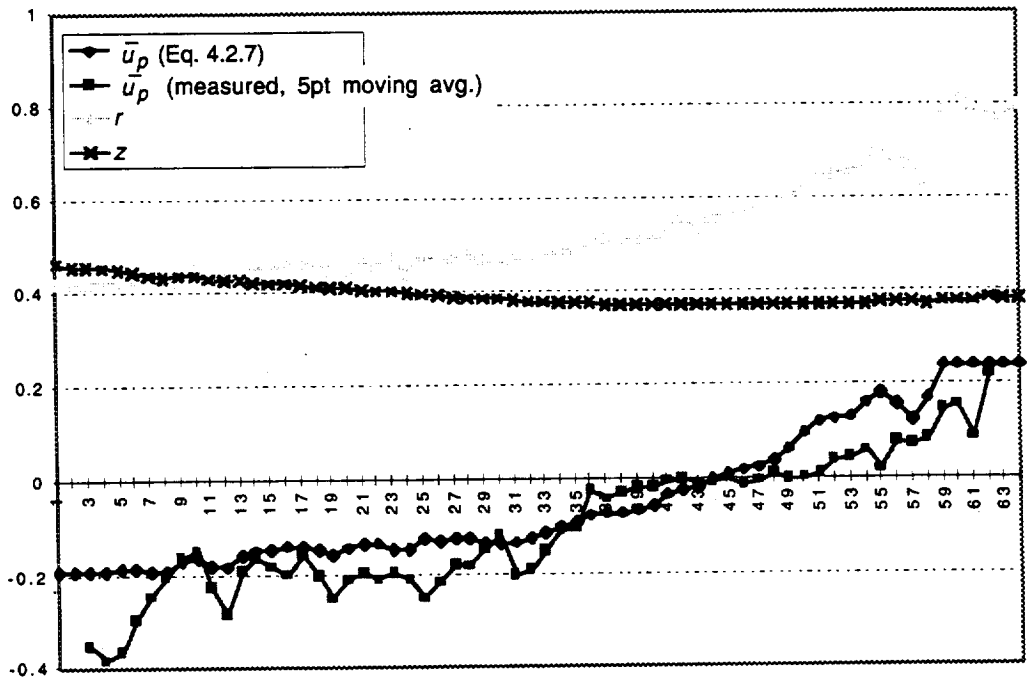

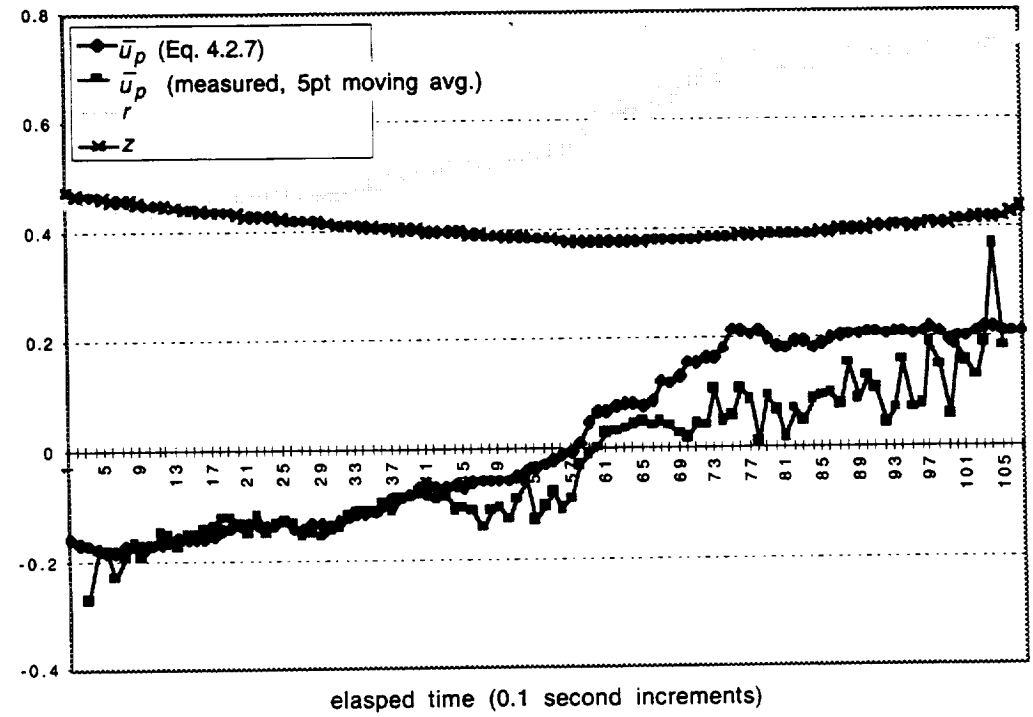

Figure 37. Plots of measured and calculated axial particle velocity $\bar{u}_p(r,z)$ at given elapsed times for OPT, $\varepsilon = 0.0435$, $Va = 68$, $\tilde{U}_L = 1$, and $\phi_U = -0.125$: (a) is data from half the tube; (b) is data from the other half of the tube, symmetric about $r = 0$.

Discussion

The measured and observed axial velocities of smoke particles were well predicted by the particle velocities given by equation (79). These results provide confidence that the present theory is valid and useful.

The measured direction and magnitude of the axial centerline velocities were predicted for a BPT configuration in which the only variable parameter is Va. For Va = 34, the axial velocities in the centerline region were positive. For Va = 103, the axial centerline velocities were negative, which is in agreement with prediction. For Va = 103, a double boundary layer is predicted. Unfortunately, this could not be confirmed with the present system. Future work using more precise methods of measuring velocities over the entire flow field should be conducted to further validate the theory.

OPT operation adds $\tilde{U}_L$ and ϕ_U to Va as variable parameters. For the OPT experiments, $\tilde{U}_L$ was set to 1, and Va and ϕ_U were allowed to vary. OPT observations of the secondary streaming for Va = 137 and $\phi_U = -0.5$ were in good qualitative agreement with predictions. The smoke was observed to stretch axially owing to opposite flow between the outer layer and centerline regions. The smoke also was seen to compress radially because of a radial flow component between the outer layer and centerline region. This stretching and compressing was predicted by theory. Observations for a change in velocity phase angle, $\phi_U = -0.94$ while retaining Va = 137 showed strong positive streaming in the centerline region with little radial flow; this was also predicted.

Measurements of the axial velocity were taken for an OPT configuration, and compared with theory. Once again, the predictions were in good agreement with measurements. For Va = 68 and $\phi_U = -0.254$, smoke that began in the centerline region was observed to flow in the negative axial direction and positive radial direction. Upon entering the viscous layer near the tube wall, the smoke reversed itself and flowed in the positive axial direction. The speed and direction of this axial flow were well predicted. Also predicted were the coordinates at which the flow reversal occurred. At the point of flow reversal, a strong radial velocity was predicted and verified.

A change in the phase angle $\phi_U = -0.125$ showed the same type of flow reversal as for $\phi_U = -0.254$. In this case a weaker radial velocity at the point of flow reversal was observed, and the axial speed and direction were again well predicted by equation (79).

In general, the measured secondary mean-steady particle velocities obtained from the flow-visualization experiments indicate that the present linear theory is applicable, and can be cautiously extended to $\varepsilon \mathrm{Va} \quad 1$. Though this is beyond the $\varepsilon \mathrm{Va} \ll 1$ constraint for linearization of the momentum equation, a case can be made—from the present flow-visualization experiments—that the theory is useful for engineering calculations in the region $\varepsilon \mathrm{Va} = \boldsymbol{O}(1)$, and that the theory can be used to help understand the transport mechanisms, particularly mass streaming and enthalpy flows, in pulse tubes.

6. CONCLUDING REMARKS AND FUTURE WORK

The present study formulates a set of two-dimensional, axisymmetric differential equations for describing mean-steady secondary flows generated by periodic compression and expansion of an ideal gas in a pulse tube. An anelastic approximation of the fluid equations—mass and energy conservation, and the equation of motion—is used to construct a consistent set of linear differential equations amenable to a series-expansion solution in the small parameter ε, where ε is the inverse Strouhal number and is the ratio of gas displacement length to tube length. The anelastic approach applies when shock and acoustic energies are small compared with the energy needed to compress and expand the gas. Other parameters resulting from the formulation are the Valensi number, Va, relating system transverse length to viscous diffusion length; the Prandtl number, Pr; the Mach number, M; the velocity amplitude ratio at the tube ends; and the velocity phase angle at the tube ends. Additionally, heat transfer to a tube wall that has thin but finite thickness is considered, thus introducing the tube wall Fourier number, Fo.

The elasticity parameter λ relates ε and M and is used to order the pressure gradient in the momentum equation. It is the product of Mach number and the ratio of the oscillation frequency to the system acoustic resonance frequency, and is useful for identifying the distinguished limit between ε and M. A linear acoustic set of equations results when $\lambda = O(1)$ and $\varepsilon \ll 1$. This corresponds to a distinguished limit of $M = \varepsilon^{0.5}$. An anelastic set of equations results when $\lambda \leq \varepsilon \ll 1$. This corresponds to a distinguished limit of $M \leq \varepsilon$. For pulse tubes, $\lambda \ll \varepsilon \ll 1$, which is the limit used in this study. Additionally, a linear approximation of the momentum equation is taken. This requires the added constraint $\varepsilon \mathrm{Va} \ll 1$.

The derived set of leading-order relations requires simultaneous solution of the zeroth-, first-, and second-order set of equations. The zeroth-order temperature—which is the equilibrium bulk temperature—is coupled to the zeroth-order equation of state, the first-order oscillating advection of enthalpy, and the second-order mean-steady conversion of work flow to heat flow. The full problem is nonlinear and requires solving 15 equations in 15 unknowns—an ambitious task left for future work.

In determining the lower-order mechanisms for the mean-steady transport of momentum and enthalpy, a solution to the equations is obtained for the strong temperature case $T_{0,z} = 0$. This effectively decouples the three separate orders of equations, leaving for the basic state problem the first-order oscillating equations, which are completely self-contained.

The oscillating solution is used to compute oscillating heat transfer and shear at the tube wall. It is found that the complex Nusselt number, relating the ratio of conduction heat flux at the wall to bulk temperature difference between the gas and tube wall, is independent of the Fourier number and of the velocity boundary conditions at the tube ends. This also applies to the wall shear factor, which is similarly defined as the ratio of momentum flux to bulk velocity difference. The complex Nusselt number and shear wall factor are simply scaled by the Prandtl number. The usefulness of these two relations is to correct for transverse heat transfer and wall shear when used with a 1-D model.

The leading-order oscillating solution is taken to the next higher order to arrive at the mean-steady solutions for the Eulerian and Lagrangian velocity fields, the enthalpy flow field, and the mean-steady radial temperature profile. These are each examined as functions of Va, $\tilde{U}_L$, ϕ_U, and Fo.

Plots of the velocity fields for the basic pulse tube (BPT) and orifice pulse tube (OPT) configurations show complicated flow patterns. The flows are highly dependent on Va and ϕ_U. Examination of the higher-order mean-steady velocity equation shows that the Reynolds stress and the quadratic product of oscillating density and oscillating velocity produce the steady secondary streaming. The streaming depends on gradients of the velocity amplitude and phase angle. In general, the leading-order solutions for all properties (temperature, pressure, velocity) depend on the velocity amplitude; hence, for any mean-steady quantity the magnitude will depend on the square of the velocity amplitude.

Plots of the enthalpy flux field show the effect of heat transfer with the tube wall. For a near isothermal wall (Fo $\rightarrow$ 0), gradients in the enthalpy flux result in mean-steady heat transfer to the tube wall. This can be seen in the mean-steady enthalpy equation where the work flux is balanced by heat flux. Under these isothermal wall conditions, the thermal and viscous diffusion layers are of the same form, both pinned at the wall, and scaled only by the Prandtl number, which for most cases is of $\boldsymbol{O}(1)$ but not equal to 1. This allows a unidirectional flow of enthalpy for the BPT, because the difference in viscous and thermal diffusion lengths enables a favorable phase angle between velocity and temperature. Alternatively, for a BPT with Pr = 1, the phase angle between velocity and temperature is 90°, hence enthalpy flow is locally zero everywhere.

The OPT overcomes the necessity of heat transfer by obtaining appropriate phase angles through the axial velocity boundary conditions. This allows favorable phase angles to be present throughout the entire transverse domain, whereas for the BPT, phase angles are favorable only in the diffusion layer. Also, the inclusion of a finite velocity at the hot end of the tube allows a finite enthalpy flow at this end, whereas for the BPT the enthalpy flow goes to zero. The velocity boundary conditions also allow a more constant enthalpy flux throughout the axial domain (when compared with the BPT). Hence, there is less conversion of work flow into heat flow along the tube length, and so more of the work flow is available for enthalpy flow to the hot heat exchanger for rejection. (For the BPT, the steep decrease in work flow results in a large heat flow that is conducted back to the cold end.)

The experimental smoke-wire flow-visualization experiments confirmed the predictions of the present theory. The system was configured for BPT and OPT operation, with Va varied for both, and ϕ_U varied with $\tilde{U}_L = 1$ for the OPT. The experiments were conducted in the range $1.5 < \varepsilon \mathrm{Va} < 6$, which is not strictly within the constraint $\varepsilon \mathrm{Va} \ll 1$ required for linearization of the momentum equation. However, for all cases examined, the calculated particle velocities satisfactorily described the observed and measured experimental particle velocities, including flow reversals between the centerline regions and diffusion layers, and the locations at which flow reversal occurred.

The major points of this study can be summarized as follows.

1. Basic pulse tubes should be operated at Fo $\rightarrow$ 0 and PrVa $\approx$ 10. The first condition represents an isothermal tube wall, thereby allowing good heat transfer between the gas and the tube wall, and

the second condition ensures that most of the gas is efficiently used to transport enthalpy. Calculations also show that an isothermal wall reduces mass streaming relative to an adiabatic wall for a BPT.

2. Orifice pulse tubes should be operated for large Fo and large PrVa. The first condition represents an adiabatic tube, thereby reducing heat transfer between the gas and the tube wall, and the second confines the diffusion layer to a thin layer near the wall. Calculations also show that an adiabatic wall reduces mass streaming relative to an isothermal wall at large PrVa. However, large Va tends to increase mass streaming. Maximum enthalpy flow for orifice pulse tubes was shown to be at a phase angle of $\phi_U \approx -0.25$.

3. The mean-steady velocity increases linearly with Va for Va < 10 and can be of $\boldsymbol{O}(1)$ for Va > 100. It is strongest when $\phi_U \approx -0.25$.

4. The complex Nusselt number can be used for one-dimensional linear oscillating flow in a tube to correct for radial heat transfer. It is of the form $\hat{\mathrm{Nu}}(\mathrm{PrVa}) = \tilde{A}\, e^{i\phi}$ and is independent of Fo, velocity amplitude ratio $\tilde{U}_L$, and velocity phase angle ϕ_U at the tube ends. $\tilde{A}$ is about 4 for PrVa < 3 and is linear with PrVa for PrVa > 25. The phase angle, for PrVa < 0.5 is $\phi \to -0.5$, and for PrVa > 500 is $\phi \to -0.38$. A similar relation for the complex shear wall factor exists using Va as the independent parameter.

5. Heat transfer between the gas and the tube wall can shift the phase between the pressure and temperature phasors. This is important because 1-D models often assume adiabatic conditions on the gas and so there is a presumption that temperature is always in phase with pressure. Most pulse tubes operate at Fo = $\boldsymbol{O}(1)$, which is closer to isothermal wall conditions. Calculations indicate the phase shift between pressure and temperature to be as much as 20°.

6. The calculated particle velocities using the linear anelastic approach were supported by the measured velocities from the flow-visualization experiment for $1.5 < \varepsilon\mathrm{Va} < 6$, even though this is not strictly within the linear constraint $\varepsilon\mathrm{Va} \ll 1$.

Though this first attempt to verify the theory has proved relatively successful, there is considerable room for further validation and improvement. Possible areas for future study include the following.

1. A numerical solution to the full coupled set of equations. This would yield the leading-order equilibrium temperature T_0, and allow a better understanding of how mass streaming affects the T_0 temperature gradient, the trade-offs between enthalpy flow and heat flow, and the ability to optimize pulse tube operation by calculating entropy generation due to temperature gradients.

2. Extending the theory to individual components, such as regenerators, heat exchangers, and inertance tubes; and adding lumped-parameter boundary conditions to model an orifice and reservoir. Once accomplished, a modular approach for constructing a pulse tube engineering model from component level modules would be available.

3. A solution of the equations with different boundary conditions would yield some interesting insights. For example, a solution for the case of a slowly varying tube diameter could be used to reduce streaming losses, since streaming is a function of velocity gradients. Another example would be to relax the no-penetration condition at the tube wall and probe how this might affect

enthalpy and mass streaming; and whether such results could be used to design a "continuous-stage" pulse tube. Finally, the isothermal temperature conditions at the tube ends can be re-cast as an oscillating temperature boundary condition to determine how the temperature phasor would be affected. This boundary condition would reflect heat exchanger ineffectiveness.

4. The use of laser-Doppler velocimeters or hot-wire anemometer velocimeters to measure local velocities over the entire domain. This would substantially validate the accuracy of the linearized approach and the limits at which it breaks down.

5. The theory can be extended to other types of oscillating systems in which one is interested in the mean-steady streaming generated by oscillating flows. For example, an expansion of the conservation equations for individual species of multi-component mixtures can be performed to determine species streaming. Its usefulness would be in understanding species separation.

The formulation of the present set of anelastic equations, and the relative success of the strong-temperature solution in predicting mean-steady particle streaming provide a measure of confidence that the present theory can be used to design pulse tubes and to predict their performance.

APPENDIX A
SCALING

The governing fluid equations that describe the flow dynamics of the tube are scaled. A sketch of the system is shown in figure 38. Two problem domains are taken: the gas domain extends from $r^* = 0$ to $r^* = r_w^*$ and $z^* = 0$ to $z^* = L^*$ (starred variables are *dimensional* quantities); and the tube-wall domain extends from $y^* = 0$ to $y^* = l^*$ and from $z^* = 0$ to $z^* = L^*$, where l^* is the tube-wall thickness. Adiabatic conditions exist for the outer wall surface, and continuity of temperature and heat flux must exist between the gas and the tube-wall interface. The velocity boundary conditions are of small amplitude and periodic so that time can be represented using complex notation: at $z^* = 0$, $u = \tilde{U}_0^* e^{i\omega^*}$; and at $z^* = L^*$, $u = \tilde{U}_L^* e^{i\left(\omega^* t^* + \phi_U^*\right)}$ where $\omega^* = 2\pi f^*$ is the angular frequency and f^* is the frequency, t^* is the time, ϕ_U is the velocity phase angle between the tube ends, and $\tilde{U}_0^*$ and $\tilde{U}_L^*$ are the velocity amplitudes at each end. The energy boundary conditions at the outer tube wall are adiabatic, with the temperature at $z^* = 0$ and $z^* = L^*$ taken as $T^* = T_c^*$ and $T^* = T_h^*$, respectively. We will refer to the z-direction as the axial direction, and the r-direction as the transverse direction, and use $\chi_{,\eta} = \partial\chi/\partial\eta$ as the notation for partial derivatives.

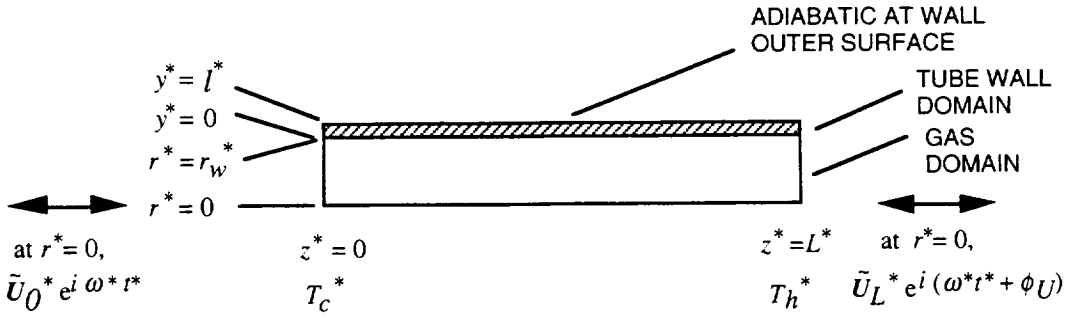

Figure 38. Two-dimensional axisymmetric system for $r_w^*/L^* \ll 1$.

The fluid equations of Bird et al. (ref. 64) are reduced for our system using the following simplifying assumptions: (1) two-dimensional, axisymmetric cylindrical geometry; (2) ideal gas; (3) constant transport properties; (4) Stokes assumption for the second viscosity; and (5) $r_w^{*2}/L^{*2} \ll 1$ (implying that $\partial p^*/\partial r^* \approx 0$ so that the r-momentum equation can be decoupled from the rest of the problem and axial viscous transport is negligible). The reduced fluid equations for mass conservation, equation of motion, energy conservation, and equation of state become, respectively,

$$\rho^*_{,t^*} + \frac{\left(\rho^* v^* r^*\right)_{,r^*}}{r^*} + \left(\rho^* u^*\right)_{,z^*} = 0 \tag{A1}$$

$$\rho^*\left[u^*_{,t^*} + v^* u^*_{,r^*} + u^* u^*_{,z^*}\right] = -p^*_{,z^*} + \frac{\mu^*}{r^*}\left(r^* u^*_{,r^*}\right)_{,r^*} \tag{A2}$$

$$\rho^* C_p^* \left[T_{,t}^* + v^* T_{,r}^* + u^* T_{,z}^* \right] = -\left(p_{,t}^* + u^* p_{,z}^* \right) + \frac{\kappa^*}{r^*} \left(r^* T_{,r}^* \right)_{,r^*} + \kappa^* T_{,z^* z^*}^* + \mu^* u_{,r}^{*2} \tag{A3}$$

$$p^* = \rho^* R^* T^* \tag{A4}$$

The energy conservation equation for the tube-wall domain for $l^* \ll r_w^*$ is

$$\rho_w^* C_{pw}^* \theta_{,t}^* = k_w^* \left(\theta_{,y^* y^*}^* + \theta_{,z^* z^*}^* \right) \tag{A5}$$

where θ is the temperature of the tube wall. The mean-steady (time-averaged) enthalpy flow is of primary interest since it represents refrigeration,

$$\overline{H}^* = 2\pi\omega^* \oint_{1/\omega^*} \left(\int_0^{r_w^*} \rho^* u^* C_p^* T^* r^* dr^* \right) dt^* \tag{A6}$$

where the overbar represents time-averaged over a cycle. The kinematic velocity components in the z^* and r^* direction are u^* and v^*; the thermodynamic gas variables p^*, ρ^*, and T^* are pressure, density, and temperature; the density of the tube wall material is ρ_w^*; gas properties, μ^*, k^*, and C_p^*, are the dynamic viscosity, thermal conductivity, and heat capacity; and the tube-wall properties, k_w^* and C_{pw}^*, are the thermal conductivity and heat capacity of the tube wall.

The above dimensional equations are scaled (normalized) resulting in dimensionless variables ranging from 0 to $O(1)$ (order 1). The variables are scaled as follows: r^* is scaled with r_w^*, z^* is scaled with L^*, y^* is scaled with the tube-wall thickness l^*, and t^* is scaled with the angular frequency ω^*; u^* is scaled with the axial boundary condition velocity $\tilde{U}_0^*$; v_0^* is scaled with $(\tilde{U}_0^* r_w^* / L^*)$; and p^*, ρ^*, and T^*, are scaled with mean pressure p_0^* and reference density and temperature ρ_0^* and T_0^*. The transport properties μ^*, k^*, C_p^*, k_w^* and C_{pw}^*, and the tube-wall density ρ_w^* are taken as constant and so they are in themselves the scaling factors. These scaling parameters are substituted into the dimensional equations (A1)–(A6) and rearranged to give the corresponding dimensionless form (unstarred variables are *dimensionless*) for mass conservation, equation of motion, energy conservation, equation of state, tube-wall energy conservation, and mean-steady enthalpy flow,

$$\rho_{,t} + \varepsilon \left[\frac{(\rho v r)_{,r}}{r} + (\rho u)_{,z} \right] = 0 \tag{A7}$$

$$\rho \left[u_{,t} + \varepsilon \left(v u_{,r} + u u_{,z} \right) \right] = -\frac{1}{\lambda} p_{,z} + \frac{1}{\mathrm{Va}} \frac{\left(r u_{,r} \right)_{,r}}{r} \tag{A8}$$

$$\rho \left[T_{,t} + \varepsilon \left(v T_{,r} + u T_{,z} \right) \right] = \frac{\gamma - 1}{\gamma} \left(p_{,t} + \varepsilon u p_{,z} \right) + \frac{1}{\mathrm{PrVa}} \left(\frac{\left(r T_{,r} \right)_{,r}}{r} + \frac{r_w^{*2}}{L^{*2}} T_{,zz} \right) + (\gamma - 1) \frac{\mathrm{M}^2}{\mathrm{Va}} u_{,r}^2 \tag{A9}$$

$$p = \rho T \tag{A10}$$

$$\theta_{,t} = \mathrm{Fo}\left(\theta_{,yy} + \frac{l^{*2}}{L^{*2}}\theta_{,zz}\right) \tag{A11}$$

$$\overline{H} = \omega \int_0^1 \left[\oint_{1/\omega} \rho u T dt \right] dr \tag{A12}$$

The mean-steady enthalpy flow of the gas, equation (A12), is scaled by the leading-order oscillating enthalpy flow, $\overline{H}_0^* = \pi r_w^{*2} \rho_0^* C_p^* U_0^* T_l^*$. The above set of equations identifies six dimensionless scaling groups, five of which are independent. Two additional dimensionless groups, ϕ_U and $\tilde{U}_L$, enter through the boundary conditions. The dimensionless groups are listed in table 7 along with their physical interpretations. The relative magnitudes of the groups provide an understanding of the importance of the various effects (friction, heat transfer, compressibility, etc.).

Table 7. Dimensionless scaling groups.

	Name	**Definition**	**Length scales**	**Time scales**
ε	Inverse Strouhal number	$\tilde{U}_0^* / \left(\omega^* L^*\right) = d_o^* / L^*$	Displacement length to tube length	Period of oscillation to residence time
λ	Acoustic resonance parameter	$\frac{\gamma \mathrm{M}^2}{\varepsilon} = \gamma \frac{\tilde{U}_0^*}{a^*} \frac{L^* \omega^*}{a^*}$	Mach number times ratio of sound wavelength to system length	Mach number times ratio oscillation to resonance frequency
Va	Valensi number	$r_w^{*2} \omega^* / \nu^*$	Transverse system length to viscous diffusion length	Viscous diffusion time to oscillation time
Pr	Prandtl number	ν^* / α^*	Viscous to thermal diffusion lengths	Thermal diffusion to viscous diffusion times
M^2	Mach number squared	$\tilde{U}_0^{*2} / \gamma R T_0^*$	Ratio of velocity amplitude at z = 0 to speed of sound	Period of oscillation to acoustic time
Fo	Fourier number	$\alpha_w^* / \left(l^{*2} \omega^*\right)$	Thermal diffusion to tube wall thickness	Oscillation time to thermal diffusion time

The numbers also represent time ratios. If the residence-time scale is L^* / U_0^* (time in which a particle of velocity U_0^* travels the length of the tube L^*) then ε is the ratio of the velocity time-scale to the residence time-scale. Va is the ratio of viscous diffusion time-scale to velocity time-scale, Pr is the ratio of thermal-to-viscous diffusion time-scales, and M is the ratio of acoustic time-to-residence-time scales.

APPENDIX B
PARTICLE VELOCITY

For a two-dimensional system, the two directional components of the mass flux vector $\rho\mathbf{u}$ can be combined into a single scalar function—the stream function ψ—which exactly satisfies the differential equation for mass conservation. For the case of axisymmetric cylindrical geometry, the stream function is defined as $-\psi_{,r} = \rho u r$, and $+\psi_{,z} = \rho v r$ where r and z are the radial and axial directions and v and u are the corresponding directional velocities.

The stream function represents lines of mass flow. For truly steady-state flow, the loci of points where the derivative of the stream function is zero ($d\psi = 0$) represents lines of constant mass flow ($d\psi = \rho \mathbf{u} dA = d\dot{m} = 0$) or streamlines. A parametric plot for the condition $d\psi = \rho u r dr = \rho v r dz = 0$ over the domain gives the streamlines, with the difference between any two streamlines being numerically equal to the difference in mass flow between those two lines.

Streamlines in the Eulerian reference frame for steady-state flow also represent particle paths. However, for the oscillating flow investigated in the experiments, Eulerian mean-steady streamlines are not equivalent to mean-steady particle paths. The mean-steady particle paths are best represented in the Lagrangian reference frame because—as in the experiments—it is the visual tracking of a distinguishable particle over time. Here we derive the equations for the particle path.

The exercise here is to determine the particle velocity field $\mathbf{u}_p(\mathbf{x},t)$, given the Eulerian velocity field $\overline{\mathcal{U}}(\mathbf{x},t)$. Consider a particle at position $\mathbf{x}$ and time t that initially was at position $\mathbf{x}_0$ at time $t = 0$. Its velocity is

$$\mathbf{u}_p(\mathbf{x},t;\mathbf{x}_0) = \mathbf{u}_p\left(\mathbf{x}_0 + \int_0^t \mathbf{u}_p(\mathbf{x},\tau)\, d\tau, t\right) \tag{B1}$$

It is understood that for any given position and time, the velocity of a particle is equal to the Eulerian velocity,

$$\mathbf{u}_p(\mathbf{x},t) = \mathcal{U}(\mathbf{x},t) \tag{B2}$$

hence equation (B1) is

$$\mathbf{u}_p(\mathbf{x},t;\mathbf{x}_0) = \mathcal{U}\left(\mathbf{x}_0 + \int_0^t \mathbf{u}_p(\mathbf{x},\tau)\, d\tau, t\right) \tag{B3}$$

For small particle displacements (small time increments) of $O(\varepsilon)$, equation (B3) can be expanded in a Taylor series, about $\mathbf{x}_0$,

$$\mathrm{u}_p(\mathrm{x},t;\mathrm{x}_0) \approx \mathcal{U}(\mathrm{x}_0,t) + \varepsilon\left(\int_0^t \mathrm{u}_p(\mathrm{x},\tau)\, d\tau \cdot \nabla \mathrm{u}_p(\mathrm{x},t)\right)_{\mathrm{x}_0} + \cdots \tag{B4}$$

Now $\mathcal{U}$ and $\mathbf{u}_p$ are both expandable in ε,

$$\mathcal{U}(\mathbf{x},t) = \mathcal{U}_0 + \varepsilon\mathcal{U}_1 + O\left(\varepsilon^2\right) \tag{B5}$$

$$\mathbf{u}_p(\mathbf{x},t) = \mathbf{u}_{p0} + \varepsilon\mathbf{u}_{p1} + O\left(\varepsilon^2\right) \tag{B6}$$

Substituting equations (B5) and (B6) into equation (B4), and equating like orders in ε,

$$\mathbf{u}_{p0}(\mathbf{x},t;\mathbf{x}_0) = \mathcal{U}_0(\mathbf{x}_0,t) \tag{B7}$$

$$\mathbf{u}_{p1}(\mathbf{x},t;\mathbf{x}_0) = \mathcal{U}_1(\mathbf{x}_0,t) + \int_0^t \mathbf{u}_{p0}(\mathbf{x}_0,t)\, d\tau \cdot \nabla\mathbf{u}_{p0}(\mathbf{x}_0,t) \tag{B8}$$

Recalling the relation of equation (B2), equation (B8) becomes

$$\mathbf{u}_{p1}(\mathbf{x},t;\mathbf{x}_0) = \mathcal{U}_1(\mathbf{x}_0,t) + \int_0^t \mathcal{U}_0(\mathbf{x}_0,t)\, d\tau \cdot \nabla\mathcal{U}_0(\mathbf{x}_0,t) \tag{B9}$$

The mean-steady observed velocities of equations (B7) and (B9) can be rewritten in terms of the mean-steady velocity produced by the Reynolds stresses. The applicable relations are $\mathcal{U}_0 = \mathbf{u}_0$ and $\mathcal{U}_1 = \mathbf{u}_1 + \frac{\rho_1\mathbf{u}_0}{\rho_0}$ and they are given by equation (76). Using these relations, equations (B7) and (B9) become

$$\mathbf{u}_{p0}(\mathbf{x},t;\mathbf{x}_0) = \mathbf{u}_0(\mathbf{x}_0,t) \tag{B10}$$

and

$$\mathbf{u}_{p1}(\mathbf{x},t;\mathbf{x}_0) = \left(\mathbf{u}_1 + \frac{\rho_1\mathbf{u}_0}{\rho_0}\right)_{\mathbf{x}_0} + \left(\int_0^t \mathbf{u}_0\, d\tau \cdot \nabla\mathbf{u}_0\right)_{\mathbf{x}_0} \tag{B11}$$

Equations (B10) and (B11) are now time-averaged over a cycle to arrive at the particle velocity,

$$\bar{\mathbf{u}}_{p0}(\mathbf{x};\mathbf{x}_0) = \oint \mathbf{u}_{p0}\, dt = 0 \tag{B12}$$

and

$$\bar{\mathbf{u}}_{p1}(\mathbf{x};\mathbf{x}_0) = \left(\bar{\mathbf{u}}_1 + \overline{\frac{\rho_1\mathbf{u}_0}{\rho_0}}\right)_{\mathbf{x}_0} + \left(\overline{\int_0^t \mathbf{u}_0\, d\tau \cdot \nabla\mathbf{u}_0}\right)_{\mathbf{x}_0} \tag{B13}$$

where the overbars represent time-averaged quantities. The quantity $\bar{\mathbf{u}}_{p1}$ is the mean-steady particle velocity. It is composed of the observed mean-steady field velocity $\mathcal{U}_1 = \mathbf{u}_1 + \frac{\rho_1\mathbf{u}_0}{\rho_0}$ and the quadratic product of the mean-steady velocity produced by the Reynolds stresses as the particle transverses across the $O(\varepsilon)$ streamlines defined by $\overline{\mathcal{U}_1}$.

APPENDIX C
ANELASTIC APPROXIMATION

The definition of anelastic flow is somewhat vague and unsettled, possibly because it is so seldom used. In general though, it can be thought of as the "filtering of sound" from the fluid equations (ref. 2); its effect is "to remove acoustic phenomena from theoretical considerations" (ref. 1). Mathematically, it is an approximation of the fluid equations where pressure gradients are ignored in the mass conservation equation, but are retained in the momentum equation. This allows decoupling of the pressure gradient between the two equations and results in density variations owing to bulk pressure changes in time only, ignoring density variations caused by pressure changes in space.

To further illuminate the meaning of anelastic flow, consider once again the problem in which an ideal gas is enclosed in a cylindrical tube. Now take the scaled equation of motion in which there are no body forces given by the conservative form of equation (10):

$$(\rho\mathbf{u})_{,t} + \varepsilon\nabla\cdot(\rho\mathbf{u}\mathbf{u}) = -\frac{1}{\lambda}\nabla p - \frac{1}{\mathrm{Va}}\nabla\cdot\tau \tag{C1}$$

where $\lambda = \dfrac{\gamma \mathrm{M}^2}{\varepsilon}$. Consider[1] a series expansion for small values of ε,

$$\begin{aligned} u &= u_0 + \varepsilon u_1 + \boldsymbol{O}\left(\varepsilon^2\right) & p &= p_0 + \varepsilon p_1 + \boldsymbol{O}\left(\varepsilon^2\right) \\ v &= v_0 + \varepsilon v_1 + \boldsymbol{O}\left(\varepsilon^2\right) & \rho &= \rho_0 + \varepsilon \rho_1 + \boldsymbol{O}\left(\varepsilon^2\right) \\ & & T &= T_0 + \varepsilon T_1 + \boldsymbol{O}\left(\varepsilon^2\right) \end{aligned} \tag{C2}$$

Substitute equations (C2) into the equation of motion and collect leading-order terms. For a typical pulse tube, the leading-order pressure term is $\nabla p_0 = \boldsymbol{O}(\lambda) = \boldsymbol{O}\left(10^{-7}\right)$, a very small number, hence

$$\nabla p_0 \approx 0 \tag{C3}$$

Although the leading-order pressure is not spatially dependent, it can still be temporally dependent, $p_0 = p_0(t)$. Now, take the scaled mass conservation equation of equation (9)

$$0 = \frac{1}{\rho}\frac{D\rho}{Dt} + \varepsilon\nabla\cdot\mathbf{u} \tag{C4}$$

---

[1] Equation (C1) can be rearranged into a more familiar form by multiplying through by Va, $\mathrm{Va}(\rho\mathbf{u})_{,t} + \varepsilon\mathrm{Va}\,\nabla\cdot(\rho\mathbf{u}\mathbf{u}) = -\dfrac{\varepsilon\mathrm{Va}}{\gamma\mathrm{M}^2}\nabla p - \nabla\cdot\tau$ where the quantity $\varepsilon\mathrm{Va}$ is the dynamic Reynolds number, Re, multiplied by the length ratio $\dfrac{r_w^{\cdot}}{L^{\cdot}}$, so $\varepsilon\mathrm{Va} = \dfrac{U_0^{\cdot}}{L^{\cdot}\omega^{\cdot}}\dfrac{r_w^{\cdot 2}\omega^{\cdot}}{\nu^{\cdot}} = \dfrac{U_0^{\cdot} r_w^{\cdot}}{\nu^{\cdot}}\dfrac{r_w^{\cdot}}{L^{\cdot}} = \mathrm{Re}\dfrac{r_w^{\cdot}}{L^{\cdot}}$. This arrangement gives the momentum equation in the form $\mathrm{Va}(\rho\mathbf{u})_{,t} + \mathrm{Re}\dfrac{r_w^{\cdot}}{L^{\cdot}}\nabla\cdot(\rho\mathbf{u}\mathbf{u}) = -\dfrac{\mathrm{Re}}{\gamma\mathrm{M}^2}\dfrac{r_w^{\cdot}}{L^{\cdot}}\nabla p - \nabla\cdot\tau$.

where $\frac{D\chi}{Dt} = \chi_{,t} + \varepsilon \mathbf{u} \cdot \nabla \chi$. The equation of state for a single-phase, single-component system allows the density to be written in terms of pressure and temperature,

$$\frac{1}{\rho}\frac{D\rho}{Dt} = -\beta \frac{DT}{Dt} + \kappa \frac{Dp}{Dt} \tag{C5}$$

where $\beta = -(1/\rho)(\partial \rho / \partial T)_p$ is the thermal expansion coefficient and $\kappa = \rho(\partial p / \partial \rho)_T$ is the bulk modulus. The equation of state is substituted into the mass conservation relation, equation (C4), giving

$$\varepsilon \nabla \cdot \mathbf{u} = -\beta\left(T_{,t} + \varepsilon \mathbf{u} \cdot \nabla T\right) + \kappa\left(p_{,t} + \varepsilon \mathbf{u} \cdot \nabla p\right) \tag{C6}$$

Substituting the series expansion into equation (C6) and expanding to $\boldsymbol{O}(1)$ with β and κ constant gives

$$0 = -\beta T_{0,t} + \kappa p_{0,t} \tag{C7}$$

which states that leading-order temperature and pressure are not, in general, time-dependent. This implies that the density is not time-dependent, but it can still be spatially dependent. Equating $\boldsymbol{O}(\varepsilon)$ terms of equation (C6) gives

$$\nabla \cdot \mathbf{u}_0 = -\beta\left(T_{1,t} + \mathbf{u}_0 \cdot \nabla T_0\right) + \kappa\left(p_{1,t} + \mathbf{u}_0 \cdot \nabla p_0\right) \tag{C8}$$

or, since $\nabla p_0 \approx 0$ from equation (C3),

$$\nabla \cdot \mathbf{u}_0 \approx -\beta\left(T_{1,t} + \mathbf{u}_0 \cdot \nabla T_0\right) + \kappa p_{1,t} \tag{C9}$$

Equation (C9) shows how the problem becomes anelastic in the limit for $\nabla p_0 <<< 1$ where pressure gradients do not significantly contribute to the divergence of the velocity. The divergence of the velocity is primarily a result of bulk-pressure and bulk-temperature changes, and advection through temperature gradients. However, p_0 may still have significant temperature dependence, which will be reflected in the energy equation.

APPENDIX D
TWO-DIMENSIONAL ANELASTIC EXPANSION AND ORDERING

Expansion Series

Consider the conservation equations for mass, momentum, and energy conservation, and the equation of state for an ideal gas:

$$0 = \rho_{,t} + \varepsilon \nabla \cdot (\rho \mathbf{u}) \tag{D1}$$

$$\lambda (\rho \mathbf{u})_{,t} + \varepsilon \lambda \nabla \cdot (\rho \mathbf{u}\mathbf{u}) = -\nabla p - \frac{\lambda}{\mathrm{Va}} \nabla \cdot \tau \tag{D2}$$

$$(\rho T)_{,t} + \varepsilon \nabla \cdot (\rho \mathbf{u} T) = \frac{\gamma - 1}{\gamma} \left(p_{,t} + \varepsilon \mathbf{u} \cdot \nabla p \right) - \frac{1}{\mathrm{Pr\ Va}} \nabla \cdot \mathbf{q} + (\gamma + 1) \frac{\mathrm{M}^2}{\mathrm{Va}} \tau : \nabla \mathbf{u} \tag{D3}$$

$$p = \rho T \tag{D4}$$

where

$$\lambda << \varepsilon << 1 \tag{D5}$$

Also take Va = $\boldsymbol{O}(1)$, Pr = $\boldsymbol{O}(1)$. Assume an expansion of the variables for pressure, temperature, density, and velocity in terms of the unknown functions $f(\varepsilon,\lambda)$, $g(\varepsilon,\lambda)$, $h(\varepsilon,\lambda)$, and $j(\varepsilon,\lambda)$,

$$p = p_0 + f_1(\varepsilon,\lambda) p_1 + f_2(\varepsilon,\lambda) p_2 + \cdots \tag{D6a}$$

$$T = T_0 + g_1(\varepsilon,\lambda) T_1 + g_2(\varepsilon,\lambda) T_2 + \cdots \tag{D6b}$$

$$\rho = \rho_0 + h_1(\varepsilon,\lambda) \rho_1 + h_2(\varepsilon,\lambda) \rho_2 + \cdots \tag{D6c}$$

$$\mathrm{u} = \mathrm{u}_0 + j_1(\varepsilon,\lambda) \mathrm{u}_1 + j_2(\varepsilon,\lambda) \mathrm{u}_2 + \cdots \tag{D6d}$$

The task is to determine f, g, h, and j so that a consistent set of equations is obtained that will describe the oscillating flow problem. Substitute equations (D6a)–(D6d) into equations (D1), (D2), and (D3) and order. At $\boldsymbol{O}(1)$, mass conservation becomes

$$\rho_{0,t} = 0 \tag{D7}$$

and momentum becomes

$$\nabla p_0 = \boldsymbol{O}\left(\varepsilon^2\right)$$

or

$$\nabla p_0 = 0 \tag{D8}$$

which implies $p_{0,t} = 0$ from equation (D7) and the use of the equation of state, (D4). From the energy equation, (D3), we have

$$T_{0,t} = 0 \tag{D9}$$

The leading-order equation of state is thus $p_0 = \rho_0(z)T_0(z)$.

At next order, take the energy equation, (D3), and order,

$$g_1\rho_0 T_{1,t} + h_1 T_0 \rho_{1,t} + \varepsilon\nabla\cdot(\rho_0\mathbf{u}_0 T_0)$$
$$= \frac{\gamma-1}{\gamma}\left(f_1 p_{1,t} + \varepsilon\mathbf{u}_0\cdot\nabla p_0\right) - \frac{g_1}{\mathrm{Pr\,Va}}\nabla\cdot k\nabla T_1 + (\gamma+1)\frac{\mathrm{M}^2}{\mathrm{Va}}\tau_0:\nabla\mathbf{u}_0 \qquad \text{(D10)}$$

Note that $\nabla p_0 = 0$ from equation (D8). Equation (D10) is an order ε relation by virtue of the advection term. Viscous dissipation is negligible at $\boldsymbol{O}(\varepsilon)$, $\mathrm{M}^2 << \varepsilon$. For equation (D10) to balance, $g_1 = h_1 = f_1 = \varepsilon$ (except for the condition that $0 = \nabla\cdot(\rho_0\mathbf{u}_0 T_0) = \nabla\cdot(p_0\mathbf{u}_0) = p_0\nabla\cdot\mathbf{u}_0$ which, in this case, requires that the flow be incompressible, which does not apply to pulse tubes). Equation (D10) becomes

$$\rho_0 T_{1,t} + T_0\rho_{1,t} + \nabla\cdot(\rho_0\mathbf{u}_0 T_0) = \frac{\gamma-1}{\gamma}p_{1,t} - \frac{1}{\mathrm{Pr\,Va}}\nabla\cdot k\nabla T_1 \qquad \text{(D11)}$$

which represents a balance between oscillating bulk temperature, pressure, bulk advection, and conduction. The next-order mass conservation is

$$\rho_{1,t} + \nabla\cdot(\rho_0\mathbf{u}_0) = 0 \qquad \text{(D12)}$$

which is consistent with $\boldsymbol{O}(\varepsilon)$. The next-order momentum equation is

$$\varepsilon\nabla p_1 = \boldsymbol{O}\left(\varepsilon^2\right)$$

or

$$\nabla p_1 = 0 \qquad \text{(D13)}$$

which implies that $p_1 = p_1(t)$. This is consistent with the ordering for energy given in equation (D11). Equations (D11) and (D12) are the leading-order oscillating equations for energy and mass conservation, but we still require the leading-order relation for momentum.

Proceeding, at next order, the energy equation (D3) is

$$g_2\rho_0 T_{2,t} + h_2 T_0\rho_{1,t} + \varepsilon^2 T_1\rho_{1,t} + \varepsilon\nabla\cdot(\varepsilon\mathbf{u}_0 p_1 + j_1\mathbf{u}_1 p_0)$$
$$= \frac{\gamma-1}{\gamma}f_2 p_{2,t} + \frac{\gamma-1}{\gamma}\varepsilon\left(\varepsilon\mathbf{u}_0\cdot\nabla p_1 + j_1\mathbf{u}_1\cdot\nabla p_0\right) - \frac{g_2}{\mathrm{Pr\,Va}}\nabla\cdot k\nabla T_2 + (\gamma+1)\frac{\mathrm{M}^2}{\mathrm{Va}}\tau:\nabla\mathbf{u} \qquad \text{(D14)}$$

Note that $\nabla p_0 = 0$ and $\nabla p_1 = 0$ from equations (D8) and (D13), respectively. Equation (D14) is an $\boldsymbol{O}(\varepsilon^2)$ relation by virtue of the advection and acceleration terms. As long as $\mathrm{M}^2 << \varepsilon^2$, viscous dissipation is negligible. For equation (A14) to balance, $g_2 = h_2 = f_2 = \varepsilon$, and $j_2 = \varepsilon$. Equation (D14) becomes after time-averaging

$$\nabla\cdot(\mathbf{u}_0 p_1 + \mathbf{u}_1 p_0) = -\frac{1}{\mathrm{Pr\,Va}}\nabla\cdot k\nabla T_2 \qquad \text{(D15)}$$

which is a conversion of work to heat conduction. The next-order mass conservation is

$$\rho_{2,t} + \nabla \cdot (\rho_0 \mathbf{u}_1 + \rho_1 \mathbf{u}_0) = 0 \tag{D16}$$

which is consistent with $\boldsymbol{O}(\varepsilon^2)$. The next-order momentum equation is

$$\lambda(\rho_0 \mathbf{u}_0)_{,t} = -\varepsilon^2 \nabla p_2 - \frac{\lambda}{\mathrm{Va}} \nabla \cdot \tau_0 \tag{D17}$$

which from equation (D5) requires that $\lambda = \boldsymbol{O}(\varepsilon^2)$ if equation (D17) is to balance. Equation (D17) becomes

$$(\rho_0 \mathbf{u}_0)_{,t} = -\nabla p_2 - \frac{1}{\mathrm{Va}} \nabla \cdot \tau_0 \tag{D18}$$

which implies that $p_2 = p_2(\mathbf{x},t)$. Hence, momentum is driven by pressure gradients of $\boldsymbol{O}(\lambda)$, whereas the lower-order pressure p_0 represents the mean pressure and $p_1(t)$ represents the bulk oscillating pressure. This separation of pressure into time and space functions is the anelastic approach. Equations (D11), (D12), and (D18) are the oscillating equations for energy, mass, and momentum conservation, respectively.

Carrying out the expansion to the next order shows that the next terms are simply of $\boldsymbol{O}(\varepsilon^3)$. The expansion is thus

$$p = p_0 + \varepsilon p_1(t) + \varepsilon^2 p_2(\mathrm{x},t) + \varepsilon^3 p_3(\mathrm{x},t) + \cdots \tag{D19a}$$

$$T = T_0(\mathrm{x}) + \varepsilon T_1(\mathrm{x},t) + \varepsilon^2 T_2(\mathrm{x},t) + \varepsilon^3 T_3(\mathrm{x},t) + \cdots \tag{D19b}$$

$$\rho = \rho_0(\mathrm{x}) + \varepsilon \rho_1(\mathrm{x},t) + \varepsilon^2 \rho_2(\mathrm{x},t) + \varepsilon^3 \rho_3(\mathrm{x},t) + \cdots \tag{D19c}$$

$$\mathrm{u} = \mathrm{u}_0(\mathrm{x},t) + \varepsilon \mathrm{u}_1(\mathrm{x},t) + \varepsilon^2 \mathrm{u}_2(\mathrm{x},t) + \varepsilon^3 \mathrm{u}_3(\mathrm{x},t) + \cdots \tag{D19d}$$

Equations (D19a)–(D19d) are series expansion in ε. This would seem to be physically correct, because ε is a displacement length of the gas at the tube ends. One would reasonably expect that an oscillating displacement at the tube ends of order ε would result in oscillating-pressure, temperature, and density changes of order ε. However, the pressure gradient that drives the oscillating velocity can be much less than the speed of sound and much less than the resonance frequency of the system; hence, the pressure gradient is of higher order and an anelastic approximation is applicable.

Equations (D19) apply for the specific case of $\lambda = \boldsymbol{O}(\varepsilon^2)$. In general, however, λ can be of higher order, that is, $\lambda = \boldsymbol{O}(\varepsilon^3)$, $\lambda = \boldsymbol{O}(\varepsilon^4)$, $\lambda = \boldsymbol{O}(\varepsilon^5)$, etc. To represent these more general cases, the pressure is written as

$$p = p_0 + \varepsilon p_1(t) + \lambda p_2(\mathrm{x},t) + \varepsilon\lambda p_3(\mathrm{x},t) + \cdots \tag{D20}$$

where $\lambda << \varepsilon << 1$.

Zeroth-Order Equations

From mass conservation, the leading-order density is not a function of time:

$$\rho_{0,t} = 0 \tag{D21}$$

From the zeroth-order momentum equation, pressure is not a function of space:

$$p_{0,z} = 0 \tag{D22}$$

Integrating the energy equation over the total system volume and using the divergence theorem, the leading-order pressure is found not to be a function of time since the temperature boundary conditions are steady and there is no accumulation of energy within the system:

$$p_{0,t} = \frac{\gamma}{\mathcal{V}} \frac{1}{\mathrm{Pr\ Va}} \int_S \mathbf{n} \cdot T_{0,r}\, dS = 0 \tag{D23}$$

The above condition, $p_{0,t} = 0$, combined with the previous condition, $p_{0,z} = 0$, requires that p_0 = constant. The energy equation becomes

$$0 = \frac{1}{\mathrm{Pr\ Va}} \frac{\left(rT_{0,r}\right)_{,r}}{r} \tag{D24}$$

This is coupled to the zeroth-order energy equation for the tube wall

$$0 = \mathrm{Fo}\ \theta_{0,yy} \tag{D25}$$

through the appropriate ordering $\mathrm{Fo} = \boldsymbol{O}\left(\frac{1}{\mathrm{Pr\ Va}}\right)$. This ordering condition requires that $\frac{l^{*2}}{r_w^{*2}} = \boldsymbol{O}\left(\frac{\alpha_w^*}{\alpha_g^*}\right) \ll 1$, allowing the tube wall to be approximated as a thin flat plate with the use of rectangular coordinates in equation (D25).

The boundary conditions for equations (D24) and (D25) are at $r = 0$, $T_{0,r} = 0$; at $y = 1$, $\theta_{0,y} = 0$; and at the interface between the gas and the tube wall, the temperature and heat fluxes are continuous. These conditions require that T_0 be independent of r. Finally, pressure, temperature, and density are related through the equation of state,

$$p_0 = \rho_0(z) T_0(z) = \text{constant} \tag{D26}$$

First-Order Equations

The next-order momentum equation is

$$0 = \frac{\varepsilon}{\lambda} p_{1,z} \tag{D27}$$

which implies that $p_{1,z} \approx 0$ and hence,

$$p_1 = p_1(t) \tag{D28}$$

The next-order mass conservation and equation of state are

$$\rho_{1,t} + \nabla \cdot (\rho_0 \mathbf{u}_0) = 0 \tag{D29}$$

$$p_1 = \rho_0 T_1 + \rho_1 T_0 \tag{D30}$$

The first-order energy equation for the gas is

$$\frac{p_1'}{\gamma} + \nabla \cdot (p_0 \mathbf{u}_0) = \frac{1}{\mathrm{Pr\,Va}} \frac{(rT_{1,r})_{,r}}{r} \tag{D31}$$

This is coupled to the first-order energy equation for the tube wall,

$$\theta_{1,t} = \mathrm{Fo}\, \theta_{1,yy} \tag{D32}$$

The next-order momentum equation is

$$(\rho_0 u_0)_{,t} = -p_{2,z} + \frac{1}{\mathrm{Va}} \frac{(ru_{0,r})_{,r}}{r} \tag{D33}$$

An additional relation is needed to find $p_1(t)$. This relation is obtained from the volume integral of the energy equation

$$p_1' = \frac{\gamma}{\mathcal{V}} \left(\frac{1}{\mathrm{Pr\,Va}} \int_{\mathcal{S}} \mathbf{n} \cdot T_{1,r}\, d\mathcal{S} - \int_{\mathcal{S}} \mathbf{n} \cdot p_0 u_0\, d\mathcal{S} \right) \tag{D34}$$

which states that the periodic nature of $p_1(t)$ results from the forced oscillations from the tube ends and periodic radial heat conduction at the tube walls.

APPENDIX E
REDUCING THE FIRST-ORDER EQUATIONS USING COMPLEX EMBEDDING

Take the nonconservative form of the energy equation in terms of enthalpy

$$0 = \frac{1}{\mathrm{Pr\,Va}} \frac{\left(rT_{1,r}\right)_{,r}}{r} - \rho_0 T_{1,t} + \frac{\gamma - 1}{\gamma} p_{1,t} - \rho_0 \mathbf{u}_0 \cdot \nabla_a T_0 \tag{E1}$$

Expand $\mathbf{u}_0 \cdot \nabla_a T_0$ where $\mathbf{u}_0 \cdot \nabla_a = v_0 \frac{\partial}{\partial r} + u_0 \frac{\partial}{\partial z}$ and $T_{0,r} = 0$

$$0 = \frac{1}{\mathrm{Pr\,Va}} \frac{\left(rT_{1,r}\right)_{,r}}{r} - \rho_0 T_{1,t} + \frac{\gamma - 1}{\gamma} p_{1,t} - \rho_0 u_0 T_0' \tag{E2}$$

Equation (a) in table 4 gives the explicit r-dependence of $u_0(r,z,t)$ as

$$u_0(r,z,t) = \hat{u}_0(r,z)e^{it} = i\frac{\hat{p}_2'(z)}{\rho_0(z)}\left[1 - \zeta_0\left(r,z;\sqrt{\mathrm{Va}}\right)\right]e^{it} \tag{E3}$$

Here complex embedding is used to separate out the time dependence, $\chi = \Re\left[\hat{\chi}(\mathbf{x})e^{it}\right]$, where χ represents the real part of the complex function $\hat{\chi}(\mathbf{x})e^{it}$. In general, $\hat{\chi}(\mathbf{x})$ is spatially dependent and is itself complex. Substituting equation (E3) into (E2) and eliminating the time-dependence results in

$$0 = \frac{1}{\mathrm{Pr\,Va}} \frac{\left(r\hat{T}_{1,r}\right)_{,r}}{r} - i\rho_0 \hat{T}_1 + i\frac{\gamma - 1}{\gamma}\hat{p}_1 - iT_0'\hat{p}_2'\left[1 - \zeta_0\left(r,z;\sqrt{\mathrm{Va}}\right)\right] \tag{E4}$$

This can be solved in terms of r using the boundary conditions at $r = 0$, $\hat{T}_{1,r} = 0$, and at $r = 1$, $\hat{T}_1 = \tilde{T}_w e^{i\phi_T}$, where $\tilde{T}_w$ is the temperature amplitude and ϕ_T is the temperature phase angle at the interface between the gas and the tube wall. Using the equation of state, $1 = \rho_0(z)T_0(z)$, equation (E4) becomes

$$\begin{aligned}\hat{T}_1 = {} & \frac{\gamma - 1}{\gamma}\hat{p}_1 T_0\left[1 - \zeta_0\left(r,z;\sqrt{\mathrm{PrVa}}\right)\right] + \tilde{T}_w e^{i\phi_T}\zeta_0\left(r,z;\sqrt{\mathrm{PrVa}}\right) \\ & - T_0 T_0'\hat{p}_2'\left\{\left[1 - \zeta_0\left(r,z;\sqrt{\mathrm{PrVa}}\right)\right] - \left(\frac{\mathrm{Pr}}{\mathrm{Pr} - 1}\right)\left[\zeta_0\left(r,z;\sqrt{\mathrm{Va}}\right) - \zeta_0\left(r,z;\sqrt{\mathrm{PrVa}}\right)\right]\right\}\end{aligned} \tag{E5}$$

The quantities $\tilde{T}_w$ and ϕ_T are determined by solving the equation for the tube wall,

$$\hat{\theta}_1 = \mathrm{Fo}\,\hat{\theta}_{1,yy} \tag{E6}$$

whose solution is

$$\hat{\theta}_1 = \tilde{T}_w e^{i\phi_T}\left[e^{i\chi y} - e^{i\chi}\left(\frac{i\sin\chi y}{\cos\chi}\right)\right] \tag{E7}$$

where $\chi = \sqrt{\frac{-i}{\mathrm{Fo}}}$.

We now know $\hat{T}_1$ in terms of the unknown pressure $\hat{p}_2(z)$, the unknown oscillating bulk pressure amplitude $\hat{p}_1$, the zeroth-order temperature T_0, the interface temperature amplitude $\tilde{T}_w$, and the temperature phase angle, ϕ_T. Now substitute $\hat{T}_1$ into the first-order equation of state (eq. (h) in table 3) and use the zeroth-order equation of state to obtain $\hat{\rho}_1$ in terms of $\hat{p}_2(z)$.

$$\hat{\rho}_1 = \frac{\hat{p}_1}{T_0} - \frac{\rho_0 \hat{T}_1}{T_0} \tag{E8}$$

$$\begin{aligned}\hat{\rho}_1 = {} & \frac{\hat{p}_1}{T_0} - \frac{\rho_0}{T_0}\tilde{T}_w e^{i\phi_T}\zeta_0\left(r,z;\sqrt{\mathrm{PrVa}}\right) - \frac{\gamma-1}{\gamma}\frac{\hat{p}_1}{T_0}\left[1-\zeta_0\left(r,z;\sqrt{\mathrm{PrVa}}\right)\right] \\ & + \frac{T_0'}{T_0}\hat{p}_2'\left\{\left[1-\zeta_0\left(r,z;\sqrt{\mathrm{PrVa}}\right)\right] - \left(\frac{\mathrm{Pr}}{\mathrm{Pr}-1}\right)\left[\zeta_0\left(r,z;\sqrt{\mathrm{Va}}\right) - \zeta_0\left(r,z;\sqrt{\mathrm{PrVa}}\right)\right]\right\}\end{aligned} \tag{E9}$$

From the first-order mass conservation equation

$$\frac{(\rho_0 \hat{v}_0 r)_{,r}}{r} = -(\rho_0 \hat{u}_0)_{,z} + i\hat{\rho}_1 \tag{E10}$$

substitute for $\hat{\rho}_1$ and $\hat{u}_0$

$$\begin{aligned}\frac{(\rho_0 \hat{v}_0 r)_{,r}}{r} = -i\Bigg(& \hat{p}_2''\left[1-\zeta_0\left(r,z;\sqrt{\mathrm{Va}}\right)\right] \\ & + (\ln T_0)'\,\hat{p}_2'\left\{\left[1-\zeta_0\left(r,z;\sqrt{\mathrm{PrVa}}\right)\right] - \left(\frac{\mathrm{Pr}}{\mathrm{Pr}-1}\right)\left[\zeta_0\left(r,z;\sqrt{\mathrm{Va}}\right) - \zeta_0\left(r,z;\sqrt{\mathrm{PrVa}}\right)\right]\right\} \\ & + \frac{\hat{p}_1}{T_0} - \frac{\gamma-1}{\gamma}\frac{\hat{p}_1}{T_0}\left[1-\zeta_0\left(r,z;\sqrt{\mathrm{PrVa}}\right)\right] - \frac{\rho_0}{T_0}\tilde{T}_w e^{i\phi_T}\zeta_0\left(r,z;\sqrt{\mathrm{PrVa}}\right)\Bigg)\end{aligned} \tag{E11}$$

Integrating equation (E11), and using the boundary condition $v = 0$ at $r = 0$, results in the unknown constant being zero and a relation for $\hat{v}_0$ in terms of r,

$$\hat{v}_0 = i\Bigg(m_1\left(r,z;\sqrt{\mathrm{Va}}\right)T_0\hat{p}_2''$$

$$+\left\{m_1\left(r,z;\sqrt{\mathrm{PrVa}}\right)-\left(\frac{\mathrm{Pr}}{\mathrm{Pr}-1}\right)\left[m_3\left(r,z;\sqrt{\mathrm{Va}}\right)-m_3\left(r,z;\sqrt{\mathrm{PrVa}}\right)\right]\right\}T_0\left(\ln T_0\right)'\hat{p}_2' \qquad \text{(E12)}$$

$$+m_2\left(r,z;\sqrt{\mathrm{PrVa}}\right)p_1+m_3\left(r,z;\sqrt{\mathrm{PrVa}}\right)\frac{\tilde{T}_w}{T_0}e^{i\phi_T}\Bigg)$$

where

$$m_1(r,z;\sigma)=-\left[\frac{r}{2}-m_3(r,z;\sigma)\right] \qquad \text{(E13)}$$

$$m_2\left(r,z;\sqrt{\mathrm{PrVa}}\right)=-\left[\frac{r}{2\gamma}+\frac{\gamma-1}{\gamma}m_3\left(r,z;\sqrt{\mathrm{PrVa}}\right)\right] \qquad \text{(E14)}$$

$$m_3(r,z;\sigma)=\frac{\zeta_1(r,z;\sigma)}{\sigma\sqrt{-i\rho_0(z)}} \qquad \text{(E15)}$$

The no-penetration condition $v_0 = 0$ at $r = 1$ is used to obtain a second-order ordinary differential equation for $\hat{p}_2(z)$ in terms of the unknown bulk pressure amplitude $\hat{p}_1$,

$$0=\hat{p}_2''+\left\{\frac{m_1(1,z;)}{m_1\left(1,z;\sqrt{\mathrm{Va}}\right)}-\frac{\mathrm{Pr}}{\mathrm{Pr}-1}\left[\frac{m_3\left(1,z;\sqrt{\mathrm{Va}}\right)}{m_1\left(1,z;\sqrt{\mathrm{Va}}\right)}-\frac{m_3\left(1,z;\sqrt{\mathrm{PrVa}}\right)}{m_1\left(1,z;\sqrt{\mathrm{Va}}\right)}\right]\right\}\left(\ln T_0\right)'\hat{p}_2'$$

$$+\frac{m_2\left(1,z;\sqrt{\mathrm{PrVa}}\right)}{m_1\left(1,z;\sqrt{\mathrm{Va}}\right)}\frac{\hat{p}_1}{T_0}+\frac{m_3\left(1,z;\sqrt{\mathrm{PrVa}}\right)}{m_1\left(1,z;\sqrt{\mathrm{Va}}\right)}\frac{\tilde{T}_w}{T_0^2}e^{i\phi_T} \qquad \text{(E16)}$$

This is the pressure equation to be solved for $\hat{p}_2(z)$ with unknowns $T_0(z)$, and $\hat{p}_1$.

APPENDIX F
SOLUTION FOR THE THERMALLY STRONG CASE, $\nabla T_0 = 0$

Leading-Order Results

Oscillating First-Order Solutions

For $\nabla T_0 = 0$, we have $p_0 = T_0 = \rho_0 = 1$ and so the pressure equation given by equation (e) in table 4 reduces to

$$0 = \hat{p}_2'' + \frac{m_2\left(1;\sqrt{\mathrm{PrVa}}\right)}{m_1\left(1;\sqrt{\mathrm{Va}}\right)}\hat{p}_1 + \frac{m_3\left(1;\sqrt{\mathrm{PrVa}}\right)}{m_1\left(1;\sqrt{\mathrm{Va}}\right)}\tilde{T}_w e^{i\phi_T} \tag{F1}$$

The general solution is

$$\hat{p}_2 = -\left[\frac{m_2\left(1;\sqrt{\mathrm{PrVa}}\right)}{m_1\left(1;\sqrt{\mathrm{Va}}\right)}\hat{p}_1 + \frac{m_3\left(1;\sqrt{\mathrm{PrVa}}\right)}{m_1\left(1;\sqrt{\mathrm{Va}}\right)}\tilde{T}_w e^{i\phi_T}\right]\frac{z^2}{2} + C_1 z + C_2 \tag{F2}$$

This is substituted into the axial velocity relation given by equation (a) in table 4 to find u_0

$$\hat{u}_0 = -i\left\{C_1 + \left[\frac{m_2\left(1;\sqrt{\mathrm{PrVa}}\right)}{m_1\left(1;\sqrt{\mathrm{Va}}\right)}\hat{p}_1 + \frac{m_3\left(1;\sqrt{\mathrm{PrVa}}\right)}{m_1\left(1;\sqrt{\mathrm{Va}}\right)}\tilde{T}_w e^{i\phi_T}\right]z\right\}\left[1 - \zeta_0\left(r;\sqrt{\mathrm{Va}}\right)\right] \tag{F3}$$

The boundary conditions on axial velocity

$$\text{at } r = 0,\ z = 0,\ \hat{u}_0 = 1 \tag{F4}$$

$$\text{at } r = 0,\ z = 1,\ \hat{u}_0 = \hat{U}_L e^{it} = \tilde{U}_L e^{i(\phi_U + t)} \tag{F5}$$

are used to determine the unknown constants C_1 and $\hat{p}_1$,

$$C_1 = -\frac{i}{1 - \zeta_0\left(0;\sqrt{\mathrm{Va}}\right)} \tag{F6}$$

$$\hat{p}_1 = -i\,\frac{1 - \tilde{U}_L e^{i\phi_U}}{1 - \zeta_0\left(0;\sqrt{\mathrm{Va}}\right)}\frac{m_1\left(1;\sqrt{\mathrm{Va}}\right)}{m_2\left(1;\sqrt{\mathrm{PrVa}}\right)} - \frac{m_3\left(1;\sqrt{\mathrm{PrVa}}\right)}{m_2\left(1;\sqrt{\mathrm{PrVa}}\right)}\tilde{T}_w e^{i\phi_T} \tag{F7}$$

Substitution and simplification gives a simple relation for u_0,

$$\hat{u}_0 = \left[1 - \left(1 - \tilde{U}_L e^{i\phi_U}\right)z\right]\left\{\frac{1 - \zeta_0\left(r;\sqrt{\mathrm{Va}}\right)}{1 - \zeta_0\left(0;\sqrt{\mathrm{Va}}\right)}\right\} \tag{F8}$$

which is linear in z as would be expected in the anelastic limit. After substituting for $\hat{p}_1$ in the temperature equation given by equation (b) in table 4, and recalling $T_0' = 0$, the temperature becomes

$$\hat{T}_1 = -i\frac{\gamma-1}{\gamma}\frac{m_1\left(1;\sqrt{\mathrm{Va}}\right)}{m_2\left(1;\sqrt{\mathrm{PrVa}}\right)}\left\{\frac{1-\zeta_0\left(r;\sqrt{\mathrm{PrVa}}\right)}{1-\zeta_0\left(0;\sqrt{\mathrm{Va}}\right)}\right\}\left(1-\tilde{U}_L e^{i\phi_U}\right)$$
$$+\left(\zeta_0\left(r;\sqrt{\mathrm{PrVa}}\right)-\frac{\gamma-1}{\gamma}\frac{m_3\left(1;\sqrt{\mathrm{PrVa}}\right)}{m_2\left(1;\sqrt{\mathrm{PrVa}}\right)}\left[1-\zeta_0\left(r;\sqrt{\mathrm{PrVa}}\right)\right]\right)\tilde{T}_w e^{i\phi_T} \tag{F9}$$

and for the radial velocity given by equation (d) in table 4,

$$\hat{v}_0 = \frac{m_1\left(1;\sqrt{\mathrm{Va}}\right)}{1-\zeta_0\left(0;\sqrt{\mathrm{Va}}\right)}\left\{\frac{m_2\left(r;\sqrt{\mathrm{PrVa}}\right)}{m_2\left(1;\sqrt{\mathrm{PrVa}}\right)}-\frac{m_1\left(r;\sqrt{\mathrm{Va}}\right)}{m_1\left(1;\sqrt{\mathrm{Va}}\right)}\right\}\left(1-\tilde{U}_L e^{i\phi_U}\right)$$
$$-i\,m_3\left(1;\sqrt{\mathrm{PrVa}}\right)\left\{\frac{m_2\left(r;\sqrt{\mathrm{PrVa}}\right)}{m_2\left(1;\sqrt{\mathrm{PrVa}}\right)}-\frac{m_3\left(r;\sqrt{\mathrm{PrVa}}\right)}{m_3\left(1;\sqrt{\mathrm{PrVa}}\right)}\right\}\tilde{T}_w e^{i\phi_T} \tag{F10}$$

$\hat{\mathrm{Nu}}$ Independence on $\hat{T}_w$ and $\hat{U}_L$

Here we show that $\hat{\mathrm{Nu}}$ is independent of both $\hat{T}_w$ and $\hat{U}_L$. Consider the definition of $\hat{\mathrm{Nu}}$

$$\hat{\mathrm{Nu}} = \frac{\hat{q}_w\big|_{r=1}}{\hat{T}_1\big|_{r=1} - 2\int_0^1 r\hat{T}_1\,dr} \tag{F11}$$

where $\hat{q}_w = -\hat{T}_{1,r}$, hence

$$\hat{\mathrm{Nu}} = \frac{-\hat{T}_{1,r}\big|_{r=1}}{\hat{T}_1\big|_{r=1} - 2\int_0^1 r\hat{T}_1\,dr} \tag{F12}$$

From equation (c) in table 5, $\hat{T}_1$ is of the form

$$\hat{T}_1 = f_1 + f_2\hat{T}_w \tag{F13}$$

where

$$f_1 = f_1(r) = -A + A\zeta_0\left(r;\sqrt{\mathrm{PrVa}}\right) \quad \text{and} \quad f_2 = f_2(r) = -B + (1+B)\zeta_0\left(r;\sqrt{\mathrm{PrVa}}\right) \tag{F14}$$

with

$$A = i\frac{\gamma-1}{\gamma}\frac{m_1\left(1;\sqrt{\mathrm{Va}}\right)}{m_2\left(1;\sqrt{\mathrm{PrVa}}\right)}\frac{1-\hat{U}_L e^{i\phi_U}}{1-\zeta_0\left(0;\sqrt{\mathrm{Va}}\right)} \quad \text{and} \quad B = \frac{\gamma-1}{\gamma}\frac{m_3\left(1;\sqrt{\mathrm{PrVa}}\right)}{m_2\left(1;\sqrt{\mathrm{PrVa}}\right)} \tag{F15}$$

From equation (F13), the derivative and integral are

$$\hat{T}_{1,r}\Big|_{r=1} = f_1' + f_2'\hat{T}_w \quad \text{and} \quad 2\int_0^1 r\hat{T}_1\,dr = f_1^\circ + f_2^\circ\hat{T}_w \tag{F16}$$

where the superscript '$\circ$' indicates the definite integral from $r = 0$ to $r = 1$. Equation (F12) becomes

$$\hat{\mathrm{Nu}} = \frac{-f_1' - f_2'\hat{T}_w}{\hat{T}_w - f_1^\circ - f_2^\circ\hat{T}_w} = \frac{-f_1' - f_2'\hat{T}_w}{\left(1 - f_2^\circ\right)\hat{T}_w - f_1^\circ} \tag{F17}$$

Taking the derivative of equation (F17) with respect to $\hat{T}_w$, we obtain

$$\hat{\mathrm{Nu}}_{,\hat{T}_w} = \frac{\left(\hat{T}_w - f_1^\circ - f_2^\circ\hat{T}_w\right)\left(-f_2'\right) + \left(f_1' + f_2'\hat{T}_w\right)\left(1 - f_2^\circ\right)}{\left(\hat{T}_w - f_1^\circ - f_2^\circ\hat{T}_w\right)^2} \tag{F18}$$

and after simplifying this becomes

$$\hat{\mathrm{Nu}}_{,\hat{T}_w} = \frac{f_1^\circ f_2' + f_1'\left(1 - f_2^\circ\right)}{\left(\hat{T}_w - f_1^\circ - f_2^\circ\hat{T}_w\right)^2} \tag{F19}$$

Taking equation (F14), we obtain for f_1' and f_1°

$$f_1' = -A\sqrt{\mathrm{PrVa}}\,\zeta_1\left(1;\sqrt{\mathrm{PrVa}}\right) \quad \text{and} \quad f_1^\circ = -A + 2A\frac{\zeta_1\left(1;\sqrt{\mathrm{PrVa}}\right)}{\sqrt{\mathrm{PrVa}}} \tag{F20}$$

and for f_2' and f_2°

$$f_2'(r) = -(1+B)\sqrt{\mathrm{PrVa}}\,\zeta_1\left(r;\sqrt{\mathrm{PrVa}}\right) \quad \text{and} \quad f_2^\circ = -B + 2(1+B)\frac{\zeta_1\left(1;\sqrt{\mathrm{PrVa}}\right)}{\sqrt{\mathrm{PrVa}}} \tag{F21}$$

Substituting equations (F20) and (F21) into equation (F16) and then evaluating the numerator of equation (F12) results in

$$\hat{\mathrm{Nu}}_{,\hat{T}_w} = 0 \tag{F22}$$

showing that $\hat{\mathrm{Nu}}$ is independent of $\hat{T}_w$. Similarly, it can be shown that $\hat{\mathrm{Nu}}$ is independent of $\hat{U}_L$. Take f_1 to be of the form

$$f_1 = g_1\left(1 - \hat{U}_L\right) \tag{F23}$$

where

$$g_1 = a\left(-1 + \zeta_0\left(r;\sqrt{\mathrm{Pr\,Va}}\right)\right) \quad \text{and} \quad a = i\frac{\gamma - 1}{\gamma}\frac{m_1\left(1;\sqrt{\mathrm{Va}}\right)}{m_2\left(1;\sqrt{\mathrm{Pr\,Va}}\right)}\frac{1}{1 - \zeta_0\left(0;\sqrt{\mathrm{Va}}\right)} \tag{F24}$$

Substitute equation (F24) into (F23) and substitute the result into equation (F17)

$$\hat{\mathrm{Nu}} = \frac{-g_1'\left(1-\hat{U}_L\right) - f_2'\hat{T}_w}{\hat{T}_w - g_1^{\circ}\left(1-\hat{U}_L\right) - f_2^{\circ}\hat{T}_w} \tag{F25}$$

Now differentiate equation (F25) to give

$$\hat{\mathrm{Nu}}_{,\hat{U}_L} = \frac{\left(\hat{T}_w - g_1^{\circ}\left(1-\hat{U}_L\right) - f_2^{\circ}\hat{T}_w\right)g_1 + \left(g_1'\left(1-\hat{U}_L\right) + f_2'\hat{T}_w\right)g_1^{\circ}}{\left(\hat{T}_w - g_1^{\circ}\left(1-\hat{U}_L\right) - f_2^{\circ}\hat{T}_w\right)^2} \tag{F26}$$

and simplify the result as

$$\hat{\mathrm{Nu}}_{,\hat{U}_L} = \frac{g_1'\hat{T}_w - f_2^{\circ}g_1'\hat{T}_w + f_2'g_1^{\circ}\hat{T}_w}{\left(\hat{T}_w - g_1^{\circ}\left(1-\hat{U}_L\right) - f_2^{\circ}\hat{T}_w\right)^2} \tag{F27}$$

For $\hat{\mathrm{Nu}}$ to be independent of $\hat{T}_w$, the numerator must be equal to zero,

$$0 = g_1'\left(1-f_2^{\circ}\right) + f_2'g_1^{\circ} \tag{F28}$$

Substituting for f_2' and f_2° of equations (F21), equation (F28) becomes

$$g_1'\left(-B + 2(1+B)\frac{\zeta_1\left(1;\sqrt{\mathrm{PrVa}}\right)}{\sqrt{\mathrm{PrVa}}} - 1\right) = -(1+B)\sqrt{\mathrm{PrVa}}\,\zeta_1\left(r;\sqrt{\mathrm{PrVa}}\right)g_1^{\circ} \tag{F29}$$

or after rearranging

$$g_1'(1+B)\left(\frac{\zeta_1\left(1;\sqrt{\mathrm{PrVa}}\right)}{\sqrt{\mathrm{PrVa}}} - 1\right) = -(1+B)\sqrt{\mathrm{PrVa}}\,\zeta_1\left(r;\sqrt{\mathrm{PrVa}}\right)g_1^{\circ} \tag{F30}$$

Now from equations (F24)

$$g_1' = -a\sqrt{\mathrm{PrVa}}\zeta_1\left(r;\sqrt{\mathrm{PrVa}}\right) \quad \text{and} \quad g_1^{\circ} = -a + \frac{a\zeta_1\left(r;\sqrt{\mathrm{PrVa}}\right)}{\sqrt{\mathrm{PrVa}}} \tag{F31}$$

Substituting equations (F31) into equation (F30) gives

$$-a\sqrt{\mathrm{PrVa}}\zeta_1\left(r;\sqrt{\mathrm{PrVa}}\right)(1+B)\left(\frac{\zeta_1\left(1;\sqrt{\mathrm{PrVa}}\right)}{\sqrt{\mathrm{PrVa}}} - 1\right)$$

$$= -(1+B)\sqrt{\mathrm{PrVa}}\,\zeta_1\left(r;\sqrt{\mathrm{PrVa}}\right)\left(-a + \frac{a\zeta_1\left(r;\sqrt{\mathrm{PrVa}}\right)}{\sqrt{\mathrm{PrVa}}}\right) \tag{F32}$$

which reduces to an identity.

Mean-Steady Solutions

Eulerian Mean-Steady Velocity Vector, $\overline{U}_1$

The mean-steady velocity components produced by the Reynolds stresses are determined by equations (46) and (47). Recalling that $\rho_0 = 1$, they are respectively,

$$\frac{\left(\overline{v_0 u_0}\right)_{,r}}{r} + \left(\overline{u_0 u_0}\right)_{,z} = -\bar{p}_{3,z} + \frac{1}{\mathrm{Va}} \frac{\left(r\bar{u}_{1,r}\right)_{,r}}{r} \tag{F33}$$

$$0 = \int_0^1 \left(\overline{u_1} + \overline{\rho_1 u_0}\right) r\, dr \tag{F34}$$

The associated boundary conditions are $\bar{u}_{1,r} = 0$ at $r = 0$ (symmetry) and $\bar{u}_1 = 0$ at $r = 1$ (no slip). Equations (F33) and (F34) and boundary conditions are used to solve for $\bar{u}_1$ and $\bar{p}_{3,z}$. The mean-steady quadratic components are determined by recalling that for $\chi_1 = \Re\left[\hat{\chi}_1 e^{it}\right]$ and $\chi_2 = \Re\left[\hat{\chi}_2 e^{it}\right]$

$$\overline{\chi_1^2} = \frac{1}{2}\hat{\chi}_1 \hat{\chi}_1^{cc} \tag{F35}$$

$$\overline{\chi_1 \chi_2} = \frac{1}{2}\Re\left[\hat{\chi}_1 \hat{\chi}_2^{cc}\right] = \frac{1}{2}\Re\left[\hat{\chi}_2 \hat{\chi}_1^{cc}\right] \tag{F36}$$

where the superscript 'cc' represents the complex conjugate. Carrying out the integrations of equations (F33) and (F34) gives $\bar{u}_1$ and $\bar{p}_{3,z}$ in table 8. with the axial Eulerian mean-steady velocity given by $\overline{u}_1$,

$$\overline{u}_1 = \bar{u}_1 + \overline{\rho_1 u_0} \tag{F37}$$

Equation (48) gives the relation for the mean-steady mass flux

$$0 = \frac{\left(\overline{v_1} r + \overline{\rho_1 v_0} r\right)_{,r}}{r} + \left(\overline{u_1} + \overline{\rho_1 u_0}\right)_{,z} \tag{F38}$$

The observed radial Eulerian mean-steady velocity is given by $\overline{v}_1$,

$$\overline{v}_1 = \bar{v}_1 + \overline{\rho_1 v_0} \tag{F39}$$

Using equations (F37) and (F39), equation (F38) can be rewritten as

$$0 = \frac{\left(\overline{v}_1 r\right)_{,r}}{r} + \overline{u}_{1,z} \tag{F40}$$

A single quadrature of equation (F40) and using the boundary condition $\overline{v}_1 = 0$ at $r = 0$ gives

$$\overline{v}_1(r,z) = -\frac{1}{r}\int r\overline{u}_{1,z}\, dr \tag{F41}$$

Table 8. Mean-steady solutions for $\bar{u}_1(r,z)$.

$$\frac{\bar{u}_1}{\mathrm{Va}} = Q_2(r,z) + J_2(r,z) + \left(r^2 - 1\right)K(z) \qquad \text{(a)}$$

$$\bar{p}_{3,z} = 16\left[q_3(1,z) - \frac{1}{2}q_2(1,z) + g_3(1,z) - \frac{1}{2}g_2(1,z) + k_3\right] \qquad \text{(b)}$$

where

$$Q_2(r,z) = q_2(r,z) - q_2(1,z) \qquad \text{(c)}$$

$$G_2(r,z) = g_2(r,z) - g_2(1,z) \qquad \text{(d)}$$

$$K(z) = 4\left[k_3(z) + q_3(z) + g_3(z)\right] - 2\left[q_2(1,z) + g_2(1,z)\right] \qquad \text{(e)}$$

and

$$q_2(r,z) = \int \frac{1}{r}\int \eta\left(\frac{\hat{u}_0\hat{u}_0^{cc}r}{2}\right)_{,z} d\eta\, dr \qquad q_3(z) = \int_0^1 q_2(r,z)\, r\, dr \qquad \text{(f, g)}$$

$$g_2(r,z) = \int \frac{\Re\left[\hat{v}_0\hat{u}_0^{cc}\right]}{2} dr \qquad g_3(z) = \int_0^1 j_2(r,z)\, r\, dr \qquad \text{(h, i)}$$

$$k_3(z) = \frac{1}{\mathrm{Va}}\int_0^1 \Re\left[\frac{\hat{\rho}_1\hat{u}_0^{cc}r}{2}\right] dr \qquad \text{(j)}$$

We also note that equation (F40) defines the mean-steady stream function,

$$-\frac{\psi_{,r}}{r} = \bar{u}_1 \qquad \text{and} \qquad +\frac{\psi_{,z}}{r} = \bar{v}_1 \qquad \text{(F42)}$$

Lagrangian Mean-Steady Particle Velocity Vector, $\bar{\mathbf{u}}_p$

As previously discussed, the mean-steady particle velocity is used in describing the mean-steady particle path. The mean-steady particle velocities were presented in equations (79) and (80), and are reiterated here,

$$\bar{u}_p(r,z) = \bar{u}_1 + \overline{u_{0,r}\int_0^t v_0 d\tau} + \overline{u_{0,z}\int_0^t u_0 d\tau} \tag{F43}$$

and

$$\bar{v}_p(r,z) = \bar{v}_1 + \overline{v_{0,r}\int_0^t v_0 d\tau} + \overline{v_{0,z}\int_0^t u_0 d\tau} \tag{F44}$$

To compute, first recall that $\chi = \Re\left[\hat{\chi}e^{it}\right] = \frac{1}{2}\left(\hat{\chi}e^{it} + \hat{\chi}^{cc}e^{-it}\right)$, thus

$$\chi_{,\eta} = \frac{1}{2}\left(\hat{\chi}_{,\eta}e^{it} + \hat{\chi}^{cc}_{,\eta}e^{-it}\right) \quad \text{and} \quad \int^t \chi\, d\tau = \frac{i}{2}\left(-\hat{\chi}e^{it} + \hat{\chi}^{cc}e^{-it}\right) \tag{F45}$$

so that

$$\chi_{1,\eta}\int^t \chi_2\, d\tau = \frac{i}{4}\left(-\hat{\chi}_2\hat{\chi}_{1,\eta}e^{2it} + \hat{\chi}_2^{cc}\hat{\chi}^{cc}_{1,\eta}e^{-2it} + \hat{\chi}_2^{cc}\hat{\chi}_{1,\eta} - \hat{\chi}_2\hat{\chi}^{cc}_{1,\eta}\right) \tag{F46}$$

hence,

$$\overline{\chi_{1,\eta}\int^t \chi_2\, d\tau} = \frac{i}{4}\left(\hat{\chi}_2^{cc}\hat{\chi}_{1,\eta} - \hat{\chi}_2\hat{\chi}^{cc}_{1,\eta}\right) \tag{F47}$$

Using equation (F47), the particle velocities given by equations (F43) and (F44) become

$$\bar{u}_p(z,r) = \bar{u}_1 + \frac{i}{4}\left(\hat{v}_0^{cc}\hat{u}_{0,r} - \hat{v}_0\hat{u}^{cc}_{0,r} + \hat{u}_0^{cc}\hat{u}_{0,z} - \hat{u}_0\hat{u}^{cc}_{0,z}\right) \tag{F48}$$

and

$$\bar{v}_p(z,r) = \bar{v}_1 + \frac{i}{4}\left(\hat{v}_0^{cc}\hat{v}_{0,r} - \hat{v}_0\hat{v}^{cc}_{0,r}\right) \tag{F49}$$

since $\hat{v}_{0,z} = \hat{v}^{cc}_{0,z} = 0$.

Mean-Steady Temperature, $\bar{T}_2$

The mean-steady $\bar{T}_2$ temperature is defined by the energy equation given by equation (m) in table 3,

$$\frac{1}{\mathrm{PrVa}}\frac{\left(r\bar{T}_{2,r}\right)_{,r}}{r} = \left(\bar{u}_1 + \overline{p_1 u_0}\right)_{,z} + \frac{1}{r}\left(\bar{v}_1 r + \overline{p_1 v_0 r}\right)_{,r} - \frac{\Gamma^2}{\mathrm{PrVa}}\bar{T}_{0,zz} \tag{F50}$$

For computational purposes it is found from

$$\frac{1}{\mathrm{PrVa}}\frac{\left(r\bar{T}_{2,r}\right)_{,r}}{r} = \left(\bar{u}_1 + \Re\left[\hat{p}_1\hat{u}_0^{cc}\right]\right)_{,z} + \frac{1}{r}\left(\bar{v}_1 r + \Re\left[\hat{p}_1\hat{v}_0^{cc}r\right]\right)_{,r} - \frac{\Gamma^2}{\mathrm{PrVa}}\bar{T}_{0,zz} \tag{F51}$$

Integrating twice and applying the boundary conditions at $r=0$, $\overline{T}_{2,r}=0$ and at $r=1$, $\overline{T}_2=0$ leads to

$$\overline{T}_2(r,z)=\mathrm{PrVa}\left[w_1(r,z)-w_1(1,z)+w_2(r,z)-w_2(1,z)\right]-\frac{\Gamma^2}{4}\overline{T}_{0,zz}\left(1-r^2\right) \tag{F52}$$

or since $\nabla T_0=0$ for the thermally strong problem,

$$\overline{T}_2(r,z)=\mathrm{PrVa}\left[w_1(r,z)-w_1(1,z)+w_2(r,z)-w_2(1,z)\right] \tag{F53}$$

where

$$w_1(r,z)=\int\frac{1}{r}\int^r\sigma\left(\overline{u}_1+\Re\left[\hat{p}_1\hat{u}_0^{cc}\right]\right)_{,z}d\sigma\,dr \tag{F54}$$

and

$$w_2(r,z)=\int\left(\overline{v}_1+\Re\left[\hat{p}_1\hat{v}_0^{cc}\right]\right)dr \tag{F55}$$

APPENDIX G
COMPUTATIONAL PROGRAM

The symbolic application used to compute the solutions was Wolfram Research Mathematica v. 2.2.2. for the Macintosh. The following program code directly translates from the text.

The user must specify the variables in the cell titled 'Input system parameters and number of terms in Bessel function for 10-digit accuracy in ber and bei'. The units are noted. Each variable is commented for clarity. The variable 'TERM' is specified to provide the accuracy required of the Bessel function that is computed with a series expansion. The number of terms depends on the value for Va, and a commented field suggests the number of terms for various Va.

Immediately after running the program, a shaded cell block prints all relevant parameters, including dimensional specifications and nondimensional numbers. The program continues computing leading-order oscillating solutions:

TW	= amplitude of gas/tube wall interface temperature
PHIT	= phase angle of gas/tube wall interface temperature
u0Re	= oscillating axial velocity
v0Re	= oscillating radial velocity
p1Re	= oscillating pressure
T1Re	= oscillating temperature
rho1Re	= oscillating density
q1	= oscillating heat flux
NuC	= complex Nusselt number

and mean-steady quantities:

u0T1ReAvg	= axial enthalpy flux
u0p1ReAvg	= axial work flux
rhoSuSAvg	= axial Eulerian velocity
rhoSvSAvg	= radial Eulerian velocity
upAvg	= axial particle velocity
vpAvg	= radial particle velocity
T2	= temperature

These quantities are plotted in phasor diagrams and field plots.

```
(* FileName and prereq *)

<<Calculus`VectorAnalysis`
<<Graphics`Graphics`
Needs["Graphics`PlotField`"];
Share[];
(* conversion factors and constants *)
convertInToCm=(2.54 cm)/in;
convertInToCmSqrt=Sqrt[2.54^2 cm^2]/in;
convertCgsToDyne=dyne/(g cm/sec^2);
convertAtmtoMPa=0.10133MPa/atm;
J=W sec;
meter=(100cm);
GasConstantStar=8.3143 J/(mol K)  (*82.05cm^3 atm/(mol*K*MW)*);

(* Bounds on vector fields *)
jAxialRMSBoundIso :=(jAxialRMSFlow[0,0,0],jAxialRMSFlow[1,0,0])
jAxialRMSBoundHXfr:=(jAxialRMSFlow[0,0,TW],jAxialRMSFlow[1,0,TW])
rhoSuSBoundIso:=
      {{rhoSuS[0,0,0],rhoSuS[.67,0,0],rhoSuS[.89,0,0]},{rhoSuS[0,1,0],rhoSuS[.67,1,0],rhoSuS[.89,1,0]}};
hAxialFluxBoundIso:=
      {{hAxialFlux[0,0,0,0],hAxialFlux[.67,0,0,0],hAxialFlux[.89,0,0,0]},
       {hAxialFlux[0,1,0,0],hAxialFlux[.67,1,0,0],hAxialFlux[.89,1,0,0]}};
hAxialFluxBoundHXfr:=
      {{hAxialFlux[0,0,TW,0],hAxialFlux[.67,0,TW,0],hAxialFlux[.89,0,TW,0]},
       {hAxialFlux[0,1,TW,0],hAxialFlux[.67,1,TW,0],hAxialFlux[.89,1,TW,0]}};

(* Predefined significant digits *)
dateLock=Date[]
date:=Prepend[Drop[Drop[dateLock,1],-2],StringJoin[kindSystem,N[Va,3]]];
epsilon:=N[eps,3]
valensi:=N[Va,4]
prandlt:=N[Pr,3]
fourier:=N[Fo,5]
vpf:=valensi * prandlt * fourier
strouhal:=N[1/eps,4]
IsoPR:=N[IsoPressRatio,4]
AdiPR:=N[AdiVolPR,4]
PHIUPrint:=N[PHIU,3]
PHITPrint:=N[PHIT,4]

{1997, 3, 15, 19, 24, 57}

(* MASTER Linear & Secondary *)

(* Master Linear *)

(* I/O AND FUNCTIONS *)

(* PARAMETERS *)

   Input Parameters in English or cgs units

(* Input cgs *)

(* Input cgs Parameters *)

  (* OPT *)

(* Input system parameters and number of terms in Bessel function for 10 digit accuracy in ber and bei *)
type="";                          (* CC or Thesis *)
type2="dT/dz=0";                  (* dT/dz<>0 *)
freqStar= 3/(sec);                 (*  a freq baseline of 1Hz corresponds to Va=50.  *)
rwStar= .81649 cm;                (*  baseline=.04442cm;  2 *.00254 (*Sqrt[.1Power[.053,2]]*)cm*)
                                  (*  Va adjustment; .053cm corresponds to VaPr=1;.04442cm to Va=1  *)
LStar= 10 cm;                     (*  baseline=10cm;  eps adjustment *)
pistonDynAmpStar[0,0]= .02 cm;    (*  baseOPT=1.0cm, BPT=1.4142cm; M adj;*)
pistonDynAmpStar[0,LStar]= 1.0*pistonDynAmpStar[0,0];    (* as a percentage of pistonDynAmpCm[0,0] *)
PHIU =-.10;                       (* velocity phase angle of UL wrt U0; PHIU<0 means UL lags U0 *)
TERM=16;                          (* .1Hz is Va=5->TERM=7;.6Hz is Va=30->TERM=11; 1Hz is Va=50->TERM=13,
                                     2Hz is Va=100->TERM=15, 5Hz is Va=250->TERM=19,
                                     6Hz is Va=300->TERM=22  *)
                                  (* for PV and V-1 then TERM=6; for PV and V-10 then TERM=18;
                                     for V^2=30, TERM=10; for V^2=300, TERM=22 *)

(* Input Tube wall domain *)
rho0TubeStar= 7.820 g/cm^3;           (* stainless steel *)
Cp0TubeStar= 0.46 J/(g K);            (* stainless steel *)
kTubeStar= 0.163 W/(cm K);            (* stainless steel *)
tubeThicknessStar= .004903 cm;        (*Fo adjustment; 0.026853 cm corresponds to Fo=1 *)

(* Input gas domain *)
tempLowGasStar=50K;
tempRefGasStar= 300K;
pressureRefStar= 9.866 atm;       (*pressureMeanStar=pressureRefStar*)
Cp0GasStar= 5.2 J/(g K);          (*air at STP 300K: 1.005 J/(g K)*)     (*He: 5.2 J/(g K)*)
kGasStar= 0.00149 W/(cm K);       (*air at STP 300K:0.000267 W/(cm K)*)  (*He at STP: 0.00149 W/(cm K);
                                  (note: for kGas=.0010471552, Pr=1.000000000)*)
muStar= 2.0134*10^-4 g/(cm sec);  (*air at 300K:1.843*10^-4 g/(cm sec); He:2.0134*10^-4 g/(cm s)
                                   @ any resonable pressure*)
MWStar= 4.2*10^-3 kg/mol;         (*air at STP 300K: 32*10^-3 kg/mol; He:4.2*10^-3 kg/mol*)
GAMMA= 5/3;                       (* 7/5 for air *)(* 5/3 for He *)


(* Output gas calculations *)

rhoRefGasStar=pressureRefStar*(300K/tempRefGasStar)*1.624*10^-4 g/(atm cm^3);
                                  (*air at STP 300K: 1.170*10^-3 g/(atm cm^3)*)
                                  (*He density/atm @ 1 atm: 1.624*10^-4 g/(atm cm^3);*)
nuStar=muStar/rhoRefGasStar;      (*air at STP 300K: 0.1566 cm^2/sec; He:0.124 cm^2/sec*)
a0Star=Sqrt[GAMMA Simplify[
   GasConstantStar/MWStar tempRefGasStar J/(sec W) (kg meter^2/sec^2)/J (sec^2/cm^2)]] cm/sec;
                                  (*air at STP Anderson pg.55;
                                     He:Sqrt[GAMMA 2.08*10^7 300]cm/s;= 101,980cm/s *)

(* Ouput convert from Star=cgs to English units *)
rwInch=rwStar/convertInToCm;
LInch=LStar/convertInToCm;
tubeThicknessInch=tubeThicknessStar/convertInToCm;
pistonDynAmpInch[0,0]=pistonDynAmpStar[0,0]/convertInToCm;
pistonDynAmpInch[0,LInch]=pistonDynAmpStar[0,LStar]/convertInToCm;
pressureRefStarMPa=pressureRefStar convertAtmtoMPa;
```

```
(* Input English Parameters and convert to cgs *)

type="CC";                                          (* CC or Thesis *)
type2="dT/dz=0";                                    (* dT/dz<>0 *)
freqStar= 15/sec;                                     (* set *)
rwInch= .5*7/8 in;   (* Va adjustment *)  (* valueForV*Sqrt[nu/omegaBar]/convertInToCmSqrt allows
                                              specified value for V *)
LInch= 5 in; (* eps adj *)(* 15*+5/8* is the undisplaced tube length *)
pistonDynAmpInch[0,0]= 1 in (*LInch/(2Pi)*); (* M adj *)(*=piston dynamic amplitude;
                                                    (1.09)/2 in is 13cc compressor pistonDynAmpInch;
                                                for spec eps, pistonDynAmpInch[0,0]=eps LInch/(2Pi)*)
pistonDynAmpInch[0,LInch]= 0.2 pistonDynAmpInch[0,0];
PHIU =-0.25;                                  (* velocity phase angle of UL wrt U0; PHIU<0 means UL lags U0 *)
TERM=15;                                      (* for PV and V-1 then TERM=6; for PV and V-10 then TERM=18 *)

(* Input Tube wall domain *)
rho0TubeStar= 7.820 g/cm^3;                   (* stainless steel *)
Cp0TubeStar= 0.46 J/(g K);                    (* stainless steel *)
kTubeStar= 0.163 W/(cm K);                    (* stainless steel *)
tubeThicknessInch= 0.020 in;                  (* Fo adjustment *)

(* Input gas domain *)
tempRefGasStar= 300K;
pressureRefStar= 10 atm;            (*"pressureMeanStar=pressureRefStar")
Cp0GasStar= 5.2 J/(g K);            (*air at STP 300K: 1.005 J/(g K)")     (*He: 5.2 J/(g K)*)
kGasStar= 0.00149 W/(cm K);         (*air at STP 300K:0.000267 W/(cm K)")  (*He at STP: 0.00149 W/(cm K);
                                    (note: for kGas=.0010471552, Pr=1.0000000000)*)
muStar= 2.0134*10^-4 g/(cm sec);    (*air at 300K:1.843*10^-4 g/(cm sec);
                                       He:2.0134*10^-4 g/(cm s) @ any resonable pressure*)
MWStar= 4.2*10^-3 kg/mol;           (*air at STP 300K: 32*10^-3 kg/mol; He:4.2*10^-3 kg/mol*)
GAMMA= 5/3;                         (* 7/5 for air *)(* 5/3 for He *)

(* Output gas calculations *)
rhoRefGasStar=pressureRefStar*(tempRefGasStar/(300K))*1.624*10^-4 g/(atm cm^3);
                                  (*air at STP 300K: 1.170*10^-3 g/(atm cm^3)*)
                                  (*He density/atm @ 1 atm: 1.624*10^-4 g/(atm cm^3);*)
nuStar=muStar/rhoRefGasStar;            (*air at STP 300K: 0.1566 cm^2/sec; He:0.124 cm^2/sec*)
a0Star=Sqrt[GAMMA GasConstantStar/MWStar tempRefGasStar] cm/sec;
                           (*air at STP Anderson pg.55;He:Sqrt[GAMMA 2.08*10^7 300]cm/s;= 101,980cm/s *)

(* Ouput convert from English to Star units *)
rwStar                    =rwInch*convertInToCm;
LStar                     =LInch*convertInToCm;
tubeThicknessStar         =tubeThicknessInch*convertInToCm;
pistonDynAmpStar[0,0]     =pistonDynAmpInch[0,0]*convertInToCm;
pistonDynAmpStar[0,LStar] =pistonDynAmpInch[0,LInch]*convertInToCm;

   Calculated Parameters Used in Calculations

(* Dimensional Parameters Calculated *)
p0=1;
If[type2=="dT/dz=0",T0[z]=1,T0[z]=.];
If[type2=="dT/dz=0",T0[0]=1,T0[0]=.];
rho0[z_]:=1/T0[z];

omegaBarStar          = 2Pi freqStar;                                  (* characteristic inverse time period *)
UStar[0,0]            = omegaBarStar*pistonDynAmpStar[0,0];    (* U0=Amplitude of d/dt{[pistonDynAmpCm[0,0]
                                                                    Sin[omegaBarStar t]]*)
UStar[0,LStar]        = omegaBarStar*pistonDynAmpStar[0,LStar];(* U0=Amplitude of d/dt{[pistonDynAmpCm[0,0]
                                                                    Sin[omegaBarStar t + phiU]] *)
UStar[0,0,t_]        := UStar[0,0    ] Cos[t       ]           (* t=omegaBarStar tStar *)
UStar[0,LStar,t_]    := UStar[0,LStar] Cos[t + PHIU]

alpha0TubeStar      =kTubeStar/(rho0TubeStar Cp0TubeStar);
alpha0GasStar       =kGasStar/(rhoRefGasStar Cp0GasStar);
h0scFlux0Star       =rhoRefGasStar*Cp0GasStar*UStar[0,0]*tempRefGasStar;
xSectAreaStar       =Pi*rwStar^2//N;
h0scFlow0Star       =xSectAreaStar*h0scFlux0Star;
j0scFlux0Star       =rhoRefGasStar*UStar[0,0];
j0scFlow0Star       =xSectAreaStar*j0scFlux0Star;
qGasRadial0Star     =kGasStar*tempRefGasStar/rwStar;
wallShearStress0Star=muStar UStar[0,0]/rwStar;
tubeInnerArea       =2 Pi rwStar LStar;
drag0Star           =wallShearStress0Star tubeInnerArea convertCgsToDyne//N;
deltaTStar          =tempRefGasStar-tempLowGasStar;
deltaT              =(tempRefGasStar-tempLowGasStar)/tempRefGasStar;

volOfTubeStar := Pi rwStar^2 LStar
(*velocityCombo[t_]:=UL*Cos[2Pi t]/Cos[2Pi(t+PHIU)]*)

periodStar=1/freqStar;
tauStar=periodStar;  (* characteristic time is the period *)

(* Nondimensional Parameters Calculated *)
M       =UStar[0,0]/a0Star;
Va      =rwStar^2 omegaBarStar/nuStar;
Pr      =muStar Cp0GasStar/kGasStar;
Fo              =alpha0TubeStar/(omegaBarStar tubeThicknessStar^2);
eps     =pistonDynAmpStar[0,0]/LStar;
S       =1/eps;
LAMBDA  =M^2/(eps GAMMA);
CAPGAMMA=rwStar/(LStar*eps);
U0      =UStar[0,0]/UStar[0,0];
UL      =UStar[0,LStar]/UStar[0,0];
KGAS    =kGasStar/kTubeStar ;
KTUBE   =kTubeStar/kTubeStar;
EL      =tubeThicknessStar/rwStar//N;
Re0     =j0scFlux0Star 2 rwStar/muStar;

(* Circular (IPi: Va, VsPr, and 1/Fo used in complex solutions *)
V =Sqrt[Va];
P =Sqrt[Pr];
PV=Sqrt[Pr]*V;
F =Sqrt[1/Fo];

(* placeholders use as variables and others *)
Uo=.;Ul=.;(*Fo=.*)
d[0]=pistonDynAmpStar[0,0]    /LStar;
d[1]=pistonDynAmpStar[0,LStar]/LStar;
volSystem[t_] := 1 - d[0]Sin[2Pi t] + d[1] Sin[2Pi(t + PHIU)];
```

```
(* calc Iso and Adi pressure Ratios and assign fileNames *)
FindMinimum[volSystem[t],{t,.5}];
timeVolMin=t/.%[[2,1]];
If[timeVolMin<.5,timeVolMax=timeVolMin+.5,timeVolMax=timeVolMin-.5,timeVolMax=timeVolMin-.5];
IsoPressRatio= volSystem[timeVolMax]/volSystem[timeVolMin]//N;
AdiVolPR=(volSystem[timeVolMax]/volSystem[timeVolMin])^GAMMA//N;

(* calc CL pressure *)
p1CLhat[Uo_,Ul_,phiU_] = (-I GAMMA)*(Uo-Ul Exp[I 2Pi phiU])//ComplexExpand;
p1CL[Uo_,Ul_,phiU_,t_] = p1CLhat[Uo,Ul,phiU]*Exp[I 2Pi t]//ComplexExpand;
p1CLRe[Uo_,Ul_,phiU_,t_] = p1CL[Uo,Ul,phiU,t]-I Coefficient[p1CL[Uo,Ul,phiU,t],I]//N;
FindMinimum[eps*p1CLRe[U0,UL,PHIU,t],{t,.5}];
p1CLAdiaAmpl=Abs[%[[1]]];
p1CLAdiaPR=(1+p1CLAdiaAmpl)/(1-p1CLAdiaAmpl);

(* 1D Hflow based on u0p1 *)
(* Hflux1DStar=(AdiVolPR-1)*pressureRefStar/(AdiVolPR+1);*)

(* 1D Hflow based on Rays Eqn 2-38 NIST TN 1343 *)
HFlowRayStar[jOscWarmInGramPerSec_,THotInK_,PdynInAtm_,PmeanInAtm_]:=
   (1/2) GasConstantStar/MWStar THotInK jOscWarmInGramPerSec (PdynInAtm/PmeanInAtm) kg/(1000 g)//N
HFlowRayStar2[jOscColdInGramPerSec_,TcoldInK_,PdynInAtm_,PmeanInAtm_,phiRadians_]:=
   (1/2) jOscColdInGramPerSec GasConstantStar/MWStar TcoldInK (PdynInAtm/PmeanInAtm) Cos[phiRadians] kg/(1000 g)//N

(* Field Graphics Coordinates *)
texter=Graphics[{Text["r=0",{0.5,-.14},{0,1}],Text["r=1",{0.5,1.13},{0,-1}],
                 Text["z=0",{-.06,0.5},{1,0}],Text["z=1",{1.06,0.5},{-1,0}]}];
liner[{x1_,y1_},{x2_,y2_}]:=Graphics[Line[{{x1,y1},{x2,y2}}]];

(* Assign fileNames *)
If[d[0]==0 || d[1]==0,kindSystem=BPT,kindSystem=OPT,kindSystem=OPT];

If[kindSystem==BPT,
fileNameBPTIsoList={(*type,*)"BPT","eps","Va","Pr","VaPr","UL","PHIU","M","LAMBDA","IsoPressRatio",
                    "AdiPressRatio","CLAdiPRatio"};
fileNameBPTHXfrList={fileNameBPTIsoList,{"Fo",{"PHIT","TW"},"VaPrFo"},
                    "(totalDragAmp0, totalDragRMS/tube, HOscFlow0Star)","date"};
flowNamesBPT:={(*type,*)"BPT",epsilon,valensi,prandlt,N[valensi prandlt,5],N[UL,2],
                    "n/aPHIU",N[M,4],N[LAMBDA,3]};
PRNames:={IsoPR,AdiPR,p1CLAdiaPR};
HXferNames:={fourier, {PHITPrint,TW}, vpf};
dragNames:={drag0Star (Amp),totalDragRMSStar"(tube^-1)",hOscFlow0Star//N};
fileNameBPTIso:={flowNamesBPT,PRNames};
fileNameBPTHXfr:={fileNameBPTIso,HXferNames,dragNames,date}];

If[kindSystem==OPT,
fileNameOPTIsoList={(*type,*)"OPT","eps","Va","Pr","VaPr","UL","PHIU","M","LAMBDA","IsoPressRatio",
                    "AdiPressRatio","CLAdiPRatio"};
fileNameOPTHXfrList={fileNameOPTIsoList,{"Fo",{"PHIT","TW"},"VaPrFo"},
                   "(totalDragAmp0, totalDragRMS/tube, HOscFlow0Star)","date"};
flowNamesOPT:={(*type,*)"OPT",epsilon,valensi,prandlt,N[valensi prandlt,5],N[UL,2],PHIUPrint,N[M,4],N[LAMBDA,3]};
PRNames:={IsoPR,AdiPR,p1CLAdiaPR};
HXferNames:={fourier, {PHITPrint,TW}, vpf};
dragNames:={drag0Star (Amp),totalDragRMSStar"(tube^-1)",hOscFlow0Star//N};
fileNameOPTIso:={flowNamesOPT,PRNames};
fileNameOPTHXfr:={fileNameOPTIso,HXferNames,dragNames,date}];

(*
If[kindSystem==BPT,
fileNameBPTIsoList={type,"BPT","eps","V","P","PV","UL","PHIU","M","IsoPressRatio","AdiVolPR","CLAdiPRatio"};
fileNameBPTHXfrList={fileNameBPTIsoList,{"F",{"PHIT","TW"}},{"HOscFlow0"},date};
fileNameBPTIso:={type,"BPT",epsilon,V//N,P//N,N[PV,5],N[UL,2],"n/aPHIU",N[M,4],IsoPR,AdiPR,p1CLAdiaPR};
fileNameBPTHXfr:={fileNameBPTIso,{F//N, {PHITPrint,TW}},{hOscFlow0Star//N}}];

If[kindSystem==OPT,
fileNameOPTIsoList={type,"OPT","eps","V","P","PV","UL","PHIU","M","IsoPressRatio","AdiVolPR","CLAdiPRatio"};
fileNameOPTHXfrList={fileNameOPTIsoList,{"F",{"PHIT","TW"}},{"HOscFlow0"},date};
fileNameOPTIso:={type,"OPT",epsilon,V//N,P//N,N[PV,5],N[UL,2],PHIUPrint,N[M,4],IsoPR,AdiPR,p1CLAdiaPR};
fileNameOPTHXfr:={fileNameOPTIso,{F//N, {PHITPrint,TW}},{hOscFlow0Star//N}}];
*)
```

Print parameters

```
• DIMENSIONAL VARIABLES SPECIFIED:
{{OPT, eps, Va, Pr, VaPr, UL, PHIU, M, LAMBDA, IsoPressRatio, AdiPressRatio, CLAdiPRatio}, {Fo, {PHIT, TW}, VaPrFo},

  {totalDragAmp0, totalDragRMS/tube, HOscFlow0Star}, date}
                                                  -6        -9
{{{OPT, 0.002, 100., 0.703, 70.266, 1., -0.1, 3.789 10  , 4.31 10  }, {1.002, 1.004, 1.00413}}, {100., {PHIT, TW}, 7026.6},

  {0.00476915 Amp dyne, (tube^-1) totalDragRMSStar, 1.97349 W}, {OPT<>100., 3, 15, 19}}

-- inches:
rw =0.321453 in; L =3.93701 in; tubeThickness =0.00193031 in; pistonDynAmpInchAt0 =0.00787402 in; pistonDynAmpInchAtL =0.00787402 in


-- cgs:
                                                                        3                          2
rw =0.81649 cm; L =10 cm; tubeThickness =0.004903 cm; volOfTube =20.9436 cm ; CrossSectArea=2.09436 cm
                                                             3
pistonDynAmpAt0 =0.02 cm; pistonDynAmpAtL =0.02 cm; freq =---
                                                          sec

                0.376991 cm                 0.376991 cm               0. cm                                                 0.00160224 g
pistonSpeedU0 =------------; pistonSpeedUL =------------; ΔpistonSpeed =-----; pRef =0.999722 MPa; tempRef =300 K; rhoRef =------------
                   sec                         sec                      sec                                                       3
                                                                                                                                 cm
                       2                                                                                2
             0.045313 cm             7.82 g          0.46 sec W        0.163 W          0.045313 cm
alphaTube =-------------; rho0Tube =-------; Cp0Tube =-----------; kTube =--------; alphaTube =------------
                 sec                    3                g K            cm K                  sec
                                       cm
                       2                                                                                         2
             0.178836 cm          0.00160224 g        5.2 sec W        0.00149 W      99488.6 cm       0.125662 cm         0.00020134 g
alpha0Gas =-------------; rho0Gas =-------------; Cp0Gas =----------; kGas =----------; a0 =-----------; nu =-------------; mu =------------
                 sec                    3                 g K             cm K             sec               sec                cm sec
                                       cm
             0.942286 W                                 0.00060403 g             0.00126506 g              0.547465 W
hOscFlux0 =-----------; hOscFlow0 =1.97349 W; jOscFlux0 =-------------; jOscFlow0 =-------------; qGasRadial0 =-----------; HFlowRay =
                 2                                           2                        sec                            2
               cm                                          cm  sec                                                  cm
```

```
            0.00040268 g Pi                                        Pi
  HFlowRayStar[---------------, 300 K, 0.0203251 atm, 9.866 atm, --]
                      sec                                          6

totalDragAmpl0 =0.00476915 dyne; totalDragRMS/tube =(tube^-1) totalDragRMSStar

• NON-DIMENSIONAL SCALING VARIABLES CALCULATED:

                                                                        -6
Va=100.; Pr=0.703; Pr*Va=70.2663; S =500.; Fo=100.; EL=0.00600497; M=3.78929 10  ; Re0 =4.89902
p0=1; T0[z]=1 ; rho0[z]=1

• NON-DIMENSIONAL VARIABLES USED IN COMPLEX SOLUTION:

                                                          -6                    -9
V=10.; P=0.83825; PV=8.3825; eps=0.002; F=0.1; M=3.78929 10  ; LAMBDA=4.30762 10  ; eps*Va=0.2
                                                             5
U0=1.; UL=1.; PHIU=-0.1; TERM=16; KGAS =0.0091411; KTUBE=1.; GAMMA=-; d0=0.002; dL=0.002
                                                             3

Archive

 (* FUNCTIONS *)

   Modified Bessel fxn expansion into real and imaginary parts

ber[order_,r_,z_,sigma_,TERM]=(r sigma Sqrt[rho0[z]]/2)^order *
      Sum[Cos[(3order/4+k/2)Pi]/(Factorial[k] Gamma[order+k+1])*(((r sigma Sqrt[rho0[z]])^2)/4)^k,{k,0,TERM}];
bei[order_,r_,z_,sigma_,TERM]=(r sigma Sqrt[rho0[z]]/2)^order *
      Sum[Sin[(3order/4+k/2)Pi]/(Factorial[k] Gamma[order+k+1])*(((r sigma Sqrt[rho0[z]])^2)/4)^k,{k,0,TERM}];

ber[0,r_,z_,V,TERM]=ber[0,r,z,V,TERM];
bei[0,r_,z_,V,TERM]=bei[0,r,z,V,TERM];
ber[1,r_,z_,V,TERM]=ber[1,r,z,V,TERM];
bei[1,r_,z_,V,TERM]=bei[1,r,z,V,TERM];
ber[0,r_,z_,PV,TERM]=ber[0,r,z,PV,TERM];
bei[0,r_,z_,PV,TERM]=bei[0,r,z,PV,TERM];
ber[1,r_,z_,PV,TERM]=ber[1,r,z,PV,TERM];
bei[1,r_,z_,PV,TERM]=bei[1,r,z,PV,TERM];

ModBesselJHold[order_,r_,z_,sigma_]:=Hold[ber[order,r,z,sigma,TERM]]+I Hold[bei[order,r,z,sigma,TERM]];
(* BesselJ[0,Sqrt[-I]sigma]=ber[0,1,sigma,TERM]+I bei[0,1,sigma,TERM] *)

   (* Test expansion accuracy *)

(* BesselJ, ber+I bei, large argument approximation *)
Print["V = ",V//N,"   TERM =",TERM]
besselAccuracyList="{   {V}   ;BesselJ; (ber+I bei); ModBesselJHold; Argument->infinity approximation)";
besselAccuracyHi=N[Abs[{{V},BesselJ[0,   Sqrt[-I]V],ber[0,1   ,z,V,TERM]+I bei[0,1   ,z,V,TERM],
                  ModBesselJHold[0,   1,z,V]//ReleaseHold,Sqrt[2/(Pi*Sqrt[-I]   V)]Cos[   Sqrt[-I]V-Pi/4]}],9]
besselAccuracyLo=N[Abs[{{0.1V},BesselJ[0,0.1Sqrt[-I]V],ber[0,0.1,z,V,TERM]+I bei[0,0.1,z,V,TERM],
                  ModBesselJHold[0,0.1,z,V]//ReleaseHold,Sqrt[2/(Pi*Sqrt[-I]0.1V)]Cos[0.1Sqrt[-I]V-Pi/4]}],9]


V = 10.   TERM =16

{{9.99999925}, 149.847528, 149.847526, 149.847526, 148.537427}

{{0.999999925}, 1.01552483, 1.01552483, 1.01552483, 1.00386903}

   kse: r-coordinate fxns

kseTemplate=ComplexExpand[(aVarKse+I bVarKse)/(cVarKse+I dVarKse)];
kseImTemplate=Coefficient[kseTemplate,I];
kseReTemplate=kseTemplate-I kseImTemplate;

kseReHold[order_,r_,z_,sigma_]=kseReTemplate/.
{aVarKse->HoldForm[ber[order,r,z,sigma,TERM]],
 bVarKse->HoldForm[bei[order,r,z,sigma,TERM]],
 cVarKse->HoldForm[ber[0,1,z,sigma,TERM]],
 dVarKse->HoldForm[bei[0,1,z,sigma,TERM]]};
kseImHold[order_,r_,z_,sigma_]=kseImTemplate/.
{aVarKse->HoldForm[ber[order,r,z,sigma,TERM]],
 bVarKse->HoldForm[bei[order,r,z,sigma,TERM]],
 cVarKse->HoldForm[ber[0,1,z,sigma,TERM]],
 dVarKse->HoldForm[bei[0,1,z,sigma,TERM]]};
kseHold[order_,r_,z_,sigma_]=kseReHold[order,r,z,sigma]+I kseImHold[order,r,z,sigma];

   m: r-coordinate fxns

m3Template=
  ComplexExpand[(aVarM3+I bVarM3)(cVarM3+I dVarM3)];
m3ImTemplate=Coefficient[m3Template,I];
m3ReTemplate=m3Template-I m3ImTemplate;

mReHold[3,r_,z_,sigma_]=m3ReTemplate/.
{aVarM3->HoldForm[-1/(sigma Sqrt[2 rho0[z]])],
 bVarM3->HoldForm[-1/(sigma Sqrt[2 rho0[z]])],
 cVarM3->kseReHold[1,r,z,sigma],
 dVarM3->kseImHold[1,r,z,sigma]};
mImHold[3,r_,z_,sigma_]=m3ImTemplate/.
{aVarM3->HoldForm[-1/(sigma Sqrt[2 rho0[z]])],
 bVarM3->HoldForm[-1/(sigma Sqrt[2 rho0[z]])],
 cVarM3->kseReHold[1,r,z,sigma],
 dVarM3->kseImHold[1,r,z,sigma]};

mReHold[1,r_,z_,sigma_]=-(1/p0)(r/2 -                    mReHold[3,r,z,sigma]);
mImHold[1,r_,z_,sigma_]=-(1/p0)(    -                    mImHold[3,r,z,sigma]);
mReHold[2,r_,z_,sigma_]=-(1/p0)(r/(2 GAMMA) + ((GAMMA-1)/GAMMA) mReHold[3,r,z,sigma]);
mImHold[2,r_,z_,sigma_]=-(1/p0)(            + ((GAMMA-1)/GAMMA) mImHold[3,r,z,sigma]);

(*
mHold[1,r_,z_,sigma_]=mReHold[1,r,z,sigma] + I mImHold[1,r,z,sigma];
mHold[2,r_,z_,sigma_]=mReHold[2,r,z,sigma] + I mImHold[2,r,z,sigma];
mHold[3,r_,z_,sigma_]=mReHold[3,r,z,sigma] + I mImHold[3,r,z,sigma];
*)

mRatioTemplate=ComplexExpand[(aVarMRatio+I bVarMRatio)/(cVarMRatio+I dVarMRatio)];
mRatioImTemplate=Coefficient[mRatioTemplate,I];
mRatioReTemplate=mRatioTemplate-I mRatioImTemplate;
mRatioReHold[{kindNum_,rNum_,sigmaNum_},{kindDem_,rDem_,sigmaDem_},z_]=mRatioReTemplate/.
{aVarMRatio->mReHold[kindNum,rNum,z,sigmaNum],
 bVarMRatio->mImHold[kindNum,rNum,z,sigmaNum],
 cVarMRatio->mReHold[kindDem,rDem,z,sigmaDem],
```

```
 dVarMRatio->mImHold[kindDem,rDem,z,sigmaDem]};
mRatioImHold[{kindNum_,rNum_,sigmaNum_},{kindDem_,rDem_,sigmaDem_},z_]=mRatioImTemplate/.
{aVarMRatio->mReHold[kindNum,rNum,z,sigmaNum],
 bVarMRatio->mImHold[kindNum,rNum,z,sigmaNum],
 cVarMRatio->mReHold[kindDem,rDem,z,sigmaDem],
 dVarMRatio->mImHold[kindDem,rDem,z,sigmaDem]};
mRatioHold[{kindNum_,rNum_,sigmaNum_},{kindDem_,rDem_,sigmaDem_},z_]=
    mRatioReHold[{kindNum,rNum,sigmaNum},{kindDem,rDem,sigmaDem},z] +
  I mRatioImHold[{kindNum,rNum,sigmaNum},{kindDem,rDem,sigmaDem},z];
 (* end m's *)

   time coordinate fxn

timeHold[t_]=HoldForm[timeRe[t]]+I HoldForm[timeIm[t]];
timeRe[t_]=Cos[2Pi t];
timeIm[t_]=Sin[2Pi t];

timeTwHold[t_, phiT_]=HoldForm[timeTwRe[t],phiT]+I HoldForm[timeTwRe[t],phiT];
timeTwRe[t_,phiT_]=Cos[2Pi (t+phiT)];
timeTwIm[t_,phiT_]=Sin[2Pi (t+phiT)];
(* end time *)

   Set certain functions that remain constant to a numerical Value using ReleaseHold

Timing[
mRe[3,1,z_,V] =mReHold[3,1,z,V]//ReleaseHold//N;
mIm[3,1,z_,V] =mImHold[3,1,z,V]//ReleaseHold//N;
mRe[3,1,z_,PV]=mReHold[3,1,z,PV]//ReleaseHold//N;
mIm[3,1,z_,PV]=mImHold[3,1,z,PV]//ReleaseHold//N;
mRe[1,1,z_,V]=mReHold[1,1,z,V]//ReleaseHold//N;
mIm[1,1,z_,V]=mImHold[1,1,z,V]//ReleaseHold//N;
mRe[2,1,z_,PV]=mReHold[2,1,z,PV]//ReleaseHold//N;
mIm[2,1,z_,PV]=mImHold[2,1,z,PV]//ReleaseHold//N;

kseRe[0,r_,z_,V]=kseReHold[0,r,z,V]//ReleaseHold//N;
kseIm[0,r_,z_,V]=kseReHold[0,r,z,V]//ReleaseHold//N;
kseRe[0,r_,z_,PV]=kseReHold[0,r,z,PV]//ReleaseHold//N;
kseIm[0,r_,z_,PV]=kseReHold[0,r,z,PV]//ReleaseHold//N;

kseRe[1,r_,z_,V]=kseReHold[1,r,z,V]//ReleaseHold//N;
kseIm[1,r_,z_,V]=kseReHold[1,r,z,V]//ReleaseHold//N;
kseRe[1,r_,z_,PV]=kseReHold[1,r,z,PV]//ReleaseHold//N;
kseIm[1,r_,z_,PV]=kseReHold[1,r,z,PV]//ReleaseHold//N;

mRatioRe[{1,1,V},{2,1,PV},z_]=mRatioReHold[{1,1,V},{2,1,PV},z]//ReleaseHold//N;
mRatioIm[{1,1,V},{2,1,PV},z_]=mRatioImHold[{1,1,V},{2,1,PV},z]//ReleaseHold//N;
mRatioRe[{3,1,PV},{2,1,PV},z_]=mRatioReHold[{3,1,PV},{2,1,PV},z]//ReleaseHold//N;
mRatioIm[{3,1,PV},{2,1,PV},z_]=mRatioImHold[{3,1,PV},{2,1,PV},z]//ReleaseHold//N;

mRatioRe[{1,r_,V},{1,1,V},z_]=mRatioReHold[{1,r,V},{1,1,V},z]//ReleaseHold//N;
mRatioIm[{1,r_,V},{1,1,V},z_]=mRatioImHold[{1,r,V},{1,1,V},z]//ReleaseHold//N;
mRatioRe[{2,r_,PV},{2,1,PV},z_]=mRatioReHold[{2,r,PV},{2,1,PV},z]//ReleaseHold//N;
mRatioIm[{2,r_,PV},{2,1,PV},z_]=mRatioImHold[{2,r,PV},{2,1,PV},z]//ReleaseHold//N;
mRatioRe[{3,r_,PV},{3,1,PV},z_]=mRatioReHold[{3,r,PV},{3,1,PV},z]//ReleaseHold//N;
mRatioIm[{3,r_,PV},{3,1,PV},z_]=mRatioImHold[{3,r,PV},{3,1,PV},z]//ReleaseHold//N;
]

{12.4333 Second, Null}

   Derivatives of r,z,t fxns *)

DkseReR[0,r_,z_,V]=D[kseRe[0,r,z,V],r]//N;
DkseImR[0,r_,z_,V]=D[kseIm[0,r,z,V],r]//N;
DkseReR[0,r_,z_,PV]=D[kseRe[0,r,z,PV],r]//N;
DkseImR[0,r_,z_,PV]=D[kseIm[0,r,z,PV],r]//N;

DmRatioReR[{1,r_,V},{1,1,V},z_]=D[mRatioRe[{1,r,V},{1,1,V},z],r]//N;
DmRatioImR[{1,r_,V},{1,1,V},z_]=D[mRatioIm[{1,r,V},{1,1,V},z],r]//N;
DmRatioReR[{2,r_,PV},{2,1,PV},z_]=D[mRatioRe[{2,r,PV},{2,1,PV},z],r]//N;
DmRatioImR[{2,r_,PV},{2,1,PV},z_]=D[mRatioIm[{2,r,PV},{2,1,PV},z],r]//N;
DmRatioReR[{3,r_,PV},{3,1,PV},z_]=D[mRatioRe[{3,r,PV},{3,1,PV},z],r]//N;
DmRatioImR[{3,r_,PV},{3,1,PV},z_]=D[mRatioIm[{3,r,PV},{3,1,PV},z],r]//N;


(*
DkseReR[0,r_,z_,sigma_]=D[kseReHold[0,r,z,sigma]//ReleaseHold,r]//N;
DkseImR[0,r_,z_,sigma_]=D[kseImHold[0,r,z,sigma]//ReleaseHold,r]//N;
DkseReR[0,r_,z_,V]=D[kseReHold[0,r,z,V]//ReleaseHold,r]//N;
DkseImR[0,r_,z_,V]=D[kseImHold[0,r,z,V]//ReleaseHold,r]//N;
*)

DtimeReT[t_]=D[timeRe[t],t];
DtimeImT[t_]=D[timeIm[t],t];
DtimeTwReT[t_,phiT_]=D[timeTwRe[t,phiT],t];
DtimeTwImT[t_,phiT_]=D[timeTwIm[t,phiT],t];


(*
Du0hatRTemplate = (Uo-(Uo-Ul Exp[I 2Pi phiU])z)(1-(DkseRe0rzVR + I DkseIm0rzVR))/(1-(kseRe00zV + I kseIm00zV));
Du0hatZTemplate = D[(Uo-(Uo-Ul Exp[I 2Pi phiU])z)(1-(kseRe0rzV + I kseIm0rzV))/(1-(kseRe00zV + I kseIm00zV)),z];

Dv0hatRTemplate = ((mRe11zV + I mIm11zV)/(1-(kseRe00zV+I kseIm00zV)))*
     ((DmRatioRe2rPV21PVzR + I DmRatioIm2rPV21PVzR)-(DmRatioRe1rV11VzR + I DmRatioIm1rV11VzR))(Uo-Ul Exp[I 2Pi phiU]) -
              I*(mRe31zPV+I mIm31zPV)*((DmRatioRe2rPV21PVzR+I DmRatioIm2rPV21PVzR)-
                (DmRatioRe3rPV31PVzR+I DmRatioIm3rPV31PVzR))*Tw*Exp[I 2Pi phiT];

Dv0hatZTemplate = ((mRe11zV + I mIm11zV)/(1-(kseRe00zV+I kseIm00zV)))*
     ((mRatioRe2rPV21PVz + I mRatioIm2rPV21PVz)-(mRatioRe1rV11Vz + I mRatioIm1rV11Vz))(Uo-Ul Exp[I 2Pi phiU]) -
              I*(mRe31zPV+I mIm31zPV)*((mRatioRe2rPV21PVz+I mRatioIm2rPV21PVz)-
               (mRatioRe3rPV31PVz+I mRatioIm3rPV31PVz))*Tw*Exp[I 2Pi phiT];

Dv0hatZTemplate = 0; (* for at least the gratT0=0 case *)
*)


(* Thin tube-wall solution 2-D planar limit ComplexExpansion.
   This cell contains TIRe defined interms of unknown Tw and phiT and
   Derivatives of theta1Re wrt y, and TIRe wrt r.  Note that these are not
   multiplied by eps.  Solution for the wall temp coupling does not require
   eps - it cancels out. *)
```

```
(* thetaTemplate to be used for finding temp coupling theta1 and for the actual temp
   distribution over the tube wall domain, of course  with appropriate assignments *)
si=F Sqrt[-I];
(* differential eqn. for thetaX *)
thetaIFindTw=ComplexExpand[Tw*Exp[I 2Pi phiT] Exp[I 2Pi t](Exp[I si y]-Exp[I si] I Sin[si y]/Cos[si])];
thetaIReFindTw[y_,t_,F_,phiT_,Tw_]=thetaIFindTw-I Coefficient[thetaIFindTw,I];

(* theta1 derivative is easy for the amount of Mathematica memory available *)
DthetaIReFindTwY[y_,t_,F_,phiT_,Tw_]=Collect[D[thetaIReFindTw[y,t,F,phiT,Tw],y],Tw]//N;

(* DT1RTemplateFindTw is a specific template used to find Tw. *)
DT1RTemplateFindTw = ComplexExpand[(-I (((GAMMA-1)/GAMMA) (Uo-Ul Exp[I 2Pi phiU]}
        (mRatioRe11V21PVz+I mRatioIm11V21PVz)*
        (0-(DkseReR0rzPV+I DkseImR0rzPV)) / (1-(kseRe00zV+I kseIm00zV))) +
             (  (DkseReR0rzPV+I DkseImR0rzPV)-(((GAMMA-1)/GAMMA)(mRatioRe13PV21PVz+I mRatioIm31PV21PVz)*
             (0-(DkseReR0rzPV+I DkseImR0rzPV)))) Tw Exp[I 2Pi phiT])*Exp[I 2Pi t]];
DT1ImRTemplateFindTw = Coefficient[DT1RTemplateFindTw,I];
DT1ReRTemplateFindTw = DT1RTemplateFindTw-I DT1ImRTemplateFindTw;

(* take derivative manually term-by-term to save time *)
DT1ReFindTwRHoldTemp[r_,z_,t_,V,PV,Uo_,Ul_,phiU_,phiT_,Tw_]=DT1ReRTemplateFindTw/.
       {mRatioRe11V21PVz->HoldForm[mRatioRe[{1,1,V},{2,1,PV},z]],
        mRatioIm11V21PVz->HoldForm[mRatioIm[{1,1,V},{2,1,PV},z]],
        DkseReR0rzPV->HoldForm[DkseReR[0,r,z,PV]],
       DkseImR0rzPV->HoldForm[DkseImR[0,r,z,PV]],
        kseRe00zV->HoldForm[kseRe[0,0,z,V]],
        kseIm00zV->HoldForm[kseIm[0,0,z,V]],
        mRatioRe31PV21PVz->HoldForm[mRatioRe[{3,1,PV},{2,1,PV},z]],
        mRatioIm31PV21PVz->HoldForm[mRatioIm[{3,1,PV},{2,1,PV},z]]};
DT1ReFindTwRHold[r_,z_,t_,V,PV,Uo_,Ul_,phiU_,phiT_,Tw_]=
  Collect[Expand[DT1ReFindTwRHoldTemp[r,z,t,V,PV,Uo,Ul,phiU,phiT,Tw]],Tw];

DT1ImFindTwRHoldTemp[r_,z_,t_,V,PV,Uo_,Ul_,phiU_,phiT_,Tw_]=DT1ImRTemplateFindTw/.
       {mRatioRe11V21PVz->HoldForm[mRatioRe[{1,1,V},{2,1,PV},z]],
        mRatioIm11V21PVz->HoldForm[mRatioIm[{1,1,V},{2,1,PV},z]],
        DkseReR0rzPV->HoldForm[DkseReR[0,r,z,PV]],
       DkseImR0rzPV->HoldForm[DkseImR[0,r,z,PV]],
        kseRe00zV->HoldForm[kseRe[0,0,z,V]],
        kseIm00zV->HoldForm[kseIm[0,0,z,V]],
        mRatioRe31PV21PVz->HoldForm[mRatioRe[{3,1,PV},{2,1,PV},z]],
        mRatioIm31PV21PVz->HoldForm[mRatioIm[{3,1,PV},{2,1,PV},z]]};
DT1ImFindTwRHold[r_,z_,t_,V,PV,Uo_,Ul_,phiU_,phiT_,Tw_]=
  Collect[Expand[DT1ImFindTwRHoldTemp[r,z,t,V,PV,Uo,Ul,phiU,phiT,Tw]],Tw];


(* Data list for fitting He conductivity to curve *)

condDataStar={{.8, 20,.02830},{.8, 25,.03108},{.8, 30,.03518},{.8, 40,.04160},{.8,50,.04766},{.8,60,.05342},
              {.8, 80,.06426},{.8,100,.07439},{.8,120,.08396},{.8,140,.09310},{.8,160,.1019},{.8,180,.1103},
              {.8,200,.1185} ,{.8,220,.1265} ,{.8,240, .1343},{.8,260,.1418} ,{.8,280,.1492},{.8,300,.1565},
              {.8,350,.1740} ,{.8,400,.1909}};
condFitStar[p_,T_]=Fit[condDataStar,{1,p,T,p^2,T^2,p^3,T^3},{p,T}];


================================================

(* SOLVE FOR TW AND PHIT *)

(* Solve for TWhat here *)

For Po = 99.9996
TWhat = 0.31027 - 0.0779612 I
TW = 0.319915
PHIT = -0.0391796


(* OLD Solve for TW *)

   First Round: Solve for implicit function

(* Equate heat flux at the wall.  Solve for Tw and make the assignment to
   Twall[z,t,V,PV,Uo,Ul,phiU,phiT,KGAS,F,KTube].
   We can retain the z-dependence in Tw, but to first order, Tw is constant in z.
   So we can take the value of Tw at z=0 to speed-up the calc *)

Timing[
tempVar=Solve[DthetaIReFindTwY[0,t,F,phiT,Tw]==KGAS DT1ReFindTwRHold[1,z,t,V,PV,Uo,Ul,phiU,phiT,Tw],Tw];
Twall[1,z_,t_,V,PV,Uo_,Ul_,phiU_,phiT_,KGAS,F,KTUBE]=Tw/.tempVar[[1,1]]//ReleaseHold//N;
deltaTw[1,z_,{t1_,t2_},V,PV,Uo_,Ul_,phiU_,phiT_,KGAS,F,KTUBE]=
 Twall[1,z,t2,V,PV,Uo,Ul,phiU,phiT,KGAS,F,KTUBE]-Twall[1,z,t1,V,PV,Uo,Ul,phiU,phiT,KGAS,F,KTUBE];]

{17.6667 Second, Null}

   Second Round: Numerical Root Finder

   Numerically find phiT and Tw if you can make a good guess.
                  Otherwise, use 'plotting tools' below.
                  If root found, assign it to PHIT and Tw.
   Check the value found for PHIT. Tw should be constant for all z.

tempVar=N[FindRoot[deltaTw[1,0,{.1,.45},V,PV,U0,UL,PHIU,phiT,KGAS,F,KTUBE]==0,{phiT,.3}]];

tempPHIT = 0.260785; tempTW = -0.516552
PHIT=-0.239215
Twall={0.516552, 0.516552, 0.516552, 0.516552, 0.516552, {0.516552}}

(* check z (in)dependence of Twall *)

Plot[Twall[1,z,0,V,PV,U0,UL,PHIU,PHIT,KGAS,F,KTUBE],{z,0,1}]


-Graphics-

   Additional resources for finding Tw and PHIT: Plotting tools and intermediate saving of Parameters!!

(* Plotting Tools to find root *)

(* Plots to find approximate value of PHIT at Tw=0. D[Twall t] continuous *)

(* Plot over ENTIRE RANGE *)

Timing[Block[{t1=.1,t2=.45},Plot[deltaTw[1,0,{t1,t2},V,PV,U0,UL,PHIU,phiT,KGAS,F,KTUBE],
      (phiT,0,1),(*PlotRange->{-.1,.1},*)AxesLabel->{"phiT","ΔTw"}]]]
```

```
{3.05 Second, -Graphics-}

(* Plot over ZOOM-IN RANGE. *)

(* Increase the spread in t   up to Δt->0.5 for steeper curves that are closer    to the singularity
   Decrease the spread in t down to Δt->0   for shallow curves that are farther from the singularity *)
Timing[Block[{t1=.45,t2=.55},Plot[deltaTw[1,0,{t1,t2},V,PV,U0,UL,PHIU,phiT,KGAS,F,KTUBE],
      {phiT,.35,.45},(*PlotRange->{-.1,.1},*)AxesLabel->{"phiT","ΔTw"}]]]


{0.483333 Second, -Graphics-}

(* Try to Numerically find PHIT and TW again *)

(* If you can now make a good guess for starting point. Use the plotting tools above to get an approximate
   idea of where the root is. The numerical method used is secant method. *)
FindRoot[deltaTw[1,0,{.45,.55},V,PV,U0,UL,PHIU,phiT,KGAS,F,KTUBE]==0,
         {phiT,{.36,.38}}]
(*PHIT=phiT/.%[[1]];*)
If[Less[tempTW,0],PHIT=tempPHIT-.5,PHIT=tempPHIT];
(*If[Greater[tempPHIT,+0.5],PHIT=tempPHIT- 1,PHIT=tempPHIT];*)

Print["PHIT=",PHIT];
Print["Twall=",{Twall[1,0,.0,      V,PV,U0,UL,PHIU,PHIT,KGAS,F,KTUBE],
                Twall[1,0,.125,    V,PV,U0,UL,PHIU,PHIT,KGAS,F,KTUBE],
                Twall[1,0,.25,     V,PV,U0,UL,PHIU,PHIT,KGAS,F,KTUBE],
                Twall[1,0,.50,     V,PV,U0,UL,PHIU,PHIT,KGAS,F,KTUBE],
                Twall[1,0,Random[],V,PV,U0,UL,PHIU,PHIT,KGAS,F,KTUBE]}];

          TW = Twall[1,0,Random[],V,PV,U0,UL,PHIU,PHIT,KGAS,F,KTUBE];

(* intermediate saving of ParameterList *)

Print["(* INTERMEDIATE SAVING OF CALCULATED Twall[1,0,t,V,PV,U0,UL,PHIU,phiT,KGAS,F,KTUBE] *)"];
Print["(* FOR ParameterList[",pListVar,"]",", *)"];
Print["Twall[1,0,t_,V,PV,U0,UL,PHIU,phiT_,KGAS,F,KTUBE]=",Twall[1,0,t,V,PV,U0,UL,PHIU,phiT,KGAS,F,KTUBE],";"];


(* INTERMEDIATE SAVING OF CALCULATED lambdaAt1 and Twall[1,0,t,V,PV,U0,UL,PHIU,phiT,KGAS,F,KTUBE] *)
(* FOR ParameterList[pListVar] *)
lambdaAt1=0.00394773 - 0.0000298093 I; lambdaAt1Re=0.00394773; lambdaAt1Im=-0.0000298093;
Twall[1,0,t_,V,PV,U0,UL,PHIU,phiT_,KGAS,F,KTUBE]=

  (-0.00807124 (77.2504 Cos[6.28319 t] + 88.2443 Sin[6.28319 t])) /

   (15.1675 Cos[1.3376 - 6.28319 phiT - 6.28319 t] - 6.39891 Cos[6.28319 (phiT + t)] -

     84.1828 Cos[6.28319 phiT + 6.28319 t] - 8.66834 Sin[1.3376 - 6.28319 phiT - 6.28319 t] +

     0.526423 Sin[6.28319 (phiT + t)] + 84.1828 Sin[6.28319 phiT + 6.28319 t]);

========= (* AUTOBREAK *) ===========
• PARAMETER LIST (for use in exporting to plot routines)
ParameterList={V,PV,KGAS,KTUBE,U0,UL,M,eps,GAMMA,PHIU,F,TERM,N[TW,5],N[PHIT,5]}
                                                                       -6              5
ParameterList={5.6419 Sqrt[Pi], 4.72932 Sqrt[Pi], 0.0091411, 1., 1., 1., 1.20617 10   Pi, 0.002, -, -0.1, 0.0564191 Sqrt[Pi], 16, 0.31991, -0.03918}
                                                                                               3

• SOLUTION OF TW AT PHIT FOR CONTINUITY OF HEAT FLUX AT GAS/TUBE BOUNDARY
TW=0.319915 at PHIT=-0.0391796

• RANDOM TIME CHECK, ALL VALUES FOR TW SHOULD BE THE SAME
tRandom=0.215549
PHIT=-0.0391796
Twall={Twall[1., 0, 0., 10., 8.3825, 1., 1., -0.1, -0.0391796, 0.0091411, 0.1, 1.],

   Twall[1., 0, 0.125, 10., 8.3825, 1., 1., -0.1, -0.0391796, 0.0091411, 0.1, 1.],

   Twall[1., 0, 0.25, 10., 8.3825, 1., 1., -0.1, -0.0391796, 0.0091411, 0.1, 1.],

   Twall[1., 0, 0.5, 10., 8.3825, 1., 1., -0.1, -0.0391796, 0.0091411, 0.1, 1.],

   Twall[1., 0, 0.215549, 10., 8.3825, 1., 1., -0.1, -0.0391796, 0.0091411, 0.1, 1.]}
Bessel Fxn Accuracy= (    (V)    ;BesselJ; (ber+I bei); ModBesselJHold; Argument->infinity approximation)
Bessel Accuracy Hi = {(9.99999925), 149.847528, 149.847526, 149.847526, 148.537427}
Bessel Accuracy Lo = {(0.999999925), 1.01552483, 1.01552483, 1.01552483, 1.00386903}

• NON-DIMENSIONAL SCALING VARIABLES CALCULATED:
                                                                                   -6
Va=100.; Pr=0.703; Pr*Va=70.2663; S =500.; Fo=100.; EL=0.00600497; M=3.78929 10   ; Re0 =4.89902
p0=1; T0[z]=1 ; rho0[z]=1

• NON-DIMENSIONAL VARIABLES USED IN COMPLEX SOLUTION:
                                                      -6                       -9
V=10.; P=0.83825; PV=8.3825; eps=0.002; F=0.1; M=3.78929 10   ; LAMBDA=4.30762 10   ; eps*Va=0.2
                                                                       5
U0=1.; UL=1.; PHIU=-0.1; TERM=16; KGAS =0.0091411; KTUBE=1.; GAMMA=-; d0=0.002; dL=0.002; PHIT=-0.0391796; TW=0.319915
                                                                       3

..............

ARCHIVE Parameter List

(* NEW *)

(* For Thesis *)

(* For [illegible] *)

 (* Cases, Isothermal *)

(* For Thesis old *)

================================================

(* LINEAR FLOW periodic velocity scalars and T, p and rho in the diffusion layer *)

Answers to linear flow

(* ANSWERS to First Order Flow *)

(* u0, v0, T1, p1, rho1 *)

   (* Templates *)

p1hatTemplate = ((-I/(1-(kseRe00zV+I kseIm00zV)))*
          (mRatioRe11V21PVz  + I mRatioIm11V21PVz )(Uo-U1 Exp[I 2Pi phiU])-
          (mRatioRe31PV21PVz + I mRatioIm31PV21PVz) Exp[I 2Pi phiT]Tw);
p1hatTemplateTwhat = ((-I/(1-(kseRe00zV+I kseIm00zV)))*
```

```
          (mRatioRe11V21PVz  + I mRatioIm11V21PVz )(Uo-Ul Exp[I 2Pi phiU])-
          (mRatioRe31PV21PVz + I mRatioIm31PV21PVz) Twhat);
p2hatTemplate = I ((Uo-Ul Exp[I 2Pi phiU])/(1-(kseRe00zV+I kseIm00zV))) (z^2/2) - I z/(1-(kseRe00zV+I kseIm00zV));
u0hatTemplate = (Uo-(Uo-Ul Exp[I 2Pi phiU])z)(1-(kseRe0rzV + I kseIm0rzV))/(1-(kseRe00zV + I kseIm00zV));
T1hatTemplate = (-I (((GAMMA-1)/GAMMA) (Uo-Ul Exp[I 2Pi phiU]) (mRatioRe11V21PVz+I mRatioIm11V21PVz) *
      (1-(kseRe0rzPV+I kseIm0rzPV)) / (1-(kseRe00zV+I kseIm00zV))) +
            ((kseRe0rzPV+I kseIm0rzPV)-(((GAMMA-1)/GAMMA)(mRatioRe31PV21PVz+I mRatioIm31PV21PVz)*
          (1-(kseRe0rzPV+I kseIm0rzPV)))) Tw Exp[I 2Pi phiT]);
v0hatTemplate = ((mRe11zV + I mIm11zV)/(1-(kseRe00zV+I kseIm00zV)))*
     ((mRatioRe2rPV21PVz + I mRatioIm2rPV21PVz)-(mRatioRe1rV11Vz + I mRatioIm1rV11Vz))(Uo-Ul Exp[I 2Pi phiU]) -
              I*(mRe31zPV+I mIm31zPV)*((mRatioRe2rPV21PVz+I mRatioIm2rPV21PVz)-(mRatioRe3rPV31PVz+I mRatioIm3rPV31PVz))*
               Tw*Exp[I 2Pi phiT];
rho1hatTemplate  = p1hatTemplate/T0[z] - rho0[z] T1hatTemplate/T0[z];
particleTracehatTemplate = -I(do-(do-dl Exp[I 2Pi phiU])z)(1-(aD0Re+I aD0Im))/(1-(bD0Re+I bD0Im));
p1VolhatTemplate = (-I 2 GAMMA (r (DT1hatReRVar+I DT1hatImRVar)/Power[PV,2] -
             (mRe11zV+I mIm11zV) (Uo-Ul Exp[I 2Pi phiU]))/(1-(kseRe00zV + I kseIm00zV))));

p1Template = ComplexExpand[Exp[I 2Pi t] p1hatTemplate];
u0Template = ComplexExpand[Exp[I 2Pi t] u0hatTemplate];
T1Template = ComplexExpand[Exp[I 2Pi t] T1hatTemplate];
v0Template = ComplexExpand[Exp[I 2Pi t] v0hatTemplate];
particleTraceTemplate = ComplexExpand[Exp[I 2Pi t] particleTracehatTemplate];
p1VolTemplate = ComplexExpand[Exp[I 2Pi t] p1VolhatTemplate];
rho1Template = ComplexExpand[Exp[I 2Pi t] rho1hatTemplate];

p1ReTemplate = p1Template-I Coefficient[p1Template,I];
u0ReTemplate = u0Template-I Coefficient[u0Template,I];
T1ReTemplate = T1Template-I Coefficient[T1Template,I];
v0ReTemplate = v0Template-I Coefficient[v0Template,I];
particleTraceReTemplate = particleTraceTemplate-I Coefficient[particleTraceTemplate,I];
p1VolReTemplate = p1VolTemplate-I Coefficient[p1VolTemplate,I];
rho1ReTemplate  = p1ReTemplate/T0[z] - rho0[z] T1ReTemplate/T0[z];

(*
p1RehatTemplate = p1hatTemplate-I Coefficient[p1hatTemplate,I];
u0RehatTemplate = u0hatTemplate-I Coefficient[u0hatTemplate,I];
T1RehatTemplate = T1hatTemplate-I Coefficient[T1hatTemplate,I];
v0RehatTemplate = v0hatTemplate-I Coefficient[v0hatTemplate,I];
particleTraceRehatTemplate = particleTracehatTemplate-I Coefficient[particleTracehatTemplate,I];
p1VolRehatTemplate = p1VolhatTemplate-I Coefficient[p1VolhatTemplate,I];
rho1RehatTemplate  = p1RehatTemplate/T0[z] + rho0[z] T1RehatTemplate/T0[z];
*)

u0hatImTemplate=Coefficient[ComplexExpand[u0hatTemplate],I];
u0hatReTemplate=ComplexExpand[u0hatTemplate] -I u0hatImTemplate;
u0hatCCTemplate=u0hatReTemplate-I u0hatImTemplate;

v0hatImTemplate=Coefficient[ComplexExpand[v0hatTemplate],I];
v0hatReTemplate=ComplexExpand[v0hatTemplate] -I v0hatImTemplate;
v0hatCCTemplate=v0hatReTemplate-I v0hatImTemplate;

T1hatImTemplate=Coefficient[ComplexExpand[T1hatTemplate],I];
T1hatReTemplate=ComplexExpand[T1hatTemplate] -I T1hatImTemplate;
T1hatCCTemplate=T1hatReTemplate-I T1hatImTemplate;

p1hatImTemplate=Coefficient[ComplexExpand[p1hatTemplate],I];
p1hatReTemplate=ComplexExpand[p1hatTemplate] -I p1hatImTemplate;
p1hatCCTemplate=p1hatReTemplate-I p1hatImTemplate;

p1VolhatImTemplate=Coefficient[ComplexExpand[p1VolhatTemplate],I];
p1VolhatReTemplate=ComplexExpand[p1VolhatTemplate] -I p1VolhatImTemplate;
p1VolhatCCTemplate=p1VolhatReTemplate-I p1VolhatImTemplate;

rho1hatImTemplate=Coefficient[ComplexExpand[rho1hatTemplate],I];
rho1hatReTemplate=ComplexExpand[rho1hatTemplate] -I rho1hatImTemplate;
rho1hatCCTemplate=rho1hatReTemplate-I rho1hatImTemplate;

DT1hatRTemplate = ComplexExpand[(-I (((GAMMA-1)/GAMMA) (Uo-Ul Exp[I 2Pi phiU]) (mRatioRe11V21PVz+I mRatioIm11V21PVz)*
        (0-(DkseReR0rzPV+I DkseImR0rzPV)) / (1-(kseRe00zV+I kseIm00zV))) +
              (  (DkseReR0rzPV+I DkseImR0rzPV)-(((GAMMA-1)/GAMMA)(mRatioRe31PV21PVz+I mRatioIm31PV21PVz)*
              (0-(DkseReR0rzPV+I DkseImR0rzPV)))) Tw Exp[I 2Pi phiT])];
DT1hatImRTemplate = Coefficient[DT1hatRTemplate,I];
DT1hatReRTemplate = DT1hatRTemplate-I DT1hatImRTemplate;

DT1hatReRHoldTemp[r_,z_,t_,V,PV,Uo_,Ul_,phiU_,phiT_,Tw_]=DT1hatReRTemplate/.
       {mRatioRe11V21PVz->HoldForm[mRatioRe[{1,1,V},{2,1,PV},z]],
        mRatioIm11V21PVz->HoldForm[mRatioIm[{1,1,V},{2,1,PV},z]],
        DkseReR0rzPV->HoldForm[DkseReR[0,r,z,PV]],
       DkseImR0rzPV->HoldForm[DkseImR[0,r,z,PV]],
        kseRe00zV->HoldForm[kseRe[0,0,z,V]],
        kseIm00zV->HoldForm[kseIm[0,0,z,V]],
        mRatioRe31PV21PVz->HoldForm[mRatioRe[{3,1,PV},{2,1,PV},z]],
        mRatioIm31PV21PVz->HoldForm[mRatioIm[{3,1,PV},{2,1,PV},z]]};
DT1hatReRHold[r_,z_,t_,V,PV,Uo_,Ul_,phiU_,phiT_,Tw_]=
  Collect[Expand[DT1hatReRHoldTemp[r,z,t,V,PV,Uo,Ul,phiU,phiT,Tw]],Tw];

DT1hatImRHoldTemp[r_,z_,t_,V,PV,Uo_,Ul_,phiU_,phiT_,Tw_]=DT1hatImRTemplate/.
       {mRatioRe11V21PVz->HoldForm[mRatioRe[{1,1,V},{2,1,PV},z]],
        mRatioIm11V21PVz->HoldForm[mRatioIm[{1,1,V},{2,1,PV},z]],
        DkseReR0rzPV->HoldForm[DkseReR[0,r,z,PV]],
       DkseImR0rzPV->HoldForm[DkseImR[0,r,z,PV]],
        kseRe00zV->HoldForm[kseRe[0,0,z,V]],
        kseIm00zV->HoldForm[kseIm[0,0,z,V]],
        mRatioRe31PV21PVz->HoldForm[mRatioRe[{3,1,PV},{2,1,PV},z]],
        mRatioIm31PV21PVz->HoldForm[mRatioIm[{3,1,PV},{2,1,PV},z]]};
DT1hatImRHold[r_,z_,t_,V,PV,Uo_,Ul_,phiU_,phiT_,Tw_]=
  Collect[Expand[DT1hatImRHoldTemp[r,z,t,V,PV,Uo,Ul,phiU,phiT,Tw]],Tw];

(*
v0hatTemplate//ComplexExpand
%==v0hatReTemplate+I v0hatImTemplate
*)

(*
p1hatCCTemplate = p1RehatTemplate-I Coefficient[p1hatTemplate,I];
v0hatCCTemplate = v0RehatTemplate-I Coefficient[v0hatTemplate,I];
particleTracehatCCTemplate = particleTraceRehatTemplate-I Coefficient[particleTracehatTemplate,I];
p1VolhatCCTemplate = p1VolRehatTemplate-I Coefficient[p1VolhatTemplate,I];
*)
```

```
  (* Assignments and Compilations *)

    (* p1 *)

p1Assign={kseRe00zV->HoldForm[kseReHold[0,0,z,sigmaV]],
        kseIm00zV->HoldForm[kseImHold[0,0,z,sigmaV]],
       mRatioRe11V21PVz->HoldForm[mRatioReHold[{1,1,sigmaV},{2,1,sigmaPV},z]],
        mRatioIm11V21PVz->HoldForm[mRatioImHold[{1,1,sigmaV},{2,1,sigmaPV},z]],
        mRatioRe31PV21PVz->HoldForm[mRatioReHold[{3,1,sigmaPV},{2,1,sigmaPV},z]],
        mRatioIm31PV21PVz->HoldForm[mRatioImHold[{3,1,sigmaPV},{2,1,sigmaPV},z]]};
p1ReHold[z_,t_,sigmaV_,sigmaPV_,Uo_,Ul_,phiU_,phiT_,Tw_]=p1ReTemplate/.p1Assign;
p1Re[z_,t_,sigmaV_,sigmaPV_,Uo_,Ul_,phiU_,phiT_,Tw_]:=p1ReHold[z,t,sigmaV,sigmaPV,Uo,Ul,phiU,phiT,Tw]//
  ReleaseHold//ReleaseHold//N;
p1Re[z_,t_,V,PV,U0,UL,PHIU,PHIT,TW]=p1Re[z,t,V,PV,U0,UL,PHIU,PHIT,TW];
p1Re[z_,t_,V,PV,U0,UL,PHIU,PHIT,0]=p1Re[z,t,V,PV,U0,UL,PHIU,PHIT,0];

p1hatHold[z_,sigmaV_,sigmaPV_,Uo_,Ul_,phiU_,phiT_,Tw_]=p1hatTemplate/.p1Assign;
p1hat[z_,sigmaV_,sigmaPV_,Uo_,Ul_,phiU_,phiT_,Tw_]:=p1hatHold[z,sigmaV,sigmaPV,Uo,Ul,phiU,phiT,Tw]//
  ReleaseHold//ReleaseHold//N;
p1hat[z_,V,PV,U0,UL,PHIU,PHIT,Tw_] =p1hat[z,V,PV,U0,UL,PHIU,PHIT,Tw]//ComplexExpand;

p1hatHold[z_,sigmaV_,sigmaPV_,Uo_,Ul_,phiU_,Twhat_]=p1hatTemplateTwhat/.p1Assign;
p1hat[z_,sigmaV_,sigmaPV_,Uo_,Ul_,phiU_,Twhat_]:=p1hatHold[z,sigmaV,sigmaPV,Uo,Ul,phiU,Twhat]//
  ReleaseHold//ReleaseHold//N;
p1hat[z_,V,PV,U0,Ul_,phiU_,fo_] =p1hat[z,V,PV,U0,Ul,phiU,Twhat[Ul,phiU,fo]];



    (* p2 *)

p2hatHold[z_,sigmaV_,Uo_,Ul_,phiU_]=p2hatTemplate/.p1Assign;
p2hat[z_,sigmaV_,Uo_,Ul_,phiU_]:=p2hatHold[z,sigmaV,Uo,Ul,phiU]//ReleaseHold//ReleaseHold//N
(*p2hat[z_,V,U0,UL,PHIU] =p2hat[z,V,U0,UL,PHIU]//ComplexExpand;*)
Dp2hatZ[z_,V,Uo_,Ul_,phiU_]=D[p2hat[z,V,Uo,Ul,phiU],z];
Dp2hatZ[z_,V,U0,UL,PHIU]=D[p2hat[z,V,U0,UL,PHIU],z];

    (* p1Vol *)

p1VolAssign={mRe11zV->HoldForm[mRe[1,1,z,V]],
        mIm11zV->HoldForm[mIm[1,1,z,V]],
       kseRe00zV->HoldForm[kseReHold[0,0,z,V]],
        kseIm00zV->HoldForm[kseImHold[0,0,z,V]],
       DT1hatReRVar->HoldForm[DT1hatReRHold[1,z,t,V,PV,Uo,Ul,phiU,phiT,Tw]],
        DT1hatImRVar->HoldForm[DT1hatImRHold[1,z,t,V,PV,Uo,Ul,phiU,phiT,Tw]],
        r->1};
p1VolReHold[z_,t_,sigmaV_,sigmaPV_,Uo_,Ul_,phiU_,phiT_,Tw_]=p1VolReTemplate/.p1VolAssign;
p1VolRe[z_,t_,sigmaV_,sigmaPV_,Uo_,Ul_,phiU_,phiT_,Tw_]:=p1VolReHold[z,t,sigmaV,sigmaPV,Uo,Ul,phiU,phiT,Tw]//
  ReleaseHold//ReleaseHold//N;
p1VolRe[z_,t_,V,PV,U0,UL,PHIU,PHIT,TW]=p1VolRe[z,t,V,PV,U0,UL,PHIU,PHIT,TW];
p1VolRe[z_,t_,V,PV,U0,UL,PHIU,PHIT,0]=p1VolRe[z,t,V,PV,U0,UL,PHIU,PHIT,0];



    (* T1 *)

T1Assign={mRatioRe11V21PVz->HoldForm[mRatioReHold[{1,1,sigmaV},{2,1,sigmaPV},z]],
        mRatioIm11V21PVz->HoldForm[mRatioImHold[{1,1,sigmaV},{2,1,sigmaPV},z]],
        kseRe00zV->HoldForm[kseReHold[0,0,z,sigmaV]],
        kseIm00zV->HoldForm[kseImHold[0,0,z,sigmaV]],
        mRatioRe31PV21PVz->HoldForm[mRatioReHold[{3,1,sigmaPV},{2,1,sigmaPV},z]],
        mRatioIm31PV21PVz->HoldForm[mRatioImHold[{3,1,sigmaPV},{2,1,sigmaPV},z]],
             kseRe0rzPV->HoldForm[kseReHold[0,r,z,sigmaPV]],
        kseIm0rzPV->HoldForm[kseImHold[0,r,z,sigmaPV]]};
T1ReHold[r_,z_,t_,sigmaV_,sigmaPV_,Uo_,Ul_,phiU_,phiT_,Tw_]=T1ReTemplate/.T1Assign;
T1Re[r_,z_,t_,sigmaV_,sigmaPV_,Uo_,Ul_,phiU_,phiT_,Tw_]:=
  T1ReHold[r,z,t,sigmaV,sigmaPV,Uo,Ul,phiU,phiT,Tw]//ReleaseHold//ReleaseHold//N;
T1Re[r_,z_,t_,V,PV,U0,UL,PHIU,PHIT,0]=T1Re[r,z,t,V,PV,U0,UL,PHIU,PHIT,0];
T1Re[r_,z_,t_,V,PV,U0,UL,PHIU,PHIT,TW]=T1Re[r,z,t,V,PV,U0,UL,PHIU,PHIT,TW];

q1[r_,z_,t_,V,PV,U0,UL,PHIU,PHIT,0] =-Expand[D[T1Re[r,z,t,V,PV,U0,UL,PHIU,PHIT,0], r]];
q1[r_,z_,t_,V,PV,U0,UL,PHIU,PHIT,TW]=-Expand[D[T1Re[r,z,t,V,PV,U0,UL,PHIU,PHIT,TW],r]];

T1hatHold[r_,z_,sigmaV_,sigmaPV_,Uo_,Ul_,phiU_,phiT_,Tw_]=T1hatTemplate/.T1Assign;
T1hat[r_,z_,sigmaV_,sigmaPV_,Uo_,Ul_,phiU_,phiT_,Tw_]:=
  T1hatHold[r,z,sigmaV,sigmaPV,Uo,Ul,phiU,phiT,Tw]//ReleaseHold//ReleaseHold//N;
T1hat[r_,z_,V,PV,U0,UL,PHIU,PHIT,Tw_] =T1hat[r,z,V,PV,U0,UL,PHIU,PHIT,Tw]//ComplexExpand;
            (* Expand for some unknown reason keeps in a form for DT1hatR to be in Re+I Im form*)

DT1hatR[r_,z_,V,PV,U0,Ul_,phiU_,PHIT,Tw_]=D[T1hat[r,z,V,PV,U0,Ul,phiU,PHIT,Tw],r](*//ComplexExpand*);
DT1hatR[r_,z_,V,PV,U0,UL,PHIU,PHIT,Tw_]=D[T1hat[r,z,V,PV,U0,UL,PHIU,PHIT,Tw],r](*//ComplexExpand*);

q1hat[r_,z_,V,PV,U0,UL,PHIU,PHIT,0] =-DT1hatR[r,z,V,PV,U0,UL,PHIU,PHIT,0];
q1hat[r_,z_,V,PV,U0,UL,PHIU,PHIT,TW]=-DT1hatR[r,z,V,PV,U0,UL,PHIU,PHIT,TW];

IntT1hatR01[z_,V,PV,U0,UL,PHIU,PHIT,Tw_]=
  2 Integrate[r T1hat[r,z,V,PV,U0,UL,PHIU,PHIT,Tw],{r,0,1}](*//ComplexExpand*);
NuC[z_,V,PV,U0,UL,PHIU,PHIT,Tw_]=
  -DT1hatR[1,z,V,PV,U0,UL,PHIU,PHIT,Tw]/(Tw Exp[I 2Pi PHIT] - IntT1hatR01[z,V,PV,U0,UL,PHIU,PHIT,Tw])
            (*//ComplexExpand*)//N;

(* CAN't Do this, cannot specify PHIT and TW independent of phiU and Ul!!!!
IntT1hatR01[z_,V,PV,U0,Ul_,phiU_,PHIT,Tw_]=
  2 Integrate[r T1hat[r,z,V,PV,U0,Ul,phiU,PHIT,Tw],{r,0,1}](*//ComplexExpand*);
NuC[z_,V,PV,U0,Ul_,phiU_,PHIT,Tw_]=
  -DT1hatR[1,z,V,PV,U0,Ul,phiU,PHIT,Tw]/(Tw Exp[I 2Pi PHIT] - IntT1hatR01[z,V,PV,U0,Ul,phiU,PHIT,Tw])
            (*//ComplexExpand*)//N;
*)
(*DT1hatTwhatR[r_,z_,V,PV,U0,Ul_,phiU_,Twhat_]=
  Collect[Expand[D[T1hatTwhat[r,z,V,PV,U0,Ul,phiU,Twhat],r]],Twhat];*)

IntT1hatR01[z_,V,PV,U0,Ul_,phiU_,Twhat_]=
  Collect[2 Integrate[r T1hatTwhat[r,z,V,PV,U0,Ul,phiU,Twhat],{r,0,1}],Twhat](*//ComplexExpand*);
NuC[z_,V,PV,U0,Ul_,phiU_,fo_]=
  - (DT1hatTwhatR[1,z,V,PV,U0,Ul,phiU,Twhat[Ul,phiU,fo]]/(Twhat[Ul,phiU,fo] -
     IntT1hatR01[z,V,PV,U0,Ul,phiU,Twhat[Ul,phiU,fo]]))
            (*//ComplexExpand//N*);

DeltaT1hat[0,V,PV,U0,UL,PHIU,PHIT,0] =T1hat[1,0,V,PV,U0,UL,PHIU,PHIT,0]-IntT1hatR01[0,V,PV,U0,UL,PHIU,PHIT,0];
DeltaT1hat[0,V,PV,U0,UL,PHIU,PHIT,TW]=T1hat[1,0,V,PV,U0,UL,PHIU,PHIT,TW]-IntT1hatR01[0,V,PV,U0,UL,PHIU,PHIT,TW];

DeltaT1[0,t_,V,PV,U0,UL,PHIU,PHIT,0] =Re[DeltaT1hat[0,V,PV,U0,UL,PHIU,PHIT,0]  Exp[I 2Pi t]]//N;
DeltaT1[0,t_,V,PV,U0,UL,PHIU,PHIT,TW]=Re[DeltaT1hat[0,V,PV,U0,UL,PHIU,PHIT,TW] Exp[I 2Pi t]]//N;
```

```
T1[r_,z_,t_,V,PV,U0,UL,PHIU,PHIT,0]  =Re[T1hat[r,z,V,PV,U0,UL,PHIU,PHIT,0]  Exp[I 2Pi t]]//N;
T1[r_,z_,t_,V,PV,U0,UL,PHIU,PHIT,TW]  =Re[T1hat[r,z,V,PV,U0,UL,PHIU,PHIT,TW]  Exp[I 2Pi t]]//N;


     (* rho1 *)

rho1ReHold[r_,z_,t_,sigmaV_,sigmaPV_,Uo_,Ul_,phiU_,phiT_,Tw_]=
  (p1ReHold[z,t,sigmaV,sigmaPV,Uo,Ul,phiU,phiT,Tw]-T1ReHold[r,z,t,sigmaV,sigmaPV,Uo,Ul,phiU,phiT,Tw]);
rho1Re[r_,z_,t_,sigmaV_,sigmaPV_,Uo_,Ul_,phiU_,phiT_,Tw_]:=
  rho1ReHold[r,z,t,sigmaV,sigmaPV,Uo,Ul,phiU,phiT,Tw]//ReleaseHold//ReleaseHold//N;
rho1Re[r_,z_,t_,V,PV,U0,UL,PHIU,PHIT,TW]=rho1Re[r,z,t,V,PV,U0,UL,PHIU,PHIT,TW];
rho1Re[r_,z_,t_,V,PV,U0,UL,PHIU,PHIT,0]=rho1Re[r,z,t,V,PV,U0,UL,PHIU,PHIT,0];


     (* theta1 *)

theta1=ComplexExpand[Tw*Exp[I 2Pi phiT] Exp[I 2Pi t](Exp[I si y]-Exp[I si] I Sin[si y]/Cos[si])];
theta1Re[y_,t_,fo_,phiT_,Tw_]=N[theta1-I Coefficient[theta1,I]];
theta1Re[y_,t_,fo_,PHIT,TW]=theta1Re[y,t,fo,PHIT,TW];
theta1Re[y_,t_,fo_,PHIT,0]=theta1Re[y,t,fo,PHIT,0];


     (* u0 *)

u0Assign={kseRe0rzV->HoldForm[kseReHold[0,r,z,sigmaV]],
       kseIm0rzV->HoldForm[kseImHold[0,r,z,sigmaV]],
      kseRe00zV->HoldForm[kseReHold[0,0,z,sigmaV]],
       kseIm00zV->HoldForm[kseImHold[0,0,z,sigmaV]]};
u0ReHold[r_,z_,t_,sigmaV_,Uo_,Ul_,phiU_]=u0ReTemplate/.u0Assign;
u0Re[r_,z_,t_,sigmaV_,Uo_,Ul_,phiU_]:=u0ReHold[r,z,t,sigmaV,Uo,Ul,phiU]//ReleaseHold//ReleaseHold//N;
u0Re[r_,z_,t_,V,U0,UL,PHIU]=u0Re[r,z,t,V,U0,UL,PHIU];

u0hatHold[r_,z_,sigmaV_,Uo_,Ul_,phiU_]=u0hatTemplate/.u0Assign;
u0hat[r_,z_,sigmaV_,Uo_,Ul_,phiU_]:=u0hatHold[r,z,sigmaV,Uo,Ul,phiU]//ReleaseHold//ReleaseHold//N;
u0hat[r_,z_,V,Uo_,Ul_,phiU_] =u0hat[r,z,V,Uo,Ul,phiU]//ComplexExpand;

Intu0hatR01[z_,V,Uo_,Ul_,phiU_]=2 Integrate[r u0hat[r,z,V,Uo,Ul,phiU],{r,0,1}]//ComplexExpand;
Intu0hatR[z_,V,Uo_,Ul_,phiU_]=2 Integrate[r u0hat[r,z,V,Uo,Ul,phiU],r]//ComplexExpand;
fC[z_,V,Uo_,Ul_,phiU_]=Dp2hatZ[z,V,Uo,Ul,phiU]/(I rho0[z] Intu0hatR01[z,V,Uo,Ul,phiU])//ComplexExpand//N;

u0hat[r_,z_,V,U0,UL,PHIU] =u0hat[r,z,V,U0,UL,PHIU]//ComplexExpand;
Intu0hatR01[z_,V,U0,UL,PHIU]=2 Integrate[r u0hat[r,z,V,U0,UL,PHIU],{r,0,1}]//ComplexExpand;
Intu0hatR[r_,z_,V,U0,UL,PHIU]=2 Integrate[r u0hat[r,z,V,U0,UL,PHIU],r]//ComplexExpand;
fC[z_,V]=Dp2hatZ[z,V,U0,UL,PHIU]/(I rho0[z] Intu0hatR01[z,V,U0,UL,PHIU])//Simplify;

localWallShearStress[z_,t_,V,U0,UL,PHIU]=Expand[2 Pi D[u0Re[r,z,t,V,U0,UL,PHIU],r]/.r->1];
  (*2Pi is for integration around circumference*)
localWallShearStressSquared[z_,t_,V,U0,UL,PHIU]=Power[localWallShearStress[z,t,V,U0,UL,PHIU],2]//Expand;
localWallShearStressRMS[z_,V,U0,UL,PHIU]=Sqrt[Integrate[localWallShearStressSquared[z,t,V,U0,UL,PHIU],{t,0,1}]];

totalDragRMS[V,U0,UL,PHIU]=Integrate[localWallShearStressRMS[z,V,U0,UL,PHIU],{z,0,1}]//N;
totalDragRMSStar=totalDragRMS[V,U0,UL,PHIU]*drag0Star;
totalDragRMS[t,V,U0,UL,PHIU]=Integrate[localWallShearStress[z,t,V,U0,UL,PHIU],{z,0,1}]//N;


     (* v0 *)


v0Assign={mRe1lzV->Hold[mReHold[1,1,z,sigmaV]], mIm1lzV->Hold[mImHold[1,1,z,sigmaV]],
       kseRe00zV->Hold[kseReHold[0,0,z,sigmaV]], kseIm00zV->Hold[kseImHold[0,0,z,sigmaV]],
        mRatioRe2rPV21PVz->Hold[mRatioReHold[{2,r,sigmaPV},{2,1,sigmaPV},z]],mRatioIm2rPV21PVz->
          Hold[mRatioImHold[{2,r,sigmaPV},{2,1,sigmaPV},z]],
        mRatioRe1rV11Vz->Hold[mRatioReHold[{1,r,sigmaV },{1,1,sigmaV },z]],mRatioIm1rV11Vz->
          Hold[mRatioImHold[{1,r,sigmaV },{1,1,sigmaV },z]],
        mRe31zPV->Hold[mReHold[3,1,z,sigmaPV]],mIm31zPV->Hold[mImHold[3,1,z,sigmaPV]],
        mRatioRe3rPV31PVz->Hold[mRatioReHold[{3,r,sigmaPV},{3,1,sigmaPV},z]],mRatioIm3rPV31PVz->
          Hold[mRatioImHold[{3,r,sigmaPV},{3,1,sigmaPV},z]],
        mRatioRe2rPV21PVz->Hold[mRatioReHold[{2,r,sigmaPV},{2,1,sigmaPV},z]],mRatioIm2rPV21PVz->
          Hold[mRatioImHold[{2,r,sigmaPV},{2,1,sigmaPV},z]]};
v0ReHold[r_,z_,t_,sigmaV_,sigmaPV_,Uo_,Ul_,phiU_,phiT_,Tw_]= v0ReTemplate/.v0Assign;
v0Re[r_,z_,t_,sigmaV_,sigmaPV_,Uo_,Ul_,phiU_,phiT_,Tw_]:=
  v0ReHold[r,z,t,sigmaV,sigmaPV,Uo,Ul,phiU,phiT,Tw]//ReleaseHold//ReleaseHold//N;
v0Re[r_,z_,t_,V,PV,U0,UL,PHIU,PHIT,0]=v0Re[r,z,t,V,PV,U0,UL,PHIU,PHIT,0];
v0Re[r_,z_,t_,V,PV,U0,UL,PHIU,PHIT,TW]=v0Re[r,z,t,V,PV,U0,UL,PHIU,PHIT,TW];


     (* d0 *)

d0Assign={aD0Re->HoldForm[kseReHold[0,r,z,sigma]],
        aD0Im->HoldForm[kseImHold[0,r,z,sigma]],
       bD0Re->HoldForm[kseReHold[0,0,z,sigma]],
        bD0Im->HoldForm[kseImHold[0,0,z,sigma]]};
d0ReHold[r_,z_,t_,sigma_,do_,dl_,phiU_]=particleTraceReTemplate/.d0Assign;
d0Re[r_,z_,t_,sigmaV_,do_,dl_,phiU_]:=d0ReHold[r,z,t,sigmaV,do,dl,phiU]//ReleaseHold//ReleaseHold//N;
d0Re[r_,z_,t_,V,d[0],d[1],PHIU]=d0Re[r,z,t,V,d[0],d[1],PHIU];

 (* Save to a notebook file ,theta1,p1,rho1,T1,u0,v0 *)

Save[fileNameHXfr,theta1,p1,rho1,T1,u0,v0]


(* print test *)

(* {{eps, Va, Pr, UL, PHIU, M, appPRatio}, {Fo, {PHIT, TW}}, Date}        *)
(* {{p1[0, t=0.1,0.2,0.3]}, p1[TW at t=.2], pisDynAmp[0,0], v0[0,.8,.2], u0[0,.8,.2], {T[0,0,.1],T[0,0,.2],T[0,0,.3]}}  *)

If[kindSystem==OPT,Print[fileNameOPTHXfr],,Print[fileNameBPTHXfr]];
Print[{{p1Re[0,.1,V,PV,U0,UL,PHIU,PHIT,0],p1Re[0,.2,V,PV,U0,UL,PHIU,PHIT,0],p1Re[0,.3,V,PV,U0,UL,PHIU,PHIT,0]},
        p1Re[0,.2,V,PV,U0,UL,PHIU,PHIT,TW],N[pistonDynAmpInch[0,0]/LInch],
        v0Re[.8,0,0,V,PV,U0,UL,PHIU,PHIT,0],u0Re[.8,0,0,V,PV,U0,UL,PHIU],
       {T1Re[0,0,.1,V,PV,U0,UL,PHIU,PHIT,0],T1Re[0,0,.2,V,PV,U0,UL,PHIU,PHIT,0],
        T1Re[0,0,.3,V,PV,U0,UL,PHIU,PHIT,0]}}]


                                                                -6          -9
{{{BPT, 0.002, 1., 0.703, 0.70266, 0., n/aPHIU, 3.789 10   , 4.31 10   }, {1.004, 1.007, 1.00669}},
                                                    -          -
  {10.001, {0.1022, 0.000203363}, 7.02719}, {0.00476915 Amp dyne, 0.00338034 (tube^-1) dyne, 0.0197349 W},
   {BPT<>1., 2, 21, 18}}
```

```
{{0.317212, 0.485368, 0.46813}, 0.485313, 0.002, 0.0722032, u0Re[0.8, 0, 0, 0.56419 Sqrt[Pi],
   0.472932 Sqrt[Pi], 1., 0., -0.3],

  {0.0297984, 0.0133024, -0.00827462}}

{{CC, OPT, 0.698, 6.016 10E-7, 0.703, 0.66, -0.1, 0.003208, 1.427, 1.808}, {1.7559 10E6, {-0.125, 0.00407989}}, {1994, 8, 24, 17, 7, 5}}
{{2.97577, 2.68448, 1.36781}, 2.68702, 0.111111, 2.76102, 0.36, {1.25176 10E-7, -3.63274 10E-7, -7.12965 10E-7}}

(* phasors *)
                                                        -6         -9
{{{OPT, 0.002, 100., 0.703, 70.266, 1., -0.1, 3.789 10  , 4.31 10  }, {1.002, 1.004, 1.00413}}, {100., {-0.03918, 0.319915}, 7026.6},

  {0.00476915 Amp dyne, 0.199157 (tube^-1) dyne, 1.97349 W}, {OPT<>100., 3, 15, 19}}
Phasors:  Amp        PHI       TWAmp      PHITW          Re+Im                ReTW+ImTW
U0        1.         0
u0(z=.5)  0.951      -0.05
u0(z=.7)  0.959      -0.0706
u0(z=.85) 0.975      -0.0856
UL        1.         -0.1
p1        0.805      -0.0116    0.883      -0.026
T1Re(0)   0.318      -0.0137    0.353      -0.0264
T1Re(1)   0.                    0.32       -0.0392
T1hat(0,z)0.318      -0.0137    0.353      -0.0264
T1hat(1,z)0.          0         0.32       -0.0392
T1bulk    0.272       0.0176    0.343      -0.0256       0.2706 + 0.03006 I      0.339 - 0.05502 I
DT1       0.272      -0.482     0.0368      -0.393      -0.271 - 0.0301 I      -0.0288 - 0.0229 I
u0p1(z=0) 0.403     -0.0058     0.401      -0.013
v0(r=.8)  0.0743     -0.845     0.0504     -0.856
q1(r=1)   2.59       -0.879     0.35       -0.79
q1hat(1,z)2.59        0.121     0.35        0.21         1.87988 + 1.78154 I      0.086417 + 0.339135 I
NuCSimple 9.51        0.603     9.51        0.603      -7.58476 - 5.74094 I      -7.58476 - 5.74094 I
NuC       9.51       -0.397     9.51       -0.397       -7.585 - 5.741 I        -7.585 - 5.741 I
fC(0)     1.15        0.476                             -1.138 + 0.1741 I
fC(z)     1.15        0.476                             -1.138 + 0.1741 I

================================================

(* SECONDARY FLOW specific enthalpy flux and streaming velocities in the diffusion layer *)

(* Enthalpy Streaming and Phasors*)

  (* Prelim *)

    Calcs

     u0T1

twoTimesu0T1AvgTemplate   =  u0hatTemplate * T1hatCCTemplate //ComplexExpand;
twoTimesu0T1ReAvgTemplate =  twoTimesu0T1AvgTemplate  -I Coefficient[twoTimesu0T1AvgTemplate,I];
twoTimesu0T1ReAvgFluxHold[r_,z_,sigmaV_,sigmaPV_,Uo_,Ul_,phiU_,phiT_,Tw_]=
  twoTimesu0T1ReAvgTemplate/.Union[u0Assign,T1Assign];

u0T1ReAvgFlux[r_,z_,sigmaV_,sigmaPV_,Uo_,Ul_,phiU_,phiT_,Tw_]:= 1/2 *
  twoTimesu0T1ReAvgFluxHold[r,z,sigmaV,sigmaPV,Uo,Ul,phiU,phiT,Tw]//ReleaseHold//ReleaseHold//ReleaseHold//N;

u0T1ReAvgFlux[r_,z_,V,PV,U0,UL,PHIU,PHIT,0] =u0T1ReAvgFlux[r,z,V,PV,U0,UL,PHIU,PHIT,0]//Expand;
u0T1EpsReAvgFlux[r_,z_,V,PV,U0,UL,PHIU,PHIT,0] =eps u0T1ReAvgFlux[r,z,V,PV,U0,UL,PHIU,PHIT,0]//Expand;

u0T1ReAvgFlux[r_,z_,V,PV,U0,UL,PHIU,PHIT,TW]=u0T1ReAvgFlux[r,z,V,PV,U0,UL,PHIU,PHIT,TW]//Expand;
u0T1EpsReAvgFlux[r_,z_,V,PV,U0,UL,PHIU,PHIT,TW]=eps u0T1ReAvgFlux[r,z,V,PV,U0,UL,PHIU,PHIT,TW]//Expand;

AxialHFlowNoEps[z_,0] =2 Integrate[r u0T1ReAvgFlux[r,z,V,PV,U0,UL,PHIU,PHIT,0], {r,0,1}];
AxialHFlowStarNoEps[z_,0]=hOscFlow0Star*AxialHFlowNoEps[z,0];
AxialHFlowStarNormalizedNoEps[z_,0]=AxialHFlowStarNoEps[z,0]/xSectAreaStar;

AxialHFlowNoEps[z_,TW]=2 Integrate[r u0T1ReAvgFlux[r,z,V,PV,U0,UL,PHIU,PHIT,TW],{r,0,1}];
AxialHFlowStarNoEps[z_,TW]=hOscFlow0Star*AxialHFlowNoEps[z,TW];
AxialHFlowStarNormalizedNoEps[z_,TW]=AxialHFlowStarNoEps[z,TW]/xSectAreaStar;

AxialHFlow[z_,0]=2 Integrate[r u0T1EpsReAvgFlux[r,z,V,PV,U0,UL,PHIU,PHIT,0],{r,0,1}];
AxialHFlowStar[z_,0]=hOscFlow0Star*AxialHFlow[z,0];
AxialHFlowStarNormalized[z_,0]=AxialHFlowStar[z,0]/xSectAreaStar;

AxialHFlow[z_,TW]=2 Integrate[r u0T1EpsReAvgFlux[r,z,V,PV,U0,UL,PHIU,PHIT,TW],{r,0,1}];
AxialHFlowStar[z_,TW]=hOscFlow0Star*AxialHFlow[z,TW];
AxialHFlowStarNormalized[z_,TW]=AxialHFlowStar[z,TW]/xSectAreaStar;

(* u0T1 at r=0 *)
AxialHFlow1D[z_,0]=2 Integrate[r u0T1EpsReAvgFlux[0,z,V,PV,U0,UL,PHIU,PHIT,0],{r,0,1}];
AxialHFlow1DStar[z_,0]=hOscFlow0Star*AxialHFlow1D[z,0];
AxialHFlow1DStarNormalized[z_,0]=AxialHFlow1DStar[z,0]/xSectAreaStar;
AxialHFlow1D[z_,TW]=2 Integrate[r u0T1EpsReAvgFlux[0,z,V,PV,U0,UL,PHIU,PHIT,TW],{r,0,1}];
AxialHFlow1DStar[z_,TW]=hOscFlow0Star*AxialHFlow1D[z,TW];
AxialHFlow1DStarNormalized[z_,TW]=AxialHFlow1DStar[z,TW]/xSectAreaStar;


     (* u0p1at r equal 0) *)

twoTimesu0p1AvgTemplate   =  u0hatTemplate * p1hatCCTemplate //ComplexExpand;
twoTimesu0p1ReAvgTemplate =  twoTimesu0p1AvgTemplate  -I Coefficient[twoTimesu0p1AvgTemplate,I];
twoTimesu0p1ReAvgFluxHold[r_,z_,sigmaV_,sigmaPV_,Uo_,Ul_,phiU_,phiT_,Tw_]=
  twoTimesu0p1ReAvgTemplate/.Union[u0Assign,p1Assign];

u0p1ReAvgFlux[0,z_,sigmaV_,sigmaPV_,Uo_,Ul_,phiU_,phiT_,Tw_]:= 1/2 *
  twoTimesu0p1ReAvgFluxHold[0,z,sigmaV,sigmaPV,Uo,Ul,phiU,phiT,Tw]//ReleaseHold//ReleaseHold//ReleaseHold//N;

u0p1EpsReAvgFlux[0,z_,V,PV,U0,UL,PHIU,PHIT,0] =eps u0p1ReAvgFlux[0,z,V,PV,U0,UL,PHIU,PHIT,0] //Expand;
u0p1EpsReAvgFlux[0,z_,V,PV,U0,UL,PHIU,PHIT,TW]=eps u0p1ReAvgFlux[0,z,V,PV,U0,UL,PHIU,PHIT,TW]//Expand;

Axialu0p1Flow[z_,0]=2 Integrate[r u0p1EpsReAvgFlux[0,z,V,PV,U0,UL,PHIU,PHIT,0],{r,0,1}];
Axialu0p1FlowStar[z_,0]=hOscFlow0Star*Axialu0p1Flow[z,0];
Axialu0p1FlowStarNormalized[z_,0]=Axialu0p1FlowStar[z,0]/xSectAreaStar;

Axialu0p1Flow[z_,TW]=2 Integrate[r u0p1EpsReAvgFlux[0,z,V,PV,U0,UL,PHIU,PHIT,TW],{r,0,1}];
Axialu0p1FlowStar[z_,TW]=hOscFlow0Star*Axialu0p1Flow[z,TW];
Axialu0p1FlowStarNormalized[z_,TW]=Axialu0p1FlowStar[z,TW]/xSectAreaStar;


     (* u0p1MaxWorkAmplat r=0, am0] *)

MaxWorkAmpStar[0,0]=hOscFlow0Star*MaxWorkAmp;
MaxWorkAmpStarNormalized[0,0]=MaxWorkAmpStar[0,0]/xSectAreaStar;
```

```
MaxWorkAmpStar[1,0]=hOscFlow0Star*MaxWorkAmp;
MaxWorkAmpStarNormalized[1,0]=MaxWorkAmpStar[1,0]/xSectAreaStar;


MaxWorkAmpStar[0,TW]=hOscFlow0Star*MaxWorkAmpTW;
MaxWorkAmpStarNormalized[0,TW]=MaxWorkAmpStar[0,TW]/xSectAreaStar;

MaxWorkAmpStar[1,TW]=hOscFlow0Star*MaxWorkAmpTW;
MaxWorkAmpStarNormalized[1,TW]=MaxWorkAmpStar[1,TW]/xSectAreaStar;


     (* u0p1VolWorkIntoTube[Tw] Macroscopic Volume Integrated PV-FlowWork for U0(r=0)*)

twoTimesu0p1VolAvgTemplate   =  u0hatTemplate * p1VolhatCCTemplate //ComplexExpand;
twoTimesu0p1VolReAvgTemplate =  twoTimesu0p1VolAvgTemplate  -I Coefficient[twoTimesu0p1VolAvgTemplate,I];
twoTimesu0p1VolReAvgFluxHold[r_,z_,sigmaV_,sigmaPV_,Uo_,Ul_,phiU_,phiT_,Tw_]=
  twoTimesu0p1VolReAvgTemplate/.Union[u0Assign,p1VolAssign];

u0p1VolReAvgFlux[r_,z_,sigmaV_,sigmaPV_,Uo_,Ul_,phiU_,phiT_,Tw_]:= 1/2 *
  twoTimesu0p1VolReAvgFluxHold[r,z,sigmaV,sigmaPV,Uo,Ul,phiU,phiT,Tw]//ReleaseHold//ReleaseHold//ReleaseHold//N;

u0p1VolEpsReAvgFlux[r_,z_,V,PV,U0,UL,PHIU,PHIT,0] =eps u0p1VolReAvgFlux[r,z,V,PV,U0,UL,PHIU,PHIT,0] //Expand;
u0p1VolEpsReAvgFlux[r_,z_,V,PV,U0,UL,PHIU,PHIT,TW]=eps u0p1VolReAvgFlux[r,z,V,PV,U0,UL,PHIU,PHIT,TW]//Expand;

u0p1VolFlow[z_,0]=2 Integrate[r u0p1VolEpsReAvgFlux[r,z,V,PV,U0,UL,PHIU,PHIT,0],{r,0,1}];
u0p1VolFlowStar[z_,0]=hOscFlow0Star*u0p1VolFlow[z,0];
u0p1VolFlowStarNormalized[z_,0]=u0p1VolFlowStar[z,0]/xSectAreaStar;

u0p1VolFlow[z_,TW]=2 Integrate[r u0p1VolEpsReAvgFlux[r,z,V,PV,U0,UL,PHIU,PHIT,TW],{r,0,1}];
u0p1VolFlowStar[z_,TW]=hOscFlow0Star*u0p1VolFlow[z,TW];
u0p1VolFlowStarNormalized[z_,TW]=u0p1VolFlowStar[z,TW]/xSectAreaStar;

(*
u0p1VolWorkIntoTubeStarInMinusOutAvg[z_,0] =u0p1VolFlowStar[z,0]-u0p1VolFlowStar[z,0]//N;
u0p1VolWorkIntoTubeStarInMinusOutAvg[z_,TW]=u0p1VolFlowStar[z,TW]-u0p1VolFlowStar[z,TW]//N;
u0p1VolWorkIntoTubeStarNormalizedInMinusOutAvg[z_,0] =u0p1VolFlowStarNormalized[z,0]-u0p1VolFlowStarNormalized[z,0]//N;
u0p1VolWorkIntoTubeStarNormalizedInMinusOutAvg[z_,TW]=(u0p1VolFlowStar[z,TW]-u0p1VolFlowStar[z,TW])/xSectAreaStar//N;
*)

     (* u0rhol(at r equal 0) *)

twoTimesu0rholAvgTemplate   =  u0hatTemplate * rholhatCCTemplate //ComplexExpand;
twoTimesu0rholReAvgTemplate =  twoTimesu0rholAvgTemplate  -I Coefficient[twoTimesu0rholAvgTemplate,I];
twoTimesu0rholReAvgFluxHold[r_,z_,sigmaV_,sigmaPV_,Uo_,Ul_,phiU_,phiT_,Tw_]=
  twoTimesu0rholReAvgTemplate/.Union[u0Assign,plAssign,TlAssign];

u0rholReAvgFlux[0,z_,sigmaV_,sigmaPV_,Uo_,Ul_,phiU_,phiT_,Tw_]:= 1/2 *
  twoTimesu0rholReAvgFluxHold[0,z,sigmaV,sigmaPV,Uo,Ul,phiU,phiT,Tw]//ReleaseHold//ReleaseHold//ReleaseHold//N;

u0rholEpsReAvgFlux[0,z_,V,PV,U0,UL,PHIU,PHIT,0] =eps u0rholReAvgFlux[0,z,V,PV,U0,UL,PHIU,PHIT,0] //Expand;
u0rholEpsReAvgFlux[0,z_,V,PV,U0,UL,PHIU,PHIT,TW]=eps u0rholReAvgFlux[0,z,V,PV,U0,UL,PHIU,PHIT,TW]//Expand;

Axialu0rholFlow[z_,0]=2 Integrate[r u0rholEpsReAvgFlux[0,z,V,PV,U0,UL,PHIU,PHIT,0],{r,0,1}];
Axialu0rholFlowStar[z_,0]=hOscFlow0Star*Axialu0rholFlow[z,0];
Axialu0rholFlowStarNormalized[z_,0]=Axialu0rholFlowStar[z,0]/xSectAreaStar;

Axialu0rholFlow[z_,TW]=2 Integrate[r u0rholEpsReAvgFlux[0,z,V,PV,U0,UL,PHIU,PHIT,TW],{r,0,1}];
Axialu0rholFlowStar[z_,TW]=hOscFlow0Star*Axialu0rholFlow[z,TW];
Axialu0rholFlowStarNormalized[z_,TW]=Axialu0rholFlowStar[z,TW]/xSectAreaStar;


     (* v0T1 *)

twoTimesv0T1AvgTemplate   = v0hatTemplate * T1hatCCTemplate //ComplexExpand;
twoTimesv0T1ReAvgTemplate = twoTimesv0T1AvgTemplate - I Coefficient[twoTimesv0T1AvgTemplate,I];
twoTimesv0T1ReAvgFluxHold[r_,z_,sigmaV_,sigmaPV_,Uo_,Ul_,phiU_,phiT_,Tw_]=
  twoTimesv0T1ReAvgTemplate/.Union[v0Assign,T1Assign];

v0T1ReAvgFlux[r_,z_,sigmaV_,sigmaPV_,Uo_,Ul_,phiU_,phiT_,Tw_]:= 1/2 *
  twoTimesv0T1ReAvgFluxHold[r,z,sigmaV,sigmaPV,Uo,Ul,phiU,phiT,Tw]//ReleaseHold//ReleaseHold//ReleaseHold//N
v0T1ReAvgFlux[r_,z_,V,PV,U0,UL,PHIU,PHIT,0] =v0T1ReAvgFlux[r,z,V,PV,U0,UL,PHIU,PHIT,0]//Expand;
v0T1ReAvgFlux[r_,z_,V,PV,U0,UL,PHIU,PHIT,TW]=v0T1ReAvgFlux[r,z,V,PV,U0,UL,PHIU,PHIT,TW]//Expand;
```

Phasors

```
                                                    -6          -9
{{{OPT, 0.002, 100., 0.703, 70.266, 1., -0.1, 3.789 10  , 4.31 10  }, {1.002, 1.004, 1.00413}}, {100.,
   {-0.03918, 0.319915}, 7026.6},

  {0.00476915 Amp dyne, 0.199157 (tube^-1) dyne, 1.97349 W}, {OPT<>100., 3, 15, 19}}
```

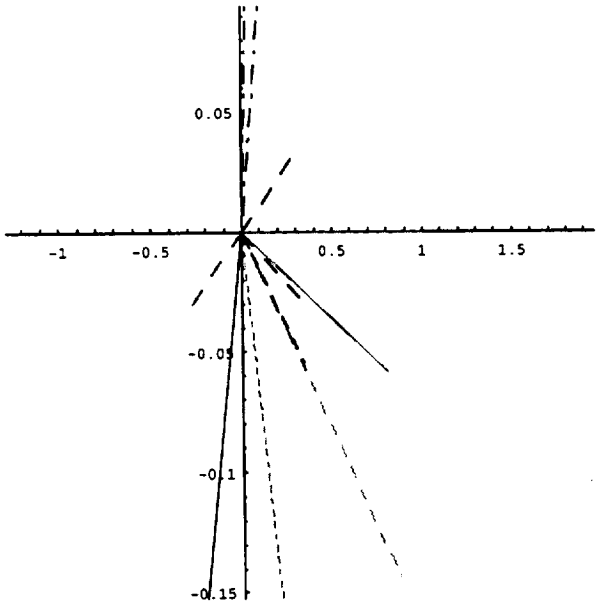

-Graphics-

Enthalpy Flow Plots

(* Enthalpy Flux Plot u0pl, u0plVol and HFlow *)

{{{OPT, 0.002, 100., 0.703, 70.266, 1., -0.1, 3.789 10^-6, 4.31 10^-9}, {1.002, 1.004, 1.00413}},
 {100., {-0.03918, 0.319915}, 7026.6},

 {0.00476915 Amp dyne, 0.199157 (tube^-1) dyne, 1.97349 W}, {OPT<>100., 3, 15, 19}}

c*	-> H [z=0 z=1]	uP [z=0 z=1]	HFlowRay [iso]	MaxWorkAmp [z=0 z=1]	
cTW*	-> HTW[z=0 z=1]	uPTW[z=0 z=1]	HFlowRay[adia]	MaxWorkAmpTW[z=0 z=1]	
c*/Href* (1/eps)	-> 0.137 0.113;	0.402 0.342;	0.118;	0.403	
c*/Href* (1/eps)	-> 0.145 0.143;	0.436 0.395;	0.196;	0.401	
c* (W/eps)	-> 0.269568 0.222384;	0.793 0.675;	0.232;	0.795;	0.795
cTW* (W/eps)	-> 0.285877 0.282791;	0.86 0.779;	0.387;	0.791;	0.791
c* /Ax*(W/cm2eps)	-> 0.128711 0.106182;	0.378 0.322;	0.111;	0.379;	0.379
cTW*/Ax*(W/cm2eps)	-> 0.136499 0.135025;	0.411 0.372;	0.185;	0.378;	0.378
c* /up* (W/Weps)	-> 0.34 0.281;	1.000 0.852;	0.293;	1.;	1.
cTW*/up* (W/Weps)	-> 0.361 0.357;	1.09 0.983;	0.488;	0.999;	0.999
c* /max* (W/Weps)	-> 0.339 0.28;	0.997 0.85;	0.292;	1.000;	1.
cTW*/max* (W/Weps)	-> 0.36 0.356;	1.08 0.98;	0.487;	0.996;	0.996

Href* = hOscFlow0Star =1.97349 W
CrossSectionalArea =2.09436 cm^2
blue is iso, red is thin wall, green is Radebaugh, purple is local area integrated plu0 flow-work
==========
AxialHFlow(1/eps) vs z
AxialHFlow(1/eps) and RayAdiaCalc(1/eps) vs z
AxialHFlowStar(W/eps) vs z
AxialHFlowStarNormalized(W/cm^2eps) vs z
==========
HFlow/u0plFlowWork(W/W) vs z
u0T1(1/eps) vs t for isothermal Wall
u0T1(1/eps) vs t for thin-wall

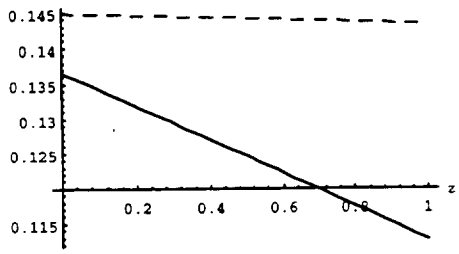

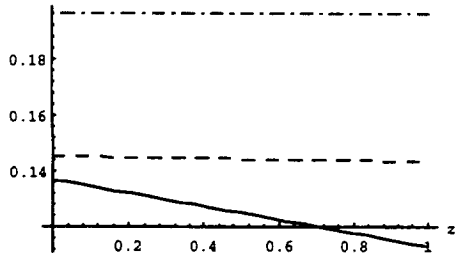

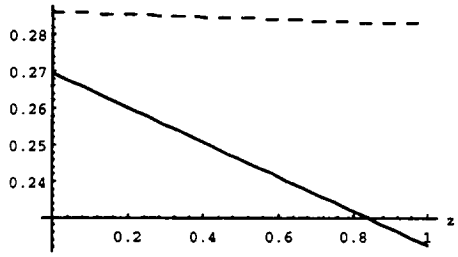

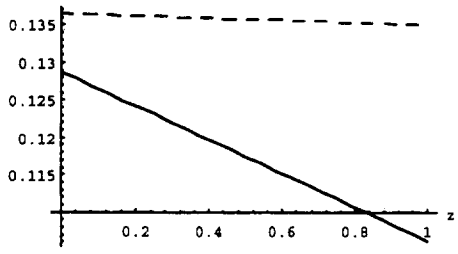

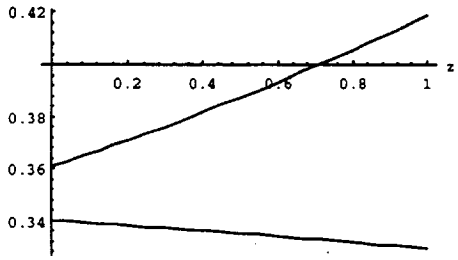

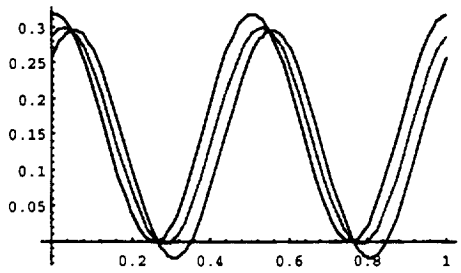

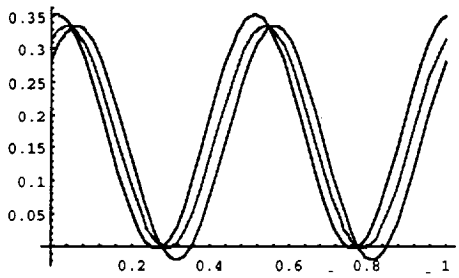

(* **Gas Conduction Loss Plot** (for a linear temp gradient) *)

```
Plot[((deltaTStar)/(LStar))*(condFitStar[pressureRefStarMPa/MPa,(z*tempRefGasStar+50K)/K](W/(M K)))*
     (M/(100 cm))(*xSectAreaStar*)cm^2/W,{z,0,1},AxesLabel->{"z","q* (W/cm^2)"}];
```

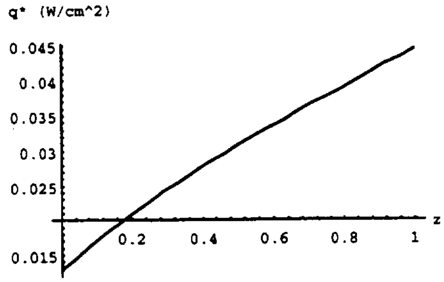

Listing;

```
• DIMENSIONAL VARIABLES SPECIFIED:
{{OPT, eps, Va, Pr, VaPr, UL, PHIU, M, LAMBDA, IsoPressRatio, AdiPressRatio, CLAdiPRatio}, {Fo, {PHIT, TW}, VaPrFo},

   {totalDragAmp0, totalDragRMS/tube, HOscFlow0Star}, date}scalingNames
                                                       -6          -9
{{{OPT, 0.002, 100., 0.703, 70.266, 1., -0.1, 3.789 10  , 4.31 10  }, {1.002, 1.004, 1.00413}}, {100., {-0.03918, 0.319915}, 7026.6},

   {0.00476915 Amp dyne, 0.199157 (tube^-1) dyne, 1.97349 W}, {OPT<>100., 3, 15, 19}}, scaling

-- inches:
rw =0.321453 in; L =3.93701 in; tubeThickness =0.00193031 in; pistonDynAmpInchAt0 =0.00787402 in; pistonDynAmpInchAtL =0.00787402 in


-- cgs:
                                                                  3                            2
rw =0.81649 cm; L =10 cm; tubeThickness =0.004903 cm; volOfTube =20.9436 cm ; CrossSectArea=2.09436 cm
                                                         3
pistonDynAmpAt0 =0.02 cm; pistonDynAmpAtL =0.02 cm; freq =---
                                                         sec

                  0.376991 cm                 0.376991 cm               0. cm                                                           0.00160224 g
pistonSpeedU0 =------------; pistonSpeedUL =------------; ΔpistonSpeed =------; pRef =0.999722 MPa; tempRef =300 K; rhoRef =------------
                    sec                         sec                      sec                                                                  3
                                                                                                                                            cm

                     2                                                                              2
           0.045313 cm              7.82 g         0.46 sec W        0.163 W             0.045313 cm
alphaTube =------------; rho0Tube =------; Cp0Tube =----------; kTube =--------; alphaTube =------------
              sec                      3             g K            cm K                    sec
                                     cm

                     2                                                                                              2
           0.178836 cm             0.00160224 g           5.2 sec W       0.00149 W     99488.6 cm       0.125662 cm        0.00020134 g
alpha0Gas =------------; rho0Gas =------------; Cp0Gas =----------; kGas =----------; a0 =----------; nu =------------; mu =------------
              sec                       3                 g K            cm K            sec              sec               cm sec
                                      cm

          0.942286 W                                            0.00060403 g              0.00126506 g               0.547465 W
hOscFlux0 =----------; HOscFlow0 =1.97349 W; jOscFlux0 =-------------; jOscFlow0 =-------------; qGasRadial0 =----------; HFlowRay =
              2                                                  2                          sec                         2
            cm                                              cm  sec                                                 cm

             0.00040268 g Pi                                    Pi
  HFlowRayStar[---------------, 300 K, 0.0203251 atm, 9.866 atm, --]
                  sec                                            6

totalDragAmpl0 =0.00476915 dyne; totalDragRMS/tube =0.199157 dyne

• PARAMETER LIST (for use in exporting to plot routines)
ParameterList={V,PV,KGAS,KTUBE,U0,UL,M,eps,GAMMA,PHIU,F,TERM,N[TW,5],N[PHIT,5]}
                                                                                   -6               5
ParameterList={5.6419 Sqrt[Pi], 4.72932 Sqrt[Pi], 0.0091411, 1., 1., 1., 1.20617 10   Pi, 0.002, -, -0.1, 0.0564191 Sqrt[Pi],
              16, 0.31991, -0.03918}
                                                                                                    3

• SOLUTION OF TW AT PHIT FOR CONTINUITY OF HEAT FLUX AT GAS/TUBE BOUNDARY
TW=0.319915 at PHIT=-0.0391796

• RANDOM TIME CHECK, ALL VALUES FOR TW SHOULD BE THE SAME
tRandom=0.657914
PHIT=-0.0391796
Twall={Twall[1., 0, 0., 10., 8.3825, 1., 1., -0.1, -0.0391796, 0.0091411, 0.1, 1.],

   Twall[1., 0, 0.125, 10., 8.3825, 1., 1., -0.1, -0.0391796, 0.0091411, 0.1, 1.],

   Twall[1., 0, 0.25, 10., 8.3825, 1., 1., -0.1, -0.0391796, 0.0091411, 0.1, 1.],

   Twall[1., 0, 0.5, 10., 8.3825, 1., 1., -0.1, -0.0391796, 0.0091411, 0.1, 1.],

   Twall[1., 0, 0.657914, 10., 8.3825, 1., 1., -0.1, -0.0391796, 0.0091411, 0.1, 1.]}
Bessel Fxn Accuracy= (   (V)   ;BesselJ; (ber+I bei); ModBesselJHold; Argument->infinity approximation)
Bessel Accuracy Hi = {(9.99999925}, 149.847528, 149.847526, 149.847526, 148.537427}
Bessel Accuracy Lo = {(0.999999925}, 1.01552483, 1.01552483, 1.01552483, 1.00386903}

• PHASORS:
           Amp       PHI       TWAmp     PHITW
U0         1.        0
UL         1.        -0.1
p1         0.805     -0.0116   0.883     -0.026
T1(r=0)    0.318     -0.0137   0.353     -0.0264
T1(r=1)    0.                  0.32      -0.0392
v0(r=.8)   0.0743    -0.845    0.0504    -0.856

• NON-DIMENSIONAL SCALING VARIABLES CALCULATED:
                                                                               -6
Va=100.; Pr=0.703; Pr*Va=70.2663; S =500.; Fo=100.; EL=0.00600497; M=3.78929 10   ; Re0 =4.89902
p0=1; T0[z]=1 ; rho0[z]=1

• NON-DIMENSIONAL VARIABLES USED IN COMPLEX SOLUTION:
```

V=10.; P=0.83825; PV=8.3825; eps=0.002; F=0.1; M=3.78929 10^-6; LAMBDA=4.30762 10^-9; eps*Va=0.2

U0=1.; UL=1.; PHIU=-0.1; TERM=16; KGAS =0.0091411; KTUBE=1.; GAMMA=5/3; d0=0.002; dL=0.002; PHIT=-0.0391796; TW=0.319915

ARCHIVE

Enthalpy **Flux** Fields

{{{OPT, 0.002, 100., 0.703, 70.266, 1., -0.1, 3.789 10^-6, 4.31 10^-9}, {1.002, 1.004, 1.00413}}, {100.,
{-0.03918, 0.319915}, 7026.6},

{0.00476915 Amp dyne, 0.199157 (tube^-1) dyne, 1.97349 W}, {OPT<>100., 3, 15, 19}}

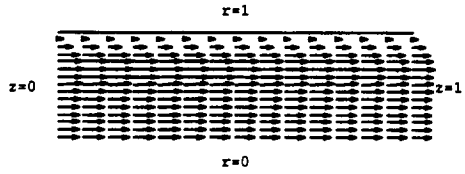

-Graphics-

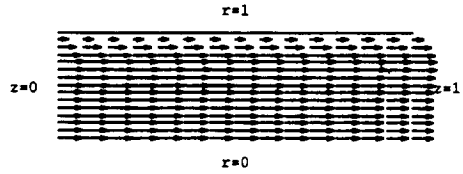

-Graphics-

Enthalpy **Flux Plots**

Isothermal and thin wall comparison at z=0, .5, 1

{{{OPT, 0.002, 100., 0.703, 70.266, 1., -0.1, 3.789 10^-6, 4.31 10^-9}, {1.002, 1.004, 1.00413}}, {100.,
{-0.03918, 0.319915}, 7026.6},

{0.00476915 Amp dyne, 0.199157 (tube^-1) dyne, 1.97349 W}, {OPT<>100., 3, 15, 19}}

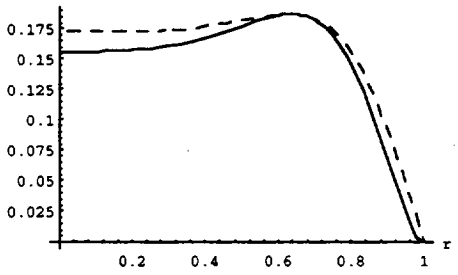

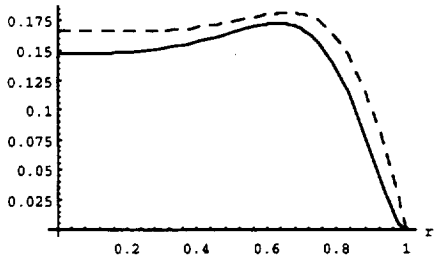

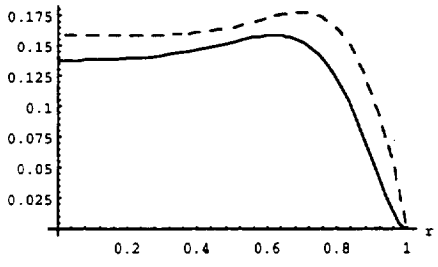

q: heat flux at wall

```
If[kindSystem==OPT,Print[fileNameOPTHXfr],,Print[fileNameBPTHXfr]];
Plot[{q1[1,0,t,V,PV,U0,UL,PHIU,PHIT,0],q1[1,0,t,V,PV,U0,UL,PHIU,PHIT,TW],T1Fa[0,0,t,V,PV,U0,UL,PHIU,PHIT,0],
      DeltaT1[0,t,V,PV,U0,UL,PHIU,PHIT,0],DeltaT1[0,t,V,PV,U0,UL,PHIU,PHIT,TW]},{t,0.1},
```

```
      PlotStyle->{{},  {Dashing[{0.03,0.03}]} ,{Dashing[{0.005,0.02,0.03,0.02}],RGBColor[1,0,0]},{},{RGBColor[0,0,1],
      Dashing[{0.03,0.03}]}   },PlotRange->All];

If[kindSystem==OPT,Print[fileNameOPTHXfr],,Print[fileNameBPTHXfr]];
Plot[{q1[1,0,t,V,PV,U0,UL,PHIU,PHIT,0],q1[1,0,t,V,PV,U0,UL,PHIU,PHIT,TW],
      DeltaT1[0,t,V,PV,U0,UL,PHIU,PHIT,0],DeltaT1[0,t,V,PV,U0,UL,PHIU,PHIT,TW]},{t,0,1},
      PlotStyle->{{},  {Dashing[{0.03,0.03}]} ,{RGBColor[0,0,1]},{RGBColor[0,0,1],Dashing[{0.03,0.03}]}   },
        PlotRange->All];

(* {{Thesis, OPT, eps, V, P, PV, UL, PHIU, M, IsoPressRatio, AdiVolPR, CLAdiPRatio}, {F, {PHIT, TW}},
  {HOscFlow0}, {date}} *)

                                                          -6          -9
{{{OPT, 0.002, 100., 0.703, 70.266, 1., -0.1, 3.789 10   , 4.31 10   }, {1.002, 1.004, 1.00413}}, {100.,
  {-0.03918, 0.319915}, 7026.6},

  {0.00476915 Amp dyne, 0.199157 (tube^-1) dyne, 1.97349 W}, {OPT<>100., 3, 15, 19}}
                                                          -6          -9
{{{OPT, 0.002, 100., 0.703, 70.266, 1., -0.1, 3.789 10   , 4.31 10   }, {1.002, 1.004, 1.00413}}, {100.,
  {-0.03918, 0.319915}, 7026.6},

  {0.00476915 Amp dyne, 0.199157 (tube^-1) dyne, 1.97349 W}, {OPT<>100., 3, 15, 19}}
```

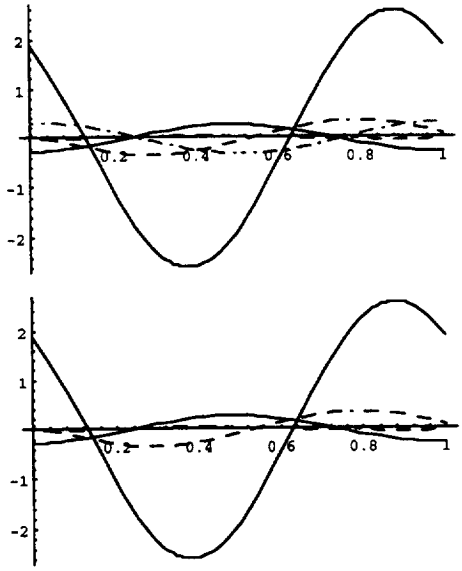

Tw=at wall

```
(* TW vs Fo *)
If[kindSystem==OPT,Print[fileNameOPTHXfr],,Print[fileNameBPTHXfr]];
AmpPlotTw[V,PV,U0,0,PHIU,fo]=LogLogPlot[Tw[0,phiU,fo],{fo,.1,150},PlotRange->All]
                                                          -6          -9
{{{OPT, 0.002, 100., 0.703, 70.266, 1., -0.1, 3.789 10   , 4.31 10   }, {1.002, 1.004, 1.00413}}, {100.,
  {-0.03918, 0.319915}, 7026.6},

  {0.00476915 Amp dyne, 0.199157 (tube^-1) dyne, 1.97349 W}, {OPT<>100., 3, 15, 19}}
```

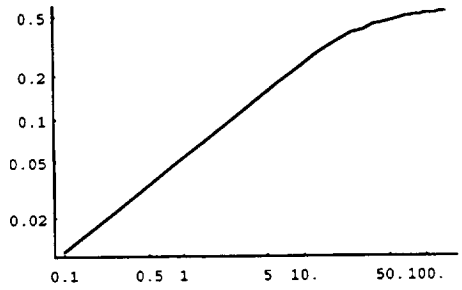

-Graphics-

```
(* PhiT vs Fo *)
ArgPlotTw[V,PV,U0,0,PHIU,fo]=LogLogPlot[-phiT[0,phiU,fo],{fo,.1,150},PlotRange->All]
```

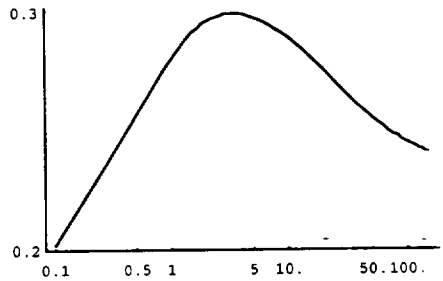

```
-Graphics-

(* Code for Graphics Plots *)

 If[kindSystem==OPT,Print[fileNameOPTHXfr],,Print[fileNameBPTHXfr]];

                                                              -6          -9
{{{OPT, 0.002, 100., 0.703, 70.266, 1., -0.1, 3.789 10   , 4.31 10   }, {1.002, 1.004, 1.00413}}, {100., {-0.03918, 0.319915}, 7026.6},

  {0.00476915 Amp dyne, 0.199157 (tube^-1) dyne, 1.97349 W}, {OPT<>100., 3, 15, 19}}

?PhasorPlot

Global`PhasorPlot

PhasorPlot[All, 31.83098385134257*Pi, 1., -0.1, 314.1578982435413/Pi] =
  Graphics[{Line[{{0, 0}, {-7.584757533613621, -5.740944894744813}}],
    {Dashing[{0.03, 0.03}], Line[{{0, 0}, {0.3165449091259993, -0.02735771620622396}}]},
    {Dashing[{0.005, 0.02, 0.03, 0.02}], Line[{{0, 0}, {1.879881736290323, 1.781540335669683}}]},
    {Dashing[{0.01, 0.01}], RGBColor[0, 1, 0], Line[{{0, 0}, {1, 0}}]},
    {Dashing[{0.01, 0.01}], RGBColor[0, 1, 0], Line[{{0, 0}, {0.809016994374948, -0.5877852522924733}}]},
    {Dashing[{}], RGBColor[0, 1, 1], Line[{{0, 0}, {0.803281420362929, -0.05861243832123366}}]},
    {Dashing[{0.02, 0.02}], RGBColor[0, 1, 1], Line[{{0, 0}, {0.871707058032187, -0.1436918561245787}}]},
    {Dashing[{0.03, 0.03}], RGBColor[0, 0, 1], Line[{{0, 0}, {0.2706043229945105, 0.03006237550349716}}]},
    {Dashing[{0.03, 0.03}], RGBColor[1, 0, 1], Line[{{0, 0}, {-0.2706043229945105, -0.03006237550349716}}]},
    {Dashing[{0.02, 0.02}], RGBColor[0, 0, 1], Line[{{0, 0}, {0.3390299606637685, -0.05501704229984794}}]},
    {Dashing[{0.03, 0.03}], RGBColor[1, 0, 0], Line[{{0, 0}, {0.3484200046661029, -0.05826763675797807}}]},
    {RGBColor[1, 0, 0], Line[{{0, 0}, {-7.58475753361361, -5.740944894744814}}]},
    {Dashing[{0.005, 0.02, 0.03, 0.02}], RGBColor[1, 0, 0], Line[{{0, 0}, {0.0864170124197421, 0.3391354590856961}}]}},
   {DisplayFunction -> (Display[$Display, #1] & ), AspectRatio -> 1, PlotRange -> Automatic, AspectRatio -> GoldenRatio^(-1),
    DisplayFunction :> Identity, ColorOutput -> Automatic, Axes -> Automatic, AxesOrigin -> Automatic, PlotLabel -> None, AxesLabel -> None,
    Ticks -> Automatic, GridLines -> None, Prolog -> {}, Epilog -> {}, AxesStyle -> Automatic, Background -> Automatic, DefaultColor -> Automatic,
    DefaultFont :> $DefaultFont, RotateLabel -> True, Frame -> False, FrameStyle -> Automatic, FrameTicks -> Automatic, FrameLabel -> None,
    PlotRegion -> Automatic}]

PhasorPlot[NuC, 31.83098385134257*Pi, 1., -0.1, 0] =
  Graphics[{Line[{{0, 0}, {-7.584757533613621, -5.740944894744813}}],
    {Dashing[{0.005, 0.02, 0.03, 0.02}], Line[{{0, 0}, {1.879881736290323, 1.781540335669683}}]},
    {Dashing[{0.01, 0.01}], RGBColor[0, 1, 0], Line[{{0, 0}, {1, 0}}]},
    {Dashing[{0.01, 0.01}], RGBColor[0, 1, 0], Line[{{0, 0}, {0.809016994374948, -0.5877852522924733}}]},
    {Dashing[{0.03, 0.03}], RGBColor[0, 0, 1], Line[{{0, 0}, {0.2706043229945105, 0.03006237550349716}}]},
    {Dashing[{0.03, 0.03}], RGBColor[1, 0, 1], Line[{{0, 0}, {-0.2706043229945105, -0.03006237550349716}}]}},
   {DisplayFunction -> Identity, PlotRange -> Automatic, AspectRatio -> GoldenRatio^(-1), DisplayFunction :> Identity, ColorOutput -> Automatic,
    Axes -> Automatic, AxesOrigin -> Automatic, PlotLabel -> None, AxesLabel -> None, Ticks -> Automatic, GridLines -> None, Prolog -> {}, Epilog -> {},
    AxesStyle -> Automatic, Background -> Automatic, DefaultColor -> Automatic, DefaultFont :> $DefaultFont, RotateLabel -> True, Frame -> False,
    FrameStyle -> Automatic, FrameTicks -> Automatic, FrameLabel -> None, PlotRegion -> Automatic}]

PhasorPlot[NuC, 31.83098385134257*Pi, 1., -0.1, 314.1578982435413/Pi] =
  Graphics[{{RGBColor[1, 0, 0], Line[{{0, 0}, {-7.58475753361361, -5.740944894744814}}]},
    {Dashing[{0.005, 0.02, 0.03, 0.02}], RGBColor[1, 0, 0], Line[{{0, 0}, {0.0864170124197421, 0.3391354590856961}}]},
    {Dashing[{0.01, 0.01}], RGBColor[0, 1, 0], Line[{{0, 0}, {1, 0}}]},
    {Dashing[{0.01, 0.01}], RGBColor[0, 1, 0], Line[{{0, 0}, {0.809016994374948, -0.5877852522924733}}]},
    {Dashing[{0.02, 0.02}], RGBColor[0, 0, 1], Line[{{0, 0}, {0.3390299606637685, -0.05501704229984794}}]},
    {Dashing[{0.03, 0.03}], RGBColor[1, 0, 1], Line[{{0, 0}, {-0.02876004518396047, -0.02294412494308133}}]}},
   {DisplayFunction -> Identity, PlotRange -> Automatic, AspectRatio -> GoldenRatio^(-1), DisplayFunction :> Identity, ColorOutput -> Automatic,
    Axes -> Automatic, AxesOrigin -> Automatic, PlotLabel -> None, AxesLabel -> None, Ticks -> Automatic, GridLines -> None, Prolog -> {}, Epilog -> {},
    AxesStyle -> Automatic, Background -> Automatic, DefaultColor -> Automatic, DefaultFont :> $DefaultFont, RotateLabel -> True, Frame -> False,
    FrameStyle -> Automatic, FrameTicks -> Automatic, FrameLabel -> None, PlotRegion -> Automatic}]

PhasorPlot[PTU, 31.83098385134257*Pi, 1., -0.1, 314.1578982435413/Pi] =
  Graphics[{{Dashing[{0.01, 0.01}], RGBColor[0, 1, 0], Line[{{0, 0}, {1, 0}}]},
    {Dashing[{0.01, 0.01}], RGBColor[0, 1, 0], Line[{{0, 0}, {0.809016994374948, -0.5877852522924733}}]},
    {Dashing[{}], RGBColor[0, 1, 1], Line[{{0, 0}, {0.803281420362929, -0.05861243832123366}}]},
    {Dashing[{0.02, 0.02}], RGBColor[0, 1, 1], Line[{{0, 0}, {0.871707058032187, -0.1436918561245787}}]},
    {Dashing[{0.03, 0.03}], RGBColor[0, 0, 1], Line[{{0, 0}, {0.2706043229945105, 0.03006237550349716}}]},
    {Dashing[{0.02, 0.02}], RGBColor[0, 0, 1], Line[{{0, 0}, {0.3390299606637685, -0.05501704229984794}}]}},
   {DisplayFunction -> (Display[$Display, #1] & ), AspectRatio -> 1, PlotRange -> {{-0.2, 1}, {-1, 0.2}}, PlotRange -> Automatic,
    AspectRatio -> GoldenRatio^(-1), DisplayFunction :> Identity, ColorOutput -> Automatic, Axes -> Automatic, AxesOrigin -> Automatic,
    PlotLabel -> None, AxesLabel -> None, Ticks -> Automatic, GridLines -> None, Prolog -> {}, Epilog -> {}, AxesStyle -> Automatic,
    Background -> Automatic, DefaultColor -> Automatic, DefaultFont :> $DefaultFont, RotateLabel -> True, Frame -> False, FrameStyle -> Automatic,
    FrameTicks -> Automatic, FrameLabel -> None, PlotRegion -> Automatic}]

?PhasorPlotBlack

Global`PhasorPlotBlack

PhasorPlotBlack[NuC, 31.83098385134257*Pi, 1., -0.1, 0] =
  Graphics[{Line[{{0, 0}, {-7.584757533613621, -5.740944894744813}}],
    {Dashing[{0.005, 0.02, 0.03, 0.02}], Line[{{0, 0}, {1.879881736290323, 1.781540335669683}}]}, {Dashing[{0.01, 0.01}], Line[{{0, 0}, {1, 0}}]},
    {Dashing[{0.01, 0.01}], Line[{{0, 0}, {0.809016994374948, -0.5877852522924733}}]},
    {Dashing[{0.03, 0.03}], Line[{{0, 0}, {0.2706043229945105, 0.03006237550349716}}]},
    {Dashing[{0.03, 0.03}], Line[{{0, 0}, {-0.2706043229945105, -0.03006237550349716}}]}},
   {DisplayFunction -> Identity, PlotRange -> Automatic, AspectRatio -> GoldenRatio^(-1), DisplayFunction :> Identity, ColorOutput -> Automatic,
    Axes -> Automatic, AxesOrigin -> Automatic, PlotLabel -> None, AxesLabel -> None, Ticks -> Automatic, GridLines -> None, Prolog -> {}, Epilog -> {},
    AxesStyle -> Automatic, Background -> Automatic, DefaultColor -> Automatic, DefaultFont :> $DefaultFont, RotateLabel -> True, Frame -> False,
    FrameStyle -> Automatic, FrameTicks -> Automatic, FrameLabel -> None, PlotRegion -> Automatic}]

PhasorPlotBlack[NuC, 31.83098385134257*Pi, 1., -0.1, 314.1578982435413/Pi] =
  Graphics[{{Line[{{0, 0}, {-7.58475753361361, -5.740944894744814}}]},
    {Dashing[{0.005, 0.02, 0.03, 0.02}], Line[{{0, 0}, {0.0864170124197421, 0.3391354590856961}}]}, {Dashing[{0.01, 0.01}], Line[{{0, 0}, {1, 0}}]},
    {Dashing[{0.01, 0.01}], Line[{{0, 0}, {0.809016994374948, -0.5877852522924733}}]},
    {Dashing[{0.02, 0.02}], Line[{{0, 0}, {0.3390299606637685, -0.05501704229984794}}]},
    {Dashing[{0.03, 0.03}], Line[{{0, 0}, {-0.02876004518396047, -0.02294412494308133}}]}},
   {DisplayFunction -> Identity, PlotRange -> Automatic, AspectRatio -> GoldenRatio^(-1), DisplayFunction :> Identity, ColorOutput -> Automatic,
    Axes -> Automatic, AxesOrigin -> Automatic, PlotLabel -> None, AxesLabel -> None, Ticks -> Automatic, GridLines -> None, Prolog -> {}, Epilog -> {},
    AxesStyle -> Automatic, Background -> Automatic, DefaultColor -> Automatic, DefaultFont :> $DefaultFont, RotateLabel -> True, Frame -> False,
    FrameStyle -> Automatic, FrameTicks -> Automatic, FrameLabel -> None, PlotRegion -> Automatic}]

PhasorPlotBlack[PTU, 31.83098385134257*Pi, 1., -0.1, 314.1578982435413/Pi] =
  Graphics[{{Dashing[{0.01, 0.01}], Line[{{0, 0}, {1, 0}}]}, {Dashing[{0.01, 0.01}], Line[{{0, 0}, {0.809016994374948, -0.5877852522924733}}]},
    {Dashing[{}], Line[{{0, 0}, {0.803281420362929, -0.05861243832123366}}]},
    {Dashing[{0.02, 0.02}], Line[{{0, 0}, {0.871707058032187, -0.1436918561245787}}]},
    {Dashing[{0.03, 0.03}], Line[{{0, 0}, {0.2706043229945105, 0.03006237550349716}}]},
    {Dashing[{0.02, 0.02}], Line[{{0, 0}, {0.3390299606637685, -0.05501704229984794}}]}},
   {DisplayFunction -> (Display[$Display, #1] & ), AspectRatio -> 1, PlotRange -> {{-0.2, 1}, {-1, 0.2}}, PlotRange -> Automatic,
    AspectRatio -> GoldenRatio^(-1), DisplayFunction :> Identity, ColorOutput -> Automatic, Axes -> Automatic, AxesOrigin -> Automatic,
    PlotLabel -> None, AxesLabel -> None, Ticks -> Automatic, GridLines -> None, Prolog -> {}, Epilog -> {}, AxesStyle -> Automatic,
    Background -> Automatic, DefaultColor -> Automatic, DefaultFont :> $DefaultFont, RotateLabel -> True, Frame -> False, FrameStyle -> Automatic,
    FrameTicks -> Automatic, FrameLabel -> None, PlotRegion -> Automatic}]

AmpPlotTw[5.641895413009938*Pi^(1/2), 4.729318913240664*Pi^(1/2), 1., 0, -0.1, fo] =
```

```
Graphics[{{{Line[{{-1., -1.9278633654111739}, {0.8024886616244436, -0.7490199905926986}, {1.1000832182914, -0.5574421622358031},
      {1.275023265322688, -0.4700519011933161}, {1.399385249546218, -0.4196936259076566}, {1.495948843114022, -0.3869530852775928},
      {1.574898989258946, -0.3639836092490773}, {1.641680632207503, -0.3469931894273173}, {1.699548677948487, -0.3339242959739331},
      {1.750604808323138, -0.3235644698694219}, {1.79628516981876, -0.3151533050972453}, {1.837614739188246, -0.3081900048869743},
      {1.875350696579289, -0.3023314621012289}, {1.910068287208911, -0.2973348150100153}, {1.942214810694346, -0.2930233835759382},
      {1.972144959458221, -0.289265596918928}, {2.00014474070519, -0.285961481476084}, {2.026448140455147, -0.2830337261160283},
      {2.051249021610516, -0.2804216135760304}, {2.074709803628545, -0.2780768007838732}, {2.096967915078924, -0.2759603231885111},
      {2.118140671487759, -0.2740404283127187}, {2.138329018246402, -0.2722909827598751}, {2.157620441425085, -0.2706902832036441},
      {2.176091259055681, -0.2692201567724531}}}}}, {DisplayFunction -> (Display[$Display, #1] & ),
  PlotRange -> {{-1.079402281476392, 2.255493540532073}, {-1.969329445627721, -0.2277540765564709}},
  AxesOrigin -> {-1.079402281476392, -1.969329445627721}, PlotRange -> All, AspectRatio -> GoldenRatio^(-1), DisplayFunction :> Identity,
  ColorOutput -> Automatic, Axes -> Automatic, AxesOrigin -> Automatic, PlotLabel -> None, AxesLabel -> None, Ticks -> {LogScale, LogScale},
  GridLines -> None, Prolog -> {}, Epilog -> {}, AxesStyle -> Automatic, Background -> Automatic, DefaultColor -> Automatic,
  DefaultFont :> $DefaultFont, RotateLabel -> True, Frame -> False, FrameStyle -> Automatic, FrameTicks -> {LogScale, LogScale, LogScale, LogScale},
  FrameLabel -> None, PlotRegion -> Automatic}]

Clear[PhasorPlot,PhasorPlotBlack,AmpPlot,ArgPlot,AmpPlotTw]

================================================

(* Mass Flux Field *)

  (* Calculations *)

  rhoSuSAvg: axial secondary mass flux

(* AXIAL REYNOLDS STRESS - Axial Reynolds Stress - u0u0 *)

twoTimesDrho0u0u0ZAvgTemplate   = D[rho0[z] u0hatTemplate u0hatCCTemplate,z] //ComplexExpand;
twoTimesDrho0u0u0ZReAvgTemplate =
  (twoTimesDrho0u0u0ZAvgTemplate - I Coefficient[twoTimesDrho0u0u0ZAvgTemplate,I]);
twoTimesDrho0u0u0ZReAvgFluxHold[r_,z_,sigmaV_,Uo_,Ul_,phiU_]=twoTimesDrho0u0u0ZReAvgTemplate/.u0Assign;

Drho0u0u0ZReAvgFlux[r_,z_,sigmaV_,Uo_,Ul_,phiU_]:= 1/2 twoTimesDrho0u0u0ZReAvgFluxHold[r,z,sigmaV,Uo,Ul,phiU]
                                        //ReleaseHold//ReleaseHold//N;
Drho0u0u0ZReAvgFlux[r_,z_,V,U0,UL,PHIU] = Drho0u0u0ZReAvgFlux[r,z,V,U0,UL,PHIU]//Expand;
axialStress[r_,z_]=Integrate[Integrate[r*Drho0u0u0ZReAvgFlux[r,z,V,U0,UL,PHIU],r]/r,r]//Expand;
  (*axialStress=q2*)
(* q3[r_,z_]=Integrate[r * axialStress[r,z],r]//Expand; *)(*don't really need r-dependence ...
  coded here for completeness*)
q3[z_]   =Integrate[r * axialStress[r,z],{r,0,1}]//Expand;


(****** time-averaged u-velocity, or mean-steady Reynolds Stress? ******)
twoTimesrho0u0u0AvgTemplate   = (rho0[z] u0hatTemplate u0hatCCTemplate) //ComplexExpand;
twoTimesrho0u0u0ReAvgTemplate = (twoTimesrho0u0u0AvgTemplate - I Coefficient[twoTimesrho0u0u0AvgTemplate,I]);
twoTimesrho0u0u0ReAvgFluxHold[r_,z_,sigmaV_,Uo_,Ul_,phiU_]=twoTimesrho0u0u0ReAvgTemplate/.u0Assign;

rho0u0u0ReAvgFlux[r_,z_,sigmaV_,Uo_,Ul_,phiU_]:= 1/2 twoTimesrho0u0u0ReAvgFluxHold[r,z,sigmaV,Uo,Ul,phiU]
                                        //ReleaseHold//ReleaseHold//N;
rho0u0u0ReAvgFlux[r_,z_,V,U0,UL,PHIU] = rho0u0u0ReAvgFlux[r,z,V,U0,UL,PHIU]//Expand;
  (* average velocity amplitude for rho0=1*)

localReynoldsStress[z_]=Integrate[r*rho0u0u0ReAvgFlux[r,z,V,U0,UL,PHIU],{r,0,1}]//Expand;
RMSReynoldsStress[z_]=Sqrt[localReynoldsStress[z]];


(* RADIAL REYNOLDS STRESS - Radial Reynolds Stress equals simply, the Int[rho[z]v0u0,r]*)

twoTimesrho0v0u0AvgTemplate   = rho0[z] v0hatTemplate u0hatCCTemplate //ComplexExpand;
twoTimesrho0v0u0ReAvgTemplate = twoTimesrho0v0u0AvgTemplate - I Coefficient[twoTimesrho0v0u0AvgTemplate,I];
twoTimesrho0v0u0ReAvgFluxHold[r_,z_,sigmaV_,sigmaPV_,Uo_,Ul_,phiU_,phiT_,Tw_]=twoTimesrho0v0u0ReAvgTemplate/.
                                                        Union[v0Assign,u0Assign];

rho0v0u0ReAvgFlux[r_,z_,sigmaV_,sigmaPV_,Uo_,Ul_,phiU_,phiT_,Tw_]:= 1/2 *
  twoTimesrho0v0u0ReAvgFluxHold[r,z,sigmaV,sigmaPV,Uo,Ul,phiU,phiT,Tw]//ReleaseHold//ReleaseHold//N;

rho0v0u0ReAvgFlux[r_,z_,V,PV,U0,UL,PHIU,PHIT,0] = rho0v0u0ReAvgFlux[r,z,V,PV,U0,UL,PHIU,PHIT,0]//Expand;
rho0v0u0ReAvgFlux[r_,z_,V,PV,U0,UL,PHIU,PHIT,TW] = rho0v0u0ReAvgFlux[r,z,V,PV,U0,UL,PHIU,PHIT,TW]//Expand;

radialStress[r_,z_,0]=Integrate[rho0v0u0ReAvgFlux[r,z,V,PV,U0,UL,PHIU,PHIT,0],r]//Expand; (*radialStress=j2*)
radialStress[r_,z_,TW]=Integrate[rho0v0u0ReAvgFlux[r,z,V,PV,U0,UL,PHIU,PHIT,TW],r]//Expand;

j3[r_,z_,0]= Integrate[r * radialStress[r,z,0],r]//Expand;
j3[z_,0]= Integrate[r * radialStress[r,z,0],{r,0,1}]//Expand;

(* j3[r_,z_,TW]= Integrate[r * radialStress[r,z,TW],r]//Expand;*)
              (*don't really need r-dependence ... coded here for completeness*)
j3[z_,TW]= Integrate[r * radialStress[r,z,TW],{r,0,1}]//Expand;


(* MASS FLUX STRESS - "Stress" due to Mass Conservation - rholu0 *)

twoTimesrholu0AvgTemplate = rholhatTemplate u0hatCCTemplate //ComplexExpand;
twoTimesrholu0ReAvgTemplate = twoTimesrholu0AvgTemplate - I Coefficient[twoTimesrholu0AvgTemplate,I];
twoTimesrholu0ReAvgFluxHold[r_,z_,sigmaV_,sigmaPV_,Uo_,Ul_,phiU_,phiT_,Tw_]=twoTimesrholu0ReAvgTemplate/.
                                                        Union[plAssign,TlAssign,u0Assign];

rholu0ReAvgFlux[r_,z_,sigmaV_,sigmaPV_,Uo_,Ul_,phiU_,phiT_,Tw_]:=
                                1/2 twoTimesrholu0ReAvgFluxHold[r,z,sigmaV,sigmaPV,Uo,Ul,phiU,phiT,Tw]
                                        //ReleaseHold//ReleaseHold//N;
rholu0ReAvgFlux[r_,z_,V,PV,U0,UL,PHIU,PHIT,0]  = rholu0ReAvgFlux[r,z,V,PV,U0,UL,PHIU,PHIT, 0]//Expand;
rholu0ReAvgFlux[r_,z_,V,PV,U0,UL,PHIU,PHIT,TW] = rholu0ReAvgFlux[r,z,V,PV,U0,UL,PHIU,PHIT,TW]//Expand;

k3[z_,0] = (1/Power[V,2]) Integrate[r*rholu0ReAvgFlux[r,z,V,PV,U0,UL,PHIU,PHIT,0], {r,0,1}]//Expand//N;
  (*massFluxStress=k3*)
k3[z_,TW]= (1/Power[V,2]) Integrate[r*rholu0ReAvgFlux[r,z,V,PV,U0,UL,PHIU,PHIT,TW],{r,0,1}]//Expand//N;


(* AXIAL SECONDARY MASS FLUX - rhoSuSAvg
   STEADY (observed!) SECONDARY AXIAL VELOCITY - u1Avg - due to Reynolds' stresses *)

K[r_,z_,0] = 4 (k3[z,0]  + q3[z] + j3[z,0])  - 2 (axialStress[1,z] + radialStress[1,z,0]) //Expand;
K[r_,z_,TW]= 4 (k3[z,TW] + q3[z] + j3[z,TW]) - 2 (axialStress[1,z] + radialStress[1,z,TW])//Expand;

rho0u1Avg[r_,z_,0]  =Power[V,2]((axialStress[r,z]-axialStress[1,z])+(radialStress[r,z,0] -
                      radialStress[1,z,0]) +(r^2-1) K[r,z,0])//Expand;
rho0u1Avg[r_,z_,TW] =Power[V,2]((axialStress[r,z]-axialStress[1,z])+(radialStress[r,z,TW]-
                      radialStress[1,z,TW])+(r^2-1) K[r,z,TW])//Expand;

rhoSuSAvg[r_,z_,0]  = rho0u1Avg[r,z,0] + rholu0ReAvgFlux[r,z,V,PV,U0,UL,PHIU,PHIT,0];
rhoSuSAvg[r_,z_,TW] = rho0u1Avg[r,z,TW] + rholu0ReAvgFlux[r,z,V,PV,U0,UL,PHIU,PHIT,TW];
```

rhoSvSAvg: radial secondary mass flux

```
(* RADIAL SECONDARY MASS FLUX - rhoSvSAvg *)

rhoSvSAvg[r_,z_,0]  = - 1/r * Integrate[r*D[rhoSuSAvg[r,z,0], z],r] //Expand;
rhoSvSAvg[r_,z_,TW] = - 1/r * Integrate[r*D[rhoSuSAvg[r,z,TW],z],r] //Expand;

(* RADIAL MASS FLUX STRESS - rho1v0 *)

twoTimesrho1v0AvgTemplate   = rho1hatTemplate v0hatCCTemplate //ComplexExpand;
twoTimesrho1v0ReAvgTemplate = twoTimesrho1v0AvgTemplate - I Coefficient[twoTimesrho1v0AvgTemplate,I];
twoTimesrho1v0ReAvgFluxHold[r_,z_,sigmaV_,sigmaPV_,Uo_,U1_,phiU_,phiT_,Tw_]=twoTimesrho1v0ReAvgTemplate/.
                                                                    Union[p1Assign,T1Assign,v0Assign];

rho1v0ReAvgFlux[r_,z_,sigmaV_,sigmaPV_,Uo_,U1_,phiU_,phiT_,Tw_]:=
                              1/2 twoTimesrho1v0ReAvgFluxHold[r,z,sigmaV,sigmaPV,Uo,U1,phiU,phiT,Tw]
                              //ReleaseHold//ReleaseHold//N;
rho1v0ReAvgFlux[r_,z_,0]  = rho1v0ReAvgFlux[r,z,V,PV,U0,UL,PHIU,PHIT,0]//Expand;
rho1v0ReAvgFlux[r_,z_,TW] = rho1v0ReAvgFlux[r,z,V,PV,U0,UL,PHIU,PHIT,TW]//Expand;

rho0v1Avg[r_,z_,0] =(rhoSvSAvg[r,z,0] -rho1v0ReAvgFlux[r,z,0] );
rho0v1Avg[r_,z_,TW]=(rhoSvSAvg[r,z,TW]-rho1v0ReAvgFlux[r,z,TW]);


  (* Fields *)

If[kindSystem==OPT,Print[fileNameOPTHXfrList];Print[fileNameOPTHXfr],,Print[fileNameBPTHXfrList];
            Print[fileNameBPTHXfr]];
Timing[massFlux[1,meanSteady,0] =PlotVectorField[{rhoSuSAvg[r,z,0],rhoSvSAvg[r,z,0]},  {z,0,1},{r,0,1},
                              AspectRatio->1/3,DisplayFunction->Identity]];
Timing[massFlux[1,meanSteady,TW]=PlotVectorField[{rhoSuSAvg[r,z,TW],rhoSvSAvg[r,z,TW]},{z,0,1},{r,0,1},
                              AspectRatio->1/3,DisplayFunction->Identity]];
Show[{massFlux[1,meanSteady,0],liner[{0,1},{1,1}],texter},DisplayFunction->$DisplayFunction]
Show[{massFlux[1,meanSteady,TW],liner[{0,1},{1,1}],texter},DisplayFunction->$DisplayFunction]

{{OPT, eps, Va, Pr, VaPr, UL, PHIU, M, LAMBDA, IsoPressRatio, AdiPressRatio, CLAdiPRatio},
   {Fo, {PHIT, TW}, VaPrFo},

  {totalDragAmp0, totalDragRMS/tube, HOscFlow0Star}, date}
                                                     -6        -9
{{{OPT, 0.002, 100., 0.703, 70.266, 1., -0.1, 3.789 10  , 4.31 10  }, {1.002, 1.004, 1.00413}},
    {100., {-0.03918, 0.319915}, 7026.6}},

  {0.00476915 Amp dyne, 0.199157 (tube^-1) dyne, 1.97349 W}, {OPT<>100., 3, 15, 19}}
```

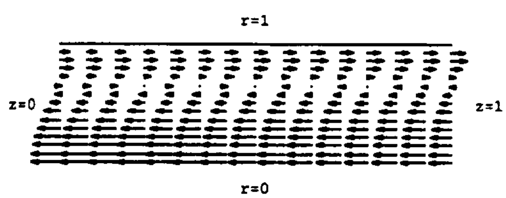

-Graphics-

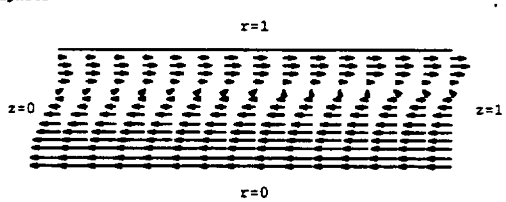

-Graphics-

```
Show[{massFlux[1,meanSteady,0], liner[{0,1},{1,1}],texter},DisplayFunction->$DisplayFunction]
Show[{massFlux[1,meanSteady,TW],liner[{0,1},{1,1}],texter},DisplayFunction->$DisplayFunction]
```

-Graphics-

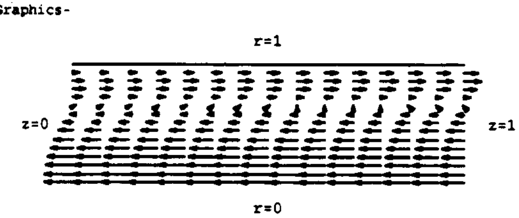

-Graphics-

```
  (* Plots *)  (* of mass flux at a given z, Check for zero net mass flow *)

If[kindSystem==OPT,(*Print[fileNameOPTHXfrList];*)Print[fileNameOPTHXfr],,(*Print[fileNameBPTHXfrList];*)
   Print[fileNameBPTHXfr]]
Block[{z=.5},
Plot[{rhoSuSAvg[r,z,0],rhoSuSAvg[r,z,TW](*,  rhoSuSAvg[r,1,0]*)   },{r,0,1},
       PlotStyle->{{},{Dashing[{0.03,0.03}],RGBColor[0,0,1]}   ,{Dashing[{0.005,0.02,0.03,0.02}],
       RGBColor[1,0,0]}   },
       PlotRange->All,AxesLabel->{"r",""}]   (*rhoSuSAvg*);
Timing[NIntegrate[rhoSuSAvg[r,z,0]*r,{r,0,1}]]]
(*
{{BPT, eps, Va, Pr, VaPr, UL, PHIU, M, LAMBDA, IsoPressRatio, AdiPressRatio, CLAdiPRatio},
   {Fo, {PHIT, TW}},
    {totalDragAmp0, totalDragRMS/tube, HOscFlow0Star}, date}
*)
                                                     -6        -9
{{{OPT, 0.002, 100., 0.703, 70.266, 1., -0.1, 3.789 10  , 4.31 10  }, {1.002, 1.004, 1.00413}},
```

```
{100., {-0.03918, 0.319915}, 7026.6},

{0.00476915 Amp dyne, 0.199157 (tube^-1) dyne, 1.97349 W}, {OPT<>100., 3, 15, 19}}
```

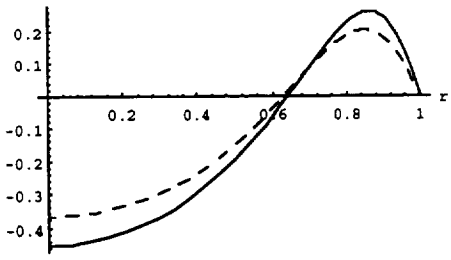


```
                                  -16
{51.9333 Second, 2.53812 10    }
```

Other

```
Plot[{rhoSuSAvg[r,0,0],rho0ulAvg[r,0,0],rholu0ReAvgFlux[r,0,V,PV,U0,UL,PHIU,PHIT,0]},{r,0,1},
PlotStyle->{{RGBColor[0,0,1]},{RGBColor[0,1,0]},{RGBColor[1,0,0]}},
PlotRange->All,AxesLabel->{"r","rhoSuSAvg"}];
```

rhoSuSAvg

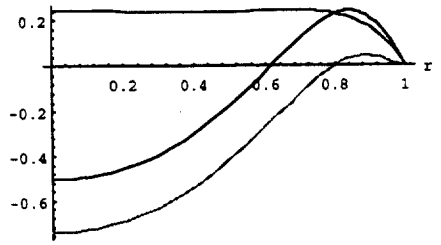


```
    (* Plot of Integrated over area Transverse RMS Reynolds Stress (integration  z *)
Plot[RMSReynoldsStress[z],{z,0,1},PlotStyle->{{RGBColor[1,0,0]}}];
```

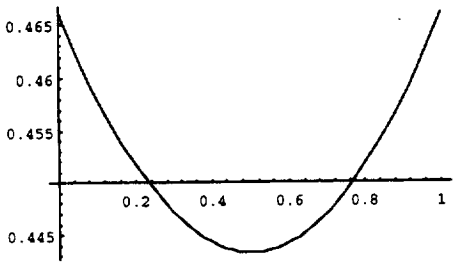


```
ARCHIVE

OTHER FLOW COMPONENTS

   (* Steady rho0U1Flux Field *)

If[kindSystem==OPT,Print[fileNameOPTHXfrList];Print[fileNameOPTHXfr],,Print[fileNameBPTHXfrList];Print[fileNameBPTHXfr]];
Timing[rho0U1Flux[1,quasiSteady,0] =PlotVectorField[{rho0ulAvg[r,z,0], rho0v1Avg[r,z,0]} ,{z,0,1},{r,0,1},AspectRatio->1/3
                                   (*,AxesLabel->{"r/rw","z/L"},Axes->True,*)]]
Timing[rho0U1Flux[1,quasiSteady,TW]=PlotVectorField[{rho0ulAvg[r,z,TW],rho0v1Avg[r,z,TW]},{z,0,1},{r,0,1},AspectRatio->1/3
                                   (*,AxesLabel->{"r/rw","z/L"},Axes->True,*)]]

{{BPT, eps, Va, Pr, VaPr, UL, PHIU, M, LAMBDA, IsoPressRatio, AdiPressRatio, CLAdiPRatio}, {Fo, {PHIT, TW}},

  {totalDragAmp0, totalDragRMS/tube, HOscFlow0Star}, date}
                                                                                    -7
{{{BPT, 0.1, 250., 0.703, 13.254, 0., n/aPHIU, 0.0003158, 5.98 10   }, {1.222, 1.397, 1.4}}, {20., {-0.288669, 0.490179}},

  {0.397429 Amp dyne, 2.17228 (tube^-1) dyne, 246.69 W}, {BPT<>250., 6, 7, 13}}

$Aborted
```

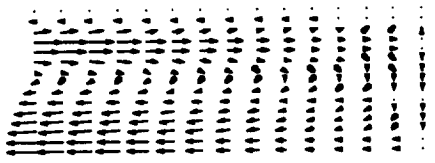

```
{60.8833 Second, -Graphics-}

   (* Steady rhol U0Flux Field *)

If[kindSystem==OPT,Print[fileNameOPTHXfrList];Print[fileNameOPTHXfr],,Print[fileNameBPTHXfrList];Print[fileNameBPTHXfr]];
Timing[rho10U0Flux[1,quasiSteady,0] =PlotVectorField[{rholu0ReAvgFlux[r,z,V,PV,U0,UL,PHIU,PHIT,0], rholv0ReAvgFlux[r,z,0]} ,
                                   {z,0,1},{r,0,1},AspectRatio->1/3{*,AxesLabel->{"r/rw","z/L"},Axes->True,*}]]
Timing[rho10U0Flux[1,quasiSteady,TW]=PlotVectorField[{rholu0ReAvgFlux[r,z,V,PV,U0,UL,PHIU,PHIT,TW],rholv0ReAvgFlux[r,z,TW]},
                                   {z,0,1},{r,0,1},AspectRatio->1/3{*,AxesLabel->{"r/rw","z/L"},Axes->True,*}]]
```

```
{{BPT, eps, Va, Pr, VaPr, UL, PHIU, M, LAMBDA, IsoPressRatio, AdiPressRatio, CLAdiPRatio}, {Fo, {PHIT, TW}},
  {totalDragAmp0, totalDragRMS/tube, HOscFlow0Star}, date}
                                                                    -7
{{{BPT, 0.1, 250., 0.703, 13.254, 0., n/aPHIU, 0.0003158, 5.98 10   }, {1.222, 1.397, 1.4}}, {20., {-0.288669, 0.490179}},
  {0.397429 Amp dyne, 2.17228 (tube^-1) dyne, 246.69 W}, {BPT<>250., 6, 7, 13}}
```

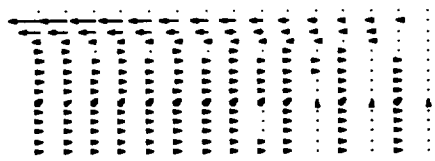

```
{43.1333 Second, -Graphics-}
```

```
{45.1667 Second, -Graphics-}

    (* Isothermal Flow movie *)

Block[{tEnd=.95},If[kindSystem==OPT,Print[fileNameOPTHXfrList];Print[fileNameOPTHXfr],,Print[fileNameBPTHXfrList];Print[fileNameBPTHXfr]];
Timing[Do[velField[2,t,0]=PlotVectorField[
  {u0Re[r,z,t,V,U0,UL,PHIU]+eps rhoSuSAvg[r,z,0],v0Re[r,z,t,V,PV,U0,UL,PHIU,PHIT,0]+eps rhoSvSAvg[r,z,0]},{z,0,1},{r,0,1},
  AspectRatio->1/3,(*AxesLabel->{"r/rw","z/L"},Axes->True,*)PlotLabel->t],{t,0,tEnd,.05}]]]

    (* thin wall Flow movie *)

Block[{tEnd=.95},If[kindSystem==OPT,Print[fileNameOPTHXfrList];Print[fileNameOPTHXfr],,Print[fileNameBPTHXfrList];Print[fileNameBPTHXfr]];
Timing[Do[velField[2,t,TW]=PlotVectorField[
  {u0Re[r,z,t,V,U0,UL,PHIU]+eps rhoSuSAvg[r,z,TW],v0Re[r,z,t,V,PV,U0,UL,PHIU,PHIT,TW]+eps rhoSvSAvg[r,z,TW]},{z,0,1},{r,0,1},
  AspectRatio->1/3,(*AxesLabel->{"r/rw","z/L"},Axes->True,*)PlotLabel->t],{t,0,tEnd,.05}]]]

================================================

(* Mean-steady Particle Velocity *)

  (* Calculations *)

Du0ReR[r_,z_,t_,V,U0,UL,PHIU] = D[u0Re[r,z,t,V,U0,UL,PHIU],r];
Du0ReZ[r_,z_,t_,V,U0,UL,PHIU] = D[u0Re[r,z,t,V,U0,UL,PHIU],z];
Du0ReRIv0ReTAvgFlux[r_,z_,0] :=
  Integrate[Du0ReR[r,z,t,V,U0,UL,PHIU] Integrate[v0Re[r,z,t,V,PV,U0,UL,PHIU,PHIT,0],t],{t,0,1}]
Du0ReRIv0ReTAvgFlux[r_,z_,TW]:=
  Integrate[Du0ReR[r,z,t,V,U0,UL,PHIU] Integrate[v0Re[r,z,t,V,PV,U0,UL,PHIU,PHIT,TW],t],{t,0,1}]
Du0ReZIu0ReTAvgFlux[r_,z_]   :=
  Integrate[Du0ReZ[r,z,t,V,U0,UL,PHIU] Integrate[u0Re[r,z,t,V,U0,UL,PHIU],t],{t,0,1}]
upAvg[r_,z_,0]               := rhoSuSAvg[r,z,0]  + Du0ReRIv0ReTAvgFlux[r,z,0]  + Du0ReZIu0ReTAvgFlux[r,z]//N
upAvg[r_,z_,TW]              := rhoSuSAvg[r,z,TW] + Du0ReRIv0ReTAvgFlux[r,z,TW] + Du0ReZIu0ReTAvgFlux[r,z]//N

Dv0ReR[r_,z_,t_,V,PV,U0,UL,PHIU,PHIT,0] = D[v0Re[r,z,t,V,PV,U0,UL,PHIU,PHIT,0],r];
Dv0ReZ[r_,z_,t_,V,PV,U0,UL,PHIU,PHIT,0] = D[v0Re[r,z,t,V,PV,U0,UL,PHIU,PHIT,0],z];
Dv0ReR[r_,z_,t_,V,PV,U0,UL,PHIU,PHIT,TW] = D[v0Re[r,z,t,V,PV,U0,UL,PHIU,PHIT,TW],r];
Dv0ReZ[r_,z_,t_,V,PV,U0,UL,PHIU,PHIT,TW] = D[v0Re[r,z,t,V,PV,U0,UL,PHIU,PHIT,TW],z];
Dv0ReRIv0ReTAvgFlux[r_,z_,0] :=
  Integrate[Dv0ReR[r,z,t,V,PV,U0,UL,PHIU,PHIT,0] Integrate[v0Re[r,z,t,V,PV,U0,UL,PHIU,PHIT,0],t],{t,0,1}]
Dv0ReZIu0ReTAvgFlux[r_,z_,0] :=
  Integrate[Dv0ReZ[r,z,t,V,PV,U0,UL,PHIU,PHIT,0] Integrate[u0Re[r,z,t,V,U0,UL,PHIU],t],{t,0,1}]
Dv0ReRIv0ReTAvgFlux[r_,z_,TW] :=
  Integrate[Dv0ReR[r,z,t,V,PV,U0,UL,PHIU,PHIT,TW] Integrate[v0Re[r,z,t,V,PV,U0,UL,PHIU,PHIT,TW],t],{t,0,1}]
Dv0ReZIu0ReTAvgFlux[r_,z_,TW] :=
  Integrate[Dv0ReZ[r,z,t,V,PV,U0,UL,PHIU,PHIT,TW] Integrate[u0Re[r,z,t,V,U0,UL,PHIU],t],{t,0,1}]
vpAvg[r_,z_,0]               := rhoSvSAvg[r,z,0]  + Dv0ReRIv0ReTAvgFlux[r,z,0]  + Dv0ReZIu0ReTAvgFlux[r,z,0]//N
vpAvg[r_,z_,TW]              := rhoSvSAvg[r,z,TW] + Dv0ReRIv0ReTAvgFlux[r,z,TW] + Dv0ReZIu0ReTAvgFlux[r,z,TW]//N


  (* Plots *)

    (* upAvg *)

uSPlot[{r,.5),0]=Plot[rhoSuSAvg[r,.5,0],{r,0,1}];
uSPlot[{r,1),0]=Plot[rhoSuSAvg[r,1,0],{r,0,1}];


Show[{uSPlot[{r,0),0], Graphics[{Dashing[{0.02,0.02}],RGBColor[0,0,1],upAvgPlot[0,0]}]},Axes->True]
(*Show[{uSPlot[{r,.5),0], Graphics[{Dashing[{0.02,0.02}],RGBColor[0,0,1],upAvgPlot[.5,0]}]},Axes->True]*)
Show[{uSPlot[{r,1),0], Graphics[{Dashing[{0.02,0.02}],RGBColor[0,0,1],upAvgPlot[1,0]}]},Axes->True]
Show[Graphics[{upAvgPlot[0,0], {Dashing[{0.02,0.02}],RGBColor[0,0,1],upAvgPlot[0,TW]}} ],Axes->True]


Show[{uSPlot[{r,0),0], Graphics[{Dashing[{0.02,0.02}],RGBColor[0,0,1],upAvgPlot[0,0]}]},
     {uSPlot[{r,1),0], Graphics[{Dashing[{0.02,0.02}],RGBColor[0,0,1],upAvgPlot[1,0]}]},Axes->True]


(*
Show[Graphics[{{                                    upAvgPlot[0,0]},
     {Dashing[ {0.02,0.02}],           RGBColor[0,0,1],upAvgPlot[.5,0]},
     {Dashing[ {0.005,0.02,0.03,0.02}],RGBColor[1,0,0],upAvgPlot[1,0]}
           }],Axes->True]

Show[Graphics[{Du0ReRIv0ReTAvgFluxPlot[0,0],{Dashing[{0.02,0.02}],RGBColor[0,0,1],
  Du0ReRIv0ReTAvgFluxPlot[0,TW]}}],Axes->True]
Show[Graphics[ Du0ReZIu0ReTAvgFluxPlot[0]],Axes->True]
*)
```

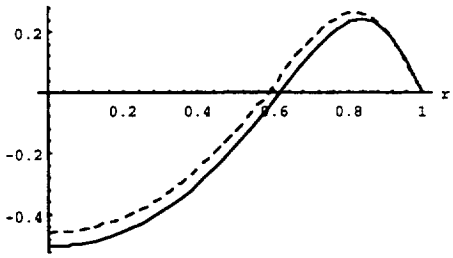

-Graphics-

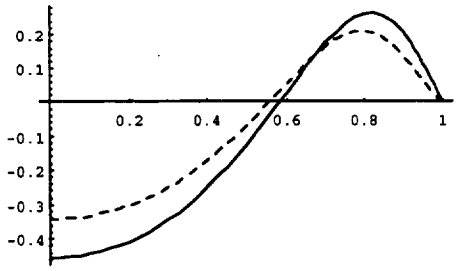

-Graphics-

```
(* vpAvg *)

Show[{vSPlot[{r,0},0], Graphics[{Dashing[{0.02,0.02}],RGBColor[0,0,1],vpAvgPlot[0,0]}]},Axes->True]
Show[Graphics[{vpAvgPlot[0,0],{Dashing[{0.02,0.02}],RGBColor[0,0,1],vpAvgPlot[0,TW]}]},Axes->True]

(*
Show[Graphics[{{                                    vpAvgPlot[0,0]},
     {Dashing[ {0.02,0.02}],          RGBColor[0,0,1],vpAvgPlot[.5,0]},
     {Dashing[ {0.005,0.02,0.03,0.02}],RGBColor[1,0,0],vpAvgPlot[1,0]}
              }],Axes->True]
Show[Graphics[{Dv0ReRIv0ReTAvgFluxPlot[0,0],{Dashing[{0.02,0.02}],RGBColor[0,0,1],
  Dv0ReRIv0ReTAvgFluxPlot[0,TW]}]},Axes->True]
Show[Graphics[{Dv0ReZIu0ReTAvgFluxPlot[0,0],{Dashing[{0.02,0.02}],RGBColor[0,0,1],
  Dv0ReZIu0ReTAvgFluxPlot[0,TW]}]},Axes->True]
*)
```

-Graphics-

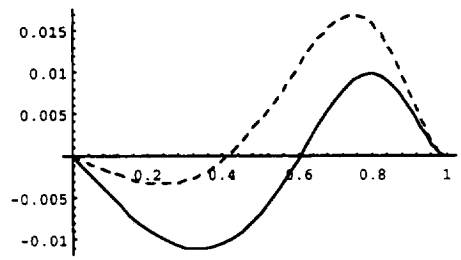

-Graphics-

```
(* Fields *)

If[kindSystem==OPT,Print[fileNameOPTHXfrList];Print[fileNameOPTHXfr],,Print[fileNameBPTHXfrList];
  Print[fileNameBPTHXfr]];
Timing[particleVelField[1,meanSteady,0] =PlotVectorField[{Re[upAvg[r,z,0]], Re[vpAvg[r,z,0]] },{z,0,1},
  {r,0,1},AspectRatio->1/3,DisplayFunction->Identity]];
Timing[particleVelField[1,meanSteady,TW]=PlotVectorField[{upAvg[r,z,TW],vpAvg[r,z,TW]},{z,0,1},{r,0,1},
  AspectRatio->1/3,DisplayFunction->Identity]];
 Show[{particleVelField[1,meanSteady,0], liner[{0,1},{1,1}],texter},DisplayFunction->$DisplayFunction]
 Show[{particleVelField[1,meanSteady,TW],liner[{0,1},{1,1}],texter},DisplayFunction->$DisplayFunction]


{{OPT, eps, Va, Pr, VaPr, UL, PHIU, M, LAMBDA, IsoPressRatio, AdiPressRatio, CLAdiPRatio}, {Fo, {PHIT, TW}, VaPrFo},

  {totalDragAmp0, totalDragRMS/tube, HOscFlow0Star}, date}
                                                  -6          -9
{{{OPT, 0.002, 100., 0.703, 70.266, 1., -0.1, 3.789 10  , 4.31 10  }, {1.002, 1.004, 1.00413}},
  {100., {-0.03918, 0.319915}, 7026.6},

  {0.00476915 Amp dyne, 0.199157 (tube^-1) dyne, 1.97349 W}, {OPT<>100., 3, 15, 19}}


(* T2 Solution *)

(* Calculations *)

ulAvg[r_,z_,0] =rho0ulAvg[r,z,0]/ rho0[z]//Expand;
ulAvg[r_,z_,TW]=rho0ulAvg[r,z,TW]/rho0[z]//Expand;

DulAvgZ[r_,z_,0] =D[ulAvg[r,z,0],z];
DulAvgZ[r_,z_,TW]=D[ulAvg[r,z,TW],z];
```

```
(*********************************)

twoTimesplu0AvgTemplate   = plhatTemplate * u0hatCCTemplate //ComplexExpand;
twoTimesplu0ReAvgTemplate = twoTimesplu0AvgTemplate - I Coefficient[twoTimesplu0AvgTemplate,I];
twoTimesplu0ReAvgFluxHold[r_,z_,sigmaV_,sigmaPV_,Uo_,Ul_,phiU_,phiT_,Tw_]=twoTimesplu0ReAvgTemplate/.
  Union[plAssign,u0Assign];

plu0ReAvgFlux[r_,z_,sigmaV_,sigmaPV_,Uo_,Ul_,phiU_,phiT_,Tw_]:= 1/2 *
  twoTimesplu0ReAvgFluxHold[r,z,sigmaV,sigmaPV,Uo,Ul,phiU,phiT,Tw]//ReleaseHold//ReleaseHold//
    ReleaseHold//N
plu0ReAvgFlux[r_,z_,V,PV,U0,UL,PHIU,PHIT,0] =plu0ReAvgFlux[r,z,V,PV,U0,UL,PHIU,PHIT,0]//Expand;
plu0ReAvgFlux[r_,z_,V,PV,U0,UL,PHIU,PHIT,TW]=plu0ReAvgFlux[r,z,V,PV,U0,UL,PHIU,PHIT,TW]//Expand;

Dplu0ReAvgFluxZ[r_,z_,0] =D[plu0ReAvgFlux[r,z,V,PV,U0,UL,PHIU,PHIT,0], z];
Dplu0ReAvgFluxZ[r_,z_,TW]=D[plu0ReAvgFlux[r,z,V,PV,U0,UL,PHIU,PHIT,TW],z];

w1[r_,z_,0] =Integrate[1/r * Integrate[r*(DulAvgZ[r,z,0] +Dplu0ReAvgFluxZ[r,z,0]),r ],r];
w1[r_,z_,TW]=Integrate[1/r * Integrate[r*(DulAvgZ[r,z,TW]+Dplu0ReAvgFluxZ[r,z,TW]),r],r];

(*********************************)

v1Avg[r_,z_,0] =rho0v1Avg[r,z,0]/ rho0[z]//Expand;
v1Avg[r_,z_,TW]=rho0v1Avg[r,z,TW]/rho0[z]//Expand;

twoTimesplv0AvgTemplate   = plhatTemplate * v0hatCCTemplate //ComplexExpand;
twoTimesplv0ReAvgTemplate = twoTimesplv0AvgTemplate - I Coefficient[twoTimesplv0AvgTemplate,I];
twoTimesplv0ReAvgFluxHold[r_,z_,sigmaV_,sigmaPV_,Uo_,Ul_,phiU_,phiT_,Tw_]=twoTimesplv0ReAvgTemplate/.
  Union[plAssign,v0Assign];

plv0ReAvgFlux[r_,z_,sigmaV_,sigmaPV_,Uo_,Ul_,phiU_,phiT_,Tw_]:= 1/2 *
  twoTimesplv0ReAvgFluxHold[r,z,sigmaV,sigmaPV,Uo,Ul,phiU,phiT,Tw]//ReleaseHold//ReleaseHold//ReleaseHold//N
plv0ReAvgFlux[r_,z_,V,PV,U0,UL,PHIU,PHIT,0] =plv0ReAvgFlux[r,z,V,PV,U0,UL,PHIU,PHIT,0]//Expand;
plv0ReAvgFlux[r_,z_,V,PV,U0,UL,PHIU,PHIT,TW]=plv0ReAvgFlux[r,z,V,PV,U0,UL,PHIU,PHIT,TW]//Expand;

w2[r_,z_,0] =Integrate[v1Avg[r,z,0]  + plv0ReAvgFlux[r,z,V,PV,U0,UL,PHIU,PHIT,0], r]//Expand;
w2[r_,z_,TW]=Integrate[v1Avg[r,z,TW] + plv0ReAvgFlux[r,z,V,PV,U0,UL,PHIU,PHIT,TW],r]//Expand;

(*********************************)

T2[r_,z_,0]  = (PV)^2 (w1[r,z,0] -w1[1,z,0] +w2[r,z,0] -w2[1,z,0])  -
  CAPGAMMA^2 D[T0[z],{z,2}] 1/4 (1-r^2)//Expand;
T2[r_,z_,TW] = (PV)^2 (w1[r,z,TW]-w1[1,z,TW]+w2[r,z,TW]-w2[1,z,TW]) -
  CAPGAMMA^2 D[T0[z],{z,2}] 1/4 (1-r^2)//Expand;

(* plots *)

If[kindSystem==OPT,Print[fileNameOPTHXfrList];Print[fileNameOPTHXfr],,Print[fileNameBPTHXfrList];
  Print[fileNameBPTHXfr]];
T2Iso=Plot[{T2[r,0.0,0],T2[r,.25,0],
      T2[r,.50,0],T2[r,.75,0],
      T2[r,1.0,0]},{r,0,1},
      PlotStyle->{{RGBColor[0,0,.6]},{RGBColor[0,0,.9]},{RGBColor[0,0,.8]},{RGBColor[0,0,.7]},{RGBColor[0,0,1]}},
      PlotRange->All,DisplayFunction->Identity];
T2TW=Plot[{T2[r,0.0,TW],T2[r,.25,TW],
      T2[r,.50,TW],T2[r,.75,TW],
      T2[r,1.0,TW]},{r,0,1},
      PlotStyle->{{RGBColor[.6,0,0]},{RGBColor[.9,0,0]},{RGBColor[.8,0,0]},{RGBColor[.7,0,0]},{RGBColor[1,0,0]}},
      PlotRange->All,DisplayFunction->Identity];
Show[{T2Iso,T2TW},DisplayFunction->$DisplayFunction,AxesLabel->{"z",""}]


-Graphics-

ARCHIVE

ARCHIVE

{{Thesis, OPT, eps, V, P, PV, UL, PHIU, M, IsoPressRatio, AdiVolPR, CLAdiPRatio}, {F, {PHIT, TW}}, {HFlow0}, {1995, 12, 13, 13, 2, 59}}
{{Thesis, OPT, 0.1, 22.5122, 0.83825, 18.871, 0.3, -0.5, 0.0006315, 1.299, 1.546, 1.55319}, {0.000372373, {-0.253, 0.881585}}, {500.081 W}}
```

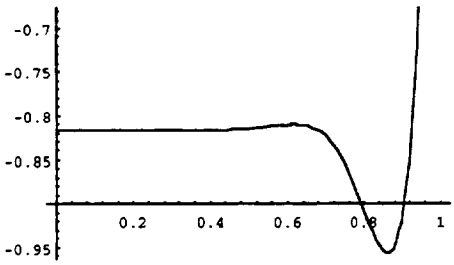

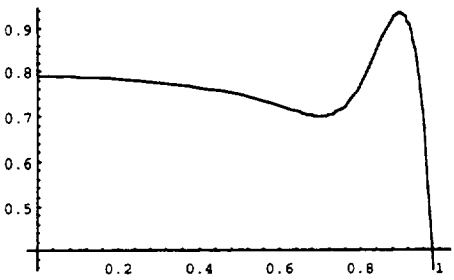

APPENDIX H
EXPERIMENTAL DATA

The data presented are for Runs 1, 2, 5, and 6 discussed in section 5. The columns are generally self-explanatory. The first two columns list the frequency and phase angle. The raw data give position and calculate axial particle velocity, which is then converted into dimensionless velocity. The system parameters ε and U_0 are then listed. The calculated axial particle velocity corresponding to the measured position is in the next column. The final four shaded columns are used in the plots of section 5. The first shaded column lists the single-point velocity, the second column lists the 3-point running average of the single point velocity, and the third column lists the 5-point running average. The last column lists the corresponding calculated axial velocity.

			Experiment raw data			L=	40.39			Calc. Dimensionless Coordinates				System parameters		Velocities from Model				
	1/sec	1/sec	(cm)	(cm)	(cm)	(cm)	(cm)	(sec)	(cm/s)	[]	[]	[]	[]		(cm/s)	[]	[]	(cm/s)	[]	[]
Case	f@z=0	f@z=1	r0	z0	rF	zF	delta z	delta t	upAvgExp	r0	z0	rF	zF	eps	U0	upO(r,z)	upF(r,z)	AvgupCalc	ExpRun3	ExpRun5
BPT																				
BPT 'cs.2.2 23.1/2-Feb-94									0.0000											
17.09.03-17.22.26	0	5	0.000	27.174	0.000	27.210	0.036	0.2	0.1605	0.0000	0.6728	0.0000	0.6737	0.0435	54.66	0.1009	0.1006	0.2396		
			0.000	27.210	0.000	27.246	0.036	0.2	0.1800	0.0000	0.6737	0.0000	0.6746	0.0435	54.66	0.1006	0.1004	0.2390	0.0758	
			0.000	27.246	0.000	27.282	0.036	0.2	0.1800	0.0000	0.6746	0.0000	0.6755	0.0435	54.66	0.1004	0.1001	0.2383	0.0750	0.0888
			0.000	27.282	0.000	27.317	0.035	0.2	0.1750	0.0000	0.6755	0.0000	0.6763	0.0435	54.66	0.1001	0.0998	0.2377	0.0974	0.0887
			0.000	27.317	0.000	27.385	0.068	0.2	0.3400	0.0000	0.6763	0.0000	0.6780	0.0435	54.66	0.0998	0.0993	0.2368	0.0974	0.0980
			0.000	27.385	0.000	27.421	0.036	0.2	0.1800	0.0000	0.6780	0.0000	0.6789	0.0435	54.66	0.0993	0.0990	0.2358	0.1136	0.0980
			0.000	27.421	0.000	27.479	0.058	0.2	0.2900	0.0000	0.6789	0.0000	0.6803	0.0435	54.66	0.0990	0.0986	0.2350	0.0911	0.0984
			0.000	27.479	0.000	27.515	0.036	0.2	0.1800	0.0000	0.6803	0.0000	0.6812	0.0435	54.66	0.0986	0.0983	0.2341	0.0911	0.1039
			0.000	27.515	0.000	27.551	0.036	0.2	0.1800	0.0000	0.6812	0.0000	0.6821	0.0435	54.66	0.0983	0.0980	0.2335	0.1072	0.1072
			0.000	27.551	0.000	27.632	0.081	0.2	0.4050	0.0000	0.6821	0.0000	0.6841	0.0435	54.66	0.0980	0.0974	0.2324	0.1129	0.1018
			0.000	27.632	0.000	27.676	0.044	0.2	0.2200	0.0000	0.6841	0.0000	0.6852	0.0435	54.66	0.0974	0.0971	0.2313	0.1192	0.1131
			0.000	27.676	0.000	27.721	0.045	0.2	0.2250	0.0000	0.6852	0.0000	0.6863	0.0435	54.66	0.0971	0.0966	0.2304	0.1065	0.1093
			0.000	27.721	0.000	27.784	0.063	0.2	0.3150	0.0000	0.6863	0.0000	0.6879	0.0435	54.66	0.0968	0.0963	0.2295	0.0946	0.1093
			0.000	27.784	0.000	27.811	0.027	0.2	0.1350	0.0000	0.6879	0.0000	0.6886	0.0435	54.66	0.0963	0.0960	0.2286	0.1199	0.1060
			0.000	27.811	0.000	27.892	0.081	0.2	0.4050	0.0000	0.6886	0.0000	0.6906	0.0435	54.66	0.0960	0.0954	0.2276	0.1009	0.0980
			0.000	27.892	0.000	27.928	0.036	0.2	0.1800	0.0000	0.6906	0.0000	0.6915	0.0435	54.66	0.0954	0.0951	0.2266	0.1002	0.0980
			0.000	27.928	0.000	27.954	0.026	0.2	0.1300	0.0000	0.6915	0.0000	0.6921	0.0435	54.66	0.0951	0.0950	0.2260	0.0876	0.1169
			0.000	27.954	0.000	28.017	0.063	0.2	0.3150	0.0000	0.6921	0.0000	0.6937	0.0435	54.66	0.0950	0.0945	0.2252	0.1129	0.1018
			0.000	28.017	0.000	28.089	0.072	0.2	0.3600	0.0000	0.6937	0.0000	0.6954	0.0435	54.66	0.0945	0.0939	0.2240	0.1262	0.0942
			0.000	28.089	0.000	28.134	0.045	0.2	0.2250	0.0000	0.6954	0.0000	0.6966	0.0435	54.66	0.0939	0.0936	0.2229	0.0946	0.1245
			0.000	28.134	0.000	28.152	0.018	0.2	0.0900	0.0000	0.6966	0.0000	0.6970	0.0435	54.66	0.0936	0.0935	0.2223	0.1129	0.1056
			0.000	28.152	0.000	28.250	0.098	0.2	0.4900	0.0000	0.6970	0.0000	0.6994	0.0435	54.66	0.0935	0.0927	0.2213	0.0939	0.1056
			0.000	28.250	0.000	28.268	0.018	0.2	0.0900	0.0000	0.6994	0.0000	0.6999	0.0435	54.66	0.0927	0.0926	0.2203	0.1318	0.1207
			0.000	28.268	0.000	28.340	0.072	0.2	0.3600	0.0000	0.6999	0.0000	0.7017	0.0435	54.66	0.0926	0.0920	0.2194	0.1199	0.1451
			0.000	28.340	0.000	28.421	0.081	0.2	0.4050	0.0000	0.7017	0.0000	0.7037	0.0435	54.66	0.0920	0.0914	0.2180	0.1605	0.1136
			0.000	28.421	0.000	28.497	0.076	0.2	0.3800	0.0000	0.7037	0.0000	0.7055	0.0435	54.66	0.0914	0.0908	0.2166	0.1262	0.1548
			0.000	28.497	0.000	28.520	0.023	0.2	0.1150	0.0000	0.7055	0.0000	0.7061	0.0435	54.66	0.0908	0.0906	0.2157	0.1507	0.1396
			0.000	28.520	0.000	28.636	0.116	0.2	0.5800	0.0000	0.7061	0.0000	0.7090	0.0435	54.66	0.0906	0.0897	0.2145	0.1227	0.1434
			0.000	28.636	0.000	28.672	0.036	0.2	0.1800	0.0000	0.7090	0.0000	0.7099	0.0435	54.66	0.0897	0.0895	0.2131	0.1696	0.1228
			0.000	28.672	0.000	28.762	0.090	0.2	0.4500	0.0000	0.7099	0.0000	0.7121	0.0435	54.66	0.0895	0.0888	0.2119	0.1072	0.1321
			0.000	28.762	0.000	28.789	0.027	0.2	0.1350	0.0000	0.7121	0.0000	0.7128	0.0435	54.66	0.0888	0.0886	0.2109	0.1136	0.0984
			0.000	28.789	0.000	28.834	0.045	0.2	0.2250	0.0000	0.7128	0.0000	0.7139	0.0435	54.66	0.0886	0.0882	0.2102	0.0757	0.1018
			0.000	28.834	0.000	28.870	0.036	0.2	0.1800	0.0000	0.7139	0.0000	0.7148	0.0435	54.66	0.0882	0.0880	0.2095	0.0876	0.0564
			0.000	28.870	0.000	28.914	0.044	0.2	0.2200	0.0000	0.7148	0.0000	0.7159	0.0435	54.66	0.0880	0.0878	0.2087	0.0435	0.0509
			0.000	28.914	0.000	28.896	-0.018	0.2	-0.0900	0.0000	0.7159	0.0000	0.7154	0.0435	54.66	0.0878	0.0878	0.2085	0.0280	0.0244
			0.000	28.896	0.000	28.924	0.028	0.4	0.0700	0.0000	0.7154	0.0000	0.7161	0.0435	54.66	0.0878	0.0876	0.2084	-0.0154	-0.0059
			0.000	28.924	0.000	28.906	-0.018	0.2	-0.0900	0.0000	0.7161	0.0000	0.7157	0.0435	54.66	0.0876	0.0877	0.2083	-0.0260	-0.0093
			0.000	28.906	0.000	28.870	-0.036	0.2	-0.1800	0.0000	0.7157	0.0000	0.7148	0.0435	54.66	0.0877	0.0880	0.2088	-0.0126	0.0076
			0.000	28.870	0.000	28.906	0.036	0.2	0.1800	0.0000	0.7148	0.0000	0.7157	0.0435	54.66	0.0880	0.0877	0.2088	0.0154	0.0093
			0.000	28.906	0.000	28.928	0.022	0.2	0.1100	0.0000	0.7157	0.0000	0.7162	0.0435	54.66	0.0877	0.0875	0.2083	0.0533	0.0341
			0.000	28.928	0.000	28.946	0.018	0.2	0.0900	0.0000	0.7162	0.0000	0.7167	0.0435	54.66	0.0875	0.0874	0.2079	0.0568	0.0604
			0.000	28.946	0.000	28.987	0.041	0.2	0.2050	0.0000	0.7167	0.0000	0.7177	0.0435	54.66	0.0874	0.0871	0.2074	0.0599	
			0.000	28.987	0.000	29.040	0.053	0.4	0.1325	0.0000	0.7177	0.0000	0.7190	0.0435	54.66	0.0871	0.0867	0.2065		
														0.0435						

			Experiment raw data			L=	40.39			Calc. Dimensionless Coordinates				System parameters		Velocities from Model			Calc parameters		
	1/sec	1/sec	(cm)	(cm)	(cm)	(cm)	(cm)	(sec)	(cm/s)	[]	[]	[]	[]		(cm/s)	[]	[]	(cm/s)	[]	[]	[]
Case	f@z=0	f@z=1	r0	z0	rF	zF	delta z	delta t	upAvgExp	r0	z0	rF	zF	eps	U0	upO(r,z)	upF(r,z)	AvgupCalc	ExpRun3	ExpRun5	AvgExp
13.51.19-14.26.17	0	15							0.0000	bouancy-				0.0435							
BPT			0.130	27.574	0.130	27.253	-0.321	0.2	-1.6068	0.1170	0.6827	0.1170	0.6747	0.0435	167	-0.0568	-0.0583	-0.4181			
Flow at near center			0.130	27.253	0.130	26.988	-0.265	0.2	-1.3256	0.1170	0.6747	0.1170	0.6682	0.0435	167	-0.0583	-0.0595	-0.4279	-0.1843		
			0.130	26.988	0.130	26.771	-0.217	0.2	-1.0846	0.1170	0.6682	0.1170	0.6628	0.0435	167	-0.0595	-0.0604	-0.4355	-0.1438	-0.1504	
			0.130	26.771	0.130	26.626	-0.145	0.2	-0.7231	0.1170	0.6628	0.1170	0.6592	0.0435	167	-0.0604	-0.0611	-0.4413	-0.1161	-0.1239	
			0.130	26.626	0.130	26.482	-0.145	0.2	-0.7231	0.1170	0.6592	0.1170	0.6558	0.0435	167	-0.0611	-0.0617	-0.4460	-0.0958	-0.1029	
			0.130	26.482	0.130	26.353	-0.129	0.2	-0.6427	0.1170	0.6558	0.1170	0.6525	0.0435	167	-0.0617	-0.0624	-0.4508	-0.0885	-0.0896	
			0.130	26.353	0.130	26.241	-0.112	0.2	-0.5624	0.1170	0.6525	0.1170	0.6497	0.0435	167	-0.0624	-0.0627	-0.4544	-0.0829	-0.0852	
			0.130	26.241	0.130	26.120	-0.121	0.2	-0.6026	0.1170	0.6497	0.1170	0.6467	0.0435	167	-0.0627	-0.0633	-0.4576	-0.0793	-0.0708	
			0.130	26.120	0.130	26.008	-0.112	0.2	-0.5624	0.1170	0.6467	0.1170	0.6439	0.0435	167	-0.0633	-0.0638	-0.4616	-0.0627	-0.0675	
			0.130	26.008	0.130	25.967	-0.040	0.2	-0.2009	0.1170	0.6439	0.1170	0.6429	0.0435	167	-0.0638	-0.0640	-0.4642	-0.0590	-0.0641	
			0.130	25.967	0.130	25.863	-0.104	0.2	-0.5222	0.1170	0.6429	0.1170	0.6403	0.0435	167	-0.0640	-0.0645	-0.4668	-0.0535	-0.0597	
			0.130	25.863	0.130	25.775	-0.088	0.2	-0.4419	0.1170	0.6403	0.1170	0.6381	0.0435	167	-0.0645	-0.0649	-0.4701	-0.0645	-0.0564	
			0.130	25.775	0.130	25.686	-0.088	0.2	-0.4419	0.1170	0.6381	0.1170	0.6360	0.0435	167	-0.0649	-0.0652	-0.4725	-0.0608		
			0.130	25.686	0.130	25.598	-0.088	0.2	-0.4419	0.1170	0.6360	0.1170	0.6338	0.0435	167	-0.0652	-0.0656	-0.4751			

			Experiment raw data			L=	40.39			Calc. Dimensionless Coordinates				System parameters		Velocities from Model				
	1/sec	1/sec	(cm)	(cm)	(cm)	(cm)	(cm)	(sec)	(cm/s)	[]	[]	[]	[]		(cm/s)	[]	[]	(cm/s)	[]	[]
Case	f@z=0	f@z=f	r0	z0	rF	zF	delta z	delta t	upAvgExp	r0	z0	rF	zF	eps	U0	upO(r,z)	upF(r,z)	AvgupCalc	ExpRun3	ExpRun5
OPT																				
29.12.17-29.36.28**																				
flow at CL SkewTop	10		-0.050						0.0000	bouancy-		0.0840	0.4648							
14.21-14.24	10		-0.050	18.775	-0.050	18.402	-0.373	0.1	-3.7340	-0.0450	0.4648	-0.0450	0.4556	0.0435	111.3	-0.6016	-0.6019	-2.9146		
14.24-14.27	-0.254		-0.050	18.402	-0.006	17.979	-0.423	0.1	-4.2270	-0.0450	0.4556	-0.0058	0.4451	0.0435	111.3	-0.6019	-0.5871	-2.8795	-0.7859	
14.27-15.00			-0.006	17.979	-0.040	17.633	-0.346	0.1	-3.4590	-0.0058	0.4451	-0.0355	0.4366	0.0435	111.3	-0.5871	-0.5994	-2.8734	-0.7896	-0.7640
15.00-15.03			-0.040	17.633	-0.023	17.254	-0.379	0.1	-3.7880	-0.0355	0.4366	-0.0209	0.4272	0.0435	111.3	-0.5994	-0.5940	-2.8901	-0.7254	-0.7617
15.03-15.06			-0.023	17.254	-0.050	16.925	-0.329	0.1	-3.2940	-0.0209	0.4272	-0.0450	0.4190	0.0435	111.3	-0.5940	-0.6031	-2.8991	-0.7406	-0.7255
15.06-15.09			-0.050	16.925	-0.013	16.557	-0.368	0.1	-3.6790	-0.0450	0.4190	-0.0112	0.4099	0.0435	111.3	-0.6031	-0.5900	-2.8895	-0.7104	-0.7118
15.09-15.12			-0.013	16.557	-0.050	16.222	-0.335	0.1	-3.3490	-0.0112	0.4099	-0.0450	0.4016	0.0435	111.3	-0.5900	-0.6037	-2.8909	-0.6990	-0.7096
15.12-15.15			-0.050	16.222	-0.029	15.909	-0.313	0.1	-3.1290	-0.0450	0.4016	-0.0264	0.3939	0.0435	111.3	-0.6037	-0.5969	-2.9077	-0.7028	-0.6960
15.15-15.18			-0.029	15.909	-0.013	15.536	-0.373	0.1	-3.7340	-0.0264	0.3939	-0.0115	0.3846	0.0435	111.3	-0.5969	-0.5905	-2.8756	-0.6763	-0.6801
15.18-15.21			-0.013	15.536	-0.006	15.239	-0.296	0.1	-2.9640	-0.0115	0.3846	-0.0055	0.3773	0.0435	111.3	-0.5905	-0.5875	-2.8527	-0.6877	-0.6597
15.21-15.24			-0.006	15.239	0.016	14.910	-0.330	0.1	-3.2950	-0.0055	0.3773	0.0141	0.3691	0.0435	111.3	-0.5875	-0.5765	-2.8190	-0.6272	-0.6484
15.24-15.27			0.016	14.910	0.005	14.624	-0.285	0.1	-2.8540	0.0141	0.3691	0.0041	0.3621	0.0435	111.3	-0.5765	-0.5824	-2.8067	-0.6197	-0.6257
15.27-16.00			0.005	14.624	-0.001	14.339	-0.285	0.1	-2.8550	0.0041	0.3621	-0.0009	0.3550	0.0435	111.3	-0.5824	-0.5852	-2.8276	-0.6121	-0.5703
16.00-16.03			-0.001	14.339	-0.012	14.020	-0.319	0.1	-3.1850	-0.0009	0.3550	-0.0110	0.3471	0.0435	111.3	-0.5852	-0.5906	-2.8476	-0.5274	-0.5735
16.03-16.06			-0.012	14.020	-0.029	13.858	-0.162	0.1	-1.6230	-0.0110	0.3471	-0.0259	0.3431	0.0435	111.3	-0.5906	-0.5979	-2.8783	-0.5630	-0.5305
16.06-16.09			-0.029	13.858	0.009	13.521	-0.337	0.1	-3.3730	-0.0259	0.3431	0.0085	0.3348	0.0435	111.3	-0.5979	-0.5798	-2.8521	-0.4685	-0.4489
16.09-16.12			0.009	13.521	0.004	13.340	-0.181	0.1	-1.8120	0.0085	0.3348	0.0034	0.3303	0.0435	111.3	-0.5798	-0.5828	-2.8156	-0.4173	-0.3718
16.12-16.15			0.004	13.340	0.059	13.252	-0.088	0.1	-0.8780	0.0034	0.3303	0.0527	0.3281	0.0435	111.3	-0.5828	-0.5482	-2.7392	-0.2758	-0.3478
16.15-16.18			0.059	13.252	0.086	13.120	-0.132	0.1	-1.3180	0.0527	0.3281	0.0774	0.3248	0.0435	111.3	-0.5482	-0.5266	-2.6031	-0.2229	-0.2607
16.18-16.21			0.086	13.120	0.175	13.016	-0.104	0.1	-1.0430	0.0774	0.3248	0.1576	0.3222	0.0435	111.3	-0.5266	-0.4369	-2.3336	-0.2494	-0.2924
16.21-16.24			0.175	13.016	0.208	12.889	-0.126	0.1	-1.2630	0.1576	0.3222	0.1871	0.3191	0.0435	111.3	-0.4369	-0.3961	-2.0175	-0.3363	
16.24-16.27			0.208	12.889	0.186	12.631	-0.258	0.1	-2.5800	0.1871	0.3191	0.1672	0.3127	0.0435	111.3	-0.3961	-0.4224	-1.9823		
flow at BottomSide			0.050						0.0000			0.3210	0.4790							
14.21-14.24	10		0.500	19.346	0.544	19.280	-0.066	0.1	-0.6590	0.4499	0.4790	0.4898	0.4773	0.0435	111.3	-0.2300	-0.1563	-0.9353		
14.24-14.27	10		0.544	19.280	0.512	19.181	-0.099	0.1	-0.9880	0.4898	0.4773	0.4603	0.4749	0.0435	111.3	-0.1563	-0.2099	-0.8867	-0.2305	
14.27-15.00	-0.254		0.512	19.181	0.534	19.011	-0.170	0.1	-1.7020	0.4603	0.4749	0.4802	0.4707	0.0435	111.3	-0.2099	-0.1717	-0.9241	-0.3325	-0.3242
15.00-15.03			0.534	19.011	0.490	18.797	-0.214	0.1	-2.1420	0.4802	0.4707	0.4408	0.4654	0.0435	111.3	-0.1717	-0.2409	-0.9991	-0.4270	-0.4103
15.03-15.06			0.490	18.797	0.496	18.561	-0.236	0.1	-2.3600	0.4408	0.4654	0.4459	0.4595	0.0435	111.3	-0.2409	-0.2297	-1.1397	-0.4987	-0.4376
15.06-15.09			0.496	18.561	0.496	18.286	-0.275	0.1	-2.7450	0.4459	0.4595	0.4460	0.4527	0.0435	111.3	-0.2297	-0.2270	-1.1082	-0.4647	-0.3741
15.09-15.12			0.496	18.286	0.496	18.122	-0.165	0.1	-1.6480	0.4460	0.4527	0.4462	0.4487	0.0435	111.3	-0.2270	-0.2252	-1.0952	-0.3136	-0.3786
15.12-15.15			0.496	18.122	0.495	18.105	-0.016	0.1	-0.1640	0.4462	0.4487	0.4451	0.4483	0.0435	111.3	-0.2252	-0.2270	-1.0952	-0.2796	-0.3355
15.15-15.18			0.495	18.105	0.496	17.880	-0.225	0.1	-2.2510	0.4451	0.4483	0.4463	0.4427	0.0435	111.3	-0.2270	-0.2228	-1.0893	-0.2569	-0.3061
15.18-15.21			0.496	17.880	0.495	17.748	-0.132	0.1	-1.3180	0.4463	0.4427	0.4452	0.4394	0.0435	111.3	-0.2228	-0.2235	-1.0809	-0.3854	-0.3083
15.21-15.24			0.495	17.748	0.489	17.545	-0.203	0.1	-2.0310	0.4452	0.4394	0.4404	0.4344	0.0435	111.3	-0.2235	-0.2302	-1.0988	-0.3476	-0.3423
15.24-15.27			0.489	17.545	0.484	17.375	-0.170	0.1	-1.7020	0.4404	0.4344	0.4355	0.4302	0.0435	111.3	-0.2302	-0.2373	-1.1322	-0.3250	-0.2679
15.27-16.00			0.484	17.375	0.490	17.276	-0.099	0.1	-0.9890	0.4355	0.4302	0.4407	0.4277	0.0435	111.3	-0.2373	-0.2272	-1.1250	-0.2494	-0.2857
16.00-16.03			0.490	17.276	0.484	17.183	-0.093	0.1	-0.9330	0.4407	0.4277	0.4358	0.4254	0.0435	111.3	-0.2272	-0.2350	-1.1195	-0.2192	-0.2426
16.03-16.06			0.484	17.183	0.495	17.056	-0.126	0.1	-1.2630	0.4358	0.4254	0.4454	0.4223	0.0435	111.3	-0.2350	-0.2166	-1.0944	-0.2191	-0.2312
16.06-16.09			0.495	17.056	0.490	16.958	-0.099	0.1	-0.9880	0.4454	0.4223	0.4410	0.4198	0.0435	111.3	-0.2166	-0.2238	-1.0671	-0.2531	-0.2471
16.09-16.12			0.490	16.958	0.490	16.815	-0.143	0.1	-1.4270	0.4410	0.4198	0.4412	0.4163	0.0435	111.3	-0.2238	-0.2221	-1.0800	-0.2607	-0.2652
16.12-16.15			0.490	16.815	0.485	16.678	-0.137	0.1	-1.3730	0.4412	0.4163	0.4364	0.4129	0.0435	111.3	-0.2221	-0.2295	-1.0937	-0.2871	-0.2652
16.15-16.18			0.485	16.678	0.485	16.540	-0.137	0.1	-1.3720	0.4364	0.4129	0.4364	0.4095	0.0435	111.3	-0.2295	-0.2282	-1.1084	-0.2758	-0.2611
16.18-16.21			0.485	16.540	0.495	16.414	-0.126	0.1	-1.2630	0.4364	0.4095	0.4452	0.4064	0.0435	111.3	-0.2282	-0.2113	-1.0644	-0.2758	-0.2584
16.21-16.24			0.495	16.414	0.495	16.277	-0.137	0.1	-1.3730	0.4452	0.4064	0.4454	0.4030	0.0435	111.3	-0.2113	-0.2097	-1.0195	-0.2418	-0.2743
16.24-16.27			0.495	16.277	0.479	16.189	-0.088	0.1	-0.8780	0.4454	0.4030	0.4306	0.4006	0.0435	111.3	-0.2097	-0.2354	-1.0779	-0.2758	-0.2584
16.27-17.00			0.479	16.189	0.484	16.013	-0.176	0.1	-1.7570	0.4306	0.4006	0.4357	0.3965	0.0435	111.3	-0.2354	-0.2248	-1.1144	-0.2493	-0.2607

			Experiment raw data			L=	40.39			Calc. Dimensionless Coordinates				System parameters		Velocities from Model				
	1/sec	1/sec	(cm)	(cm)	(cm)	(cm)	(cm)	(sec)	(cm/s)	[]	[]	[]	[]		(cm/s)	[]	[]	(cm/s)	[]	[]
Case	f@z=0	f@z=f	r0	z0	rF	zF	delta z	delta t	upAvgExp	r0	z0	rF	zF	eps	U0	upO(r,z)	upF(r,z)	AvgupCalc	ExpRun3	ExpRun5
17.00-17.03			0.484	16.013	0.484	15.915	-0.099	0.1	-0.9880	0.4357	0.3965	0.4358	0.3940	0.0435	111.3	-0.2248	-0.2237	-1.0861	-0.2796	-0.2539
17.03-17.06			0.484	15.915	0.490	15.783	-0.132	0.1	-1.3180	0.4358	0.3940	0.4409	0.3908	0.0435	111.3	-0.2237	-0.2133	-1.0584	-0.2418	-0.2698
17.06-17.09			0.490	15.783	0.485	15.662	-0.121	0.1	-1.2080	0.4409	0.3908	0.4361	0.3878	0.0435	111.3	-0.2133	-0.2209	-1.0516	-0.2608	-0.2539
17.09-17.12			0.485	15.662	0.479	15.536	-0.126	0.1	-1.2630	0.4361	0.3878	0.4313	0.3846	0.0435	111.3	-0.2209	-0.2284	-1.0881	-0.2845	-0.2517
17.12-17.15			0.479	15.536	0.474	15.398	-0.137	0.1	-1.3720	0.4313	0.3846	0.4265	0.3812	0.0435	111.3	-0.2284	-0.2357	-1.1239	-0.2456	-0.2449
17.15-17.18			0.474	15.398	0.484	15.305	-0.093	0.1	-0.9340	0.4265	0.3812	0.4353	0.3789	0.0435	111.3	-0.2357	-0.2191	-1.1015	-0.2360	-0.2873
18.18-17.21			0.484	15.305	0.484	15.190	-0.115	0.1	-1.1530	0.4353	0.3789	0.4353	0.3761	0.0435	111.3	-0.2191	-0.2181	-1.0589	-0.2976	-0.2720
17.21-17.24			0.484	15.190	0.484	14.966	-0.224	0.1	-2.2370	0.4353	0.3761	0.4353	0.3705	0.0435	111.3	-0.2181	-0.2161	-1.0516	-0.2947	-0.2653
17.24-17.27			0.484	14.966	0.484	14.877	-0.089	0.1	-0.8920	0.4353	0.3705	0.4353	0.3683	0.0435	111.3	-0.2161	-0.2153	-1.0448	-0.2985	-0.2562
17.27-18.00			0.484	14.877	0.484	14.756	-0.121	0.1	-1.2080	0.4353	0.3683	0.4353	0.3653	0.0435	111.3	-0.2153	-0.2142	-1.0402	-0.1937	-0.3037
18.00-18.03			0.484	14.756	0.462	14.685	-0.071	0.1	-0.7140	0.4353	0.3653	0.4156	0.3636	0.0435	111.3	-0.2142	-0.2489	-1.1215	-0.2909	-0.2363
18.03-18.06			0.462	14.685	0.478	14.454	-0.231	0.1	-2.3050	0.4156	0.3636	0.4303	0.3579	0.0435	111.3	-0.2489	-0.2206	-1.1371	-0.2493	-0.2358
18.06-18.09			0.478	14.454	0.478	14.394	-0.060	0.1	-0.6040	0.4303	0.3579	0.4303	0.3564	0.0435	111.3	-0.2206	-0.2201	-1.0674	-0.2607	-0.2244
18.09-18.12			0.478	14.394	0.489	14.306	-0.088	0.1	-0.8790	0.4303	0.3564	0.4402	0.3542	0.0435	111.3	-0.2201	-0.2012	-1.0203	-0.1663	-0.2607
18.12-18.15			0.489	14.306	0.489	14.213	-0.093	0.1	-0.9330	0.4402	0.3542	0.4402	0.3519	0.0435	111.3	-0.2012	-0.2004	-0.9725	-0.2343	-0.2245
18.15-18.18			0.489	14.213	0.500	14.053	-0.159	0.1	-1.5920	0.4402	0.3519	0.4501	0.3479	0.0435	111.3	-0.2004	-0.1805	-0.9223	-0.2720	-0.2494
18.18-18.21			0.500	14.053	0.495	13.911	-0.143	0.1	-1.4280	0.4501	0.3479	0.4452	0.3444	0.0435	111.3	-0.1805	-0.1883	-0.8931	-0.2910	-0.2356
18.21-18.24			0.495	13.911	0.522	13.790	-0.121	0.1	-1.2080	0.4452	0.3444	0.4699	0.3414	0.0435	111.3	-0.1883	-0.1403	-0.7958	-0.2189	-0.1610
18.24-18.27			0.522	13.790	0.506	13.735	-0.055	0.1	-0.5450	0.4699	0.3414	0.4551	0.3401	0.0435	111.3	-0.1403	-0.1681	-0.7468	-0.0604	-0.1270
18.27-19.00			0.506	13.735	0.528	13.823	0.087	0.1	0.8750	0.4551	0.3401	0.4749	0.3422	0.0435	111.3	-0.1681	-0.1310	-0.7242	-0.0302	-0.1065
19.00-19.03			0.528	13.823	0.517	13.746	-0.077	0.1	-0.7690	0.4749	0.3422	0.4650	0.3403	0.0435	111.3	-0.1310	-0.1493	-0.6787	-0.0569	-0.0635
19.03-19.06			0.517	13.746	0.517	13.653	-0.093	0.1	-0.9330	0.4650	0.3403	0.4650	0.3380	0.0435	111.3	-0.1493	-0.1484	-0.7209	-0.1285	-0.0387
19.06-19.09			0.517	13.653	0.539	13.636	-0.017	0.1	-0.1650	0.4650	0.3380	0.4847	0.3376	0.0435	111.3	-0.1484	-0.1101	-0.6259	-0.0718	-0.0567
19.09-19.12			0.539	13.636	0.572	13.642	0.005	0.1	0.0550	0.4847	0.3376	0.5144	0.3377	0.0435	111.3	-0.1101	-0.0516	-0.3915	0.0226	-0.0476
19.12-19.15			0.572	13.642	0.594	13.685	0.044	0.1	0.4390	0.5144	0.3377	0.5341	0.3388	0.0435	111.3	-0.0516	-0.0129	-0.1563	-0.0038	0.0725
19.15-19.18			0.594	13.685	0.594	13.631	-0.055	0.1	-0.5490	0.5341	0.3388	0.5341	0.3375	0.0435	111.3	-0.0129	-0.0124	-0.0614	0.1285	0.1587
19.18-19.21			0.594	13.631	0.714	13.828	0.198	0.1	1.9770	0.5341	0.3375	0.6428	0.3424	0.0435	111.3	-0.0124	0.1886	0.4267	0.2305	0.2244
19.21-19.24			0.714	13.828	0.775	14.020	0.192	0.1	1.9210	0.6428	0.3424	0.6971	0.3471	0.0435	111.3	0.1886	0.2657	1.1002	0.3816	0.2176
19.24-19.27			0.775	14.020	0.835	14.185	0.165	0.1	1.6470	0.6971	0.3471	0.7515	0.3512	0.0435	111.3	0.2657	0.3141	1.4041	0.2645	0.3537
19.27-20.00			0.835	14.185	0.835	14.213	0.027	0.1	0.2750	0.7515	0.3512	0.7517	0.3519	0.0435	111.3	0.3141	0.3143	1.5218	0.3212	0.2633
20.00-20.03			0.835	14.213	0.846	14.487	0.275	0.1	2.7450	0.7517	0.3519	0.7614	0.3587	0.0435	111.3	0.3143	0.3195	1.5348	0.2267	0.3378
20.03-20.06			0.846	14.487	0.863	14.514	0.027	0.1	0.2740	0.7614	0.3587	0.7762	0.3594	0.0435	111.3	0.3195	0.3245	1.5595	0.4307	0.2630
20.06-20.09			0.863	14.514	0.852	14.838	0.324	0.1	3.2400	0.7762	0.3594	0.7663	0.3674	0.0435	111.3	0.3245	0.3224	1.5665	0.2305	0.3854
20.09-20.12			0.852	14.838	0.857	14.822	-0.016	0.1	-0.1650	0.7663	0.3674	0.7713	0.3670	0.0435	111.3	0.3224	0.3241	1.5657	0.4345	0.3196
20.12-20.15			0.857	14.822	0.863	15.146	0.324	0.1	3.2390	0.7713	0.3670	0.7762	0.3750	0.0435	111.3	0.3241	0.3267	1.5761	0.2909	0.4103
20.15-20.18			0.863	15.146	0.852	15.261	0.115	0.1	1.1530	0.7762	0.3750	0.7663	0.3778	0.0435	111.3	0.3267	0.3234	1.5745	0.4722	0.4103
20.18-20.21			0.852	15.261	0.835	15.508	0.247	0.1	2.4690	0.7663	0.3778	0.7515	0.3840	0.0435	111.3	0.3234	0.3156	1.5476	0.4722	0.3967
20.21-20.24			0.835	15.508	0.824	15.832	0.324	0.1	3.2400	0.7515	0.3840	0.7416	0.3920	0.0435	111.3	0.3156	0.3083	1.5108	0.3590	0.2653
20.24-20.27			0.824	15.832	0.835	15.783	-0.049	0.1	-0.4930	0.7416	0.3920	0.7514	0.3908	0.0435	111.3	0.3083	0.3158	1.5114	0.1928	0.2562
20.27-21.00			0.835	15.783	0.852	15.788	0.006	0.1	0.0550	0.7514	0.3908	0.7663	0.3909	0.0435	111.3	0.3158	0.3248	1.5514	0.0341	0.2188
21.00-21.03			0.852	15.788	0.841	15.882	0.093	0.1	0.9330	0.7663	0.3909	0.7568	0.3932	0.0435	111.3	0.3248	0.3196	1.5606	0.1756	0.1111
21.06-21.09			0.841	15.882	0.841	16.038	0.156	0.1	1.5630	0.7568	0.3932	0.7568	0.3971	0.0435	111.3	0.3196	0.3199	1.5486	0.2153	0.1723
21.09-21.12			0.841	16.038	0.857	16.101	0.063	0.1	0.6330	0.7568	0.3971	0.7713	0.3986	0.0435	111.3	0.3199	0.3280	1.5690	0.2192	0.2108
21.12-21.15			0.857	16.101	0.852	16.200	0.099	0.1	0.9890	0.7713	0.3986	0.7663	0.4011	0.0435	111.3	0.3280	0.3258	1.5835	0.1798	0.2176
21.15-21.18 Follow centroid brightn			0.852	16.200	0.852	16.299	0.099	0.1	0.9880	0.7663	0.4011	0.7663	0.4035	0.0435	111.3	0.3258	0.3261	1.5788	0.2116	0.2030
20.18-20.21			0.852	16.299	0.846	16.409	0.110	0.1	1.0980	0.7663	0.4035	0.7614	0.4063	0.0435	111.3	0.3261	0.3235	1.5731	0.2268	0.2290
20.21-20.24			0.846	16.409	0.852	16.530	0.121	0.1	1.2093	0.7614	0.4063	0.7664	0.4092	0.0435	111.3	0.3235	0.3267	1.5747	0.2455	0.2153
20.24-20.27			0.852	16.530	0.852	16.656	0.126	0.1	1.2607	0.7664	0.4092	0.7666	0.4124	0.0435	111.3	0.3267	0.3272	1.5836	0.2153	0.2448
20.27-21.00			0.852	16.656	0.852	16.722	0.066	0.1	0.6590	0.7666	0.4124	0.7663	0.4140	0.0435	111.3	0.3272	0.3272	1.5847	0.2492	0.2267
21.00-21.03			0.852	16.722	0.852	16.892	0.170	0.1	1.7020	0.7663	0.4140	0.7664	0.4182	0.0435	111.3	0.3272	0.3277	1.5859	0.2078	0.2062

			Experiment raw data			L=	40.39			Calc. Dimensionless Coordinates				System parameters		Velocities from Model				
	t/sec	t/sec	(cm)	(cm)	(cm)	(cm)	(cm)	(sec)	(cm/s)	[]	[]	[]	[]		(cm/s)	[]	[]	(cm/s)	[]	[]
Case	t@z=0	t@z=1	r0	z0	rF	zF	delta z	delta t	upAvgExp	r0	z0	rF	zF	eps	U0	upO(r,z)	upF(r,z)	AvgupCalc	ExpRun3	ExpRun5
21.03-21.06			0.852	16.892	0.852	16.958	0.066	0.1	0.6590	0.7664	0.4182	0.7664	0.4198	0.0435	111.3	0.3277	0.3278	1.5875	0.2116	0.1700
21.06-21.09			0.852	16.958	0.846	17.029	0.071	0.1	0.7140	0.7664	0.4198	0.7614	0.4216	0.0435	111.3	0.3278	0.3248	1.5805	0.1209	0.1927
21.09-21.12			0.846	17.029	0.852	17.067	0.038	0.1	0.3840	0.7614	0.4216	0.7664	0.4226	0.0435	111.3	0.3248	0.3261	1.5812	0.1587	0.1700
21.12-21.15			0.852	17.067	0.852	17.188	0.121	0.1	1.2080	0.7664	0.4226	0.7666	0.4256	0.0435	111.3	0.3261	0.3286	1.5903	0.1689	0.1564
21.15-21.18			0.852	17.188	0.852	17.304	0.115	0.1	1.1530	0.7666	0.4256	0.7667	0.4284	0.0435	111.3	0.3286	0.3289	1.5922	0.1851	0.1202
21.18-21.21			0.852	17.304	0.852	17.336	0.033	0.1	0.3290	0.7667	0.4284	0.7669	0.4292	0.0435	111.3	0.3289	0.3291	1.5936	0.0907	0.1655
21.21-21.24			0.852	17.336	0.852	17.320	-0.016	0.1	-0.1640	0.7669	0.4292	0.7663	0.4288	0.0435	111.3	0.3291	0.3287	1.5931	0.1133	0.1632
21.24-21.27			0.852	17.320	0.852	17.468	0.148	0.1	1.4820	0.7663	0.4288	0.7664	0.4325	0.0435	111.3	0.3287	0.3291	1.5931	0.1701	0.0725
21.27-22.00			0.852	17.468	0.852	17.584	0.115	0.1	1.1530	0.7664	0.4325	0.7666	0.4353	0.0435	111.3	0.3291	0.3296	1.5952	0.1096	0.1655
22.00-22.03			0.852	17.584	0.852	17.479	-0.104	0.1	-1.0430	0.7666	0.4353	0.7667	0.4328	0.0435	111.3	0.3296	0.3294	1.5958	0.1851	0.2267
22.03-22.06			0.852	17.479	0.852	17.737	0.258	0.1	2.5800	0.7667	0.4328	0.7667	0.4391	0.0435	111.3	0.3294	0.3300	1.5969	0.1965	0.1814
22.06-22.09			0.852	17.737	0.852	17.869	0.132	0.1	1.3180	0.7667	0.4391	0.7670	0.4424	0.0435	111.3	0.3300	0.3306	1.5999	0.2947	0.1451
22.09-22.12			0.852	17.869	0.852	17.907	0.038	0.1	0.3840	0.7670	0.4424	0.7667	0.4434	0.0435	111.3	0.3306	0.3305	1.6009	0.1361	0.2582
22.12-22.15			0.852	17.907	0.863	17.935	0.027	0.1	0.2750	0.7667	0.4434	0.7763	0.4440	0.0435	111.3	0.3305	0.3365	1.6154	0.1587	0.1746
22.15-22.18			0.863	17.935	0.857	18.100	0.165	0.1	1.6470	0.7763	0.4440	0.7716	0.4481	0.0435	111.3	0.3365	0.3343	1.6246	0.1738	0.2290
22.18-22.21			0.857	18.100	0.858	18.160	0.060	0.1	0.6040	0.7716	0.4481	0.7717	0.4496	0.0435	111.3	0.3343	0.3345	1.6197	0.3363	0.2607
22.21-22.24			0.858	18.160	0.858	18.424	0.264	0.1	2.6350	0.7717	0.4496	0.7717	0.4561	0.0435	111.3	0.3345	0.3353	1.6223	0.3023	0.2448
22.24-22.27			0.858	18.424	0.857	18.539	0.115	0.1	1.1530	0.7717	0.4561	0.7713	0.4590	0.0435	111.3	0.3353	0.3354	1.6245	0.2531	0.1111
22.27-23.00			0.857	18.539	0.857	18.528	-0.011	0.1	-0.1100	0.7713	0.4590	0.7714	0.4587	0.0435	111.3	0.3354	0.3355	1.6248	-0.0378	
23.00-23.03			0.857	18.528	0.852	18.369	-0.159	0.1	-1.5920	0.7714	0.4587	0.7666	0.4548	0.0435	111.3	0.3355	0.3320	1.6184		
bigAvgOver 0.9 Sec			0.886	18.846	0.886	19.648	0.802	0.9	0.8906	0.7972	0.4666	0.7972	0.4665	0.0435	111.3	0.3209	0.3219	1.5567		
flow at BotSideBL rear sighting			0.050									0.7280	0.4340							
			0.809	17.529	0.797	17.781	0.253	0.1	2.5250	0.7280	0.4340	0.7169	0.4402	0.0435	111.3	0.2938	0.2797	1.3889		
			0.797	17.781	0.808	17.693	-0.088	0.1	-0.8780	0.7169	0.4402	0.7269	0.4361	0.0435	111.3	0.2797	0.2923	1.3853	0.2569	
			0.808	17.693	0.808	17.902	0.209	0.1	2.0860	0.7269	0.4361	0.7271	0.4432	0.0435	111.3	0.2923	0.2923	1.4159	0.0831	0.1723
			0.808	17.902	0.808	17.902	0.000	0.1	0.0000	0.7271	0.4432	0.7272	0.4432	0.0435	111.3	0.2923	0.2925	1.4162	0.1738	0.0907
			0.808	17.902	0.808	17.946	0.044	0.1	0.4400	0.7272	0.4432	0.7274	0.4443	0.0435	111.3	0.2925	0.2926	1.4170	0.0681	0.2040
			0.808	17.946	0.808	18.001	0.055	0.1	0.5490	0.7274	0.4443	0.7275	0.4457	0.0435	111.3	0.2926	0.2927	1.4176	0.1965	0.2449
			0.808	18.001	0.809	18.187	0.187	0.1	1.8660	0.7275	0.4457	0.7276	0.4503	0.0435	111.3	0.2927	0.2926	1.4175	0.3778	
			0.809	18.187	0.809	18.495	0.308	0.1	3.0750	0.7276	0.4503	0.7277	0.4579	0.0435	111.3	0.2926	0.2924	1.4168		
flow at TopSide			-0.050									0.3897	0.3963							
16.18-16.21	10		0.433	16.008	0.433	15.739	-0.269	0.1	-2.6900	0.3897	0.3963	0.3897	0.3897	0.0435	111.3	-0.3034	-0.3014	-1.4646		
16.21-16.24	10		0.433	15.739	0.422	15.574	-0.165	0.1	-1.6470	0.3897	0.3897	0.3798	0.3856	0.0435	111.3	-0.3014	-0.3161	-1.4955	-0.4194	
16.24-16.27	-0.254		0.422	15.574	0.427	15.398	-0.176	0.1	-1.7570	0.3798	0.3856	0.3845	0.3812	0.0435	111.3	-0.3161	-0.3072	-1.5097	-0.3212	-0.3718
16.27-17.00			0.427	15.398	0.427	15.272	-0.126	0.1	-1.2630	0.3845	0.3812	0.3844	0.3781	0.0435	111.3	-0.3072	-0.3065	-1.4862	-0.3212	-0.3582
17.00-17.03			0.427	15.272	0.422	15.107	-0.165	0.1	-1.6470	0.3844	0.3781	0.3794	0.3740	0.0435	111.3	-0.3065	-0.3133	-1.5010	-0.3627	-0.3061
17.03-17.06			0.422	15.107	0.410	14.871	-0.236	0.1	-2.3610	0.3794	0.3740	0.3693	0.3682	0.0435	111.3	-0.3133	-0.3278	-1.5528	-0.3023	-0.2675
17.06-17.09			0.410	14.871	0.421	14.833	-0.038	0.1	-0.3840	0.3693	0.3682	0.3791	0.3672	0.0435	111.3	-0.3278	-0.3118	-1.5491	-0.2456	-0.3582
17.09-17.12			0.421	14.833	0.427	14.751	-0.082	0.1	-0.8240	0.3791	0.3672	0.3839	0.3652	0.0435	111.3	-0.3118	-0.3034	-1.4899	-0.3212	-0.3514
17.12-17.15			0.427	14.751	0.416	14.405	-0.346	0.1	-3.4590	0.3839	0.3652	0.3739	0.3566	0.0435	111.3	-0.3034	-0.3171	-1.5027	-0.3967	-0.3537
17.15-17.18			0.416	14.405	0.433	14.256	-0.148	0.1	-1.4820	0.3739	0.3566	0.3897	0.3530	0.0435	111.3	-0.3171	-0.2900	-1.4704	-0.5063	-0.3718
17.18-17.21			0.433	14.256	0.422	14.015	-0.242	0.1	-2.4160	0.3897	0.3530	0.3799	0.3470	0.0435	111.3	-0.2900	-0.3045	-1.4398	-0.3249	-0.3741
17.21-17.24			0.422	14.015	0.472	13.933	-0.082	0.1	-0.8230	0.3799	0.3470	0.4244	0.3449	0.0435	111.3	-0.3045	-0.2267	-1.2866	-0.2634	-0.1576
17.24-17.27			0.472	13.933	0.466	13.845	-0.088	0.1	-0.8790	0.4244	0.3449	0.4194	0.3428	0.0435	111.3	-0.2267	-0.2350	-1.1182	0.0056	-0.2290
17.27-18.00			0.466	13.845	0.444	14.023	0.178	0.1	1.7840	0.4194	0.3428	0.3996	0.3472	0.0435	111.3	-0.2350	-0.2713	-1.2262	-0.1587	-0.1043
18.00-18.03			0.444	14.023	0.450	13.702	-0.321	0.1	-3.2110	0.3996	0.3472	0.4046	0.3392	0.0435	111.3	-0.2713	-0.2600	-1.2868	-0.0566	-0.1133
18.03-18.06			0.450	13.702	0.488	13.762	0.060	0.1	0.6040	0.4046	0.3392	0.4391	0.3407	0.0435	111.3	-0.2600	-0.1983	-1.1100	-0.2512	-0.0816

			Experiment raw data			L=	40.39			Calc. Dimensionless Coordinates				System parameters		Velocities from Model					
	1/sec	1/sec	(cm)	(cm)	(cm)	(cm)	(cm)	(sec)	(cm/s)	[]	[]	[]	[]		(cm/s)	[]	[]	(cm/s)	[]	[]
Case	f@z=0	f@z=f	r0	z0	rF	zF	delta z	delta t	upAvgExp	r0	z0	rF	zF	eps	U0	upO(r,z)	upF(r,z)	AvgupCalc	ExpRun3	ExpRun5
16.06-16.09			0.488	13.762	0.472	13.658	-0.104	0.1	-1.0430	0.4391	0.3407	0.4244	0.3382	0.0435	111.3	-0.1983	-0.2244	-1.0237	-0.0378	-0.1553
16.09-16.12			0.472	13.658	0.477	13.647	-0.011	0.1	-0.1100	0.4244	0.3382	0.4293	0.3379	0.0435	111.3	-0.2244	-0.2154	-1.0650	-0.0793	-0.0249
16.12-16.15			0.477	13.647	0.483	13.647	0.000	0.1	0.0000	0.4293	0.3379	0.4343	0.3379	0.0435	111.3	-0.2154	-0.2062	-1.0208	-0.0114	-0.0816
16.15-16.18			0.483	13.647	0.477	13.642	-0.005	0.1	-0.0550	0.4343	0.3379	0.4293	0.3377	0.0435	111.3	-0.2062	-0.2153	-1.0207	-0.0567	-0.0544
16.18-16.21			0.477	13.642	0.466	13.565	-0.077	0.1	-0.7690	0.4293	0.3377	0.4194	0.3358	0.0435	111.3	-0.2153	-0.2326	-1.0847	-0.0831	-0.1315
16.21-16.24			0.466	13.565	0.461	13.526	-0.038	0.1	-0.3840	0.4194	0.3358	0.4145	0.3349	0.0435	111.3	-0.2326	-0.2411	-1.1471	-0.2153	-0.0431
16.24-16.27			0.461	13.526	0.499	13.329	-0.198	0.1	-1.9760	0.4145	0.3349	0.4490	0.3300	0.0435	111.3	-0.2411	-0.1758	-1.0096	-0.0151	0.0725
16.27-19.00			0.499	13.329	0.433	13.543	0.214	0.1	2.1410	0.4490	0.3300	0.3897	0.3353	0.0435	111.3	-0.1758	-0.2845	-1.1148	0.2003	0.1043
19.00-19.03			0.433	13.543	0.521	13.817	0.275	0.1	2.7450	0.3897	0.3353	0.4688	0.3421	0.0435	111.3	-0.2845	-0.1427	-1.0346	0.3363	
19.03-19.06			0.521	13.817	0.603	13.817	0.000	0.1	0.0000	0.4688	0.3421	0.5426	0.3421	0.0435	111.3	-0.1427	0.0025	-0.3394		
flow at TopSide NO Offset			0.000									0.4002	0.4224							
16.00-16.03	10		0.445	17.062	0.445	16.809	-0.252	0.1	-2.5250	0.4002	0.4224	0.4002	0.4162	0.0435	111.3	-0.2945	-0.2925	-1.4217		
16.03-16.06	10		0.445	16.809	0.472	16.617	-0.192	0.1	-1.9220	0.4002	0.4162	0.4249	0.4114	0.0435	111.3	-0.2925	-0.2491	-1.3118		
16.06-16.09	-0.254		0.472	16.617	0.472	16.442	-0.176	0.1	-1.7570	0.4249	0.4114	0.4249	0.4071	0.0435	111.3	-0.2491	-0.2476	-1.2031	-0.4270	
16.09-16.12			0.472	16.442	0.472	16.277	-0.165	0.1	-1.6470	0.4249	0.4071	0.4249	0.4030	0.0435	111.3	-0.2476	-0.2462	-1.1959	-0.3665	-0.3582
16.12-16.15			0.472	16.277	0.472	16.195	-0.082	0.1	-0.8230	0.4249	0.4030	0.4249	0.4010	0.0435	111.3	-0.2462	-0.2455	-1.1908	-0.2909	-0.3310
16.15-16.18			0.472	16.195	0.478	16.008	-0.187	0.1	-1.8670	0.4249	0.4010	0.4299	0.3963	0.0435	111.3	-0.2455	-0.2353	-1.1644	-0.2985	-0.3695
16.18-16.21			0.478	16.008	0.472	15.722	-0.286	0.1	-2.8550	0.4299	0.3963	0.4249	0.3893	0.0435	111.3	-0.2353	-0.2414	-1.1545	-0.3816	-0.3741
16.21-16.24			0.472	15.722	0.456	15.536	-0.187	0.1	-1.8670	0.4249	0.3893	0.4101	0.3846	0.0435	111.3	-0.2414	-0.2655	-1.2276	-1.0504	-0.6846
16.24-16.27			0.456	15.536	0.450	15.404	-0.132	0.1	-1.3170	0.4101	0.3846	0.4051	0.3814	0.0435	111.3	-0.2655	-0.2730	-1.3042	-0.4156	-0.7164
16.27-17.00			0.450	15.404	0.467	15.327	-0.077	0.1	-0.7690	0.4051	0.3814	0.4200	0.3795	0.0435	111.3	-0.2730	-0.2466	-1.2584	-0.2720	-0.3582
17.00-17.03			0.467	15.327	0.456	15.140	-0.187	0.1	-1.8670	0.4200	0.3795	0.4101	0.3749	0.0435	111.3	-0.2466	-0.2623	-1.2324	-0.2720	-0.3219
17.03-17.06			0.456	15.140	0.445	14.943	-0.198	0.1	-1.9760	0.4101	0.3749	0.4002	0.3700	0.0435	111.3	-0.2623	-0.2776	-1.3076	-0.3174	-0.3015
17.06-17.09			0.445	14.943	0.439	14.805	-0.137	0.1	-1.3730	0.4002	0.3700	0.3952	0.3666	0.0435	111.3	-0.2776	-0.2850	-1.3626	-0.3590	-0.2857
17.09-17.12			0.439	14.805	0.456	14.712	-0.093	0.1	-0.9330	0.3952	0.3666	0.4101	0.3643	0.0435	111.3	-0.2850	-0.2587	-1.3168	-0.2947	-0.4126
17.12-17.15			0.456	14.712	0.439	14.328	-0.384	0.1	-3.8430	0.4101	0.3643	0.3952	0.3547	0.0435	111.3	-0.2587	-0.2812	-1.3077	-0.4232	-0.4307
17.15-17.18			0.439	14.328	0.450	14.097	-0.231	0.1	-2.3060	0.3952	0.3547	0.4051	0.3490	0.0435	111.3	-0.2812	-0.2624	-1.3165	-0.4874	-0.4013
17.18-17.21			0.450	14.097	0.461	13.971	-0.126	0.1	-1.2630	0.4051	0.3490	0.4150	0.3459	0.0435	111.3	-0.2624	-0.2439	-1.2261	-0.5101	-0.4284
17.21-17.24			0.461	13.971	0.456	13.768	-0.203	0.1	-2.0310	0.4150	0.3459	0.4101	0.3409	0.0435	111.3	-0.2439	-0.2509	-1.1984	-0.3854	-0.4149
17.24-17.27			0.456	13.768	0.445	13.707	-0.060	0.1	-0.6040	0.4101	0.3409	0.4002	0.3394	0.0435	111.3	-0.2509	-0.2678	-1.2561	-0.2683	-0.2811
17.27-18.00			0.445	13.707	0.439	13.647	-0.060	0.1	-0.6040	0.4002	0.3394	0.3952	0.3379	0.0435	111.3	-0.2678	-0.2759	-1.3167	-0.2229	-0.1927
18.00-18.03			0.439	13.647	0.439	13.631	-0.017	0.1	-0.1650	0.3952	0.3379	0.3952	0.3375	0.0435	111.3	-0.2759	-0.2758	-1.3361	-0.0945	-0.1882
18.03-18.06			0.439	13.631	0.439	13.515	-0.115	0.1	-1.1530	0.3952	0.3375	0.3952	0.3346	0.0435	111.3	-0.2758	-0.2749	-1.3336	-0.1323	-0.1133
18.06-18.09			0.439	13.515	0.434	13.493	-0.022	0.1	-0.2190	0.3952	0.3346	0.3903	0.3341	0.0435	111.3	-0.2749	-0.2831	-1.3514	-0.1058	-0.1542
18.09-18.12			0.434	13.493	0.412	13.334	-0.159	0.1	-1.5930	0.3903	0.3341	0.3706	0.3301	0.0435	111.3	-0.2831	-0.3149	-1.4483	-0.2040	-0.2698
18.12-18.15			0.412	13.334	0.406	12.994	-0.340	0.1	-3.4040	0.3706	0.3301	0.3656	0.3217	0.0435	111.3	-0.3149	-0.3207	-1.5393	-0.3590	-0.3038
18.15-18.18			0.406	12.994	0.401	12.895	-0.099	0.1	-0.9880	0.3656	0.3217	0.3607	0.3193	0.0435	111.3	-0.3207	-0.3260	-1.5710	-0.4119	-0.2562
18.18-18.21			0.401	12.895	0.395	12.895	0.000	0.1	0.0000	0.3607	0.3193	0.3557	0.3193	0.0435	111.3	-0.3260	-0.3360	-1.6081	-0.3023	-0.2970
18.21-18.24			0.395	12.895	0.390	12.774	-0.121	0.1	-1.2080	0.3557	0.3193	0.3508	0.3163	0.0435	111.3	-0.3360	-0.3430	-1.6445	-0.1511	-0.2199
18.24-18.27			0.390	12.774	0.395	12.602	0.028	0.1	0.2750	0.3508	0.3163	0.3557	0.3169	0.0435	111.3	-0.3430	-0.3354	-1.6429	-0.0642	
FlowTopSide Stagnant			-0.050									0.3408	0.3183							
18.18-18.21	10		0.379	12.856	0.384	12.834	-0.022	0.1	-0.2200	0.3408	0.3183	0.3456	0.3178	0.0435	111.3	-0.3591	-0.3516	-1.7211		
18.21-18.24	10		0.384	12.834	0.384	12.856	0.022	0.1	0.2200	0.3456	0.3178	0.3455	0.3183	0.0435	111.3	-0.3516	-0.3518	-1.7035	-0.0454	
18.24-18.27	-0.125		0.384	12.856	0.384	12.791	-0.066	0.1	-0.6590	0.3455	0.3183	0.3453	0.3167	0.0435	111.3	-0.3518	-0.3517	-1.7039	-0.0226	-0.0114
18.27-19.00			0.384	12.791	0.395	12.802	0.011	0.1	0.1100	0.3453	0.3167	0.3552	0.3169	0.0435	111.3	-0.3517	-0.3362	-1.6660	-0.0189	0.0204
19.00-19.03			0.395	12.802	0.395	12.829	0.027	0.1	0.2740	0.3552	0.3169	0.3552	0.3176	0.0435	111.3	-0.3362	-0.3364	-1.6288	0.0642	0.0680
19.03-19.06			0.395	12.829	0.406	12.884	0.055	0.1	0.5490	0.3552	0.3176	0.3651	0.3190	0.0435	111.3	-0.3364	-0.3208	-1.5915	0.1511	0.1020
19.06-19.09			0.406	12.884	0.428	13.021	0.137	0.1	1.3730	0.3651	0.3190	0.3849	0.3224	0.0435	111.3	-0.3208	-0.2887	-1.4761	0.1436	0.0998

			Experiment raw data			L=	40.39			Calc. Dimensionless Coordinates				System parameters		Velocities from Model				
	1/sec	1/sec	(cm)	(cm)	(cm)	(cm)	(cm)	(sec)	(cm/s)	[]	[]	[]	[]		(cm/s)	[]	[]	(cm/s)	[]	[]
Case	f@z=0	f@z=L	r0	z0	rF	zF	delta z	delta t	upAvgExp	r0	z0	rF	zF	eps	U0	upO(r,z)	upF(r,z)	AvgupCalc	ExpRun3	ExpRun5
19.09-19.12			0.428	13.021	0.395	13.038	0.016	0.1	0.1650	0.3849	0.3224	0.3552	0.3228	0.0435	111.3	-0.2887	-0.3377	-1.5172	0.1096	-0.0227
19.12-19.15			0.395	13.038	0.384	13.043	0.006	0.1	0.0550	0.3552	0.3228	0.3453	0.3229	0.0435	111.3	-0.3377	-0.3533	-1.6736	-0.1701	-0.0317
19.15-19.18			0.384	13.043	0.384	12.774	-0.269	0.1	-2.6910	0.3453	0.3229	0.3453	0.3163	0.0435	111.3	-0.3533	-0.3516	-1.7072	-0.1587	-0.0612
19.18-19.21			0.384	12.774	0.384	12.807	0.033	0.1	0.3300	0.3453	0.3163	0.3453	0.3171	0.0435	111.3	-0.3516	-0.3518	-1.7037	-0.1171	-0.1134
19.21-19.24			0.384	12.807	0.384	12.873	0.066	0.1	0.6590	0.3453	0.3171	0.3453	0.3187	0.0435	111.3	-0.3518	-0.3522	-1.7052	-0.0076	-0.2063
19.24-19.27			0.384	12.873	0.351	12.763	-0.110	0.1	-1.0990	0.3453	0.3187	0.3157	0.3160	0.0435	111.3	-0.3522	-0.3959	-1.8118	-0.1814	-0.1791
19.27-20.00			0.351	12.763	0.345	12.543	-0.220	0.1	-2.1960	0.3157	0.3160	0.3106	0.3106	0.0435	111.3	-0.3959	-0.4020	-1.9324	-0.3865	-0.1791
20.00-20.03			0.345	12.543	0.356	12.340	-0.203	0.1	-2.0310	0.3106	0.3106	0.3206	0.3055	0.0435	111.3	-0.4020	-0.3865	-1.9097	-0.2663	
20.03-20.06			0.356	12.340	0.351	12.373	0.033	0.1	0.3290	0.3206	0.3055	0.3157	0.3063	0.0435	111.3	-0.3865	-0.3938	-1.8899		
OPT																				
44.11.05 Bouancy																				
29.12.17-29.36.28**																				
flow at BotSide			0.050						0.0000	bouancy-		0.4769	0.4773							
29.14.24-29.15.24	10		0.530	19.280	0.530	17.500	-1.780	1	-1.7800	0.4769	0.4773	0.4769	0.4333	0.0435	111.3	-0.2600	-0.2440	-1.2201		
29.15.24-29.16.24	10		0.530	17.500	0.530	16.270	-1.230	1	-1.2300	0.4769	0.4333	0.4769	0.4028	0.0435	111.3	-0.2440	-0.2340	-1.1571	-0.2947	
29.16.24-29.17.24	-0.254		0.530	16.270	0.540	15.000	-1.270	1	-1.2700	0.4769	0.4028	0.4859	0.3714	0.0435	111.3	-0.2340	-0.2060	-1.0651	-0.2602	
29.17.24-29.18.24			0.484	15.000	0.550	13.720	-1.280	1	-1.2800	0.4355	0.3714	0.4949	0.3397	0.0435	111.3	-0.2060	-0.1780	-0.9296		
return in BL			0.050						0.0000	bouancy+		0.6749	0.4182							
29.22.00-29.22.03	10		0.750	16.890	0.770	16.970	0.080	0.1	0.8000	0.6749	0.4182	0.6929	0.4202	0.0435	111.3	0.1450	0.1770	0.7795		
29.22.03-29.22.09	10		0.820	16.970	0.820	17.150	0.180	0.2	0.9000	0.7379	0.4202	0.7379	0.4246	0.0435	111.3	0.1770	0.2500	1.0337	0.1859	
29.22.09-29.22.15	-0.254		0.820	17.150	0.820	17.350	0.200	0.2	1.0000	0.7379	0.4246	0.7379	0.4296	0.0435	111.3	0.2500	0.2490	1.2080	0.1962	0.2251
29.22.15-29.22.21			0.820	17.350	0.820	17.540	0.190	0.2	0.9500	0.7379	0.4296	0.7379	0.4343	0.0435	111.3	0.2490	0.2480	1.2031	0.2582	
			0.820	17.540	0.840	17.900	0.360	0.2	1.8000	0.7379	0.4343	0.7559	0.4432	0.0435	111.3	0.2480	0.2730	1.2612		

			Experiment raw data			L=	40.39			Calc. Dimensionless Coordinates				System parameters		Velocities from Model					
	1/sec	1/sec	(cm)	(cm)	(cm)	(cm)	(cm)	(sec)	(cm/s)	[]	[]	[]	[]		(cm/s)	[]	[]	(cm/s)	[]	[]
Case	f@z=0	f@z=1	r0	z0	rF	zF	delta z	delta t	upAvgExp	r0	z0	rF	zF	eps	U0	upO(r,z)	upF(r,z)	AvgupCalc	ExpRun3	ExpRun5
31.03.25-31.26.17																				
flow at BotSide			0.050						0.0000	boyuancy		0.4600	0.4757							
31.05.20-31.05.26	10		0.511	19.214	0.500	18.940	-0.275	0.1	-2.7450	0.4600	0.4757	0.4501	0.4689	0.0435	111.3	-0.1530	-0.1647	-0.7692		
	10		0.500	18.940	0.495	18.841	-0.099	0.1	-0.9880	0.4501	0.4689	0.4452	0.4665	0.0435	111.3	-0.1647	-0.1704	-0.8115	-0.2645	
	-0.125		0.495	18.841	0.495	18.830	-0.011	0.1	-0.1100	0.4452	0.4665	0.4452	0.4662	0.0435	111.3	-0.1704	-0.1704	-0.8255	-0.2003	-0.2698
			0.495	18.830	0.484	18.649	-0.181	0.1	-1.8120	0.4452	0.4662	0.4353	0.4617	0.0435	111.3	-0.1704	-0.1820	-0.8535	-0.1927	-0.1814
			0.484	18.649	0.484	18.561	-0.088	0.1	-0.8780	0.4353	0.4617	0.4355	0.4595	0.0435	111.3	-0.1820	-0.1815	-0.8803	-0.2267	-0.1836
			0.484	18.561	0.484	18.500	-0.060	0.1	-0.6040	0.4355	0.4595	0.4353	0.4580	0.0435	111.3	-0.1815	-0.1816	-0.8794	-0.1738	-0.2312
			0.484	18.500	0.500	18.396	-0.104	0.1	-1.0430	0.4353	0.4580	0.4501	0.4555	0.0435	111.3	-0.1816	-0.1632	-0.8351	-0.2003	-0.1927
			0.500	18.396	0.489	18.270	-0.126	0.1	-1.2630	0.4501	0.4555	0.4402	0.4523	0.0435	111.3	-0.1632	-0.1751	-0.8193	-0.2192	-0.1678
			0.489	18.270	0.489	18.182	-0.088	0.1	-0.8790	0.4402	0.4523	0.4402	0.4502	0.0435	111.3	-0.1751	-0.1749	-0.8475	-0.1663	-0.1904
			0.489	18.182	0.495	18.155	-0.027	0.1	-0.2740	0.4402	0.4502	0.4452	0.4495	0.0435	111.3	-0.1749	-0.1686	-0.8319	-0.1587	-0.1700
			0.495	18.155	0.495	18.039	-0.115	0.1	-1.1530	0.4452	0.4495	0.4452	0.4466	0.0435	111.3	-0.1686	-0.1683	-0.8161	-0.1360	-0.1474
			0.495	18.039	0.500	17.984	-0.055	0.1	-0.5490	0.4452	0.4466	0.4501	0.4453	0.0435	111.3	-0.1683	-0.1621	-0.8003	-0.1663	-0.1496
			0.500	17.984	0.506	17.913	-0.071	0.1	-0.7140	0.4501	0.4453	0.4551	0.4435	0.0435	111.3	-0.1621	-0.1557	-0.7696	-0.1511	-0.1746
			0.506	17.913	0.500	17.820	-0.093	0.1	-0.9330	0.4551	0.4435	0.4501	0.4412	0.0435	111.3	-0.1557	-0.1617	-0.7685	-0.1738	-0.1541
			0.500	17.820	0.506	17.732	-0.088	0.1	-0.8790	0.4501	0.4412	0.4551	0.4390	0.0435	111.3	-0.1617	-0.1552	-0.7674	-0.1700	-0.1496
			0.506	17.732	0.500	17.666	-0.066	0.1	-0.6580	0.4551	0.4390	0.4503	0.4374	0.0435	111.3	-0.1552	-0.1610	-0.7658	-0.1361	-0.1451
			0.500	17.666	0.511	17.622	-0.044	0.1	-0.4400	0.4503	0.4374	0.4600	0.4363	0.0435	111.3	-0.1610	-0.1487	-0.7500	-0.1171	-0.1383
			0.511	17.622	0.517	17.562	-0.060	0.1	-0.6040	0.4600	0.4363	0.4651	0.4348	0.0435	111.3	-0.1487	-0.1420	-0.7039	-0.1247	-0.1224
			0.517	17.562	0.522	17.485	-0.077	0.1	-0.7680	0.4651	0.4348	0.4699	0.4329	0.0435	111.3	-0.1420	-0.1356	-0.6721	-0.1284	-0.1224
			0.522	17.485	0.522	17.435	-0.049	0.1	-0.4940	0.4699	0.4329	0.4699	0.4317	0.0435	111.3	-0.1356	-0.1354	-0.6562	-0.1322	-0.1337
			0.522	17.435	0.528	17.369	-0.066	0.1	-0.6590	0.4699	0.4317	0.4750	0.4300	0.0435	111.3	-0.1354	-0.1286	-0.6393	-0.1285	-0.1473
			0.528	17.369	0.522	17.298	-0.071	0.1	-0.7140	0.4750	0.4300	0.4700	0.4283	0.0435	111.3	-0.1286	-0.1349	-0.6381	-0.1587	-0.1179
			0.522	17.298	0.517	17.205	-0.093	0.1	-0.9330	0.4700	0.4283	0.4650	0.4260	0.0435	111.3	-0.1349	-0.1411	-0.6685	-0.1171	-0.1496
			0.517	17.205	0.528	17.199	-0.006	0.1	-0.0550	0.4650	0.4260	0.4749	0.4258	0.0435	111.3	-0.1411	-0.1282	-0.6523	-0.1549	-0.1337
			0.528	17.199	0.528	17.073	-0.126	0.1	-1.2630	0.4749	0.4258	0.4749	0.4227	0.0435	111.3	-0.1282	-0.1279	-0.6203	-0.1096	-0.1315
			0.528	17.073	0.506	17.046	-0.027	0.1	-0.2740	0.4749	0.4227	0.4551	0.4220	0.0435	111.3	-0.1279	-0.1533	-0.6810	-0.1511	-0.1338
			0.506	17.046	0.522	16.980	-0.066	0.1	-0.6590	0.4551	0.4220	0.4699	0.4204	0.0435	111.3	-0.1533	-0.1342	-0.6962	-0.1323	-0.1542
			0.522	16.980	0.522	16.881	-0.099	0.1	-0.9890	0.4699	0.4204	0.4699	0.4179	0.0435	111.3	-0.1342	-0.1339	-0.6491	-0.1512	-0.1496
			0.522	16.881	0.522	16.826	-0.055	0.1	-0.5490	0.4699	0.4179	0.4700	0.4166	0.0435	111.3	-0.1339	-0.1336	-0.6478	-0.1852	-0.1585
			0.522	16.826	0.517	16.711	-0.115	0.1	-1.1530	0.4700	0.4166	0.4650	0.4137	0.0435	111.3	-0.1336	-0.1398	-0.6620	-0.1473	-0.1451
			0.517	16.711	0.533	16.667	-0.044	0.1	-0.4390	0.4650	0.4137	0.4797	0.4126	0.0435	111.3	-0.1398	-0.1204	-0.6301	-0.1360	-0.1405
			0.533	16.667	0.539	16.628	-0.038	0.1	-0.3840	0.4797	0.4126	0.4849	0.4117	0.0435	111.3	-0.1204	-0.1134	-0.5663	-0.1171	-0.1178
			0.539	16.628	0.533	16.540	-0.088	0.1	-0.8780	0.4849	0.4117	0.4799	0.4095	0.0435	111.3	-0.1134	-0.1198	-0.5648	-0.0869	-0.1133
			0.533	16.540	0.539	16.540	0.000	0.1	0.0000	0.4799	0.4095	0.4847	0.4095	0.0435	111.3	-0.1198	-0.1134	-0.5648	-0.1323	-0.1111
			0.539	16.540	0.539	16.436	-0.104	0.1	-1.0440	0.4847	0.4095	0.4849	0.4089	0.0435	111.3	-0.1134	-0.1129	-0.5480	-0.0983	-0.1133
			0.539	16.436	0.561	16.398	-0.038	0.1	-0.3840	0.4849	0.4089	0.5045	0.4060	0.0435	111.3	-0.1129	-0.0862	-0.4821	-0.1285	-0.0998
			0.561	16.398	0.561	16.354	-0.044	0.1	-0.4390	0.5045	0.4060	0.5046	0.4049	0.0435	111.3	-0.0862	-0.0859	-0.4169	-0.0944	-0.1088
			0.561	16.354	0.561	16.299	-0.055	0.1	-0.5490	0.5046	0.4049	0.5045	0.4035	0.0435	111.3	-0.0859	-0.0859	-0.4162	-0.0831	-0.0876
			0.561	16.299	0.566	16.277	-0.022	0.1	-0.2200	0.5045	0.4035	0.5095	0.4030	0.0435	111.3	-0.0859	-0.0790	-0.3993	-0.0894	-0.0861
			0.566	16.277	0.577	16.224	-0.053	0.1	-0.5300	0.5095	0.4030	0.5193	0.4017	0.0435	111.3	-0.0790	-0.0652	-0.3491	-0.0756	-0.0816
			0.577	16.224	0.577	16.189	-0.035	0.1	-0.3480	0.5193	0.4017	0.5193	0.4008	0.0435	111.3	-0.0652	-0.0651	-0.3156	-0.0831	-0.0862
			0.577	16.189	0.566	16.156	-0.033	0.1	-0.3300	0.5193	0.4008	0.5094	0.4000	0.0435	111.3	-0.0651	-0.0787	-0.3484	-0.0920	-0.0929
			0.566	16.156	0.583	16.090	-0.066	0.1	-0.6590	0.5094	0.4000	0.5243	0.3964	0.0435	111.3	-0.0787	-0.0576	-0.3307	-0.0945	-0.0869
			0.583	16.090	0.572	16.052	-0.038	0.1	-0.3840	0.5243	0.3984	0.5144	0.3974	0.0435	111.3	-0.0576	-0.0715	-0.3132	-0.0982	-0.1088
			0.572	16.052	0.577	16.013	-0.038	0.1	-0.3840	0.5144	0.3974	0.5193	0.3965	0.0435	111.3	-0.0715	-0.0646	-0.3296	-0.1133	-0.1065
			0.577	16.013	0.583	15.925	-0.088	0.1	-0.8790	0.5193	0.3965	0.5243	0.3943	0.0435	111.3	-0.0646	-0.0573	-0.2953	-0.1058	-0.1111
			0.583	15.925	0.583	15.898	-0.027	0.1	-0.2740	0.5243	0.3943	0.5243	0.3936	0.0435	111.3	-0.0573	-0.0573	-0.2775	-0.1323	-0.1406
			0.583	15.898	0.583	15.821	-0.077	0.1	-0.7690	0.5243	0.3936	0.5243	0.3917	0.0435	111.3	-0.0573	-0.0570	-0.2768	-0.1473	-0.1111

			Experiment raw data			L=	40.39			Calc. Dimensionless Coordinates				System parameters		Velocities from Model				
	1/sec	1/sec	(cm)	(cm)	(cm)	(cm)	(cm)	(sec)	(cm/s)	[]	[]	[]	[]		(cm/s)	[]	[]	(cm/s)	[]	[]
Case	f@z=0	f@z=f	r0	z0	rF	zF	delta z	delta t	upAvgExp	r0	z0	rF	zF	eps	U0	upO(r,z)	upF(r,z)	AvgupCalc	ExpRun3	ExpRun5
			0.583	15.821	0.583	15.711	-0.110	0.1	-1.0980	0.5243	0.3917	0.5243	0.3890	0.0435	111.3	-0.0570	-0.0567	-0.2755	-0.1058	-0.1065
			0.583	15.711	0.583	15.744	0.033	0.1	0.3300	0.5243	0.3890	0.5243	0.3898	0.0435	111.3	-0.0567	-0.0568	-0.2749	-0.1058	-0.1270
			0.583	15.744	0.594	15.667	-0.077	0.1	-0.7690	0.5243	0.3898	0.5341	0.3879	0.0435	111.3	-0.0568	-0.0428	-0.2412	-0.0831	-0.0929
			0.594	15.667	0.599	15.591	-0.077	0.1	-0.7690	0.5341	0.3879	0.5390	0.3860	0.0435	111.3	-0.0428	-0.0356	-0.1899	-0.1021	-0.0612
			0.599	15.591	0.599	15.596	0.005	0.1	0.0550	0.5390	0.3860	0.5392	0.3861	0.0435	111.3	-0.0356	-0.0354	-0.1719	-0.0718	-0.1315
			0.599	15.596	0.610	15.563	-0.033	0.1	-0.3290	0.5392	0.3861	0.5489	0.3853	0.0435	111.3	-0.0354	-0.0215	-0.1377	-0.1133	-0.1043
			0.610	15.563	0.610	15.426	-0.137	0.1	-1.3730	0.5489	0.3853	0.5489	0.3819	0.0435	111.3	-0.0215	-0.0211	-0.1031	-0.1247	-0.0793
			0.610	15.426	0.621	15.415	-0.011	0.1	-0.1100	0.5489	0.3819	0.5588	0.3816	0.0435	111.3	-0.0211	-0.0069	-0.0678	-0.1133	-0.1088
			0.621	15.415	0.621	15.398	-0.016	0.1	-0.1640	0.5588	0.3816	0.5589	0.3812	0.0435	111.3	-0.0069	-0.0067	-0.0331	-0.0642	-0.0907
			0.621	15.398	0.648	15.333	-0.066	0.1	-0.6590	0.5589	0.3812	0.5835	0.3796	0.0435	111.3	-0.0067	0.0286	0.0529	-0.0491	-0.0317
			0.648	15.333	0.681	15.344	0.011	0.1	0.1100	0.5835	0.3796	0.6132	0.3799	0.0435	111.3	0.0286	0.0705	0.2400	-0.0340	-0.0135
			0.681	15.344	0.676	15.349	0.005	0.1	0.0550	0.6132	0.3799	0.6082	0.3800	0.0435	111.3	0.0705	0.0635	0.3246	0.0341	0.0023
			0.676	15.349	0.682	15.382	0.033	0.1	0.3300	0.6082	0.3800	0.6133	0.3808	0.0435	111.3	0.0635	0.0706	0.3247	0.0416	0.0272
			0.682	15.382	0.693	15.404	0.022	0.1	0.2190	0.6133	0.3808	0.6232	0.3814	0.0435	111.3	0.0706	0.0842	0.3749	0.0340	0.0317
			0.693	15.404	0.687	15.398	-0.005	0.1	-0.0550	0.6232	0.3814	0.6181	0.3812	0.0435	111.3	0.0842	0.0772	0.3909	0.0264	0.0340
			0.687	15.398	0.692	15.420	0.022	0.1	0.2190	0.6181	0.3812	0.6231	0.3818	0.0435	111.3	0.0772	0.0841	0.3906	0.0189	0.0430
			0.692	15.420	0.681	15.431	0.011	0.1	0.1100	0.6231	0.3818	0.6132	0.3821	0.0435	111.3	0.0841	0.0703	0.3739	0.0604	0.0453
			0.681	15.431	0.709	15.486	0.055	0.1	0.5490	0.6132	0.3821	0.6380	0.3834	0.0435	111.3	0.0703	0.1042	0.4225	0.0643	0.0408
			0.709	15.486	0.742	15.514	0.027	0.1	0.2750	0.6380	0.3834	0.6675	0.3841	0.0435	111.3	0.1042	0.1423	0.5968	0.0454	0.0453
			0.742	15.514	0.704	15.497	-0.016	0.1	-0.1650	0.6675	0.3841	0.6331	0.3837	0.0435	111.3	0.1423	0.0975	0.5807	0.0302	0.0408
			0.704	15.497	0.764	15.530	0.033	0.1	0.3290	0.6331	0.3837	0.6872	0.3845	0.0435	111.3	0.0975	0.1657	0.6376	0.0113	0.0249
			0.764	15.530	0.747	15.530	0.000	0.1	0.0000	0.6872	0.3845	0.6725	0.3845	0.0435	111.3	0.1657	0.1484	0.7607	0.0340	0.0204
			0.747	15.530	0.758	15.547	0.017	0.1	0.1650	0.6725	0.3845	0.6825	0.3849	0.0435	111.3	0.1484	0.1603	0.7475	0.0227	0.0431
			0.758	15.547	0.770	15.563	0.017	0.1	0.1650	0.6825	0.3849	0.6925	0.3853	0.0435	111.3	0.1603	0.1717	0.8039	0.0491	0.0408
			0.770	15.563	0.753	15.602	0.038	0.1	0.3840	0.6925	0.3853	0.6774	0.3863	0.0435	111.3	0.1717	0.1572	0.7964	0.0567	0.1088
			0.753	15.602	0.802	15.629	0.027	0.1	0.2750	0.6774	0.3863	0.7220	0.3870	0.0435	111.3	0.1572	0.2018	0.8693	0.1567	0.0499
			0.802	15.629	0.846	15.794	0.165	0.1	1.6470	0.7220	0.3870	0.7617	0.3910	0.0435	111.3	0.2018	0.2319	1.0504	0.0454	0.0589
			0.846	15.794	0.797	15.667	-0.126	0.1	-1.2630	0.7617	0.3910	0.7173	0.3879	0.0435	111.3	0.2319	0.1974	1.0397	0.0529	0.1043
			0.797	15.667	0.819	15.706	0.038	0.1	0.3840	0.7173	0.3879	0.7366	0.3889	0.0435	111.3	0.1974	0.2144	0.9973	0.0416	0.0861
			0.819	15.706	0.813	15.854	0.148	0.1	1.4830	0.7366	0.3889	0.7319	0.3925	0.0435	111.3	0.2144	0.2105	1.0291	0.1171	0.0068
			0.813	15.854	0.786	15.838	-0.017	0.1	-0.1650	0.7319	0.3925	0.7073	0.3921	0.0435	111.3	0.2105	0.1873	0.9634	0.0718	0.0929
			0.786	15.838	0.760	15.810	-0.027	0.1	-0.2750	0.7073	0.3921	0.7021	0.3914	0.0435	111.3	0.1873	0.1819	0.8941	0.0264	0.0657
			0.760	15.810	0.780	15.893	0.082	0.1	0.8240	0.7021	0.3914	0.7023	0.3935	0.0435	111.3	0.1819	0.1820	0.8809	0.0189	0.0181
			0.780	15.893	0.808	15.865	-0.027	0.1	-0.2750	0.7023	0.3935	0.7271	0.3928	0.0435	111.3	0.1820	0.2063	0.8816	0.0605	0.0680
			0.808	15.865	0.781	15.898	0.033	0.1	0.3300	0.7271	0.3928	0.7025	0.3936	0.0435	111.3	0.2063	0.1822	0.9994	0.0756	0.0499
			0.781	15.898	0.781	16.002	0.104	0.1	1.0430	0.7025	0.3936	0.7026	0.3962	0.0435	111.3	0.1822	0.1822	0.8826	0.0454	0.0884
			0.781	16.002	0.797	15.931	-0.071	0.1	-0.7140	0.7026	0.3962	0.7170	0.3944	0.0435	111.3	0.1822	0.1969	0.8826	0.1436	0.0929
			0.797	15.931	0.803	16.107	0.176	0.1	1.7570	0.7170	0.3944	0.7222	0.3968	0.0435	111.3	0.1969	0.2018	0.9538	0.0604	0.0975
			0.803	16.107	0.808	16.090	-0.017	0.1	-0.1650	0.7222	0.3968	0.7272	0.3984	0.0435	111.3	0.2018	0.2063	0.9773	0.1398	0.0794
			0.808	16.090	0.814	16.134	0.044	0.1	0.4400	0.7272	0.3984	0.7323	0.3995	0.0435	111.3	0.2063	0.2108	0.9995	0.0605	0.1519
			0.814	16.134	0.808	16.195	0.060	0.1	0.6040	0.7323	0.3995	0.7275	0.4010	0.0435	111.3	0.2108	0.2066	1.0210	0.1436	0.0884
			0.808	16.195	0.819	16.299	0.104	0.1	1.0430	0.7275	0.4010	0.7366	0.4035	0.0435	111.3	0.2066	0.2144	1.0006	0.1284	0.1270
			0.819	16.299	0.808	16.321	0.022	0.1	0.2190	0.7366	0.4035	0.7269	0.4041	0.0435	111.3	0.2144	0.2060	1.0384	0.1398	0.1088
			0.808	16.321	0.808	16.398	0.077	0.1	0.7690	0.7269	0.4041	0.7268	0.4060	0.0435	111.3	0.2060	0.2059	0.9978	0.0680	0.0430
			0.808	16.398	0.819	16.398	0.000	0.1	0.0000	0.7268	0.4060	0.7368	0.4060	0.0435	111.3	0.2059	0.2144	0.9972	-0.0152	0.0680
			0.819	16.398	0.808	16.299	-0.099	0.1	-0.9894	0.7368	0.4060	0.7269	0.4035	0.0435	111.3	0.2144	0.2060	1.0383	0.0454	0.1587
			0.808	16.299	0.808	16.464	0.165	0.1	1.6484	0.7269	0.4035	0.7271	0.4076	0.0435	111.3	0.2060	0.2061	0.9978	0.2116	0.0680
			0.808	16.464	0.819	16.705	0.242	0.1	2.4160	0.7271	0.4076	0.7371	0.4136	0.0435	111.3	0.2061	0.2148	1.0193	0.1814	0.0771
			0.819	16.705	0.830	16.562	-0.143	0.1	-1.4280	0.7371	0.4136	0.7471	0.4101	0.0435	111.3	0.2148	0.2226	1.0592	0.0831	0.1905
			0.830	16.562	0.797	16.584	0.022	0.1	0.2200	0.7471	0.4101	0.7174	0.4106	0.0435	111.3	0.2226	0.1969	1.0160	0.0378	0.1496

			Experiment raw data				L=	40.39			Calc. Dimensionless Coordinates				System parameters		Velocities from Model					
	1/sec	1/sec	(cm)	(cm)	(cm)	(cm)	(cm)	(sec)	(cm/s)		[]	[]	[]	[]		(cm/s)	[]	[]	(cm/s)		[]	[]
Case	f@z=0	f@z=1	r0	z0	rF	zF	delta z	delta t	upAvgExp		r0	z0	rF	zF	eps	U0	upO(r,z)	upF(r,z)	AvgupCalc		ExpRun3	ExpRun5
			0.797	16.584	0.797	16.760	0.176	0.1	1.7570		0.7174	0.4106	0.7169	0.4150	0.0435	111.3	0.1969	0.1963	0.9524		0.1813	0.0589
			0.797	16.760	0.808	16.826	0.066	0.1	0.6580		0.7169	0.4150	0.7269	0.4166	0.0435	111.3	0.1963	0.2058	0.9740		0.1813	0.1814
			0.808	16.826	0.797	16.848	0.022	0.1	0.2200		0.7269	0.4166	0.7172	0.4171	0.0435	111.3	0.2058	0.1966	0.9746		0.1662	0.1541
			0.797	16.848	0.830	17.002	0.154	0.1	1.5370		0.7172	0.4171	0.7470	0.4209	0.0435	111.3	0.1966	0.2226	1.0152		0.0907	0.1269
			0.830	17.002	0.819	16.958	-0.044	0.1	-0.4390		0.7470	0.4209	0.7372	0.4198	0.0435	111.3	0.2226	0.2148	1.0594		0.1511	0.1904
			0.819	16.958	0.830	17.067	0.110	0.1	1.0980		0.7372	0.4198	0.7473	0.4226	0.0435	111.3	0.2148	0.2229	1.0600		0.1965	0.3718
			0.830	17.067	0.798	17.287	0.220	0.1	2.1960		0.7473	0.4226	0.7178	0.4280	0.0435	111.3	0.2229	0.1969	1.0166		0.5441	0.1814
			0.798	17.287	0.831	17.748	0.461	0.1	4.6120		0.7178	0.4280	0.7475	0.4394	0.0435	111.3	0.1969	0.2231	1.0173		0.2570	
			0.831	17.748	0.798	17.441	-0.307	0.1	-3.0740		0.7475	0.4394	0.7180	0.4318	0.0435	111.3	0.2231	0.1970	1.0176			
flow at CenterLine			-0.050						0.0000		boyuancy		-0.0252	0.4530								
31.05.20-31.05.26	10		-0.028	18.297	0.027	17.979	-0.318	0.1	-3.1840		-0.0252	0.4530	0.0242	0.4451	0.0435	111.3	-0.4331	-0.4333	-2.0984			
	10		0.027	17.979	0.049	17.693	-0.286	0.1	-2.8550		0.0242	0.4451	0.0439	0.4381	0.0435	111.3	-0.4333	-0.4317	-2.0950		-0.6234	
	-0.125		0.049	17.693	-0.028	17.391	-0.302	0.1	-3.0200		0.0439	0.4381	-0.0252	0.4306	0.0435	111.3	-0.4317	-0.4335	-2.0954		-0.5970	-0.5985
			-0.028	17.391	-0.006	17.111	-0.280	0.1	-2.8000		-0.0252	0.4306	-0.0055	0.4237	0.0435	111.3	-0.4335	-0.4343	-2.1017		-0.5819	-0.5758
			-0.006	17.111	0.016	16.848	-0.264	0.1	-2.6350		-0.0055	0.4237	0.0143	0.4171	0.0435	111.3	-0.4343	-0.4342	-2.1035		-0.5554	-0.5396
			0.016	16.848	-0.001	16.584	-0.264	0.1	-2.6350		0.0143	0.4171	-0.0005	0.4106	0.0435	111.3	-0.4342	-0.4346	-2.1040		-0.4987	-0.5146
			-0.001	16.584	0.010	16.387	-0.198	0.1	-1.9770		-0.0005	0.4106	0.0094	0.4057	0.0435	111.3	-0.4346	-0.4345	-2.1048		-0.4836	-0.4964
			0.010	16.387	0.027	16.145	-0.241	0.1	-2.4150		0.0094	0.4057	0.0242	0.3997	0.0435	111.3	-0.4345	-0.4340	-2.1034		-0.4647	-0.4693
			0.027	16.145	0.021	15.909	-0.236	0.1	-2.3610		0.0242	0.3997	0.0193	0.3939	0.0435	111.3	-0.4340	-0.4344	-2.1030		-0.4647	-0.4625
			0.021	15.909	0.010	15.711	-0.198	0.1	-1.9770		0.0193	0.3939	0.0094	0.3890	0.0435	111.3	-0.4344	-0.4348	-2.1049		-0.4685	-0.4602
			0.010	15.711	0.016	15.464	-0.247	0.1	-2.4700		0.0094	0.3890	0.0143	0.3829	0.0435	111.3	-0.4348	-0.4347	-2.1058		-0.4383	-0.4330
			0.016	15.464	0.016	15.272	-0.192	0.1	-1.9220		0.0143	0.3829	0.0143	0.3781	0.0435	111.3	-0.4347	-0.4348	-2.1059		-0.4232	-0.4035
			0.016	15.272	0.016	15.096	-0.176	0.1	-1.7570		0.0143	0.3781	0.0143	0.3738	0.0435	111.3	-0.4348	-0.4349	-2.1062		-0.3665	-0.3922
			0.016	15.096	-0.001	14.932	-0.165	0.1	-1.6470		0.0143	0.3738	-0.0005	0.3697	0.0435	111.3	-0.4349	-0.4352	-2.1072		-0.3514	-0.3468
			-0.001	14.932	0.021	14.762	-0.170	0.1	-1.7020		-0.0005	0.3697	0.0193	0.3655	0.0435	111.3	-0.4352	-0.4348	-2.1069		-0.3249	-0.3151
			0.021	14.762	-0.001	14.624	-0.137	0.1	-1.3720		0.0193	0.3655	-0.0005	0.3621	0.0435	111.3	-0.4348	-0.4353	-2.1072		-0.2909	-0.2970
			-0.001	14.624	0.016	14.509	-0.115	0.1	-1.1530		-0.0005	0.3621	0.0143	0.3592	0.0435	111.3	-0.4353	-0.4351	-2.1080		-0.2645	-0.2811
			0.016	14.509	0.065	14.377	-0.132	0.1	-1.3180		0.0143	0.3592	0.0588	0.3560	0.0435	111.3	-0.4351	-0.4309	-2.0972		-0.2570	-0.3106
			0.065	14.377	0.093	14.251	-0.126	0.1	-1.2630		0.0588	0.3560	0.0834	0.3528	0.0435	111.3	-0.4309	-0.4262	-2.0757		-0.3439	-0.2539
			0.093	14.251	0.104	14.009	-0.242	0.1	-2.4160		0.0834	0.3528	0.0933	0.3469	0.0435	111.3	-0.4262	-0.4240	-2.0591		-0.2532	-0.3537
			0.104	14.009	0.175	14.009	0.000	0.1	0.0000		0.0933	0.3469	0.1576	0.3469	0.0435	111.3	-0.4240	-0.4022	-2.0009		-0.4118	-0.2679
			0.175	14.009	0.197	13.653	-0.357	0.1	-3.5680		0.1576	0.3469	0.1774	0.3380	0.0435	111.3	-0.4022	-0.3931	-1.9262		-0.2267	
			0.197	13.653	0.230	13.680	0.027	0.1	0.2740		0.1774	0.3380	0.2070	0.3387	0.0435	111.3	-0.3931	-0.3775	-1.8663			
flow at TopSide			-0.050						0.0000		boyuancy		0.4244	0.4650								
31.05.20-31.05.26	10		0.472	18.780	0.472	18.610	-0.170	0.1	-1.7020		0.4244	0.4650	0.4244	0.4608	0.0435	111.3	-0.1953	-0.1949	-0.9448			
	10		0.472	18.610	0.472	18.506	-0.104	0.1	-1.0430		0.4244	0.4608	0.4244	0.4582	0.0435	111.3	-0.1949	-0.1946	-0.9432		-0.2418	
	-0.125		0.472	18.506	0.477	18.429	-0.077	0.1	-0.7690		0.4244	0.4582	0.4293	0.4563	0.0435	111.3	-0.1946	-0.1886	-0.9280		-0.2343	-0.3514
			0.477	18.429	0.472	18.270	-0.159	0.1	-1.5920		0.4293	0.4563	0.4244	0.4523	0.0435	111.3	-0.1886	-0.1940	-0.9266		-0.3967	-0.3831
			0.472	18.270	0.483	17.929	-0.340	0.1	-3.4040		0.4244	0.4523	0.4343	0.4439	0.0435	111.3	-0.1940	-0.1814	-0.9090		-0.5139	-0.3673
			0.483	17.929	0.472	17.682	-0.247	0.1	-2.4710		0.4343	0.4439	0.4244	0.4378	0.0435	111.3	-0.1814	-0.1928	-0.9055		-0.4497	-0.2970
			0.472	17.682	0.477	17.616	-0.066	0.1	-0.6590		0.4244	0.4378	0.4293	0.4362	0.0435	111.3	-0.1928	-0.1866	-0.9182		-0.1511	-0.2449
			0.477	17.616	0.472	17.710	0.093	0.1	0.9340		0.4293	0.4362	0.4244	0.4385	0.0435	111.3	-0.1866	-0.1926	-0.9183		-0.0038	-0.2063
			0.472	17.710	0.510	17.677	-0.033	0.1	-0.3300		0.4244	0.4385	0.4589	0.4377	0.0435	111.3	-0.1926	-0.1502	-0.8303		-0.1284	-0.1655
			0.510	17.677	0.488	17.430	-0.247	0.1	-2.4700		0.4589	0.4377	0.4391	0.4315	0.0435	111.3	-0.1502	-0.1742	-0.7658		-0.2948	-0.1511
			0.488	17.430	0.477	17.282	-0.148	0.1	-1.4830		0.4391	0.4315	0.4293	0.4279	0.0435	111.3	-0.1742	-0.1857	-0.8718		-0.2934	-0.2290
			0.477	17.282	0.483	17.251	-0.031	0.1	-0.3100		0.4293	0.4279	0.4343	0.4271	0.0435	111.3	-0.1857	-0.1796	-0.8848		-0.1889	-0.2633
			0.483	17.251	0.516	17.155	-0.095	0.1	-0.9520		0.4343	0.4271	0.4639	0.4247	0.0435	111.3	-0.1796	-0.1424	-0.7799		-0.2002	-0.1904
			0.516	17.155	0.499	16.991	-0.165	0.1	-1.6470		0.4639	0.4247	0.4490	0.4207	0.0435	111.3	-0.1424	-0.1609	-0.7344		-0.1940	-0.1632

			Experiment raw data			L=	40.39			Calc. Dimensionless Coordinates				System parameters		Velocities from Model				
	1/sec	1/sec	(cm)	(cm)	(cm)	(cm)	(cm)	(sec)	(cm/s)	[]	[]	[]	[]		(cm/s)	[]	[]	(cm/s)	[]	[]
Case	f@z=0	f@z=1	r0	z0	rF	zF	delta z	delta t	upAvgExp	r0	z0	rF	zF	eps	U0	upO(r,z)	upF(r,z)	AvgupCalc	ExpRun3	ExpRun5
			0.499	16.991	0.521	16.969	-0.022	0.1	-0.2200	0.4490	0.4207	0.4688	0.4201	0.0435	111.3	-0.1609	-0.1356	-0.7179	-0.1852	-0.1844
			0.521	16.969	0.516	16.886	-0.082	0.1	-0.8240	0.4688	0.4201	0.4639	0.4161	0.0435	111.3	-0.1356	-0.1417	-0.6714	-0.1285	-0.2018
			0.516	16.886	0.521	16.804	-0.082	0.1	-0.8230	0.4639	0.4161	0.4688	0.4160	0.0435	111.3	-0.1417	-0.1351	-0.6703	-0.2078	-0.1587
			0.521	16.804	0.499	16.667	-0.137	0.1	-1.3730	0.4688	0.4160	0.4490	0.4126	0.0435	111.3	-0.1351	-0.1600	-0.7147	-0.1927	-0.2063
			0.499	16.667	0.499	16.606	-0.060	0.1	-0.6040	0.4490	0.4126	0.4490	0.4111	0.0435	111.3	-0.1600	-0.1598	-0.7746	-0.2305	-0.2516
			0.499	16.606	0.527	16.469	-0.137	0.1	-1.3720	0.4490	0.4111	0.4736	0.4077	0.0435	111.3	-0.1598	-0.1276	-0.6962	-0.2683	-0.2131
			0.527	16.469	0.510	16.277	-0.192	0.1	-1.9220	0.4736	0.4077	0.4589	0.4030	0.0435	111.3	-0.1276	-0.1464	-0.6637	-0.2191	-0.1995
			0.510	16.277	0.532	16.288	0.011	0.1	0.1100	0.4589	0.4030	0.4787	0.4033	0.0435	111.3	-0.1464	-0.1207	-0.6469	-0.1965	-0.2107
			0.532	16.288	0.488	16.184	-0.104	0.1	-1.0430	0.4787	0.4033	0.4391	0.4007	0.0435	111.3	-0.1207	-0.1710	-0.7065	-0.1244	-0.1995
			0.488	16.184	0.532	16.096	-0.088	0.1	-0.8750	0.4391	0.4007	0.4787	0.3985	0.0435	111.3	-0.1710	-0.1201	-0.7052	-0.2078	-0.2131
			0.532	16.096	0.521	15.986	-0.110	0.1	-1.1020	0.4787	0.3985	0.4688	0.3958	0.0435	111.3	-0.1201	-0.1328	-0.6127	-0.2910	-0.2539
			0.521	15.986	0.527	15.761	-0.225	0.1	-2.2510	0.4688	0.3958	0.4738	0.3902	0.0435	111.3	-0.1328	-0.1257	-0.6261	-0.2912	-0.2176
			0.527	15.761	0.532	15.673	-0.088	0.1	-0.8780	0.4738	0.3902	0.4787	0.3880	0.0435	111.3	-0.1257	-0.1190	-0.5924	-0.2267	-0.1815
			0.532	15.673	0.521	15.656	-0.017	0.1	-0.1650	0.4787	0.3880	0.4688	0.3876	0.0435	111.3	-0.1190	-0.1319	-0.6076	-0.0718	-0.1636
			0.521	15.656	0.516	15.656	0.000	0.1	0.0000	0.4688	0.3876	0.4639	0.3876	0.0435	111.3	-0.1319	-0.1383	-0.6545	-0.0907	-0.1473
			0.516	15.656	0.521	15.541	-0.115	0.1	-1.1530	0.4639	0.3876	0.4688	0.3848	0.0435	111.3	-0.1383	-0.1316	-0.6537	-0.1738	-0.1202
			0.521	15.541	0.521	15.404	-0.137	0.1	-1.3720	0.4688	0.3848	0.4688	0.3814	0.0435	111.3	-0.1316	-0.1312	-0.6366	-0.1889	-0.2040
			0.521	15.404	0.532	15.382	-0.022	0.1	-0.2200	0.4688	0.3814	0.4787	0.3808	0.0435	111.3	-0.1312	-0.1181	-0.6040	-0.2607	-0.1927
			0.532	15.382	0.543	15.162	-0.220	0.1	-2.1960	0.4787	0.3808	0.4885	0.3754	0.0435	111.3	-0.1181	-0.1044	-0.5390	-0.1474	-0.1541
			0.543	15.162	0.548	15.190	0.027	0.1	0.2740	0.4885	0.3754	0.4935	0.3761	0.0435	111.3	-0.1044	-0.0977	-0.4896	-0.1473	-0.1066
			0.548	15.190	0.565	15.168	-0.022	0.1	-0.2190	0.4935	0.3761	0.5083	0.3755	0.0435	111.3	-0.0977	-0.0774	-0.4242	-0.0114	-0.1043
			0.565	15.168	0.570	15.146	-0.022	0.1	-0.2200	0.5083	0.3755	0.5133	0.3750	0.0435	111.3	-0.0774	-0.0704	-0.3580	-0.0415	-0.0227
			0.570	15.146	0.570	15.129	-0.016	0.1	-0.1640	0.5133	0.3750	0.5133	0.3746	0.0435	111.3	-0.0704	-0.0704	-0.3410	-0.0416	-0.0408
			0.570	15.129	0.570	15.107	-0.022	0.1	-0.2200	0.5133	0.3746	0.5133	0.3740	0.0435	111.3	-0.0704	-0.0703	-0.3407	-0.0378	-0.0272
			0.570	15.107	0.581	15.091	-0.017	0.1	-0.1650	0.5133	0.3740	0.5232	0.3736	0.0435	111.3	-0.0703	-0.0565	-0.3070	-0.0189	-0.0181
			0.581	15.091	0.581	15.102	0.011	0.1	0.1100	0.5232	0.3736	0.5232	0.3739	0.0435	111.3	-0.0565	-0.0565	-0.2735	-0.0038	-0.0182
			0.581	15.102	0.620	15.102	0.000	0.1	0.0000	0.5232	0.3739	0.5578	0.3739	0.0435	111.3	-0.0565	-0.0075	-0.1549	-0.0038	-0.0045
			0.620	15.102	0.598	15.085	-0.017	0.1	-0.1650	0.5578	0.3739	0.5380	0.3735	0.0435	111.3	-0.0075	-0.0356	-0.1043	-0.0038	0.0000
			0.598	15.085	0.625	15.096	0.011	0.1	0.1100	0.5380	0.3735	0.5627	0.3738	0.0435	111.3	-0.0356	-0.0005	-0.0873	-0.0076	-0.0068
			0.625	15.096	0.631	15.091	-0.006	0.1	-0.0550	0.5627	0.3738	0.5676	0.3736	0.0435	111.3	-0.0005	0.0066	0.0148	0.0000	-0.0068
			0.631	15.091	0.636	15.085	-0.005	0.1	-0.0550	0.5676	0.3736	0.5726	0.3735	0.0435	111.3	0.0066	0.0137	0.0491	-0.0076	0.0023
			0.636	15.085	0.647	15.085	0.000	0.1	0.0000	0.5726	0.3735	0.5825	0.3735	0.0435	111.3	0.0137	0.0278	0.1006	0.0000	-0.0113
			0.647	15.085	0.647	15.091	0.005	0.1	0.0550	0.5825	0.3735	0.5825	0.3736	0.0435	111.3	0.0278	0.0278	0.1348	-0.0113	-0.0023
			0.647	15.091	0.669	15.069	-0.022	0.1	-0.2190	0.5825	0.3736	0.6022	0.3731	0.0435	111.3	0.0278	0.0558	0.2025	0.0000	0.0091
			0.669	15.069	0.686	15.085	0.016	0.1	0.1640	0.6022	0.3731	0.6171	0.3735	0.0435	111.3	0.0558	0.0769	0.3213	0.0114	0.0000
			0.686	15.085	0.724	15.107	0.022	0.1	0.2200	0.6171	0.3735	0.6516	0.3740	0.0435	111.3	0.0769	0.1229	0.4837	0.0113	0.0023
			0.724	15.107	0.724	15.085	-0.022	0.1	-0.2200	0.6516	0.3740	0.6516	0.3735	0.0435	111.3	0.1229	0.1229	0.5951	0.0078	0.0159
			0.724	15.085	0.735	15.096	0.011	0.1	0.1100	0.6516	0.3735	0.6615	0.3738	0.0435	111.3	0.1229	0.1355	0.6257	0.0000	0.0408
			0.735	15.096	0.735	15.107	0.011	0.1	0.1100	0.6615	0.3738	0.6615	0.3740	0.0435	111.3	0.1355	0.1355	0.6562	0.0681	0.0476
			0.735	15.107	0.790	15.184	0.077	0.1	0.7690	0.6615	0.3740	0.7109	0.3759	0.0435	111.3	0.1355	0.1914	0.7917	0.0869	0.0612
			0.790	15.184	0.768	15.223	0.038	0.1	0.3840	0.7109	0.3759	0.6911	0.3769	0.0435	111.3	0.1914	0.1705	0.8766	0.0869	0.0204
			0.768	15.223	0.752	15.234	0.011	0.1	0.1100	0.6911	0.3769	0.6764	0.3772	0.0435	111.3	0.1705	0.1535	0.7847	-0.0265	0.0839
			0.752	15.234	0.708	15.146	-0.088	0.1	-0.8790	0.6764	0.3772	0.6369	0.3750	0.0435	111.3	0.1535	0.1034	0.6222	0.0604	0.0748
			0.708	15.146	0.880	15.311	0.165	0.1	1.6470	0.6369	0.3750	0.7918	0.3791	0.0435	111.3	0.1034	0.2438	0.8408	0.0906	0.0861
			0.880	15.311	0.922	15.365	0.055	0.1	0.5490	0.7918	0.3791	0.8295	0.3804	0.0435	111.3	0.2438	0.2436	1.1802	0.1965	0.1473
			0.922	15.365	0.869	15.431	0.066	0.1	0.6590	0.8295	0.3804	0.7998	0.3821	0.0435	111.3	0.2436	0.2454	1.1843	0.1927	0.1565
			0.869	15.431	0.878	15.591	0.159	0.1	1.5920	0.7998	0.3821	0.7900	0.3860	0.0435	111.3	0.2454	0.2437	1.1846	0.1096	0.0907
			0.878	15.591	0.861	15.525	-0.066	0.1	-0.6580	0.7900	0.3860	0.7752	0.3844	0.0435	111.3	0.2437	0.2385	1.1679	0.0880	0.2222
			0.861	15.525	0.869	15.530	0.005	0.1	0.0540	0.7752	0.3844	0.7998	0.3845	0.0435	111.3	0.2385	0.2456	1.1724	0.2154	
			0.869	15.530	0.867	15.904	0.373	0.1	3.7340	0.7998	0.3845	0.7801	0.3937	0.0435	111.3	0.2456	0.2409	1.1782		

REFERENCES

1. Sherman, F. S.: 1990 *Viscous Flow*, McGraw Hill.
2. Paolucci, S.: 1982 On the filtering of sound from the Navier-Stokes equations, *SAND 82-8257*, Sandia National Labs, Livermore.
3. Grotberg, J. B.: 1984 Volume-cycled oscillatory flow in a tapered channel, *J. Fluid Mech.*, **141**, 249-264.
4. Hall, P.: 1974 Unsteady viscous flow in a pipe of slowly varying cross-section, *J. Fluid Mech.*, **64**, 209-226.
5. Harris, H. G.; and Goren, S. L.: 1967 Axial diffusion in a cylinder with pulsed flow, *Chem. Eng. Sci.*, **22** 1571-1576.
6. Watson, E. J.: 1983 Diffusion in oscillatory pipe flow, *J. Fluid Mech.*, **133**, 233-244.
7. Bowden, K. F.: 1965 Horizontal mixing in the sea due to a shearing current, *J. Fluid Mech.*, **21**, 84-96.
8. Schlichting, H.: 1932 Berechnung ebener periodischer Grenzschichtströmungen, *Physik. Zeitschr.*, **33**, 327-335.
9. Longsworth, R. C.: 1997 Early pulse tube refrigerator developments, *Cryocoolers 9*, Plenum Press, 261-268.
10. Kittel, P.: 1994 A short history of pulse tube refrigerators, http://ranier.oact.hq.nasa.gov/Sensors_page/Cryo/CryoPT/CryoPTHist.html.
11. Radebaugh, R.: 1990 A review of pulse tube refrigeration, *Adv Cryo. Eng.*, Plenum Press, **35B**, 1191-1205.
12. Swift, G. W.: 1988 Thermoacoustic engines, *J. Acoust. Soc. Am.*, **84** (4), 1145-1180.
13. Gifford, W. E.; and Longsworth, R. C.: 1964 Pulse tube refrigeration, *J. Eng. Industry, Transactions of the ASME*, **63**, 264-268.
14. Longsworth, R. C.: 1967 An experimental investigation of pulse tube refrigeration heat pumping rates, *Adv Cryo. Eng.*, Plenum Press, **12**, 608-618.
15. Gifford, W. E.; and Longsworth, R. C.: 1966 Surface Heat Pumping, *Adv Cryo. Eng.*, Plenum Press, **11**, 171-179.
16. de Boer, P. C. T.: 1994 Thermodynamic analysis of the basic pulse-tube refrigerator, *Cryogenics*, **34**, 699-711.
17. Wheatley, J.; Hoffler, J. H.; Swift, G. W.; and Migliori, A.: 1985 Understanding some simple phenomena in thermoacoustics with applications to acoustical heat engines, *Am. J. Phys.*, **53**, 147-162.
18. Olsen, J. R.; and Swift, G. W.: 1994 Similitude in thermoacoustic, *J. Acoust. Soc. Am.*, **95** (3), 1405-1412.

19. Hoffler, T. J.: 1988 Concepts for thermoacoustic refrigeration and a practical device, *Proc. Fifth Intl. Cryocooler Conf.*, 93-101.

20. Rott, N.: 1969 Damped and Thermally Driven Acoustic Oscillations in Wide and Narrow Tubes, *J. Apl. Math & Physics (ZAMP)*, **20**, 230-243.

21. Rott, N.: 1980 Thermoacoustics, *Adv. Appl. Mech.*, **20**, 135-175.

22. Müller, U. A.: 1982 Thermoakustishe Gasschwingungen: Definition und Optimierung eines Wirkungsgrades, *Diss. ETH Nr. 7014*, Eidegenössischen Technischen Hochschule, Zürich.

23. Rott, N.: 1973 Thermally driven acoustic oscillations, Part II: Stability limit for helium, *J. Apl Math & Physics (ZAMP)*, **24**, 54-72.

24. Rott, N.: 1976 Thermally driven acoustic oscillations, Part IV: Tubes with variable cross-section, *J. Apl Math & Physics (ZAMP)*, **27**, 197-224.

25. Rott, N.: 1976 Thermally driven acoustic oscillations, Part V: Gas-liquid oscillations, *J. Apl Math & Physics (ZAMP)*, **27**, 325-334.

26. Rott, N.: 1983 Thermally driven acoustic oscillations, part VI: Excitation and power, *J. Apl Math & Physics (ZAMP)*, **34**, 609-626.

27. Rott, N.: 1974 The heating effect connected with non-linear oscillations in a resonance tube, *J. Apl Math & Physics (ZAMP)*, **25**, 619-634.

28. Rott, N.: 1975 Thermally driven acoustic oscillations, Part III: Second-order heat flux, *J. Apl Math & Physics (ZAMP)*, **26**, 43-49.

29. Rott, N.: 1984 Thermoacoustic heating at the closed end of an oscillating gas column, *J. Fluid Mech.*, **145**, 1-9.

30. Merkli, P.; and Thomann, H.: 1975 Thermoacoustic effects in a resonance tube, *J. Fluid Mech.*, **70** (1), 161-177.

31. Mikulin, E. L.; Tarasov, A. A.; and Shkrebyonock, M. P.: 1984 Low-temperature expansion pulse tubes, *Adv Cryo. Eng.*, Plenum Press, **29**, 629-637.

32. Radebaugh, R.; Zimmerman, J.; Smith, D. R.; and Louie, B.: 1986 A comparison of three types of pulse tube refrigerators: New methods for reaching 60 K, *Adv Cryo. Eng.*, Plenum Press, **31**, 779-789.

33. Matsubara, Y.: 1994 Novel configuration of three-stage pulse tube refrigerator for temperatures below 4 K, *Cryogenics*, **34**, 259-262.

34. Tanida, K.; Gao, J. L.; Yoshimura, N.; and Matsubara, Y.: 1996 Three-staged pulse tube refrigerator controlled by four-valve method, *Adv Cryo. Eng.*, Plenum Press, **41B**, 1503-1509.

35. Storch, P. J.; Radebaugh, R.; and Zimmerman, J. E.: 1990 Analytical model for the refrigeration power of the orifice pulse tube refrigerator, *NIST Tech Note 1343*, National Institute for Standards and Technology, Boulder, CO.

36. David, M.; Mare'chal, J. -C.; Simon, Y.; and Guilpin, C.: 1993 Theory of ideal orifice pulse tube refrigerator, *Cryogenics*, **33** (2), 154-161.

37. Kittel, P.; Kashani, A.; Lee, J. M.; and Roach, P. R.: 1996 General pulse tube theory, *Cryogenics*, **36** (10), 849-857.

38. Lee, K. P.: 1983 A simplistic model of cyclic heat transfer phenomena in closed spaces, *Proc. 18th Intersociety Energy Conversion Eng. Conf.*, 720-723.

39. Kornhauser, A. A.; and Smith, J. L.: 1989 Heat transfer with oscillating pressure and oscillating flow, *Proc. 24th Intersociety Energy Conversion Eng. Conf.*, 2347-2353.

40. Kornhauser, A. A.; and Smith, J. L.: 1994 Application of a complex Nusselt number to heat transfer during compression and expansion, *J. Heat Transfer*, **116**, 536-542.

41. Roach, P.; and Kashani, A.: 1997 A simple modeling program for orifice pulse tube coolers, *Cryocoolers 9*, Plenum Press, 327-334.

42. Jeong, E. S.: 1996 Secondary flow in basic pulse tube refrigerators, *Cryogenics*, **36** (5), 317-323.

43. Lee, J. M.; Kittel, P.; Timmerhaus, K. D.; and Radebaugh, R.: 1995 Steady secondary momentum and enthalpy streaming in the pulse tube refrigerator, *Cryocoolers 8*, Plenum Press, 359-369.

44. Xiao, J. H.: 1995 Thermoacoustic heat transportation and energy transformation, Part 1: formulation of the problem, *Cryogenics* **35** (1), 15-19.

45. Xiao, J. H.: 1995 Thermoacoustic heat transportation and energy transformation, Part 2: isothermal wall thermoacoustic effects, *Cryogenics* **35** (1), 21-26.

46. Xiao, J. H.: 1995 Thermoacoustic heat transportation and energy transformation, Part 3: adiabatic wall thermoacoustic effects, *Cryogenics* **35** (1), 27-29.

47. Bauwens, L.: 1996 Entropy balance and performance characterization of the narrow basic pulse-tube refrigerator, *J. Thermophysics and Heat Transfer,* **10** (4), 663-671.

48. Bauwens, L.: 1996 Oscillating flow of a heat-conducting fluid in a narrow tube, *J. Fluid Mech.,* **342**, 135-161.

49. Shiraishi, M.; Nakamura, N.; Kaquya, S.; and Murakami, M.: 1997 Visualization study of velocity profiles and displacements of working gas inside a pulse tube refrigerator, *Cryocoolers 9*, Plenum Press, 355-364.

50. Nakamura, N.; Shiraishi, M.; Seo, K.; and Murakami, M.: 1997 Visualization study of oscillating flow inside a pulse tube refrigerator, *Cryogenic Engineering Conf.*, Portland, OR, paper APG-1.

51. Hoffman, A.; Wild, S.; and Oellrich, L. R.: 1997 Evaluation of experimental pulse tube refrigerator data with predictions of the thermoacoustic theory, *Proc. 16th International Cryogenic Eng. Conf.*, Kitakyushu, Japan, 239-242.

52. Lee, J. M.; Kittel, P.; Timmerhaus, K. D.; and Radebaugh, R.: 1993 Flow patterns intrinsic to the pulse tube refrigerator, *Proceedings of the 7th International Cryocooler Conf.*, PL-CP-93-1001, Santa Fe, 125-139.

53. Zhu, S.; Wu, P.; and Chen, Z.: 1990 Double inlet pulse tube refrigerators: an important improvement, *Cryogenics* **30** (5), 514-520.

54. Lewis, M.; and Radebaugh, R.: 1997 Effect of regenerator geometry on pulse tube refrigerator performance, *Cryogenic Engineering Conf.*, Portland, OR, paper DPG-9.

55. Seo, K.; Shiraishi, M.; Nakamura, N.; and Murakami, M.: 1997 Investigation of radial temperature and velocity profiles in oscillating flows inside a pulse tube refrigerator, *Cryocoolers 9*, Plenum Press, 365-374.

56. Shiraishi, M.; Seo, K.; and Murakami, M.: 1997 Oscillating flow behavior in pulse tube refrigerator under optimized conditions, *Cryogenic Engineering Conf.*, Portland, OR, paper APG-4.

57. Godshalk, K. M.; Jin, C.; Kwong, Y. K.; and Hershberg, E. L.: 1996 Characterization of 350 Hz thermoacoustic driven orifice pulse tube refrigerator with measurements of the phase of the mass flow and pressure, *Adv Cryo. Eng.*, Plenum Press, **41B**, 1411-1418.

58. Zhu, S. W.; Zhou, S.L.; Yoshimura, N.; and Matsubara, Y.: 1997 Phase shift effect of the long neck tube for the pulse tube refrigerator, *Cryocoolers 9*, Plenum Press, 269-278.

59. Gardner, D. L.; and Swift, G. W.: 1997 Use of inertance in orifice pulse tube refrigerators, submitted to *Cryogenics*.

60. Roach, P.; and Kashani, A.: 1997 Pulse tube coolers with an inertance tube: theory, modeling and practice, *Cryogenic Engineering Conf.*, Portland, OR, paper APE-6.

61. Batchelor, G. K.: 1967 *Introduction to Fluid Mechanics*, Cambridge University Press.

62. Lee, J. M.; Kittel, P.; Timmerhaus, K. D.; and Radebaugh, R.: 1995 Useful scaling parameters for the pulse tube, *Adv Cryo. Eng.*, Plenum Press, **41B**, 1347-1356.

63. White, F. M.: 1991 *Viscous Fluid Flow*, McGraw-Hill, Inc.

64. Bird, R. B.; Stewart, W. E.; and Lightfoot, E. N.: 1960 *Transport Phenomena*, John Wiley & Sons, Inc.

65. Anderson, J. D.: 1990 *Modern Compressible Flow*, McGraw-Hill, Inc.

66. Gedeon, D.: 1986 Mean Parameter Models of Oscillating Flow. J. Heat Transfer, 108(3), 513-518.

67. Stuart, J. T.: 1966 Double boundary layers in oscillatory viscous flow, *J. Fluid Mech.*, **24** (4), 673-687.

68. Kasuya, M.; Yuyama, J.; Geng, Q.; and Goto, E.: 1992 Optimum phase angle between pressure and gas displacement oscillations in a pulse-tube refrigerator, *Cryogenics*, **32** (3), 303-338.

SUGGESTED READING

Lighthill, Sir James: 1978 Acoustic streaming, *J. Sound and Vib.*, **61** (3), 391-418.

Mirels, H.: 1993 Linearized pulse tube cryocooler theory, *Proc. 7th Int. Cryocooler Conf.*, **1**, 222-232.

Ravikumar, K. V.; Yoshida, S.; Karlmann, P.; Myung, N. S.; and Frederking, T. H. K.: 1997 On thermodynamic aspects of pulse tube operation, *11th Intersoc. Cryogenic Sympos.*, Houston ISBM 1-890277-05-3 (Book VI), Intersociety Cryogenics '97 28-35.

Richardson, R. N.: 1988 Development of a practical pulse tube refrigerator: coaxial designs and the influence of viscosity, *Cryogenics*, **28**, 516-520.

Riley, N.: 1965 Oscillating flows, *Mathematika*, **12**, 161-175.

Riley, N.: 1967 Oscillatory viscous flows. Review and extension, *J. Inst. Maths Applics,* **3**, 419-434.

Schlichting, H.: 1968 *Boundary Layer Theory*, McGraw-Hill, Inc.

REPORT DOCUMENTATION PAGE

Form Approved
OMB No. 0704-0188

1. AGENCY USE ONLY *(Leave blank)*	2. REPORT DATE	3. REPORT TYPE AND DATES COVERED
	September 1999	Technical Memorandum

4. TITLE AND SUBTITLE

Steady Secondary Flows Generated By Periodic Compression and Expansion of an Ideal Gas in a Pulse Tube

5. FUNDING NUMBERS

UPN 632-20

6. AUTHOR(S)

Jeffrey M. Lee

7. PERFORMING ORGANIZATION NAME(S) AND ADDRESS(ES)

Ames Research Center
Moffett Field, CA 94035-1000

8. PERFORMING ORGANIZATION REPORT NUMBER

A-9901168

9. SPONSORING/MONITORING AGENCY NAME(S) AND ADDRESS(ES)

National Aeronautics and Space Administration
Washington, DC 20546-0001

10. SPONSORING/MONITORING AGENCY REPORT NUMBER

NASA/TM–1999-208769

11. SUPPLEMENTARY NOTES

Point of Contact: Jeffrey M. Lee, Ames Research Center, MS 244-10, Moffett Field, CA 94035-1000
(650) 604-5693

12a. DISTRIBUTION/AVAILABILITY STATEMENT

Unclassified — Unlimited
Subject Category 34 Distribution: Standard
Availability: NASA CASI (301) 621-0390

12b. DISTRIBUTION CODE

13. ABSTRACT ***(Maximum 200 words)***

This study establishes a consistent set of differential equations for use in describing the steady secondary flows generated by periodic compression and expansion of an ideal gas in pulse tubes. Also considered is heat transfer between the gas and the tube wall of finite thickness. A small-amplitude series expansion solution in the inverse Strouhal number is proposed for the two-dimensional axisymmetric mass, momentum and energy equations. The anelastic approach applies when shock and acoustic energies are small compared with the energy needed to compress and expand the gas.

An analytic solution to the ordered series is obtained in the strong temperature limit where the zeroth-order temperature is constant. The solution shows steady velocities increase linearly for small Valensi number and can be of order 1 for large Valensi number. A conversion of steady work flow to heat flow occurs whenever temperature, velocity or phase angle gradients are present. Steady enthalpy flow is reduced by heat transfer and is scaled by the Prandtl times Valensi numbers.

Particle velocities from a smoke-wire experiment were compared with predictions for the basic and orifice pulse tube configurations. The theory accurately predicted the observed steady streaming.

14. SUBJECT TERMS	15. NUMBER OF PAGES
Pulse tube, Anelastic, Steady secondary flows	161
	16. PRICE CODE: A08

17. SECURITY CLASSIFICATION OF REPORT	18. SECURITY CLASSIFICATION OF THIS PAGE	19. SECURITY CLASSIFICATION OF ABSTRACT	20. LIMITATION OF ABSTRACT
Unclassified	Unclassified		